Dissertation

submitted to the
Combined Faculties for the Natural Sciences and for Mathematics
of the Ruperto-Carlo University of Heidelberg, Germany
for the degree of
Doctor of Natural Sciences

Put forward by
Sadaf Pashapour, M.Sc.
Born in: Vienna, Austria

Oral examination:
21st of October 2021

Generation of Extracellular Matrix Protein-based Microcapsules for Investigating Single Cells

Referees:

Prof. Dr. Joachim P. Spatz
Institute for Mechanical Systems Engineering
Heidelberg University
Max-Planck Institute for Medical Research
Heidelberg

Prof. Dr. Reiner Dahint
Institute for Physical Chemistry
Heidelberg University

I am dedicating my thesis to my parents,
Esmail and Parvin
and my sister, Roxana.
Thank you for always supporting me.
I love you.

Zusammenfassung

Durch die Gewebsgängigkeit der Zelle kann sie auf mechanische Veränderungen der Umgebung reagieren indem die äußeren Reize entsprechende Signalwege im Inneren der Zelle aktivieren. Dieser Anstoß animiert die Zelle sich zu bewegen, zu teilen oder in einigen Fällen auch zu sterben. Die Extrazellulär Matrix (EZM) spielt in solchen vitalen Ereignissen eine zentrale Rolle. Deshalb ist es kaum verwunderlich, dass jegliche Abweichungen von der Norm zu nekrotischen oder sogar kanzerogenen Prozessen führen können. Um spezifische Zellinterkationen mit der EZM genauer untersuchen zu können, entwickelte ich im Rahmen meiner Doktorarbeit zwei neue Technologien. Mit Hilfe Tröpfchen-basierter Mikrofluidik gelang es mir EZM-basierte Proteinkapseln und EZM-beschichtete Hydrogele herzustellen. Die Proteinkapseln enthalten neben Laminin-111, Fibronektin oder Matrigel auch Zellen in der inneren Wasserphase. Die äußere Ölschicht besteht aus geladenen Surfactants, welche ihre Ladung in das Innere des Tropfens richten. Dadurch entsteht eine geladene Innenseite, an welcher die Proteine sich mit Hilfe von Ionen anordnen und eine polymerisierte Proteinschicht aufbauen. Sobald dieser erste, und gleichzeitig unentbehrliche Schritt vollzogen ist, kann man die entstandene Proteinmikrokapsel aus der stabilisierenden Ölschicht wieder befreien, sodass die Zellen im Inneren der Mikrokapseln an nährstoffreiches Medium gelangen können. Zur Untersuchung von Zellen in EZM-beschichteten Hydrogelen produzierte ich poly(ethylene) glycol diacrylate (PEGDA) Gele welche eine abgerundete Öffnung für die Beladung einzelner Zellen haben. Diese Öffnung ist mit Laminin-111 beschichtet und unterstützt die Anhaftung der Zellen. In dieser Arbeit konnte ich durch die Anwendung Tröpfchen-basierter Mikrofluidik erstmalig die Herstellung von Proteinkapseln zeigen, dessen Zusammensetzung auf vollkommen natürlichen Materialen beruht und weiters, eine schon bestehende Technologie durch die Zugabe von EZM Proteinen zu abgerundeten PEGDA Hydrogelen bereichern. Durch die Interaktion von variierenden Zelltypen mit verschiedenen Proteinen an unterschiedlich geformten Oberflächen ist es möglich diese Interaktionen genau zu untersuchen und deren oxidativen Reaktionen zu bewerten. Darüber hinaus, öffnet diese Art von Zelluntersuchung Türen zur

Beantwortung jeglicher Fragen im Bereich der Zell-Zell Kommunikation über Proteinbarrieren hindurch oder der mechanischen Manipulation von Zellen mittels Proteine.

Abstract

Interactions between cells and the extracellular matrix (ECM) activate multiple signaling pathways that initiate, drive and regulate nearly all motions of cells in their native environment. Cell-ECM interactions are also emphasizing the importance of research that aims to better understand such interactions. Consequently, engineering 3D ECM systems for controlled manipulation of cells *in vitro* has become an important strategy, particularly in medical applications. These systems will contribute to understanding the mechanisms underlying the ability of cells to perform different tasks as a response to environmental information. In this PhD thesis, I have established two novel droplet-based microfluidic approaches for the controlled assembly of; (1) cell-laden ECM-based protein microcapsules; and (2) ECM-coated crescent hydrogel-based microparticles. Towards the production of ECM-based microcapsules, water-in-oil emulsion droplets consisting of negatively or positively charged block-copolymer surfactants are used as a template for the charge-mediated formation of an either pure laminin-, laminin/collagen mixed- or fibronectin-based continuous layer on the inner droplet periphery. Following the protein layer formation, different microfluidic technologies are implemented to encapsulate cells and under the appropriate ionic conditions for the controlled polymerization of the protein layer. Sequential release of the assembled cell-laden ECM based microcapsules from the surfactant-stabilized droplets into a physiological environment allows for analysis of cell-ECM interactions on the single-cell level. The second technology, invented within the scope of this thesis, is the application of ECM-coated crescent PEGDA microparticles for the analysis of cell behavior on curved substrates. By making use of an aqueous two-phase microfluidic system, it was possible to establish PEGDA crescent microparticles with a layer of ECM proteins coating the bucket. Towards this end, ECM proteins are dissolved with dextran molecules and are encapsulated with PEGDA into water-in-oil droplets. Due to a phase separation between PEGDA and dextran the characteristic crescent shape is established. Upon polymerization of PEGDA it becomes feasible to release the particles and wash away the dextran phase, which generates a remaining protein layer on the inner bucket. By tailoring the

biochemical properties of both systems, we are able to produce a wide variety of ECM-based microcapsules that are tunable in terms of protein composition and cellular encapsulation. Ultimately, this technology will be used for investigating cell-ECM interactions in various environments and on a variety of substrate geometries.

Table of Content

Acronyms

7-AAD	7-Aminoactinomycin D
ADAM	a disintegrin and metalloprotease
ADAMT	ADAM with thrombospondin motif
ASGPR	asialoglyoprotein receptors
BrIBAM	bromoisobutyramide
BSA	bovine serum albumin
$CaCl_2$	Calcium chloride
CAF	cancer-associated fibroblasts
colIV	collagen type IV
cFN	cellular fibronectin
CLSM	confocal laser scanning microscopy
CHO	chinese hamster ovary cells
DDR	discoidin domain receptors
DMPA	α-dimyristoyl-phosphatic acid
DTT	dithiothreitol
EB	embryonic body
ECM	extracellular matrix
ER	endoplasmic reticulum
ESC	embryonic stem cells
EtOH	ethanol
ETPTA	ethoxylated trimethylolpropane triacrylate
FA	focal adhesion
FGF	Fibroblast growth factor
FN	fibronectin
GA	galactosylated alginate
GAG	glycosaminoglycans
GEL	collagen type I gel
GF	growth factors
HA	hyaluronan

HCl	Hydrogen chloride
HCR	hybridization chain reaction
HSA	human serum albumin
HSP47	Heat shock protein 47
IBAM	isobutyramide
ILK	integrin-linked protein kinase
IPTG	Isopropyl-β-D-thiogalactopyranosid
LAP	latency associated peptide
LAP	lithium phenyl-2,4,6-trimethyl-benzoylphosphinate
LbL	layer-by-layer
LN	laminin
LOX	lysyl oxidase
LSM	laser scanning microscope
LTBP	latent TGF binding protein
MAPK	mitogen-activated protein kinase
MMP	matrix metalloproteinase
NCl	non-collagenous
NaCl	Natrium chloride
OCN	osteocalcin
OPN	osteopontin
PAA	polyacrylamide
PBS	phosphate buffered saline
PCR	polymerase-chain reactions
PDMS	Polydimethylsiloxane
PEG	poly(ethylene glycol)
PEGDA	poly(ethylene glycol) diacrylate
PFA	Paraformaldehyde
PFO	1H,1H,2H,2H-Perfluoro-1-octanol
pFN	plasma fibronectin
PFPE	perfluor polyether
PG	proteoglycans
PLA	polyactic acid

PLL	poly-L-lysine
PLG	poly(lactide-co-glycolide
PMA/PAA	poly(meth) acrylic acid
PNIPAM	poly(N-isopropylacrylamide)
PSS	poly(styrene sulfonate) sodium salt
PTEN	phosphatase and tensin homolog
PVA	poly(vinyl)alcohol
rpm	rounds per minute
RT	room temperature
SLRP	small leucine-rich proteoglycans
SPARC	secreted protein acidic and rich in cysteine
TGF	tumor growth factor
TGF-β	transforming growth factor- β
TGM2	transglutaminase
TME	tumor microenvironment
TRIS	Tris(hydroxymethyl)aminomethan
TSP	thrombospondin
VEGF	vascular endothelial growth factor
W/O/W	water-in-oil-in-water

Introduction

1 Introduction

1.1 Molecular organization of tissues in the human body

Maintaining tissue stability, functionalization and organization is a complex job, fulfilled on a multicellular and multimolecular level.[1] The whole system is based on the signal transduction between cells and proteins, which are determining cell fate and organization.[2,3] Tissues are being constantly remodeled by changes in their protein and cell constellation. Cells degrade proteins and synthesize new ones, while themselves undergo a constant circle of proliferation and apoptosis to maintain tissue functionality.[4] There are two main interactions which are responsible for the construction of tissues. On the one hand, cadherin-dependent cell-cell interactions allow the cells to communicate with each other and transduce signals to the nucleus via the actomyosin cytoskeleton, while on the other hand, integrins bind the cells tightly to their underlying extracellular matrix (ECM) and propagate external mechanical cues to the inside of the cells (Figure 1).[5] Those cadherin molecules are not solely functioning as glues between cells, they are furthermore important for diverse morphogenetic impacts, such as tissue integrity, motility and *in vivo* cell sorting.[6] Cadherins are very crucial from the beginning of tissue formation. Expression of a mutant cadherin molecule in the embryo of a *Xenopus* caused many defects in tissue integrity, leading to discontinuities in the ectodermal layer.[7] Further, the most prominent example for cell motility based on cadherin levels is epithelial-mesenchymal transition/mesenchymal-epithelial transition (EMT/MET). Here, cells are in tight contact to each other over E-cadherins, but as soon as the expression level decreases, cells become loose and can migrate separately. Once reached their destination, E-cadherin levels increase again and cells adhere to each other. This extraordinary mechanism is crucial during morphogenesis, but unfortunately also during carcinogenesis.[8] The final developmental process, discussed here, is the ability of cells with different fates to disintegrate from each other and connect with cells from the same origin again.[9] This sorting behavior might base on the differential adhesion receptors between

different cell populations. Three scenarios can be observed: "Like"-cells have the ability to find and bind each other, "Unlike"-cells segregate away from each other, and the third possibility is that those distinct cell populations stay aggregated.[10] The aforementioned tasks of cadherins are just to give an overview of the importance of cell-cell interactions. However, cells also interact with the extracellular matrix (ECM) for stabilizing the tissue and providing special functionalities.[11] Cells are in tight contact to the ECM over various integrins on the cell surface. Those receptors sense the changes of the surrounding ECM, and lead to the organization of the actomyosin cytoskeleton and hence regulate cell contractility (Figure 1).[12] The interaction mechanisms between cells and their surrounding ECM will be discussed thoroughly in Chapter 1.3 Basic principles of ECM-cell interactions.

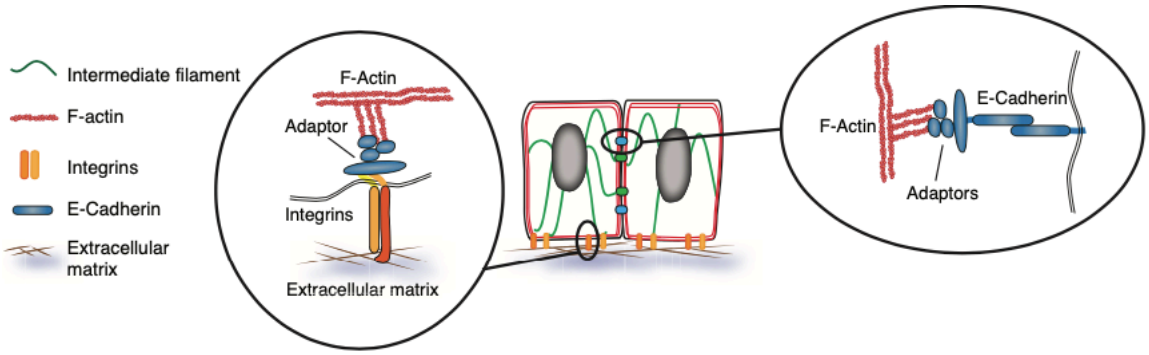

Figure 1 Scheme of cell-cell and cell-matrix interactions.
Cells bind to their neighbors over different cadherin molecules, while the adhesion to the ECM is established by integrins. Both adhesive molecules are linked to the actomyosin cytoskeleton which is organized and contracted based on the outer interaction. Figure adapted from Wickström et al., 2018.[12]

1.2 Functions of the Extracellular Matrix

The extracellular matrix (ECM) is of utmost importance for every development on a cellular and a tissue level. The first function associated with the ECM is its ability of providing a physical scaffold into which cells are embedded. Further it is also responsible for establishing signaling cues in order to initiate movements of single cells towards a specific direction. It also orchestrates higher functions, namely building, stabilizing and regulating various kinds of whole organ tissues.[13,14] The

dynamic interactions between cells and single ECM molecules leads to the rearrangement and remodeling of ECM throughout the life span of an organism.[6] The most interesting part of this system is that every tissue with its varying functionality consists of the exact same fibrous proteins, such as laminin, fibronectin or collagen, although the ECM comprises over 300 proteins, 200 glycoproteins and 30 proteoglycans.[15] The difference in functionality and stiffness of the tissues arises in precise but yet different compositions of those proteins.[1,3,4,13] To give specific examples, Figure 2 shows the relative abundance of ECM proteins presented in different tissues. The most prominent difference can be seen with collagen type I. Bone tissue consists nearly entirely of collagen type I while the presence of this protein is approximately one fourth in skeletal muscle tissue.[4]

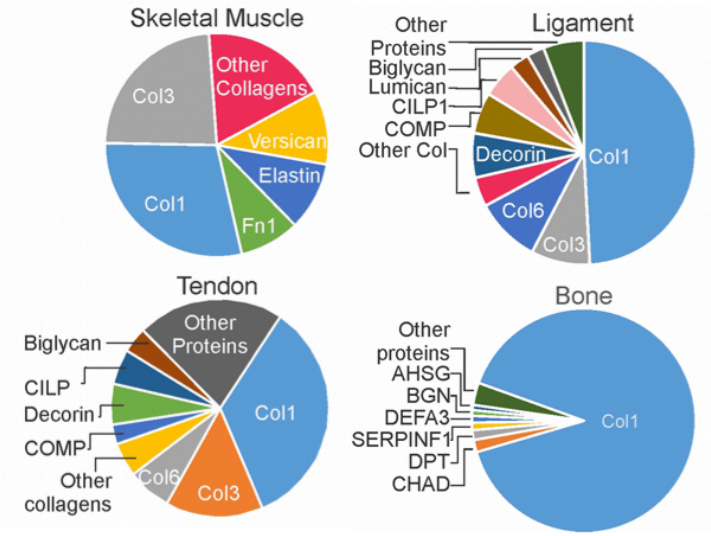

Figure 2 Overall proteomic composition of different tissues.
Relative abundance of ECM proteins in the presented tissues. Figure adapted from McKee et al., 2019.[4]

Figure 3 depicts the difference between epithelium and bone tissue very well. Here, it is clearly visible how the same proteins, e.g. different collagen types, growth factors and their receptors and integrins, are present in both tissues. Additionally, the tissues are fundamentally different in their functions and most importantly in their stiffness. This is due to the fact that bone mineralization is facilitated by ECM proteins such as SLRPs (small leucine-rich proteoglycans), OPN (osteopontin) and OCN (osteocalcin).[1] Furthermore, Figure 3A shows the multifaceted and dense

matrix, which makes up the epithelium. At a first glance it looks tumultuous and disorganized, but each and every protein has its own role and function in this system. The extracellular matrix takes over many fundamental responsibilities in order for tissues and organs to function properly, which will be highlighted in the next chapters.

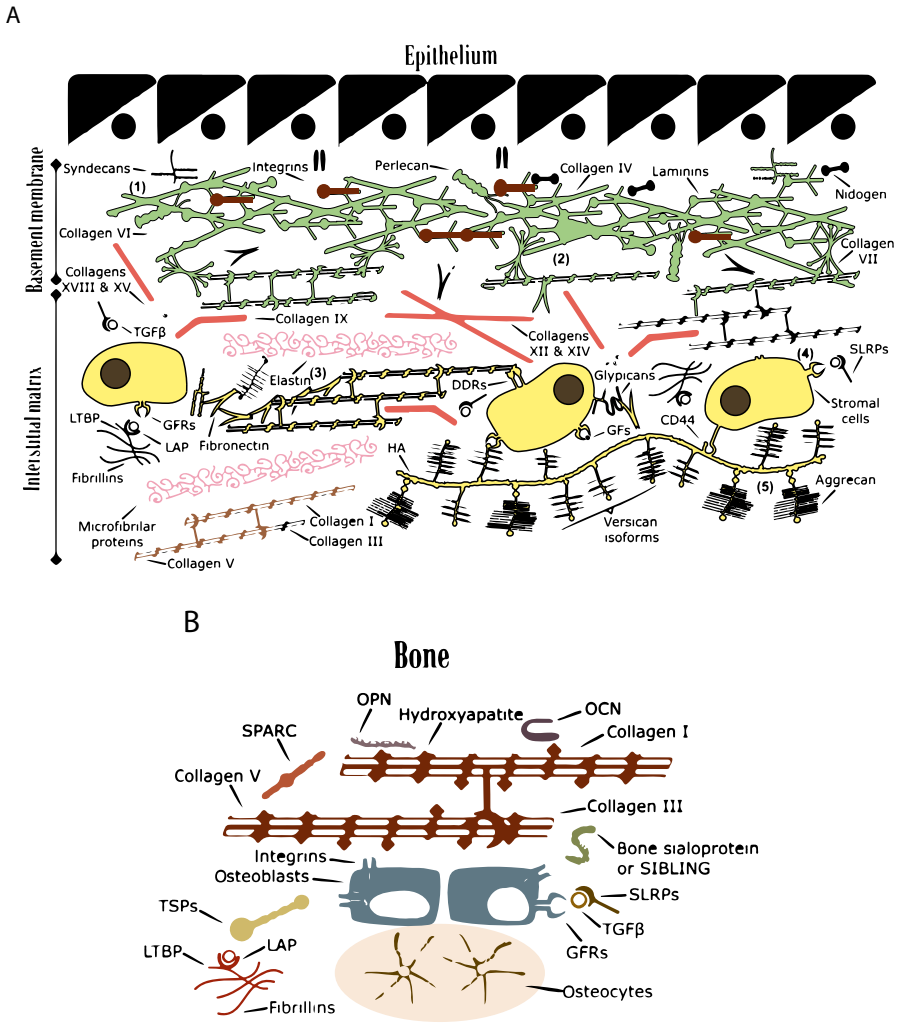

Figure 3 Schematic overview of the ECM protein composition of the epithelium in comparison to bone.
A) Two distinctive matrices, basement membrane and interstitial matrix, make up the epithelium. Collagen type IV and laminin are connected over perlecan to form a dense matrix underneath the epithelial cells. Different types of collagens are building the bridge to the interstitial matrix and are anchoring several single cells to the matrix. B) The bone tissue shows a lower amount of ECM proteins, but consists of the similar types. Bone mineralization is facilitated by ECM molecules such as OCN, SIBLING and SLRPs. DDR, discoidin domain receptors; HA, hyaluronan; LAP, latency associated peptide; LTBP, latent TGFβ binding protein; GFs, Growth Factors; TGFβ, Tumor growth factor β; OCN, osteocalcin; OPN, osteopontin; SLRP, small leucine-rich proteoglycans; SPARC, secreted protein acidic and rich in cysteine; TSP, thrombospondin. Figure adapted from Theocharis et al., 2019. [1]

Figure 4 highlights the complexity underlying every mechanical and biophysical stimulation towards a cell. The fibrous ECM compartments are interconnected with other ECM molecules such as proteoglycans to build complex three-dimensional matrices.[1,16] By changing the stiffness around those cells, the ECM helps triggering mechanical reactions which lead to deformations of the cell. For stem cells, these kinds of triggers lead to differentiation towards a needed cell type in the tissue. Biophysical cues are activated over junction proteins, such as integrins between the proteins and cells. With this interaction it is possible to initiate intrinsic pathways which lead to cell growth, migration, differentiation and morphogenesis.[17]

The ECM is roughly classified into two different categories, the interstitial and pericellular matrix.[16] Those differ mainly in composition and structure (Figure 4). The most known pericellular matrix is the basement membrane. It functions as an anchoring point for epithelial cells to prevent the epithelium from falling apart.[16] Further, both matrices interact with each other over basement membrane proteins such as collagen type IV, laminin and fibronectin to keep the system stable and functioning.[3] For example, collagen type IV and laminin molecules are interconnected with perlecan to ensure stability and additionally, this small connecting molecule impacts the tissue hydration and hence its biomechanical properties.[16,18,19] The interstitial matrix surrounds cells, meaning mostly single cells are interacting with the macromolecular ECM network without any cell-cell interactions. Unlike the pericellular matrix, the interstitial matrices are less dense and allow free cell migration.[20] All cell types (i.e., fibroblasts, epithelial cells, immune cell) are interacting with the ECM over cell-ECM connecting proteins, such as integrins, CD44 and cell surface proteoglycans. This way they can integrate the signal coming from their surrounding ECM and respond by creating their own ECM proteins and secrete those.[17] This leads to ECM remodeling based on the current need of the tissue and the ability of the cells to provide the desired proteins.[21] This capability of a fast response towards a demand of the tissue makes the ECM flexible to react in order to prevent diseases and malfunctioning of the tissue.[17] In parallel to the immediate ECM deposition the body is making use of another clever and fast way to derive various molecules such as cytokines, chemokines or growth factors.[22,23] Those molecules are released by cells and

embedded in the ECM. At developmentally and physiologically relevant timings those molecules can be withdrawn immediately, without losing time during the production process.[16,17]

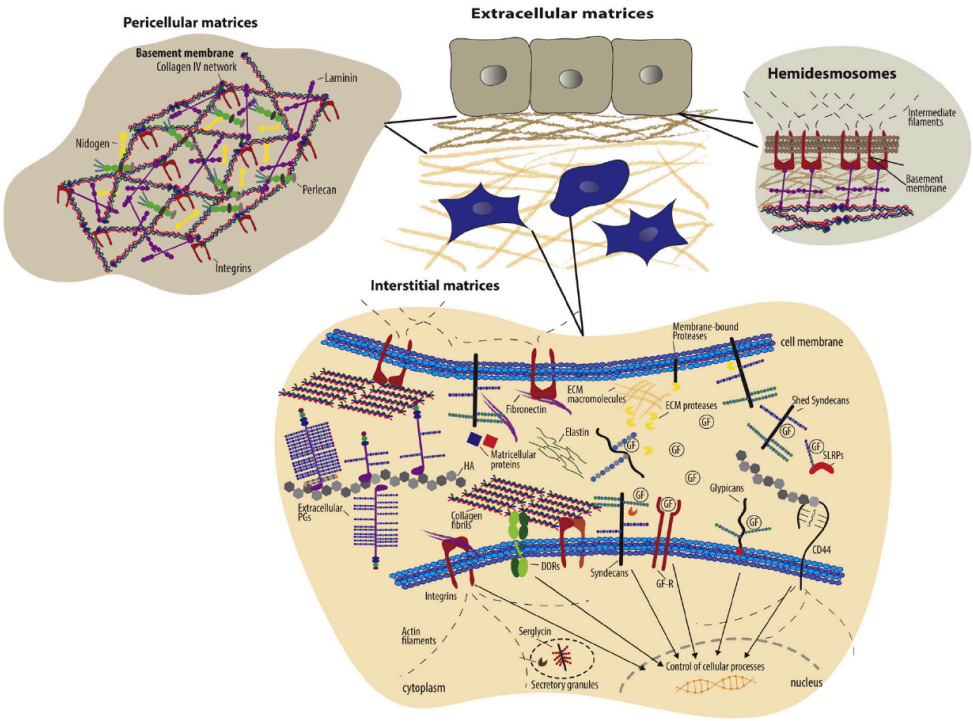

Figure 4 Schematic representation of extracellular matrices.
Cells are connected to the ECM over two different networks, the pericellular matrix and the interstitial matrix. The pericellular matrix lies directly beneath the epithelium and functions as a support for epithelial cells. Cells are connected to this matrix over integrins. The interstitial matrix surrounds mostly single cells which are connected to the ECM proteins over integrins, hyaluronan receptors CD44 and discoidin domain receptors, DDR. Figure adapted from Theocharis et al. 2016.[16]

To summarize, the functions of the ECM are widely distributed and range from functioning as an underlying adhesive substrate for cells to mechanotransducers towards cells from the surrounding tissue (Figure 5). In order to migrate in specific directions, cells need substantial anchoring points to adhere and trigger intrinsic actin cytoskeleton changes.[24] Those adhesive substrates are consisting of various ECM molecules (Figure 5A).[25,26] In a three-dimensional setting, ECM molecules provide structure for various cell types and define tissue borders.[27,28] Cells remodel and degrade the ECM components to support the growth and development of organs (Figure 5B).[29] The ECM has the ability to present specific growth factors to the according cell receptors.[30] This allows for the spatial distribution of ECM-bound

surface molecules and helps to arrange the cells in tissue complexes.[31] Through this mechanism, the ECM facilitates the interaction between ECM receptors and growth factor receptors (Figure 5C). Besides the ability of ECM molecules to interact directly with cells through protein sequences in their structure, the ECM stores various growth factors which are produced by the cells beforehand and displays them to the surrounding cells, by enzymes degrading the ECM.[32] A fast release of such molecules is mediated upon the proteolytic degradation of the ECM or cell-based forces exerting on the matrix structure. Further, morphogenic gradients can be organized in this way and allow for the specific guidance of cells in a determined direction (Figure 5D).[33] Another very important, and widely distributed attribute of the ECM is its role as a mechanosensor.[34] Hereby, it transduces mechanical changes in the surrounding tissue to the cell by interactions between the ECM and cell-surface receptors such as integrins.[35,36] Those interactions trigger intracellular pathways and order the cell to migrate, differentiate or proliferate (Figure 5E).[37,38]

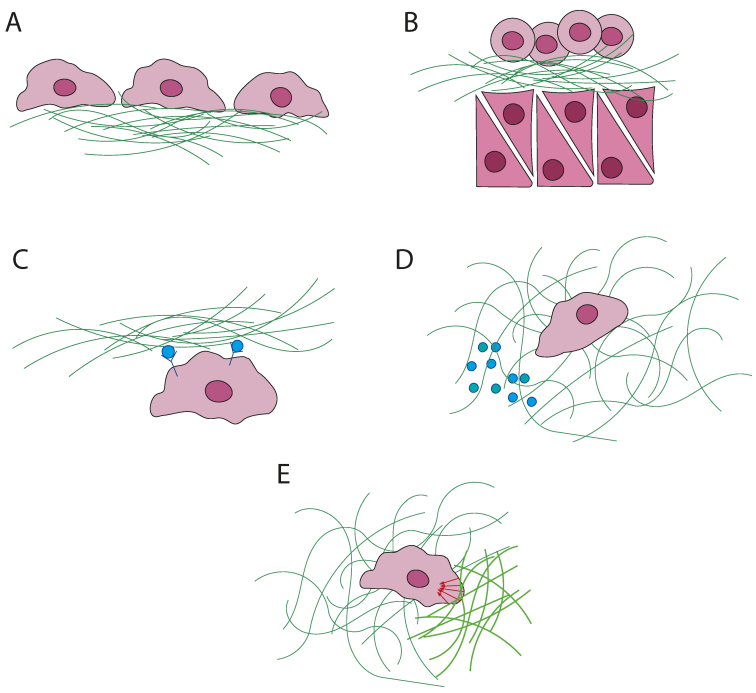

Figure 5 Functions of the extracellular matrix.
A) ECM as adhesive substrates. B) 3D structure defined by tissue boundaries provided by ECM molecules. C) Growth factor presentation to cell surface receptors to control distribution of ECM-bound surface molecules. D) Storage of growth factors for release on-demand. E) Mechanotransduction of physical stress towards the cell from the surrounding varying in stiffness.

1.2.1 Molecular composition of the ECM

The ECM consists of two classes of macromolecules: fibrous proteins and proteoglycans (PGs). The main variance is that PGs are composed of glycosaminoglycans (GAGs) which makes those proteins highly hydrophilic leading to hydrogel formations.[18,21] Those proteins are mostly filling up the space between cells in the interstitial matrix. Fibrous proteins, on the other hand, assemble into networks and help stabilizing cells and whole tissues.[3,15,17,39-41] The focus on this thesis lays on the establishment of microcapsules consisting of fibrous proteins, such as collagen, fibronectin and laminin, hence those proteins are going to be discussed in further detail.

1.2.1.1 Fibrous Collagen

Collagen functions as a triple helix which consists of 3 polypeptide-α-chains with a 7S domain on the N-terminal end and a non-collagenous (NCl) domain on the C-terminus (Figure 6). In vertebrates, 28 collagen types exist, originating from 46 distinct collagen chains.[17] Those 28 kinds are further categorized into fibril-forming collagens (e.g. types I, II and III), fibril-associated collagens, which are interrupted in the triple helix (e.g. types IX and XII), network-forming collagens (collagen type IV) and others.[17,20,42,43] As the names indicate they differ in their fibril-forming abilities. Fibril-forming collagens polymerize with each other and are able to build fibrils. Network-forming collagens such as type IV collagen are building non-fibril supramolecular structures with the help of nonfibrillar collagens. Fibril-associated collagens, instead, are more likely to assemble into fibrils in close association with other collagen fibrils.[44,45]

The biosynthesis of fibril-forming collagens starts with the generation of procollagen molecules. They comprise of several α-chains which undergo posttranslational modifications before generating a triple helix.[46] The heat shock protein 47 (HSP47) functions as the guardian of the procollagen and guides it to the endoplasmic reticulum (ER).[47] Arrived at the ER, procollagen is cleaved by A Disintegrin And Metalloproteinase with Thrombospondin motifs (ADAMTs). In

order to assemble those fibrils, collagens are covalently linked to each other via their lysine residues. This process is catalyzed by lysyl oxidase (LOX), an extracellular enzyme.[48] The tissue architecture, shape and organization of the final product is dictated by the collagenous backbone.[17,49-51] Monomer structures have a 7S domain and a NCl domain on either end. Dimerization of the protein is established over the NCl domain, while tetramers are built by linkage of the 7S domains of the proteins to each other. Those tetramers are connecting to other tetramers over the NCl domains, building a ColIV suprastructure (Figure 6).[21]

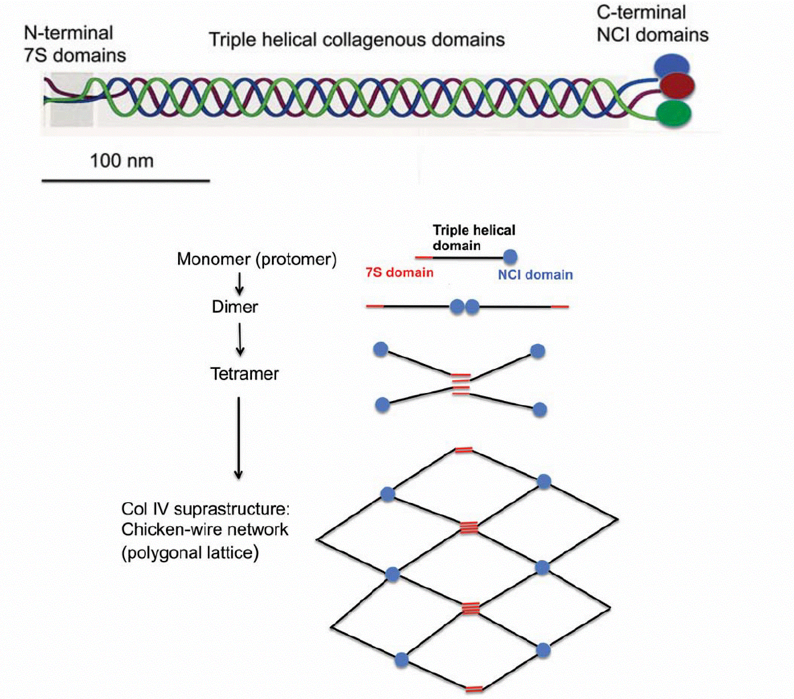

Figure 6 Overview of a triple helical collagen fiber.

Upper panel: Collagen chains consist of 3 polypeptide-α-chains, intertwined to a triple helix. Collagen chains are approximately 300-400nm in length. Lower panel: NCI domains are needed to form collagen dimers, while Tetrameric and higher order structures are assembled via 7S-domains. Figure adapted from Mak et al., 2017. [21]

1.2.1.2 Fibronectin

Another very important player in the foundation of the ECM is fibronectin (FN). This protein has binding sites to integrins and other cell receptors, which helps the protein to interact with cells and regulate their behavior. Further, fibronectin can also bind to other ECM proteins such as gelatin (Figure 7).[52,53] The protein is built as a dimer, consisting of nearly the same subunits, which are linked together at the C-terminus with disulfide bonds. Fibronectin has three different types of repeating units, which have different binding abilities (Figure 7).[54] There are 20 different variants of fibronectin in the human, which are all a product of the same gene. The difference in form arises from alternative splicing of a single mRNA. Fibronectin can be grouped in two different classes, based on its solubility: soluble plasma fibronectin (pFN) and less-soluble cellular fibronectin (cFN).[39] pFN is in comparison to cFN rather simple in its splicing pattern and is synthesized in the liver. cFN, on the other hand, consists of a more heterogenous group of FNs, and are cell type- and species-specific.[25] Cellular FN is mainly binding over different classes of integrin molecules to the cells. Besides binding to cells, fibronectin has various other binding sites to interact with heparin, collagen/gelatin and fibrin.[26] The heparin-binding domain, was proven to facilitate cell adhesion in some cell types, whereas the collagen/gelatin-binding site prefers binding to denatured collagen (gelatin), which is needed to clear the blood and tissue from this material.[53] The binding to fibrin is necessary to initiate cell adhesion or cell migration towards fibrin clots, and further help macrophages clear the circulating fibrin after inflammation.[55,56]

The role of soluble plasma fibronectin is to create extracellular fibrils. Fibrillogenesis is performed by which dynamic tension forces and integrins unmask specific fibronectin binding sites, which lead to self-assembly and the production of a fibrillar network.[57,58] Fibrillogenesis occurs through the interaction of soluble fibronectin molecules to sulfonic acid side groups present on polyanionic proteoglycans (PGs).[59] This process is extremely important to provide some elasticity to the extracellular matrix. With fibronectin assembling into such networks, other proteins can bind easier and form their own nets.[54,60] This in turn helps cells to incorporate, attach and migrate through a well-connected network.

Based on those networks the three-dimensional structure is constructed and is crucial for the health of the tissue.[61]

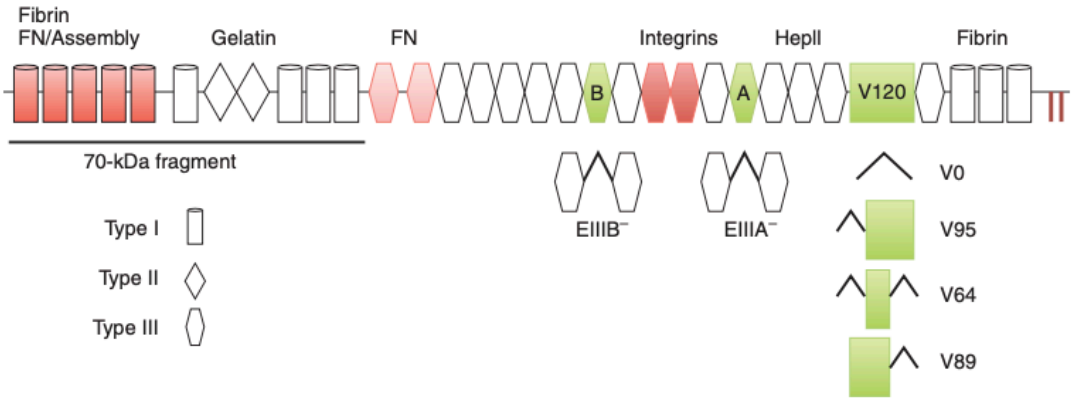

Figure 7 Fibronectin structure and different isoforms.
Each FN monomer consists of 12 different repeats from three different types. Two additional types (EIIIA and EIIIB) are included or cut out by alternative splicing such as the V region which is either fully incorporated (V120), not existent (V0) or half integrated (V95, V64 or V89). Fibronectin has the ability to form fibrils (fibrin assembly units) or bind to integrins via typeIII$_{9\text{-}10}$ regions. The typeIII$_{1\text{-}2}$ domain is important for binding to FN in order to initiate fibrillogenesis. Finally, the 70 kDa fragment contains FN and gelatin binding sites, which is needed for matrix assembly. Figure adapted from Schwarzbauer et al., 2011.[54]

1.2.1.3 Laminin

Laminin is mostly present in basement membranes, where it is responsible for forming large and wide networks via self-assembly of the protein by using calcium ions.[40] Small bridging molecules such as perlecan are connecting those networks to others such as collagen type IV or fibronectin meshes. Laminin, is functioning as a heterotrimer with three different chains. The N-terminus of each chain is spread out forming the arms of the molecule, while the main body of the protein is intertwined into a triple α-helix domain.[21] A single laminin molecule consists of three chains, namely an α-, β- and γ- chain (Figure 8A). In total the genes LAMA1-5, LAMB1-3 and LAMC1-3, encode 11 chains, however, only 18 different laminin heterotrimer consist (Figure 8B).[62] Laminin networks are built by connections over the arms to each other (Figure 8C). Those established laminin protein networks are not only building connections to other proteins to stabilize the surrounding of the cells, they are also able to interact directly with cells over their C-terminal G domain.[16]

Laminins have several cell surface receptor binding sites. The protein can interact with integrins (αLG1-3 and αLG4 domains), dystroglycan (αLG4 domain and 2αLG domains) and syndecans (αLG4 domains of all α chains and α4LG1), as well as Lutheran blood group glycoprotein (LG3 domain of the α5 chain) (Figure 8D).[1] By binding directly to cells over those transmembrane receptors, they can alter cell differentiation, adhesion and migration by affecting the actin cytoskeleton.[63-67]

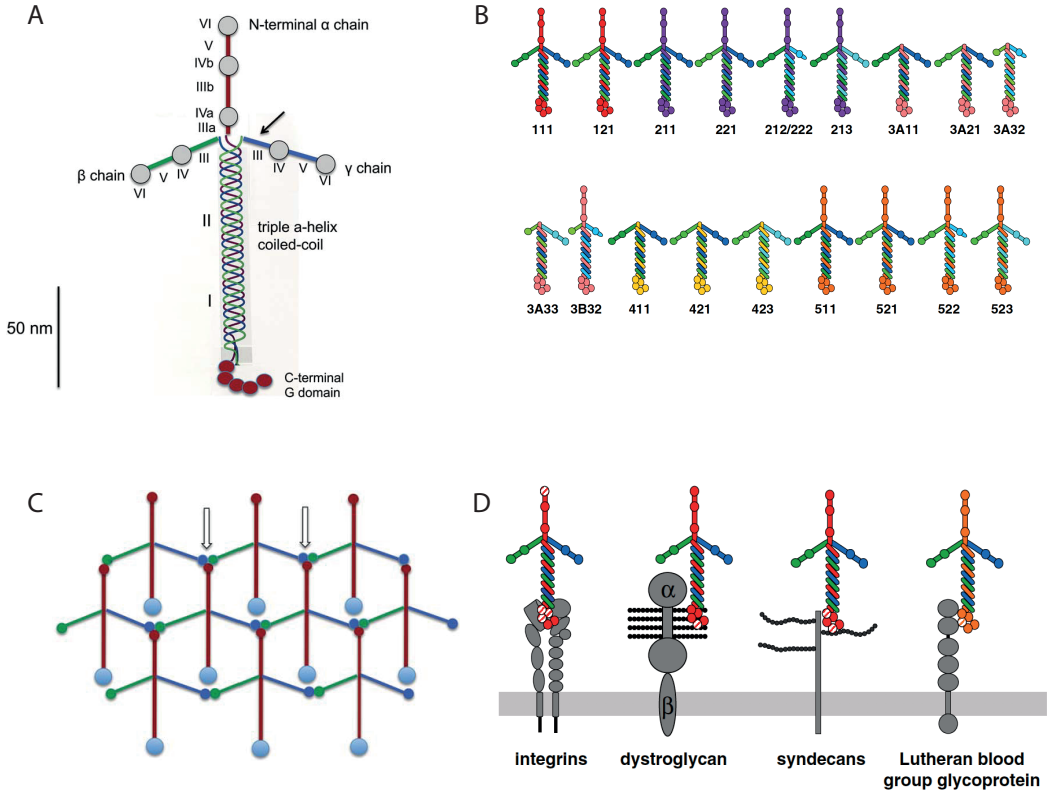

Figure 8 Schematic drawing of Laminin-111.

A) Typical shape of laminin made up by α, β and γ chains are building up the triple α-helix coiled-coil main body. The ends of those chains are reaching out separately from the center of the cross and contain globular domains (grey circles). The C-terminal G domain at the lower end of the protein, solely comes from the α-chain and is the only anchoring point of the protein to cells. The Romain numerals indicate various laminin domains on the protein. Domains I and III are representing the binding sites of the protein to cell surface receptors, while the black arrow at domain III indicates the nidogen binding site. Overall, laminin is approximately 160 nm long, of which approximately 80 nm is the length of the triple coiled-coil structure. B) All existing laminin types represented. The main difference of the proteins can be found in their arms, while the main body is always a triple α-helix coiled-coil. C) Laminin self-assembly over his three arms. The N-terminal regions of the α, β and γ chains are interacting with each other to form the network. Two white arrows are indicating those complexes. The main body is not contributing to the network formation. D) Laminin interaction with four different transmembrane receptors of the cell. The G-domains (striped circles) are interacting with integrins, dystroglycans, syndecans and Lutheran blood group glycoprotein. Figures A and C adapted from Mak et al., 2017[21], figures B and D adapted from Durbeej et al., 2010.[62]

1.3 Basic principles of ECM-cell interactions

The extracellular matrix is a complex and important supportive structure for various cells in all tissue types in the body. Cell-ECM interactions are facilitated by integrin molecules, which are binding to the actin cytoskeleton inside the cell.[68] This allows the cell to react to mechanical stimuli from the ECM and alter its behavior. On the other hand, cells are also constantly remodeling the surrounding ECM, in the sense of degradation, deposition and modification of its components by the release of enzymes.[69] Figure 9 summarizes the interactions between cells and their surrounding ECM.[17] Those aspects are going to be discussed in the following chapters in more detail and should highlight the active processes and complexity of ECM-cell interactions.

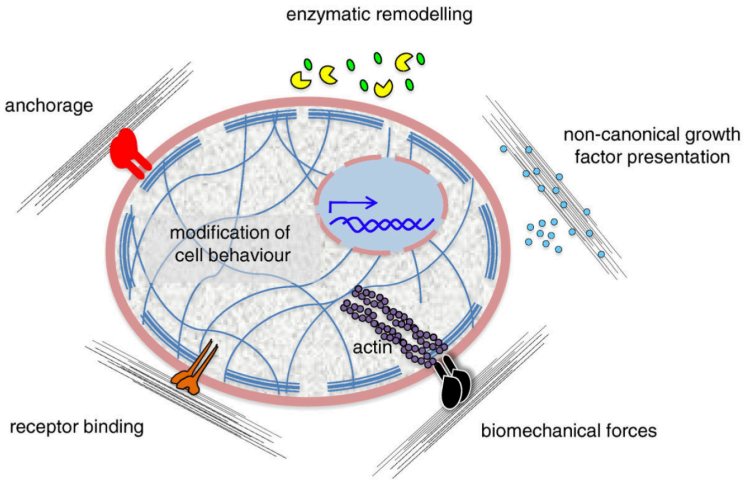

Figure 9 Impact of the ECM on cell behavior.
There are various ways how the ECM can affect the faith of a cell. By binding to different receptors on the cell it can determine cell anchorage, mechanotransduction or even regulate intrinsic pathways. Furthermore, growth factors are embedded in the ECM and can be taken up by the cell at any time needed. The ECM is also affected by the cell through the release of enzymes in order to remodel its surrounding ECM. Figure adapted from Yue, 2014.[17]

1.3.1 ECM remodeling

The ECM is surrounding and supporting cells, which makes it prone to remodeling and alteration by its inhabitants. By secreting various enzymes, the cells are actively changing their surrounding proteins, depending on their needs. For example, LOX enzymes are released to cross-link collagens and elastin, which is increasing the matrix stiffness and thereby facilitating cellular anchorage and migration. Other key players in ECM remodeling are matrix metalloproteinases (MMPs), a disintegrin and metalloproteases (ADAMs), ADAMs with thrombospondin motifs (ADAMTs) and cathepsin G and elastase.[70] Those enzymes allow for the deposition of fresh ECM proteins by the cells by degrading the existing ECM proteins. Misfunction of those regulators leads to diseases like fibrosis or cancer, as described in Chapter 1.4.1 Fibrosis and 1.4.2 Cancer, respectively.[71] Furthermore, enzymatic activity is crucial to sustain tissue functionality. By changing tissue architecture, converting structural ECM proteins to signaling molecules and activating dormant proteins through changes of their conformation, the ECM is under constant change. Those cues are necessary to maintain cell proliferation and survival.[72] MMPs are constantly expressed by the cells and embedded inside the ECM, waiting to be activated. 23 different MMPs exist, each of them have their own tasks.[70] Some MMPs are only needed to cleave pro-domains of other MMPs in order to activate them, while others are degrading ECM molecules. Specifically, tumstatin derives from the non-collagenous (NCl) domain of collagen type IV after cleavage of collagen type IV with MMPs. In turn, tumstatin is recognized by integrins on the cell surface, inducing a signaling cascade to disrupt the actin cytoskeleton and leading to cell apoptosis.[72] ADAMs and ADAMTs, are zinc-dependent metalloproteases, which are either transmembrane or secretion proteins, respectively. They are involved in the activation of cell surface receptors and growth factors and the cleavage of ECM proteins.[72,73] Additionally, to enzymatic remodeling, the ECM is also altered by cytokines, oxidative stress, mechanical stress and pressure. The Smad signaling pathway is needed for the activation of fibrillar collagen genes, and it was shown that transforming growth factor (TGF-β) is a downstream target of this signaling pathway.[17,74,75] The ECM can also store cytokines or growth factors, released by

cells, to establish concentration gradients and impact the bioavailability. TGF-β, for example, is sequestered in the ECM in its latent form until proteolysis by MMPs activates the protein. Once activated, TGF-β regulates ECM-related genes which induce the deposition of ECM proteins.[69-72,76]

1.3.2 Cell anchorage to the ECM

In order for the cell to react to changes coming from the ECM it needs to be linked to the matrix tightly.[77] Many proteins are taking over this role to ensure signal transduction which ultimately impacts cell function. The main cell-ECM linkage is built up by integrins.[11] Those proteins are anchoring the ECM to cells by binding to the actin cytoskeleton via integrin-actin linker proteins. Integrins have very special conformations, which are changed upon binding to the ECM. Those transmembrane proteins are transporting mechanical signals from the ECM to the cytoplasm and *vice versa*.[78] Figure 13 shows the structure of integrins, which are heterodimers consisting of α- and β- subunits.[79] Those subunits are composed roughly in several large extracellular-ligand binding domains (Figure 10a (a and b), a transmembrane domain and a cytoplasmic tail (Figure 10). In an inactive stage the integrin homodimer is bent and the transmembrane domain and the cytoplasmic tail are close to each other (Figure 10a). Upon intrinsic ligand activation (inside out), by for example talin or kindlins, a separation of the transmembrane and the cytoploasmic domain is initiated, which leads to the extension of the extracellular domains of integrin.[79,80] Inside-out signaling is important for the cell body to react to external cues such as injuries or inflammation. Cells are in constant proximity to various ligands, but binding of such ligands is only initiated after the activation of integrins from the inside. Extracellular ligands can bind to integrin in this extended conformation (Figure 10b).[78-80]

Outside-in signaling is triggered when extrinsic ligands, such as collagen, fibronectin or laminin, bind to the extracellular domains of integrins. This binding leads to the formation of focal adhesion (FA) complexes (Figure 10c). This complex consists of 150 different intracellular proteins and serves as the center for

intracellular transmission signals. Further, FA complexes are not static protein clusters. The proteins involved in FAs constantly associate and dissociate, depending on the signaling cues from the cell and its surrounding. Those signals are crucial for cell survival since the activated signaling cascades have an impact on cell proliferation, motility and migration. [11,77-80]

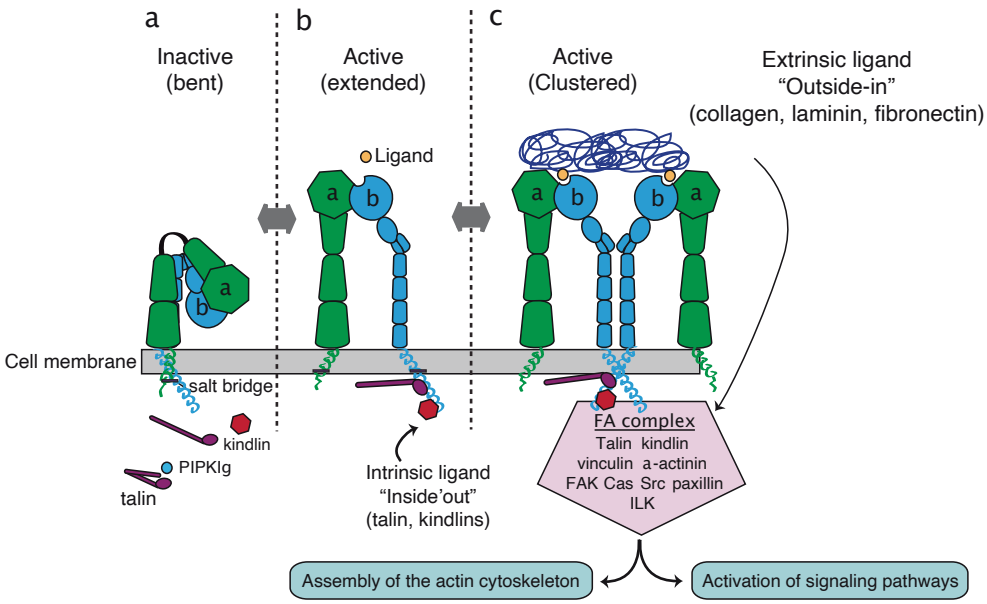

Figure 10 Overview of inside-out and outside-in integrin signaling.
a) Integrins are bent in an inactive form. b) Talins and kindlins bind from the inside to the cytoplasmic tail of integrins and trigger the activation. This leads to the extension of the protein. This mechanism is called inside-out triggering. c) Once integrins are activated they can transduce signal from the outside to the inside of the cells, by binding different ECM proteins. This leads to the assembly of focal adhesion (FA) complexes, which are important for the assembly of the actin cytoskeleton and the activation of various signaling pathways, leading to cell migration or proliferation. Figure adapted from Srichai et al., 2010.[79]

Cell migration in the extracellular matrix is based on the interplay between cell surface integrins and integrin-binding motifs on the ECM proteins. The most prominent amino acid sequence for cells to bind to is Arg-Gly-Asp (RGD). In order for a cell to start migrating, tight contacts to the surrounding ECM are established. Further, several internal changes are triggered in order for the cell to move in a specific direction (Figure 11).[81] First, the polymerization of globular (G-) actin into filamentous (F-) actin defines the leading edge of the cell (Figure 11A).[82] Further, new adhesions are generated in the membrane protrusions and establish a linkage between the underlying surface and the intracellular actin network. This new

adhesion serves as strong traction sites to the surface. Myosin II supports this movement by contracting the actin cytoskeleton (Figure 11B).[83] Finally, the combination of intracellular forces and actin movement generates the needed tension for the cell to pull its body and nucleus forward. The focal adhesions and actin filaments are disassembled at the rear end (Figure 11C).[25,84] The fact that cells can interact with their surrounding and modify the actin cytoskeleton upon ECM interaction, led to the proposal that the ECM does not only serve as anchoring points for cells inside tissues, but furthermore provides guidance for the migration of cells.[81] Lo *et al.*[85] showed that cells actively migrate from soft to stiff matrices by a gradient in ECM rigidity. The field of durotaxis (Latin: *durus;* hard, Greek: *taxis*; arrangement) was born.[81,86]

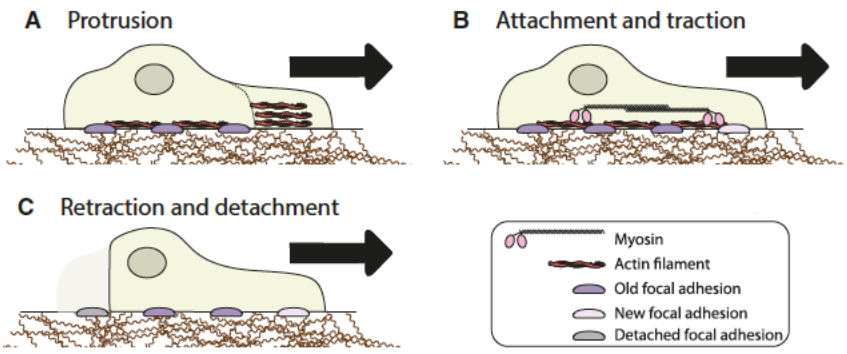

Figure 11 Intracellular changes during cell motility.
A) Protrusion is facilitated by rearrangement of the actin cytoskeleton. B) Attachment and traction are fueled by myosin which contracts the actin cytoskeleton. C) The cell fully moves by dissembling focal adhesions and retraction of the rear end. Figure reused from Shellard and Mayor, 2021.[81]

1.3.3 Mechanotransduction

The term "mechanotransduction" comes from mechanochemical transduction, which describes the conversion of mechanical signals into chemical signals. Not much is known about the exact mechanism behind this conversion of signals, however, many studies demonstrate the central role of the extracellular matrix and its stiffness around the cell.[87] The main molecule bearing the signals between cells and their surrounding ECM is integrin. This transmembrane protein mediates the adhesion of cells to the ECM and regulates the sensing between the actomyosin cytoskeleton and ECM proteins.[15] By binding the cells to the ECM, integrin initiates cell spreading, growth and proliferation, by further recruiting additional proteins.[88] The chemical signaling of integrin is based on the exchange of Na^+/H^+ ions and the control of pH, while the mechanical input comes distinctly from the interaction of this protein with focal adhesions of the cell.[13] By anchoring the cell to the ECM mechanical signals are transmitted to the inside. This specific interaction happens by integrins which are transporting information over two ways: outside-in and inside-out. The molecules are undergoing different conformations in order to signal changes towards the cell (outside-in) or the ECM (inside-out) as explained in the previous chapter.[78]

Integrin binds actin over linker proteins such as talin, vinculin, integrin-linked protein kinase (ILK), filamin and parvin (Figure 12) and initiates different pathways inside the cells.[15] Those signaling components are called mechanotransducer.[89] The most prominent signaling pathways are RHO-family small GTPases and mitogen-activated protein kinases (MAPK) with their downstream effectors.[15] Those pathways actively rearrange the actin cytoskeleton and strengthen focal adhesion assembly upon binding to ECM proteins via integrin molecules and initiate cell migration.[87] Changes in the stiffness of the ECM are immediately communicated to the cell, and further transported to the nucleus via those signaling pathways.[13,25,88]

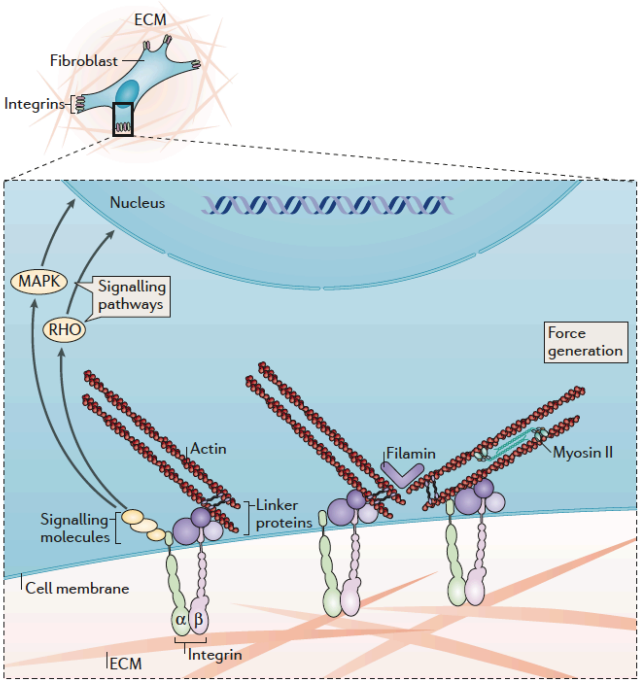

Figure 12 Signaling components between cells and their surrounding ECM.
Integrins are connected to the actomyosin cytoskeleton via various linker proteins such as talin, vinculin, parvin and filamin. Upon integrin activation signaling pathways such as RHO and mitogen-activated protein kinase (MAPK) are stimulated. Figure adapted from Humphrey et al. 2014.[15]

Studies are showing that altering the stiffness of the ECM, leads to major behavioral changes of the cell. Cells noticeably prefer stiffer substrates, based on the increased spreading morphology and assembly of larger focal adhesions than on soft matrices.[68,90,91] A stiffer substrate is not only improving cell adhesion and migration, but it also has tremendous effects on cell fate and gene expression. Mesenchymal stem cells could be directed towards special lineages just by changing the stiffness.[73] Here, the major signaling pathway being in charge of cytoskeletal re-organization and gene expression upon alterations of ECM stiffness is the Hippo pathway with its prominent YAP/TAZ proteins.[92] It was shown that this particular pathway play an important role in cell shape and elasticity. Ultimately, activated YAP/TAZ protein impact the cell cycle[93], differentiation[94] and even the regulation of transcription proteins.[95] The importance of well crosslinked and stiff ECM becomes clear when observing cells on compliant ECM. There, spreading of cells is impaired, which leads to cell death of anchorage-dependent cells.[96-98]

1.4 ECM roles in the function of diseases

The importance of the ECM becomes clear when having a look at diseases and syndromes throughout the body. Already small abnormalities in the genetic information of proteins or cells can lead from minor to severe malfunctions of the affected tissue.[99] The fact that the final shape of the tissue is already formed during development and fully dependent on the communication and interplay of cellular components with their surrounding protein microenvironment, makes it prone to mismatches.[100] If misfolded proteins are involved in the homeostasis of tissues, cancer, fibrosis, osteoarthritis and other severe diseases are the consequences.[3,101]

1.4.1 Fibrosis

Fibrosis is the result of occurring abnormalities during wound healing. This disease is affecting millions of peoples worldwide.[102] In order for a wound to heal properly, fibroblasts are attracted to the injured tissue over many different signaling molecules. When reaching their destination those cells differentiate into myofibroblasts and start synthesizing and secreting their own ECM molecule in order to close the wound.[103] In fibrosis, myofibroblasts are distorted and secrete uncontrollably stiff and disorganized ECM proteins, leading to the replacement of functional tissues and production of scars (Figure 13).[1] Those scars are stiff and non-functional sides of the skin. If occurring in lungs or hearts fibrosis can lead to organ failure.[1] The fibrotic tissue consists of untypical ECM proteins such as collagen type I, III and V fibrils. Those fibers are characteristic for disordered structures and enhanced cross-linking through the presence of lysyl oxidase (LOX). Another problem, next to stiff matrices, is that ECM signaling to cells is impaired, hence cells cannot react to the immense secretion of LOX and stiff matrix proteins to prevent the secretion.[104] Myofibroblasts are continuously receiving information from growth factors and cytokines, such as IL-4, IL-17, bone morphogenic protein (BMP) and TGFβ1, which are expressed at the site of tissue injury, leading to the progression of fibrosis. The main actuator is the interaction of the cells with TGFβ.[74] This molecule is differentiating various cells into myofibroblasts and suppressing

inflammation and epithelial cell growth, leading to immense growth of fibrotic tissue.[74,102-104] Currently, therapeutic options for fibrosis are very rare.[71] In the recent years, many studies on matrix metalloproteases (MMPs) and their effects on reducing ECM proteins was extensively studied and revealed their promising future as therapeutic options. By introducing macrophages to the site of disease, the release of MMPs is elevated and helps with the regression of the disease.[102] A different approach of treating fibrosis, is the down regulation of tissue specific cell integrins. It was shown that integrin $\alpha 2\beta 1$ and $\alpha v\beta 3$ are elevated in kidney fibrosis[105], while integrin subunit $\alpha 11$ is highly expressed in hepatic fibrosis.[106] Targeting those special integrins allows for the loss of cell-ECM contacts and leads to death of distorted cells. Fibrosis is currently not treatable but with the current methodologies there is the potential of reversing the disease to a certain extent.[102,107]

Figure 13 Malfunctioning tissue repair leading to fibrosis.
(1) Myofibroblasts are deregulated through constant stimuli via growth factors and cytokines from immune cells. Those signals force the differentiation of injury-activated fibroblasts to myofibroblasts. (2) Myofibroblasts are secreting overwhelming amounts of ECM proteins. (3) A scar is formed out of heterotypic ECM proteins, such as collagen type I, III and V, fibronectin fibrils and cross-linking enzymes such as lysyl oxidase. Figure adapted from Theocharis et al., 2019.[1]

1.4.2 Cancer

Cancerous tissue is defined by the loss of tissue organization and high numbers of transformed cells (Figure 14).[1] Due to genetic mutations and epigenetic factors, like the altered ECM structure, cells start transforming and becoming invasive.[99] The ECM is changed in that regard, that the matrix is stiffer and packed with inflammatory mediators, namely cytokines, ECM-degrading enzymes and growth factors.[108] The combination of growth factors enriched in the ECM and released by tumor cells leads to the differentiation of fibroblasts to cancer-associated fibroblasts (CAF). The main task of CAFs together with tumor cells is to secrete ECM remodeling enzymes such as matrix metalloproteinases (MMPs) and cathepsin to degrade the basement membrane and pave the way for the tumor cells into the underlying stroma to spread and invade the interstitial matrix.[109] For example, MMP-9 and MMP-2 are shown to be upregulated in colorectal cancer, to initiate the local degradation of tissue to support cancer cell growth and motility. Further, CAFs also remodel the ECM mechanically, by pulling, stretching and softening the basement membrane, which leads to enlarged gaps in the membrane through which tumor cells can migrate and escape into different tissues. If the clearance of the way is not sufficient enough and tumor cells remain at the primary tumor, CAFs can drag tumor cells out of the tumor mass by establishing contacts via N- and E-cadherins.[110] Next to the CAFs, ECM proteins also play crucial roles in the progression of cancer. Fibronectin fibrils regulate collagen I fibrillogenesis, which in turn activates the contractile phenotype of fibroblasts. Fibronectin fibrillogenesis helps cells to migrate, since the fibers are oriented anisotropic and by integrin-mediated adhesion the cancer cells can move directionally.[111] By secreting increased amounts of collagens, CAFs stiffen the matrix around the tumor cells. The collagen fibrils are aggregating and stiffening via LOX, which is also secreted by CAFs.[49,51] Extensive research has shown the elevated effects of stiff ECM on the hallmarks of cancer.[2] Cancer cell motility is directed by stiff matrix starting from the primary tumor growth to metastasis or colonization of cells at a secondary organ site (Figure 14).[108,112,113] By binding to the stiff surrounding FAK and vinculin assemble focal adhesion complexes which leads to the suppression of the tumor

suppressor PTEN (Phosphatase and tensin homolog) and p53-induced apoptosis.[2,114] After resisting cell death, the mutated cells induce angiogenesis, which was also shown to be supported by a stiff ECM environment. Based on the ability of the ECM acting as a reservoir for various growth factors, VEGF and fibroblast growth factor (FGF) are sequestered in the ECM. Stiffer surroundings show the upregulation of VEGFR2 receptors on cancer cell surfaces, which leads to higher levels of growth factors binding to the cancer cells and induce angiogenesis.[115] Finally, invasion and metastasis of the cells is facilitated by the elevated activity of Rho and Rac GTPases inside the cells upon integrin binding, which promotes actin assembly and induces migration.[116] To finally settle at a secondary tumor site, stiff ECM environment functions as anchoring points for cells which are undergoing EMT with the help of TGF-β, which is secreted by infiltrating immune cells.[117,118] Tumor cells are making use of the availability of TGF-β and change their phenotype to basal-like cells to stimulate metastasis. Many other matricellular proteins, such as laminin, elastin or hyaluronic acid (HA) are impacting the ECM stiffness and promoting motility, metastasis and invasion of cancer cells.[1] Based on the major role of the ECM, various therapeutic strategies were invented to target specific ECM proteins.[119] Here, only very few options are described. The problem of a stiff tumor microenvironment (TME) is not only the increase in cancer cell migration, it also prevents drug molecules to reach the primary tumor site.[120] Specific therapies towards the degradation of the ECM were developed.[121] Therapies targeting TGF-β promise the inhibition of excessive collagen synthesis and allows for the present collagenases to degrade the ECM which contributes to an efficient drug delivery.[121,122] However, the usage of those targeted drug therapies is limited to the progression of the cancerous tissue. Tumors at elevated stages with existing collagen networks cannot be treated, since the collagen deposition is already developed.[119] In such cases, various therapies target the cells directly. Many studies have shown that by inhibiting adhesion of cancer cell-specific integrins, such as integrin $\alpha 11\beta 1$, $\alpha 5\beta 1$, $\alpha 9\beta 1$ and $\alpha v\beta 3$, to the ECM, tumor growth can be substantially limited.[107] Despite the vast amount of current therapeutic strategies, fighting cancer remains the biggest challenge to be resolved in the medical field of the 21st century.

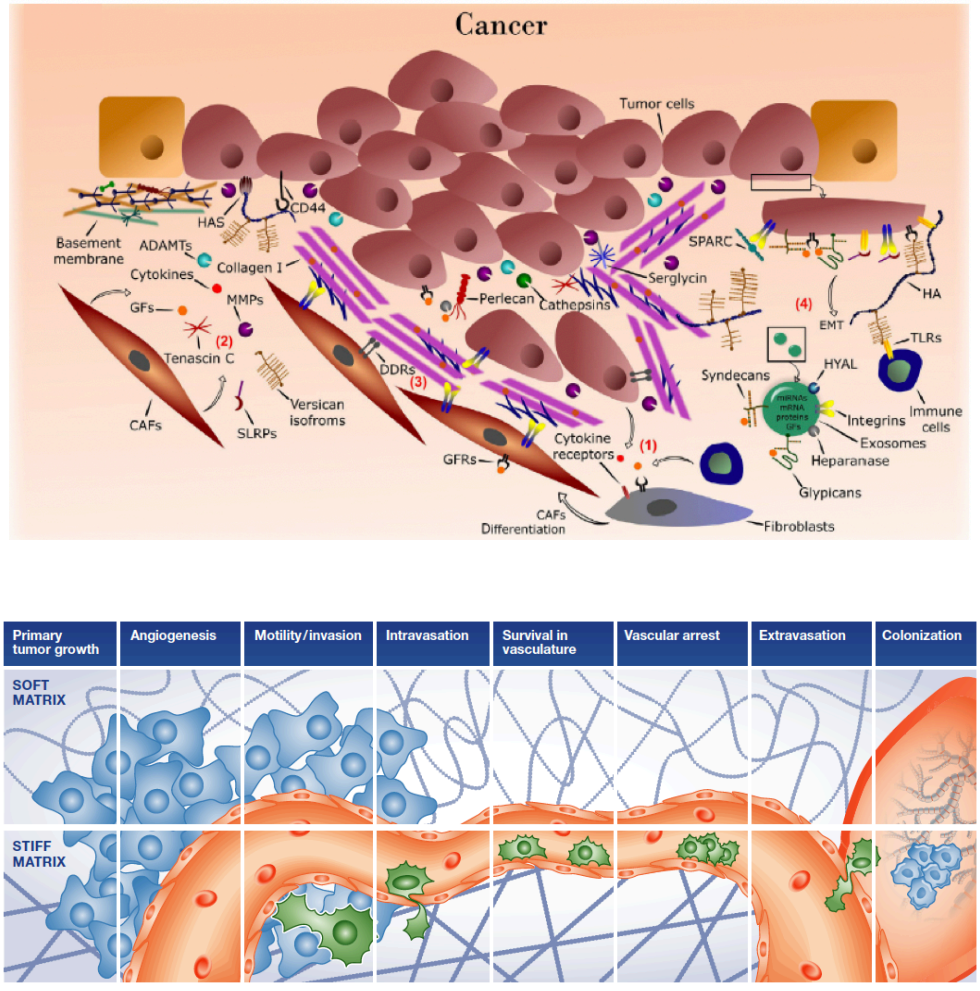

Figure 14 Influences of ECM on the Tumor growth and invasion.
<u>Upper Panel</u>. Cancer cells alter the basement membrane in order to escape the primary tumor and invade the stroma. 1) Fibroblasts differentiate into cancer-associated fibroblasts (CAFs) by the release of cytokines and growth factors from tumor and immune cells in proximity. 2) Matrix-degrading enzymes, growth factors and other molecules are released by the CAFs to facilitate tumor cell growth and migration. 3) A stiff collagen I network is assembled, with which tumor cells interact via integrins and discoidin domain receptors (DDRs) to migrate along. 4) Tumor cells interact with their environment by using their cell surface receptors and releasing exosomes. The communication of cells via integrins, syndecans and Toll-like receptors (TLRs) lead to an aggressive phenotype of the cells, while the release of exosomes helps remodeling and degrading the surrounding ECM. Figure adapted from Theocharis et al., 2019[1] <u>Lower Panel.</u> Cancer cell metastasis influenced by ECM stiffness. The journey of a cancer cell to a second organ sites starts with the mutation into an invasive phenotype. By invading the bloodstream, surviving in the circulation followed by extravasation, the cells survive and grow at a new organ site. All those steps were shown to be regulated by ECM adhesion. Figure reused from Pickup et al., 2014[2]

1.5 Investigating Cell-ECM interactions in different dimensions

To investigate the behavior of cells in vivo, it is necessary to simplify culturing conditions and mimic specific observations in vitro first. This important was realized by researchers many years ago. Hence, the generation of fundamental experimental conditions are invented to investigate the behavior of cells in simplified surroundings. In this section I am focusing on the importance of cell cultures in 2D vs. 2.5D vs. 3D and elucidate the term "2.5D" in more details.

The main differences in cell investigation techniques are the cell-cell interactions, mechanical changes and nutrient access of cells. In order to mimic *in vivo* conditions, 3D techniques are established. Scientists soon started to lose the interest in 2D models and focused on the implementation and improvement of various gels and substances for the analysis of cells in 3D environments.[123-126] However, simple 2D systems can also help gaining crucial information of cell adhesion, proliferation and migration by altering substrate stiffness and coating. A study by Pineda *et al*.[127] showed that OCT4 in mouse embryonic stem cells (ESCs) was decreased in a 2D and 3D model, showing a loss of pluripotency. The interesting part, however, was that those cells showed a faster differentiation rate on collagen type I coated glass slides than in the corresponding 3D culture.[127] This example shows that 3D studies cannot completely replace 2D techniques, even though they deliver more information about the *in vivo* situation.

While going through literature, I realized that most of the studies claiming to alter cells in two dimensions only, are in fact investigating the behavior of cells in a 2.5D surrounding. With the emergence of different kinds of cell culture methodologies, it becomes crucial to state clear definitions for the various dimensional studies. Generally spoken, 2D cultures are restricted to the x-y plane and their movement is polarized in this specific plane. Cell-ECM studies are investigated from the basal side only (Figure 15A).[128] While for 3D studies, cells are embedded in e.g. hydrogels and are not given a polarity anymore. The can move freely in any dimension (Figure 15C).[125] Over the years a combination of 2D and 3D techniques was

invented, namely 2.5D *in vitro* conditions. Hereby, cells keep the x-y polarity and can migrate in specific directions, while simultaneously having contact to ECM molecules from their apical and basal side (Figure 15B).[129] Following these rules, any study conducted on surfaces with various surface topographies, such as microgrooves or micropillars[130] can be categorized as a 2.5D study. As the cells are allowed to migrate in any direction without any given polarity, it can be claimed as 3D, such as the encapsulation of cells in hydrogel beads.

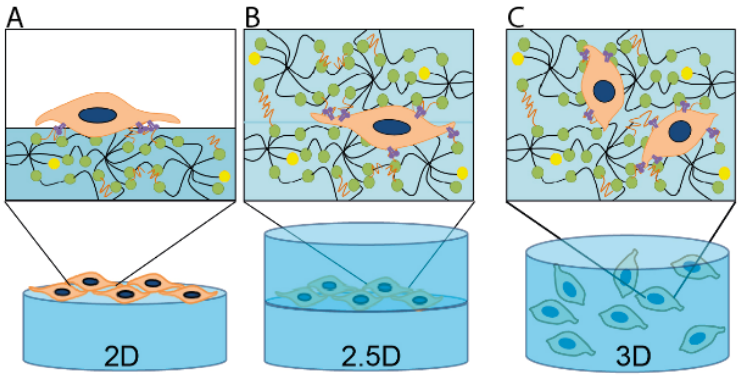

Figure 15 Comparison between 2D vs. 2.5D vs. 3D cell culture techniques.
A) 2D planar cell culturing. ECM interactions from the basal side only. B) 2.5D cell culturing technique by seeding cells in between two hydrogels. C) 3D in vitro technique. Cells are embedded in a hydrogel without any polarity. Figure adapted from Smithmeyer et al., 2019.[129]

1.5.1 2D Cell culture methods

The early beginnings of cell culturing methods based solely on the seeding of cells on simple plastic or glass surfaces. Over the years, researchers observed many limitations such as the failure of cells to adapt to the culturing conditions or the cells changed in morphology and polarity, started to proliferate extensively or even undergo apoptosis.[131] By coating substrates with extracellular matrix components those drawbacks were circumvented and reproducible and trustworthy 2D cell experiments could be conducted. Those studies allowed for many groundbreaking investigations such as the finding of a specific cell attachment region, namely the RGD sequence incorporated in fibronectin and laminin, which interacts directly with cells over integrin molecules.[132] Many revolutionary insights were given to us

by seeding cells simply on differently coated substrates. Establishing collagen gels showed the important role of this specific ECM protein in the development of organs. The differentiation, growth and plating efficiency of many cells are improved by this way.[133] Using those results, animal studies were conducted and could underline the effects observed in 2D *in vitro* culturing techniques. Transgenic mice strains inheriting damaged collagen processing mechanisms, resulted in the death of the embryos before Day 14.[134] Those results indicated the functional role of collagen during development and its importance in the structure of tissues.[131] The applications ranged from simple collagen films[43], gels or even floating gels[135] to complex matrices like pig skin[35], fibrin clots[136], bone powder[137] or liver biomatrices[138]. Based on all previous findings, nowadays new and more complex studies can be conducted in order to understand life in more details. According to the definitions set for 2D cultures defined in Chapter 1.5 Investigating Cell-ECM interactions, the only valid culturing technique broadly used these days is traction force microscopy. Thereby, cells are seeded on polyacrylamide (PAA) gels containing beads, with which the cells are interacting. After removal of the cells, the position of the beads remains the same and is analyzed to give information about the force exerted on the beads by the cells (Figure 16).[128]

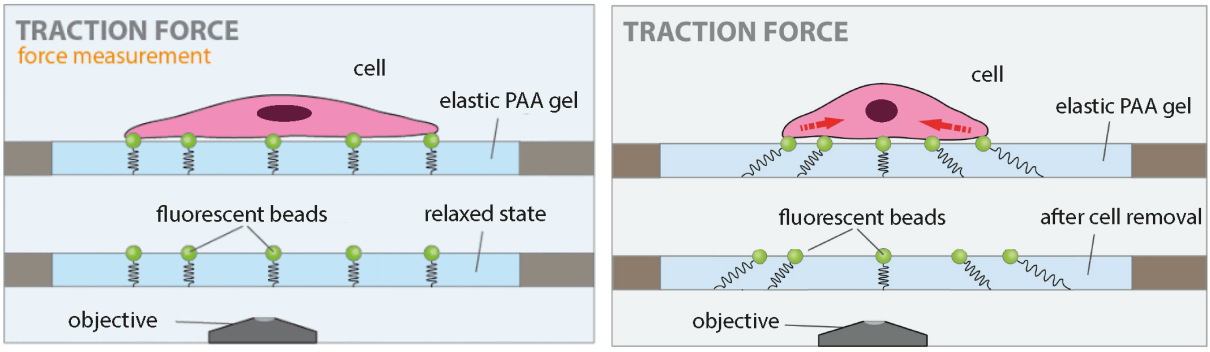

Figure 16 Basic principle of traction force microscopy.
Cells are seeded on bead-containing polyacrylamdide (PAA) gels and interact with the beads and displace them. After cell removal, the beads keep the deformed shape and the force exerted by the cells on the gel can be analyzed. Figure adapted from Menacher.[128]

1.5.2 2.5D Cell Culture Methods

The term "2.5D" describes studies, which are not fully encapsulating cells in 3D environments but culture cells on uneven substrates.[129] Most of the studies presented here are considered as 2D studies by the authors. Following the newly set definitions, those experimental set ups fall into the category of 2.5D studies. Here, mostly cells are seeded on differently shaped ECM coated substrates or sandwiched by another substrate containing ECM proteins.[139,140] 2.5D cell culture methods are used to understand the adhesion, growth and proliferation of cells, on different uneven substrates. In those conditions, cells have access to the same amounts of nutrients, which allows cell survival and additionally, simplifies the investigation of complex mechanisms. Further, to control cell shapes, analyze adhesion patters and alteration of bioactivities, scientists established microwells[130] and micro-patterned substrates such as cell-adhesive islands.[92] In the next chapters the current 2.5D culture methods and the importance of ECM-coated substrates are highlighted.

1.5.2.1 Micropatterning

Micropatterning is a broad and versatile field for studying the adhesion of cells to different substances[141], the migration on various stiffnesses[142] or even the interaction with biochemical molecules.[143] There are basically no limitations set to this technique. Mostly, islands-like chemical structures are created by various techniques, and coated by proteins to adhere to cells and are surrounded by a non-adhesive surface (Figure 17)[141], or the generation of fibronectin stripes allows for the alignment of cells.[144] Substrates for actin and paxillin are generated[145] or various polymers, such as poly(lactide-co-glycolide (PLG) are coated with ECM proteins to understand the movement of cells on rough and uneven surfaces.[146] Researchers, for example, seeded bone marrow stromal precursor cells on coated and non-coated poly-L-lactide (PLLA) surfaces and observed the differentiation into adipocytes and further the elevated lipid production compared to the non-coated surfaces.[147] Wan *et al.*[130], investigated OCT-1 osteoblast-like cell behavior on rough polystyrene (PS) pits and smooth PLLA islands and could show that cells rounded up on the PLLA substrates, while they stretched and formed single outgrowths on rough structures. These investigations lead to the understanding of cell filopodia and microspikes, which are crucial for cell migration and neurite outgrowth.[130]

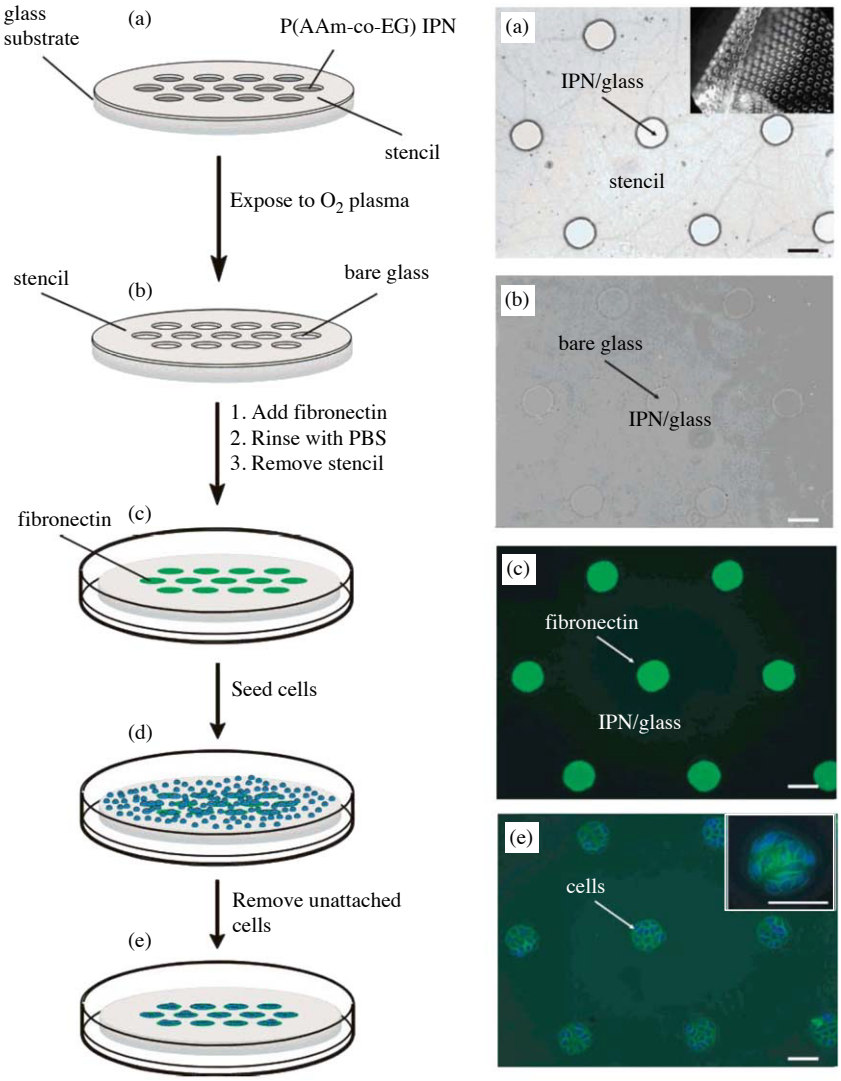

Figure 17 Schematic representation of cellular micropatterning.
a) PDMS stencils are placed on top of glass substrates. b) The stencil is used as a mask for the etching of the pattern by oxygen plasma. c)Before removal of the stencil, the glass substrates are coated with fibronectin and washed with PBS. d) Then, the stencil is removed and cells are seeded and allowed to attach to the fibronectin coated islands. e) Finally, unbound cells are removed and only cells on the islands can be observed. Figure reused from Tourovskaia et al., 2003.[141]

1.5.2.2 Sandwich culture methods

Implementing sandwich cell culturing method is the most common 2.5D technique. To not falsify experimental results by analyzing cells only on planar 2D surfaces only, a sandwich culture method was invented, which adds a layer of ECM on top of the cells. By mimicking the surrounding ECM in this way, the apical-basal polarity is removed and is not altering cell functions and behavior.[148-150] It mimics

the *in vivo* situation as close as possible, while still being in two dimensions. The sandwich culture is mostly used for culturing hepatocytes because they do not survive in traditional 2D cultures. For this method, cells are placed between two layers of polyacrylamide, collagen or ECM hydrogels. It was shown to be very effective for hepatocyte survival and especially for drug delivery purposes.[151] For example, the production of albumin of hepatocytes in sandwich cultures are comparable with the *in vivo* situation, whereas the albumin production rate on a one-gel system was decreased by ten-fold.[149] Furthermore, the bile canaliculi of hepatocytes are also well established, which are important for the study of drug uptake.[152] Figure 18 depicts the schematic sandwich technique with the bile canaliculus being established between two layers of cells. Hepatocytes are binding to the galactose moieties of galactosylated alginate (GA) over their asialoglyoprotein receptors (ASGPR). By the interaction of the cells to the sheets and simultaneously to other cells, survival is granted and further the bile canaliculi can be established.[138]

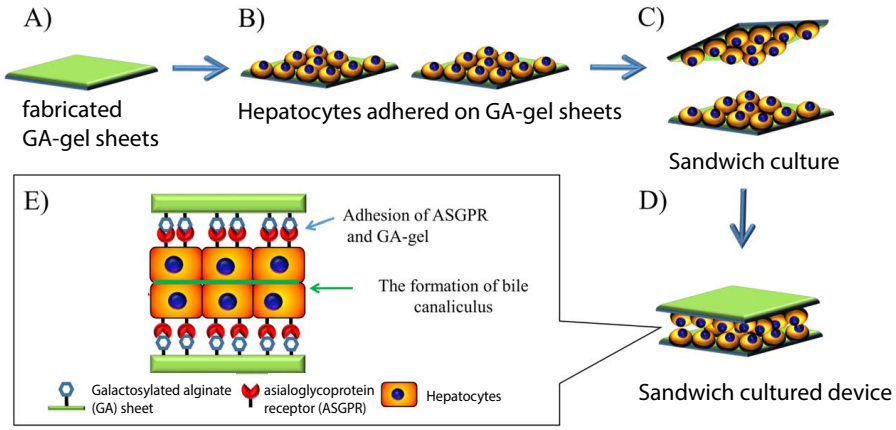

Figure 18 Sandwich cultured device production with hepatocytes.
Hepatocytes are loaded on GA-gel sheets, where they adhere via their ASPGR receptors to galactose of GA. Sheets are stacked with the cell-loaded side to establish sandwich cultures. Hepatocytes start forming bile canaliculus. Figure adapted from Arai et al. 2016.[138]

Many variants of this sandwich culturing technique exist. Mostly cells are seeded on ECM-containing hydrogels and are sandwiched by another hydrogel from the top.[140] In comparison to the study, described above, here only one layer of cells is used and the interaction to the ECM from its apical side is facilitated.[153]

By sandwiching cells between two gels, no limitations are set to the types of hydrogels used. Fischer *et al.*[154] seeded cells first on a polyacrylamide gel coated with ECM molecules, before they sandwiched the cells with a polymerized collagen gel (Figure 19).[154]

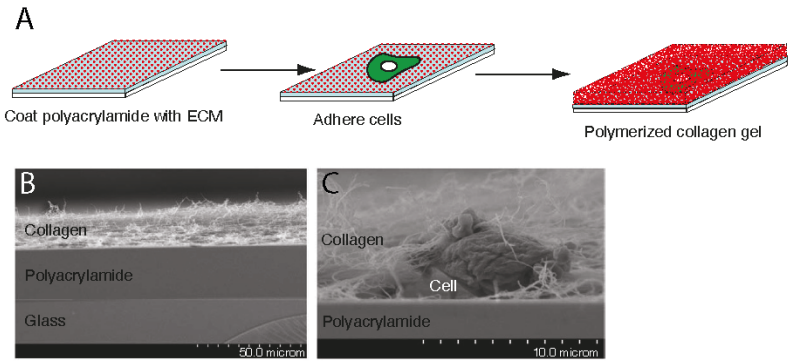

Figure 19 Sandwich culturing cells between two different gel types.

A) Cells seeded on ECM-coated polyacrylamide gels and covered with polymerized collagen gels. B) SEM image of cross sectioning of collagen and polyacrylamide gels on glass. C) SEM image of a single cell on polyacrylamide gels covered with collagen. Figure adapted from Fischer et al. [154]

1.5.3 3D Cell Culture Methods

For many decades, two-dimensional cell culture methods explained many different migration patterns and specific movements of the cells, being on a single cell level or as a collective. However, some characteristics of cells *in vivo* cannot be visualized and studied this way. Hence, many attempts were taken to overcome the limitations of 2D cell culture methods, which lead the way to 3D studies. By embedding cells in a gel or scaffold, the interactions between cells and their surrounding ECM or neighboring cells can be mimicked *in vitro*.[155] Figure 20 gives an overview of the advantages of 3D techniques over 2D culture systems. By introducing another dimension to cell studies the impact on cell differentiation, migration and proliferation was drastically improved.[124] Currently, several 3D techniques are present, but it always depends on the scientific question, whether a 3D approach is suitable.[124,126] Here, some 3D techniques will be discussed.

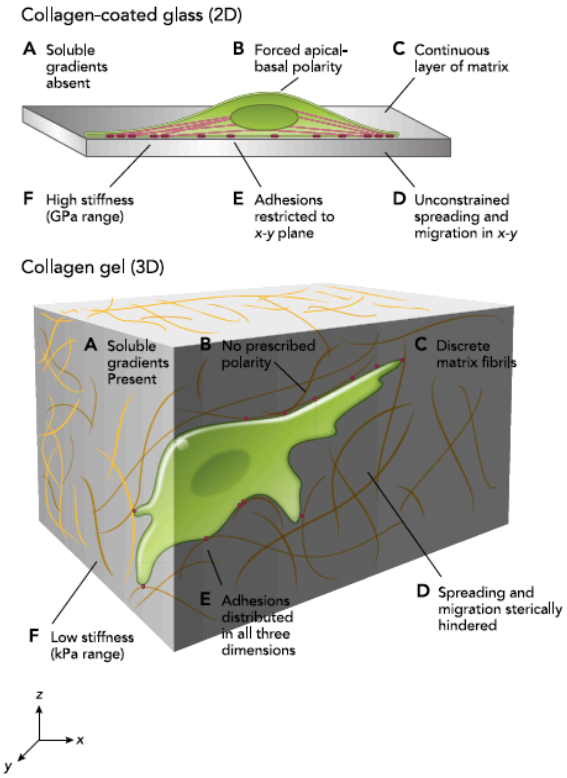

Figure 20 Cells seeded on collagen-coated glass (2D) in comparison to cells embedded in collagen gels (3D). 3D cultures mimic the in vivo situation better by allowing the cell to adhere in three dimensions, sterically hinder cell movement and let cells grow in lower stiffness areas. Figure adapted from Duval et al. [124]

1.5.3.1 Spheroid cultures

Producing spheroids became a large field, since they mimic tissues *in vitro* very well and can be utilized for many studies such as drug screening assays, for which they deliver reliable results. Further, it is possible to produce spheroids from patient-derived cells which further increases the values of those miniature tissues for biomedical research purposes.[156] Researchers are producing spheroids by the means of hanging-drop culture[157], microfluidics[158], embryonic bodies (EBs)[127] and many more (Figure 21). The beauty of all those systems is that an ECM-like surrounding can be introduced by adding e.g. Matrigel® to the growth media of the cells. To give precise examples, a very interesting study focuses on the differentiation of embryonic stem cells (ESCs) in two different 3D culturing methods[127]. Here, ESCs are grown as EBs in wither a collagen type I gel (GEL) or in parallel in low adhesion well plates. Interestingly, the GEL study showed to be less effective when it comes to the dynamic changes of the cytoskeleton compared to EBs generated in culture dishes.[127] Those results are underlying the statement that 3D cultures have to be chosen wisely when conducting experiments to resemble the *in vivo* situation. The most common spheroid technique is the hanging drop method (Figure 21B).[110] Here, cells are cultured in droplets containing cell culture media upside down. Those hanging drops are establishing a round bottom based on gravity. Cells can grow in close proximity and in constant contact to cell media. The main disadvantage of this method is the limited ability to change media of the spheroids. To overcome this issue, many other techniques were evolved such as the production of spheroids by using microfluidic channels (Figure 21F).[159] The spheroids are surrounded by media and a generated flow is ensuring a constant flow of fresh media. Many more different techniques were established in order to build the best environment for spheroids to grow in (Figure 21).[160]

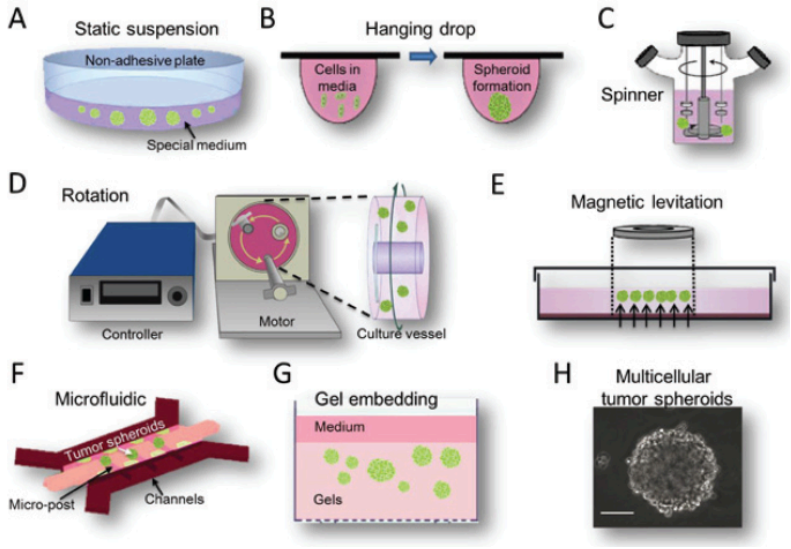

Figure 21 Various methods for the production of spheroids (A-G).
(H) The result of the depicted systems is a multicellular spheroid. Scale bar, 100 µm. Figure adapted from Lv et al. 2017 [160]

1.5.3.2 ECM protein-coated polymer scaffolds

Many different polymer scaffolds are coated with cells to function as tissue-like structures *in vitro*. The major advantage of those constructs is to deeply understand the effects of the ECM on cells and determination of their fate. The mostly used animal-derived biopolymers for this goal are collagen, gelatin, chondroitin sulfate and hyaluronic acid[161,162], while non-mammalian biopolymers such as alginate and chitosan are also fabricated into scaffolds.[163,164] The next step is to load those scaffolds with cells, were the major problem comes into play. This process often leads to low cell penetration and hence poor scaffold cellularization. To overcome this problem, building blocks-based scaffold formation was established.[123] Researchers want to aim for full control of scaffold porosity, mechanics and cellularization.[165] Since the focus of this study lays on the interaction of cells with ECM proteins, only polymer scaffolds coated with ECM proteins will be discussed further.

Ma *et al.*[166] produced polystyrene scaffolds by electro spinning fibers on glass plates. Afterwards, different laminin isoforms were used to coat the scaffold and establish a 3D ECM scaffolds for cells to attach to. U251, glioblastoma cells, were seeded onto those scaffolds and analyzed over time. This study revealed that the 3D scaffold

improved cell signaling in comparison to the 2D control. Other interesting studies are making use of PLGA scaffolds[82] coated with fibronectin or vinculin or polypropylene meshes[167,168], which are consecutively coated with collagen type IV. All those examples are highlighting the importance of cell studies conducted with close contact to an ECM in a three-dimensional set up.[124,160,169]

Another scaffold type which is coated and loaded with ECM-proteins are hydrogels. Those gels have various advantages. On the one hand, it is possible to tune the stiffness, simply by changing the hyaluronan content and crosslinking degree.[170] On the other hand, those hydrogels consist of collagen proteins and are loaded with cells on the inside to ensure ECM contact from all sides.[171] ECM hydrogels are promising *in vivo* tools because of their ability of embedding cells in an ECM environment with constant access to nutrients and other cells and they are injectable, without harming the contained cells.[172,173]

1.5.3.3 3D printing of encapsulated cells

The field of 3D bioprinting is increasing and offering many different possibilities to establish tissue-like structures *in vitro*. The three main 3D bioprinting technologies are inkjet/droplet bioprinting, extrusion-based bioprinting and laser-assisted bioprinting (Figure 22).[125]

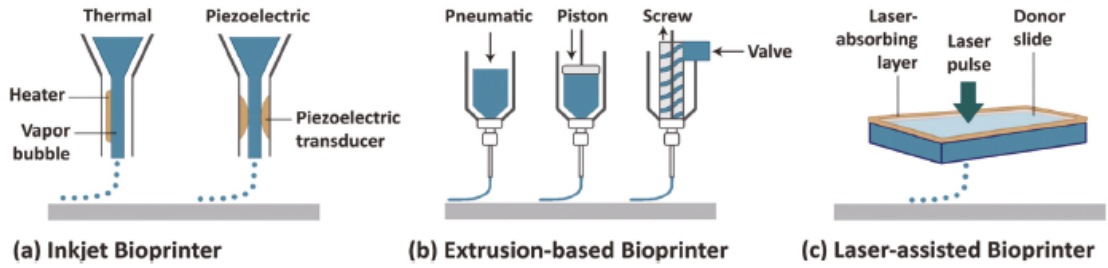

Figure 22 Schematic overview of the three main 3D bioprinting techniques.
a) Inkjet/droplet bioprinting, droplet ejection is based on thermal responses or piezoelectric triggers. b) Extrusion-based bioprinting, where the extrusion is controlled either over pneumatic or mechanical forces such as pistons or screws. c) Laser-assisted bioprinting releases a stream of droplets by focusing a laser beam onto a donor slide which forms a jet stream into the medium of choice. Figure adapted from Gungor-Ozkerim et al. 2018.[125]

Protein-based bioinks showed to be very promising when loading cells and stacking them to a tissue-like construct *in vitro*. The most common ECM protein for this purpose is collagen, because of its tissue-matching properties. Many different attempts based on loading cells in only collagen gels [35,151] or in combination with alginate [174-177] already exist but the majority of 3D bioprinting techniques stack cell-laden sheets on top of each other, rather than using cell-laden droplets. However, some droplet-based techniques exist, which are mostly produced by inkjet bioprinters. Jakab *et al.* [178] established a method by which they are using two different micropipettes, one loaded with Chinese hamster ovary (CHO) cells and the other containing collagen gel as the matrix material. First, collagen beds are established before cell aggregates are printed onto them. The aggregates started fusing over time and analysis showed minimal cell death.[178,179] The same research group mixed chicken cardiomyocytes with CHOs and human vascular endothelial cells and bioprinted those on collagen gel matrix containing vascular endothelial growth factor (VEGF). 90 h post-bioprinting synchronous beating was observed.[180] Another technique uses the ejection of cell-laden collagen droplets onto a collagen and agarose sheet which are further coated with a layer of collagen. This layering method is repeated twice to produce a tissue-like structure.[181] This technique has the advantage to introduce spacing between the cell layers, which mimics the 3D ECM more closely to the *in vivo* situation. Another, quite different approach from currently existing methods is the bioprinting set-up from Graham *et al.*[182] Here, the researchers are mixing cells in a hydrogel-based bioink and producing aqueous droplets stabilized by lipids in the oil layer (Figure 23A, B). The constructs are stable and are incorporating viable cells (Figure 23C). Further, it is possible to introduce another cell line in this construct, simple by changing the cell-laden bioink, and investigating the intercellular interactions. In order to use those constructs for further analysis it is necessary to remove the oil phase around, which was also shown to neither disturb the cell-laden construct nor cell viability (Figure 23D). This method provides a new tool for bottom-up tissue engineering.[182]

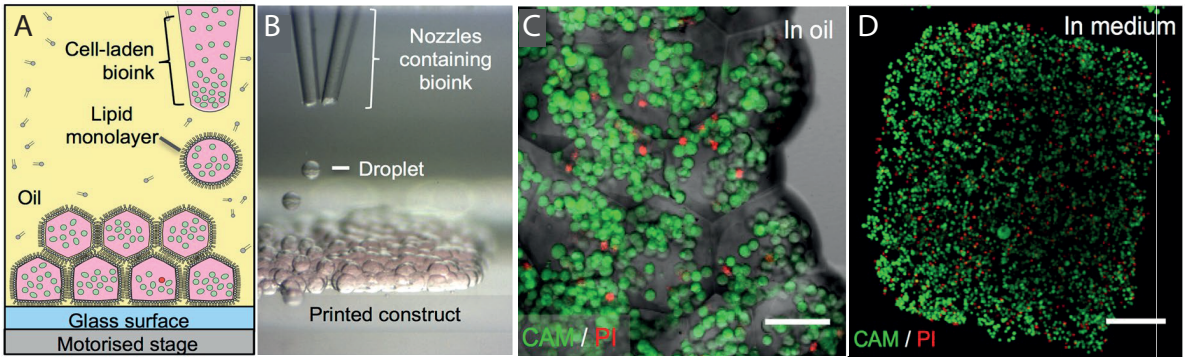

Figure 23 3D printing of HEK293T cells in oil droplets.
A) Schematic overview of cell printing by using a cell-laden bioink. The cells are dispersed into a lipid-containing oil, which form and stabilize the droplets upon ejection from the nozzle. B) Brightfield image of droplet production device containing cells. C) Fluorescence image of living (CAM) and dead (PI) cells inside the construct in oil. Scale bar, 75 µm. D) The construct is released out of oil into medium for better cell viability. Scale bar, 150 µm. Figure adapted from Graham et al., 2017.[182]

1.6 Cell microencapsulation strategies

Over the recent years the demand for encapsulation strategies ranging from small drug molecules to several cells increased. By encapsulating drugs it is ensured that the molecules reach their destination without harming the body or being captured and metabolized.[183] In this context many materials are used to produce polymer capsules[184], protein capsules[185] or a combination of both, polymer-protein capsules.[183,186,187] The advantages of those capsules do not end with just masking the content from the immune system of the recipient but further those capsules can be modified on the outside, yielding specific functionalities. Those functionalities can be f.e., specificity to a special target in order to trigger immune responses, enhance transport properties or even encode for a release switch mechanism to ensure targeted delivery.[188-190]

Another advantage coming from the research for drug delivery, is that researchers started using the materials which proved to be biocompability and effective, to encapsulate cells and bioprint them to establish tissue-like structures *in vitro*.[191] The next chapters focus on the encapsulation of cells inside various kinds of capsules. This technique is gaining more importance in the fields of biotechnology and medicine. The ability of implanting patient-derived cell clusters, grown in

biocompatible materials, can overcome several drawbacks such as graft rejection and increases the chances of treating many diseases.[192] With this aim in mind, many capsules based on biocompatible materials are established to support cell growth. The most challenging part in establishing capsules is to discover the perfect material. Many attributes need to be fulfilled that a material can be classified as a suitable foundation for capsules.[187,193-195] Additional to biocompatibility, the stability of a material is a very important aspect. If a material is too stable, encapsulated drugs cannot be released or cells can stay trapped without any access to nutrients.[196] On the other hand, if a material is weak and cannot form a capsules cells are escaping such a compartment or drug molecules cannot be retained and delivered to their final destination.[188,197,198] The most promising materials are proteins as well as natural and synthetic polymers. In the next chapters, some of the successful attempts to produce cell-laden capsules will be discussed.

1.6.1 Protein capsules

Literature is flooded by protein capsules based on alginate and bovine serum albumin (BSA).[199] Those proteins fulfill the most important aspects in order to function as strong foundations for capsules. Bovine serum albumin (BSA) or human serum albumin (HSA) has many advantages which is why it is used to establish protein capsules in various sizes.[187,200] Albumin is the most abundant protein in the body and additionally, has the ability to transport nutrient molecules due to its high number of binding sites. The structure of this protein and its availability allows for the building of protein capsules for various purposes ranging from drug delivery to cell encapsulation according to the size of the capsule.[185] Mertz *et al*.[196] were able to produce HSA capsules in the size of 5 µm in diameter, while Lu *et al.*[185] reported stable HSA microcapsules with a diameter of 100 µm. Those and many other microcapsules do not vary only in size but also in their production method. In order to produce hollow capsules researchers are either coating SiO_2 particles with layers of protein and re-functionalize the surface with bromoisobutyramide (BrIBAM) or isobutyramide (IBAM). Those chemicals are needed to stabilize the protein assemblies over hydrogen bonds. The final step is the removal of the particle after

successful polymerization of the protein with hydrofluoric acid (HF) (Figure 24A).[196] The resulting capsules are approximately 5 µm in diameter. Figure 24BI shows the BrIBAM-HSA coated SiO_2 particles with brightfield insets, while Figure 24BII shows the resulting capsules after template removal. Another approach is the pendant drop technique. Here, proteins are adsorbed to the interface of chloroform/water droplets produced at the tip of a capillary. After evaporation of the chloroform, stable protein capsules are produced (Figure 24C).[201] The droplets are stable in solution and their surface is covered in protein (Figure 24DI). Over time, the droplet dries at the air-oil interface (Figure 24DII) and the chloroform evaporates. This leads to folds in the membrane of the microcapsule (Figure 24DIII) and finally, a hollow and transparent microcapsule is produced (Figure 24DIV).[185] To bring a final example, the LbL (layer-by-Layer) technique is also broadly used to produce HSA capsules. An *et al.*[202] used the electrostatic assembly of HSA molecules and α-dimyristoyl-phosphatic acid (DMPA) to coat a melamine formaldehyde resin for several times. After core removal by HCl, lipid-protein microcapsules are established (Figure 24E). Figure 24FI shows the protein assembly around the template before removal, while Figure 24FII depicts the final product. So far, many capsules made out of HSA exist but mostly chemicals are involved in the polymerization of those microcapsules. [185,187,188,196,200,201]

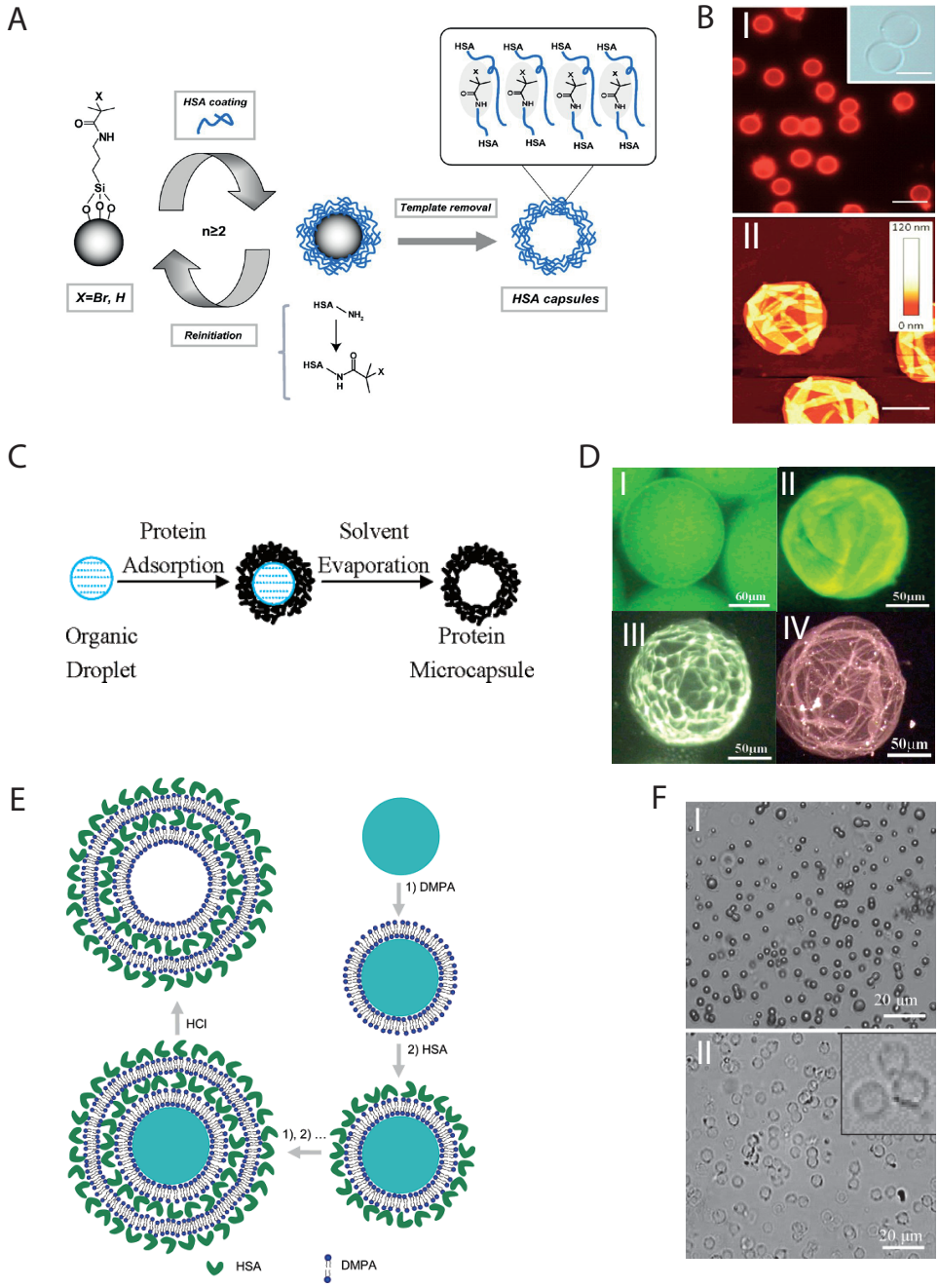

Figure 24 Different assembly approaches of human serum albumin (HSA)-based microcapsules.
A) SiO_2 beads are covered with several layers of HSA molecules and crosslinked with Br-IBAM. The template is removed by hydrofluoric acid. BI) Fluorescent image of HSA-coated SiO_2 beads, with a brightfield image as the inset. Scale bar, 5 µm. BII) AFM images of HSA capsules. Scale bar, 2 µm. C) HSA capsule formation by adsorption of proteins on an organic droplet and subsequent solvent evaporation. DI) Organic droplet with an HSA cover. DII) Drying process of droplet started. DIII) Folds on the surface are visible from the air- drying process. DIV) Final result is a hollow and transparent HSA capsule. E) Layer-by-Layer assembly of alternating layers of α-dimyristoyl-phosphatic acid (DMPA) and HSA on melamine formaldehyde resin. The template is removed by HCl. FI) Resin-coated HSA and DMPA droplets before template removal. FII) Resulting HSA-DMPA capsules. Figures adapted from Mertz et al.,2012[196] (A,B), Lu et al., 2004 [201] (C,D) and An et al.,2005 [202] (E,F).

Next to alginate and BSA/HSA capsules, microspheres made out of Laminin-biodritin[191,203] and GelMa[190] also exist. Those cell-laden droplets are mostly produced by ejection of protein-cell solutions into polymerization buffers. Hence, neither cell number nor size of the constructs are controlled.[190,203,204] Here, those proteins are mostly used in order to trap cells inside a filled gel and support cell growth and nutrient supply. The proteins are not only stable enough to keep the shape of the capsules but are also biocompatible and even biodegradable.[177] Encapsulating cells in alginate has an immense potential for implanting cells grown in such spheres.[184] Alginate beads serve as a cushion for the cells and provide them with nutrients through the porous structure of this protein.[174,198,205,206] Bochenek *et al*.[205] were able to produce alginate beads and load them with pancreatic islet cells and transplant them into macaques. With this method they could decrease the foreign-body-response and introduce cells without any immunosuppression.[205]

All in all, many protein capsules exist already, but the material is limited to HSA and alginate. They are fabricated with the goal for drug delivery purposes or are stabilized by different chemicals. If cells are encapsulated they are loaded into beads rather than hollow capsules and serve as transplantation applications.

1.6.2 Polymer capsules

To circumvent the challenges in protein capsule stability, researchers are making use of natural or synthetic polymers. The big advantage here is the ability to tune those polymers in regard of stability and functionalization. On the other hand, such polymers are mostly not biodegradable and can trigger immune reactions because of their missing biocompatibility. This can lead to severe consequences, such as graft rejection in case of cell microencapsulation. In order to prevent this issue, polymers with a low endotoxin level are used, which are considered to be biocompatible. [207] The choice of polymers to make capsules is large. Many polymers are suitable for this approach and researchers are able to establish an immense number of polymer capsules for small molecule transportation. The challenge still remains in finding a polymer mostly suitable for cell encapsulation strategies.

However, some polymers can be used for this approach. The most common ones are poly(styrene sulfonate) sodium salt (PSS)[208], poly-L-lysine (PLL)[209], and dextran[189], poly(N-isopropylacrylamide) (PNIPAM)[197], poly(meth) acrylic acid (PMA/PAA)[210,211], and many more.

In general, the methods for polymer capsule assembly are similar to the production of protein capsule assembly introduced in Chapter 1.6.1 Protein capsules and Figure 24. It can be roughly differentiated between, template-free and template-assisted methods. Self-assembly methods fall into the category of template-free assembly, while Layer-by-Layer (LbL) assembly methods of polymers are the most common template-assisted techniques.[212,213]

Several examples show the successful encapsulation of cells in various polymer capsules such as the microencapsulation of liver cells in (poly(d,l-lactide-co-glycolide (PLGA)/BSA capsules[214], encapsulation of pancreatic islet cells in poly (vinyl) alcohol (PVA) capsules[215] or beta-cells in chemically modified alginate capsules.[216] Those cell-laden polymer capsules contain several cells and are widely used for regenerative medicine[214] or studies to investigate insulin secretion *in vivo*.[215,216]

1.6.3 Crescent microgels

Another, rather new method of cell encapsulation techniques, is the production of crescent moon-shaped microparticles. Those particles are not completely enclosed but rather function as buckets to store and maintain cells. Currently, only a minority of researchers worldwide are investigating and producing this kind of microgels. To construct them, three different methods and materials are applied currently. Crescent particles consisting either of ethoxylated trimethylolpropane triacrylate (ETPTA)[217], polyactic acid (PLA)[218] or poly(ethylene glycol) diacrylate (PEGDA)[219-221] are produced for the moment (Figure 25). In order to produce ETPTA particles, fluorocarbon oil (FC- 77) and silica-ETPTA solutions are introduced into a glass capillary and droplets are produced by dripping the solution into surfactant-containing aqueous phase (Figure 25A). In order to obtain the special structure, the silica particles arrange at the water interface and are photopolymerized in place.

Finally, FC- 77 oil drops can be removed with ethanol (EtOH) and crescent shapes are visible (Figure 25B).[217] The second technique, is based on the collapse of a PLA shell.[218] Glass capillary devices are used to establish water-in-oil-in-water (W/O/W) emulsions (Figure 25C). Because of phase separation and solvent evaporation, the PLA shell collapses and Eudragit polymer-rich core-shell particles are established (Figure 25D). The last, and so far, mostly used method, is the production of crescent particles by using PEGDA.[221-223] Here, droplet-based microfluidics is used to generate aqueous two-phase droplets in hexadecane with non-polymerizable dextran and PEGDA mixed with lithium phenyl-2,4,6-trimethyl-benzoylphosphinate (LAP) in order to initiate photo-crosslinking (Figure 25E). After UV-polymerization of the PEGDA phase, dextran is washed away with EtOH and a crescent microgel is established. By changing the flow rates of dextran:PEGDA (Fd:Fp) the bucket size can be altered (Figure 25F).[221] Those PEGDA microgels are additionally loaded with cells and could serve as cell transporters[221] or collection buckets to quantify single-cell secretions.[219]

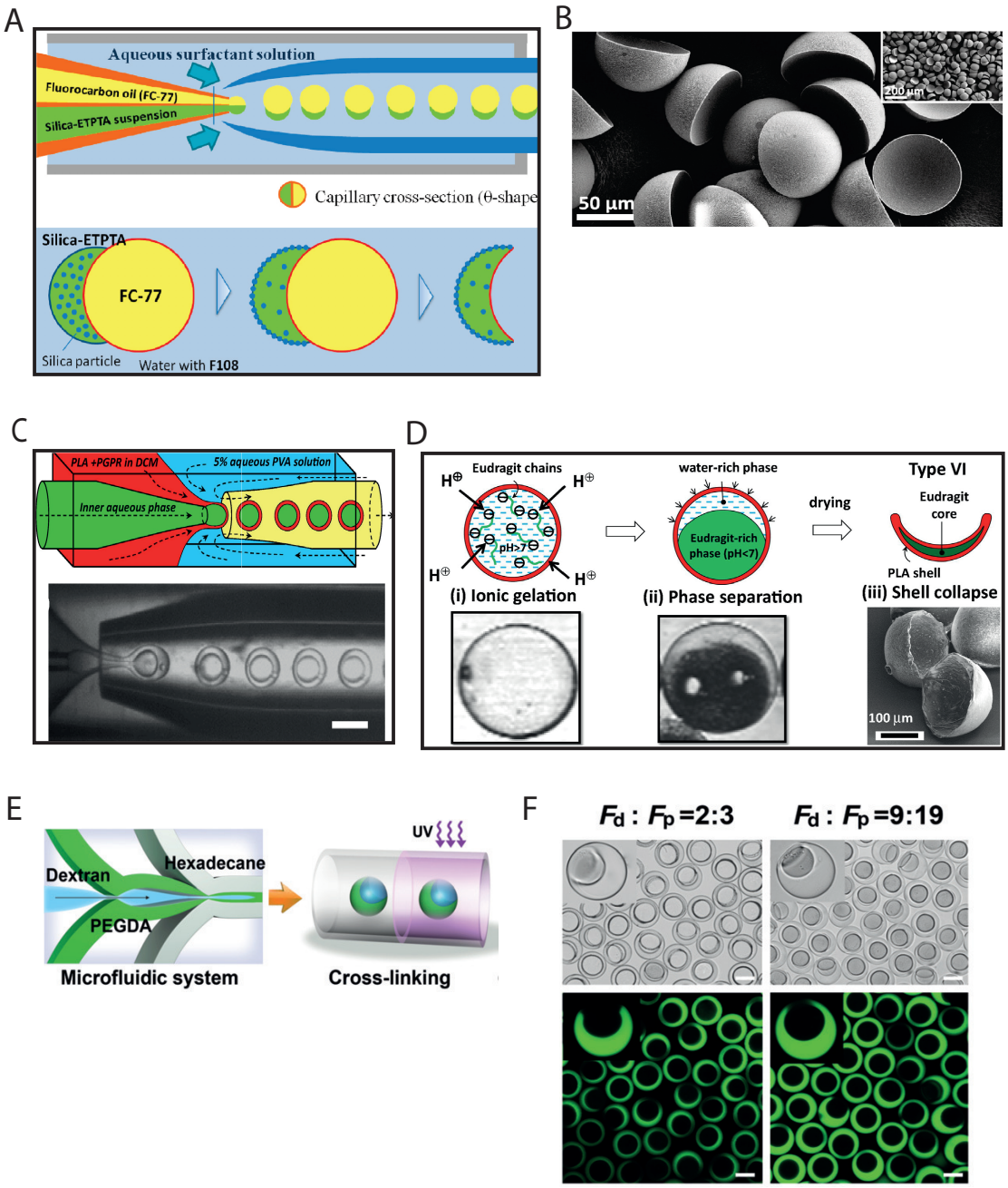

Figure 25 Overview of different crescent particles and their production techniques.
A) FC-77 and Silica-ETPTA droplets are produced by using glass capillaries. The silica particles arrange at the water phase and are photo-crosslinked in place. After removal of the FC-77 oil droplet, silica-ETPTA crescent particles are established. B) SEM image of silica-ETPTA crescent particles. C) Glass capillary system to produce W/O/W emulsions with an inner aqueous phase, a PLA shell and another aqueous phase containing PVA to stabilize the droplets in water. D) By evaporation of the water phase the PLA shell collapses and produced crescent shape particles with an eudragit-polymer core. E) A droplet-based microfluidic aqueous two-phase system (ATPS) device is used to produce dextran-PEGDA droplets in hexadecane. The PEGDA phase is crosslinked in flow via UV. F) PEGDA crescent particles after removal of dextran. By changing the production flowrates of dextran:PEGDA the bucket size of the particles can be altered. Figures adapted from Kim et al.[217] (A&B), Ekanem et al. [218] (C&D) and Liu et al. [221] (E&F).

1.7 Microfluidics

The focus of microfluidics lays on the down-scaling of (bio-) chemical reactions in the sense of volume and channel sizes to minimize processing times, study kinetics of several chemical reactions or biological properties.[224] Initially, microfluidics was used in four different fields: molecular analysis, molecular biology, microelectronics and biodefense.[225] First, this field started off with microanalytical methods such as high-pressure liquid chromatography (HPLC)[226] or gas-phase chromatography (GPC).[227] Microfluidics helped improving sensitivity and resolution of those techniques while decreasing sample sizes and hence costs. At this microscale level, cells and fluids are differently impacted by forces such as surface tension and capillary forces.[228,229] Those attributes are supporting several techniques by pumping fluids in microchannels[229], filtering various analytes[230] and forming monodisperse droplets.[231] Microfluidic technology started impacting biological experiments with the production of lab-on-a-chip devices.[232] Researchers are able to mimic the *in vivo* conditions of blood vessels[233] or even whole organs on such chips.[234] With the use of polydimethylsiloxane (PDMS) in combination with microfluidics, Whitesides *et al.*[225] invented for the first time a fast approach for the production of microfluidic devices. "Soft lithography" turned into the mostly adopted technique for fabricating microfluidic chips.[224,225] By this invention, the microfluidic field started growing and with it the numbers of available applications. Further, the mostly used field where microfluidic devices are finding use is in diagnostics.[230] Point-of-Care (POC) devices, such as glucometers or pregnancy tests, were the first ones to be established and are showing the advantages of this technique with user-friendly devices.[235] The possibilities for using microfluidic set-ups is immense and more techniques are being developed to date.[236]

1.7.1 Fluid Dynamics in Microfluidics

Fluid dynamics is a subdiscipline of fluid mechanics and describes the flow of fluids.[237] The understanding of the different fluidic behavior of fluids in microfluidic chips is crucial in order to correctly apply this powerful tool for various

applications.[228] In nature, turbulent flows are the dominant forces. In contrast to that, in microfluidic techniques laminar flows are generated and employed to the user's advantage.[228] Hereby, it becomes possible to establish fine-tuned gradients or parallel flows with little mixing.[238] The dynamics of fluids is determined by the Reynolds Number *Re*, which is defined as the ratio of inertial and viscous forces and is a non-dimensional number.[239] Depending on the magnitude of this number, the flow regime can be described. In order to calculate the *Re*, following equation is needed:

$$Re = \frac{\rho v l}{\eta}$$

To solve this equation, values for ρ the density, ν the velocity, l the characteristic length and η the dynamic viscosity are needed.[239] At high *Re* (>3000) the flow is unsteady and intrinsically chaotic which leads to turbulent flows (Figure 26A). In microfluidic channels the length (l) is small, hence low Re numbers (<<2000) are calculated and represent laminar flow regimes (Figure 26B).[229]

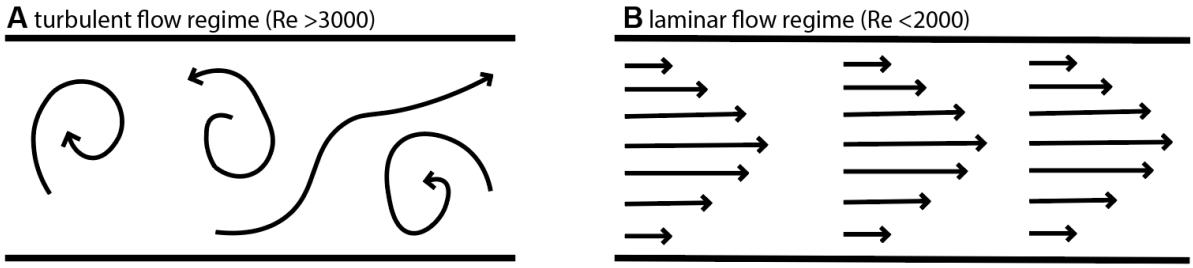

Figure 26 Turbulent and laminar flow regimes in microfluidic channels.
A) High Reynold numbers (Re) indicate a turbulent flow regime, which is unsteady and non-linear. B) Parallel streaming is occurring in laminar flows with low Re numbers.

Laminar flows are the dominant forces and produce parallel streamlines inside microfluidic channels until mixing is desired on chip. Since the fluids are miscible by nature, only the laminar flows allow for parallel streams without mixing. Upon application of a vertical flow with an immiscible fluid phase, such as an oil phase for the production of water-in-oil droplets or the incorporation of curved geometries on chip, the aqueous phases can be mixed.

1.7.2 Emulsions

Emulsions occur widely in food systems and play a crucial role in natural and processed food such as milk, ice cream or salad dressings. By using this rather simple technique it becomes feasible to modulate stability, texture, smell or even taste by fine-tuning physical and chemical characteristics of the emulsion.[231] In general, emulsions are mixtures of two immiscible fluids, where one liquid is dispersed into another liquid as droplets (Figure 27).[240] Mostly, oil is used as the continuous phase in which aqueous droplets are formed.[241] By applying enough energy to those two phases it is possible to homogenize the solution and produce an emulsion. However, without any stabilizing factors (emulsifiers), the emulsion becomes unstable and the phases separate again to minimize the contact between the oil and aqueous phases.[242] Emulsion instability includes phase inversion, where the initial continuous phase disperses into the aqueous phase (Figure 27-1).[243] When droplets produce grape-like structures because of attractive interactions beneath each other, it is called flocculation (Figure 27-2).[244] Gravitational forces can also lead to coalescence, since the droplets are aggregating and establishing a close contact to neighboring water droplets until the oil shell becomes too thin to stabilize the droplets in oil. This happens mostly when the difference in density between the continuous phase and the aqueous phase is large. This state of the droplets is called creaming (Figure 27-3).[245] Another instability process is the Ostwald ripening, where the bigger droplets coalesce with each other under the loss of smaller droplets in the same culture(Figure 27-4).[246] Mostly such instability mechanisms are elevated by temperature or physical forces such as centrifugation.[247] In order to stabilize such emulsions surfactants are mixed in the continuous layer.[248] The importance of those molecules is discussed in more detail in the next chapter.

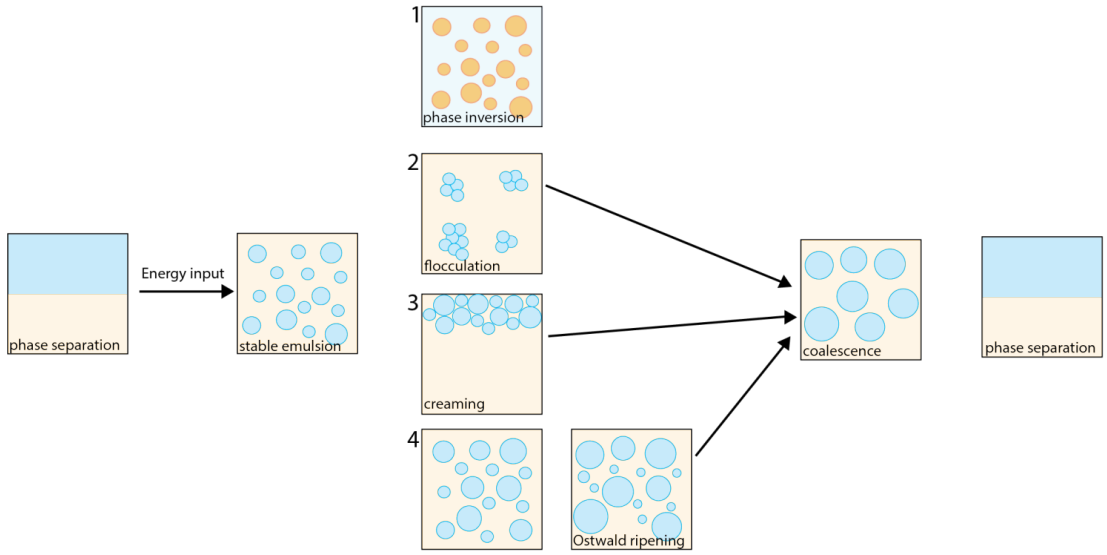

Figure 27 Schematic drawing of various instability mechanisms of water-in-oil emulsions.
Stable emulsions are established from two different immiscible phases by an energy input. As soon as the aging of the droplets start several conditions can occur. 1) Oil droplets are more favorable to establish in water, which might lead to a phase inversion. 2) Flocculation takes place if the attraction of the droplet towards each other is high. 3) Creaming happens in the case of different densities of the two phases. 4) Oswald ripening is triggered by differently sized droplets in one culture. Bigger droplets start coalescing under the dispense of smaller ones. All those mechanisms lead to coalescence of the droplets and finally, phase separation if the droplets are not stabilized well in the emulsion phase [231]

1.7.3 Surfactants

Surfactant are used to stabilize emulsions. Those molecules possess a hydrophobic tail and hydrophilic head and adsorb themselves at the interface of two phases, hence the name, surface-active agents.[249] Fluorinated oil is widely used in combination with microfluidic PDMS devices, to prevent the interaction of the device and conventional oils such as silicon or hydrocarbon oils.[250] In order to dissolve the stabilizing agents in this specific oil, fluorosurfactants are used to stabilize water-in-oil emulsions.[251] Furthermore, Perfluoropolyether (PFPE) is the surfactant of choice when it comes to their solubility and stabilizing properties of the long PFPE chains in fluorinated oil. By adding a PEG head group to such chains, non-specific adsorption of biological components to the inner periphery are prevented, based on the inert PEG head group.[248] In this thesis, I used differently charged PEG-based block copolymer fluorosurfactants to attract proteins to the

inner periphery. The most common and commercially available negatively charged fluorosurfactant is Krytox™ 157 FSH.[252] This molecule is based on a PEG-PFPE chain with a carboxylic head group attached to the PEG molecule, in order to establish a negative charge on the inside of such water-in-oil droplets.[252,253] From herein I will use the term Krytox™ when describing droplets, with a negatively charged inner layer.

PEG-PFPE are the most common block copolymers.[248,251,254] They are defined by the individual sequence of the components, which are connected to each other by covalent bonds.[255] A two component AB diblock copolymer is the simplest form of such block copolymers.[256] Depending on the final application, the choice of the surfactant becomes crucial. In order to establish stable water-in-oil emulsions a specific water/oil pair surfactant is needed.[248,251]

By the use of surfactants, it becomes feasible to stabilize water-in-oil droplets with various compounds, without the concern of coalescing droplets during longer incubation periods.[257] The interfacial tension is a very important physical concept, when aiming to stabilize two immiscible fluids as droplets in solution.[258] Surfactants are stabilizing droplets by thermodynamically decreasing the interfacial tension and hence their free energy, upon adsorption of the molecules to the interface.[259] The adsorption is mediated by the Gibbs free energy, which can be calculated by following equation:

$$\Gamma = -\frac{c}{RT}\frac{dy}{dc_b}$$

Here, Γ is the surface concentration, R is the gas constant, T is the temperature, y the surface tension and c_b the bulk concentration of the surfactant.[260] Following the equation, the amount of adsorbed surfactant molecules at the interface can be calculated, by the decrease of surface tension. It can be concluded that the chemical and physical properties of the surfactant, such as size of the head groups, or charges also affect the surface coverage.[261] Since charges of the surfactants play an important role in the context of this thesis, it is necessary to understand the underlying working mechanism. A densely packed surfactant layer with surfactants containing

a charged head group in the water phase cannot be established, since those molecules are affected by electrostatic repulsion.[262] However, upon the addition of counter ions it becomes possible to incorporate compact layers of surfactants and stabilize the droplets even further.[263]

Another very important factor in the stabilization of water-in-oil droplets is the critical micellar concentration (CMC).[248,264] This value gives information about the lowest concentration at which surfactants stay soluble.[265] Above that concentration, micelles are produced in the surrounding oil phase and interfere with the linear relation between surfactant concentration and interfacial tension.[266] Below that concentration, free surfactant monomers are available to constantly exchange at the droplet interface and stabilize the droplets in oil.[254] Typically, 4 µM are indicated as a CMC for fluorosurfactants to stabilize water-in-oil droplets.[243]

1.7.4 Physical properties of droplet stabilization

In the field of microfluidics, surface tension plays a crucial role. It describes the contraction of the surface-air interface of a fluid in order to reduce its free tension.[267] In the case of two immiscible fluids, such as water and oil, interfacial tension takes over a similar role as surface tension.[236] In order to reduce the free energy, many surfactant molecules are arranging at the oil-water interface and stabilizing the droplets in the emulsion.[268] Without the stabilizing effects of the block copolymers, the phases would separate again (Figure 27, Chapter 1.7.2 Emulsions).[269,270] Surface tension properties can be measured by using pendant drop. Hereby, the shape of a hanging oil droplet is measured, which depends on gravity and the interfacial tension (Figure 28). Briefly, the more elongated the droplet, the lower the surface tension.[271] The theory behind those measurements are based on the Young-Laplace equation.[270] The Laplace pressure through an interface with the according curvature and the interfacial tension γ are taken into consideration:

$$\gamma\left(\frac{1}{R}+\frac{1}{R_2}\right) = \Delta P \equiv \Delta P_0 - \Delta\rho g z$$

R_1 and R_2 represent the radii and the Laplace pressure is described by $\Delta P \equiv P_{in} - P_{out}$, with $\Delta\rho = \rho_d - \rho$ being the difference in density between the density of the drop phase ρ_d and the continuous phase ρ. To finally obtain the interfacial tension values the bond number, Bo has to be calculated:

$$Bo = \frac{\Delta\rho g R_0^2}{\gamma}$$

This dimensionless value allows for the calculation of the interfacial tension by the shape of the pendant drop.

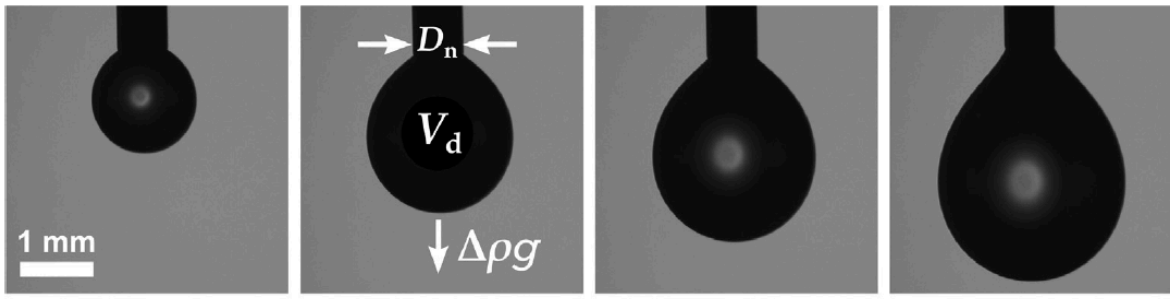

Figure 28 Interfacial tension measurements with pendant drop tensiometry.
D_n: diameter of the needle, V_d: Volume of the droplet, $\Delta\rho g$; density difference times the gravitational force.
Figure adapted from Berry et al., 2015.[270]

Once the surfactant molecules are added into the continuous oil phase of the emulsion, they adsorb to the interface and stabilize the droplet. The coverage of the interface is described by the adsorption kinetics of the surfactant molecules *per se*.[272,273] For the surfactant molecules to reach the interface, they have to overcome a specific adsorption depth h. The depth can be calculated by taking the maximum surface concentration of surfactants in equilibrium Γ_{eq} and the bulk concentration C_∞ into consideration.

$$h = \Gamma_{eq}/C_\infty$$

Knowing the adsorption depth h, allows for the calculation of the diffusion time of molecules to the interface of a sphere.[274] In general, the time for surfactants

molecules to assemble at round interfaces is faster than for planar surfaces.[263] The adsorption time to planar surfaces is quantified with following equation:

$$\tau_{2D} = h^2/D$$

In comparison to planar surfaces, the diffusion time $\tau_{D_{sphere}}$ for round surfaces is calculated the following:

$$\tau_{D_{sphere}} = hb/D$$

In both equations, D is the surfactant diffusivity and b the droplet radius.[272] The diffusion time depends also on the surfactant type, since the size of those molecules affects the diffusivity. To summarize, an interplay of various physical and chemical properties ensures droplet stability of emulsions. It is crucial to understand the importance of each single player in order to successfully establish stable water-in-oil or oil-in-water emulsions.

1.7.5 Droplet-based microfluidics

Droplet-based microfluidics is a subfield of microfluidics. Droplet-based microfluidics was established to simplify various reactions, e.g. the gelation of polymers without clogging the chips.[275] This technique is based on the separation of fluids into stable droplets in an oil phase. The major advantage of this technique is the establishment of small reactors with controllable sizes and contents.[254] Figure 29 shows the broad spectrum of droplet manipulation strategies, starting from simple manipulations such as mixing droplets with two different contents or encapsulating cells, to the pico-injection of various components or other fluids.[276,277] Based on this, microfluidic platforms for polymerase-chain reactions (PCR)[278,279], hybridization chain reaction (HCR) to sense miRNA[280] or droplet barcoding, which simplifies and upscales single-cell sequencing[281-284], and many more[229,275,285-287] were evolved. The compartmentalization of proteins, enzymes or DNA improves

reaction times of the substances and allows fast results. Another field, where droplet-based microfluidics is simplifying experiment outcomes and data interpretation is synthetic biology.[288] Researchers are mimicking tasks in simplified versions of cells and aiming for new knowledge about cell behavior.[289-291] Drug-screening platforms and drug-delivery technologies are currently also benefitting from droplet-based microfluidics and the establishment of several thousands of droplets with precise contents, high-throughput systems and a high reproducibility rate.[283,292] Finally, those established droplets can be further used for the generation of particles and microgels with the exact same size and functionalization by incorporating all needed components in droplets such as polymers, proteins or cells. To conclude, droplet-based microfluidics is a versatile tool for the production of microparticles such as polymerosomes[293], microgels[294] and colloid-filled granules[295] or allows high-throughput analysis tools such as PCRs and drug-screenings to yield fast outcomes.[224,277,296-299]

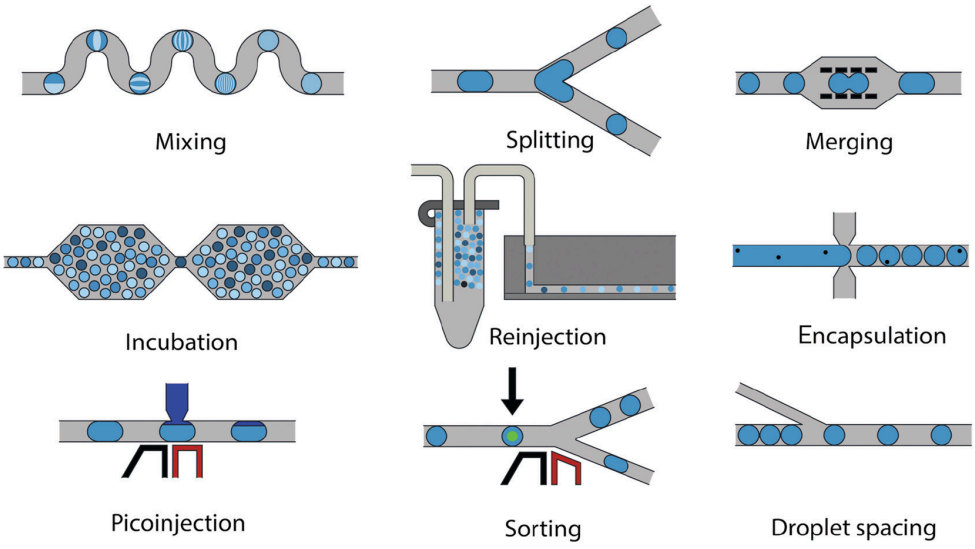

Figure 29 Various droplet manipulation techniques.

Stable droplets with two or more contents can be mixed after production. The purpose of a splitting device is to make many small droplets with the same content, while merging devices can fuse two droplets with different contents to one. Incubation chambers are holding droplets in place in order to polymerize or facilitate interactions of the contents on chip. Previously produced droplets can be reinjected into a device to be pico-injected with a different content or sorted by an electric field. Cells can be encapsulated on chip and by introducing another oil inlet the droplets can be separated from each other. Figure adapted from Suea-Ngam et al., 2019.[277]

Motivation

2 Motivation

Understanding the interaction of single cells inside dense extracellular matrix (ECM) layers is of utmost importance. The ECM has many functions, ranging from supporting cells in a tissue to inducing mechanotransduction through intracellular pathways in cells.[3] Analyzing the fundamental role of the ECM in healthy tissues leads further to a better comprehension of diseases induced by a malfunctioning ECM. [71]

Towards better understanding of 3D cell-ECM interactions several studies have been focusing on the design and development of 3D model systems, such as protein-containing hydrogels.[206] Analyzing cell behavior in three-dimensional ECM constructs allows for the resemblance of specific cell-ECM interaction occurring *in vivo*. In particular, current studies use human serum albumin (HSA) as a building block for microcapsules. The main advantage of HSA is stability in various pH and temperature environments as well as a straightforward polymerization process.[201,202] Even though this protein functions as a carrier protein for fatty acids and improves the wound healing of burn injuries, it is less significant for the induction of more complex cell behaviors such as migration, division or proliferation.[300] Next to HSA, various types of synthetic and natural polymers are used to establish capsules of various sizes.[175,194] Polymers have the advantage of ensuring high stability and facilitate straightforward assembly. However, so far most of the polymer capsules have been designed for drug delivery purposes.

To this date there are no studies that are concentrating on the design of cell-laden protein-based capsules for the advanced analysis of 3D cell-ECM interactions. The currently used production methods for protein microcapsules use harsh chemicals to remove the templates, which are coated with the polymerized proteins. Further, upon polymerization, no content can be introduced to the cavity of the microcapsules (Explained thoroughly in the introduction Chapter 1.6.2 Protein Capsules).

Hence, in this thesis my ultimate goal is to generate protein-based microcapsules that will allow for cellular-ECM interactions from multiple sides. To achieve this goal, I will implement the advantages of the modular droplet-based microfluidic technology for the production of two types of microcapsules: 1) Cell laden microcapsules consisting of ECM proteins, such as laminin-111, fibronectin or a laminin/collagen IV mixture (Figure 30B); 2) Microcapsules consisting of PEG-DA hydrogel and coated with different ECM proteins (Figure 30A). The used ECM proteins are laminin-111, fibronectin or a laminin/collagen IV mixture, which are found in all tissues of the body and play important roles in tissue homeostasis[5] as well as in diseases such as fibrosis or tumorigenesis.[1] The implemented ECM proteins will be chosen according to the type of cells and the type of tissue to be designed. For the production of ProCaps, I will aim to design and optimize the charge-mediated approach in which the polymer-stabilized water-in-oil droplets will be used as a charged scaffold for electrostatic attraction of proteins. Moreover, my additional goal will be to implement the modular microfluidic technology for the sequential loading of the developed capsules with cells. After encapsulation of cells and polymerization of the proteins inside water-in-oil droplets, the capsules will be released into physiological media.

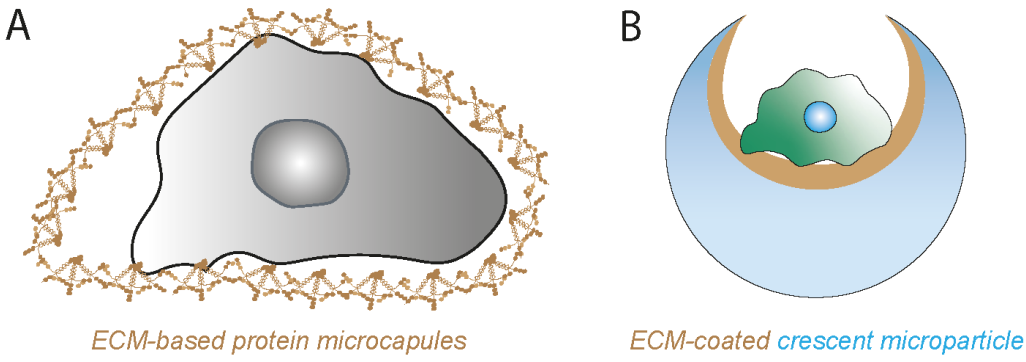

Figure 30 Schematic drawing of an extracellular matrix (ECM)-based microcapsule and ECM-coated PEGDA crescent microparticles.

A) Microcapsule consisting of ECM proteins and surrounding a single cell. B) PEGDA crescent microparticle coated by a layer of ECM proteins harboring single cells on a curved substrate.

The second part of this thesis focuses on the establishment of PEGDA crescent microparticles. Droplet-based microfluidics is used generate droplets, containing PEGDA and dextran with the ECM proteins. Next, the polymerized PEGDA particles are released and the non-polymerized dextran is safely removed. A layer of ECM proteins remains on the cavity of the particles and allows for cell-ECM interactions in a curved and semi-open environment (Figure 30B).

Both technologies are promising tools to study the behavior of single cells in tight yet differently shaped, confinements consisting of ECM proteins. Additionally, giving a three-dimensional curved environment from multiple sides might affect the interaction of the encapsulated cells with their protein surroundings.

Materials and Methods

3 Materials and Methods

In the following chapters I am going to discuss the used methods in order to generate protein-based microcapsules (ProCaps) and ECM-coated PEGDA crescent microparticles. First, I will give a general overview of the microfluidic tools and their preparation process, before I explain in more detail the specific use of each device. Further, the detailed protocols for each experiment performed are described.

3.1 Droplet-based microfluidics

Droplet-based microfluidics is a versatile tool and various device geometries can be implemented in order to produce and manipulate water-in-oil droplets. Depending on the encapsulation content and the final aim of the experiment, different devices are designed and employed. Here, I am focusing on the general aspects of device fabrication and handling. Specific flow rates and oil concentrations used in order to produce water-in-oil droplets will be discussed thoroughly in Chapter 3.6.

3.1.1 Microfluidic device fabrication

Microfluidic structures for each device are designed with the CAD software QCAD-pro (Ribbonsoft, Switzerland). All the channel sizes of the used devices are 30 µm in width and 30 µm in height if not stated otherwise. Laser lithography is the technique of choice in order to generate microfluidic devices. Silicon wafers (MicroChemicals, Germany) are covered with SU8-3025 negative photoresist (MicroChem, USA) and spin-coated (Laurell Technologies Corp., USA) at 2600 rpm to achieve a 30 µm high, uniform layer. After a soft bake (5 min at 65 °C and 15 min at 95 °C on a hot plate (IKA, C-MAG HS7)), the previously designed structure is exposed into the photoresist-coated wafer by using the Tabletop Micro Pattern Generator µPG 101 (Heidelberg Instruments, Germany) with 50 mW output laser

power and 20 % pixel-pulse duration. To harden the exposed regions the wafer is baked at 65 °C for 1 minute and for another 5 min at 95 °C. Afterwards the non-exposed photoresist is removed with mr-DEV 600 (MicroChemicals, Germany). Before soft lithography is performed the structure is harden at 150 °C for 15 min. Since the spin coating process is not yielding always the same height of the photoresist the actual height of the structures is measured with a DektakXT (Bruker). To produce microfluidic chips soft lithography is performed which is described elsewhere.[301] Briefly, PDMS (Polydimethylsiloxane, Sylgard 184, Dow Corning, USA) is prepared by mixing the oligomer with the polymerization catalyst in a 9:1 (w/w) ratio. The solution is poured over the silicon wafer, degassed in an exicator and cured for 2 h at 65 °C. A PDMS block with the structure is cut out, connection holes for the aqueous inlet is punched (Biopsy Punch, World Precision Instruments, USA) in 0.5 mm diameter, while 0.75 mm holes are punched for the oil phase inlet, electrode inlets and the droplet-collection outlet of for the PTFE-tubing (0.4 x 0.9 mm, or 0.3 x 0.6 mm Bola, Germany). As a final step the holes and the structures in the PDMS block are cleaned carefully with 70% EtOH and pressurized nitrogen gas and activated in an oxygen plasma (PVA TePla 100, PVA TePla, Germany; 0.48 mbar, 250 W, 30 sec) together with a coverslip (#1, Carl Roth, Germany, 24 x 60 mm) cleaned with Caro solution (Figure 31). The activated sides are bond to each other and left at 65 °C overnight. Directly before using the devices the micro channels are flushed with Sigmacote® (Sigma-Aldrich, Germany) to render it hydrophobic, and left for 5 min at 65 °C. Afterwards the devices are flushed with pure and filtered HFE-7500 oil and can be stored until further usage.

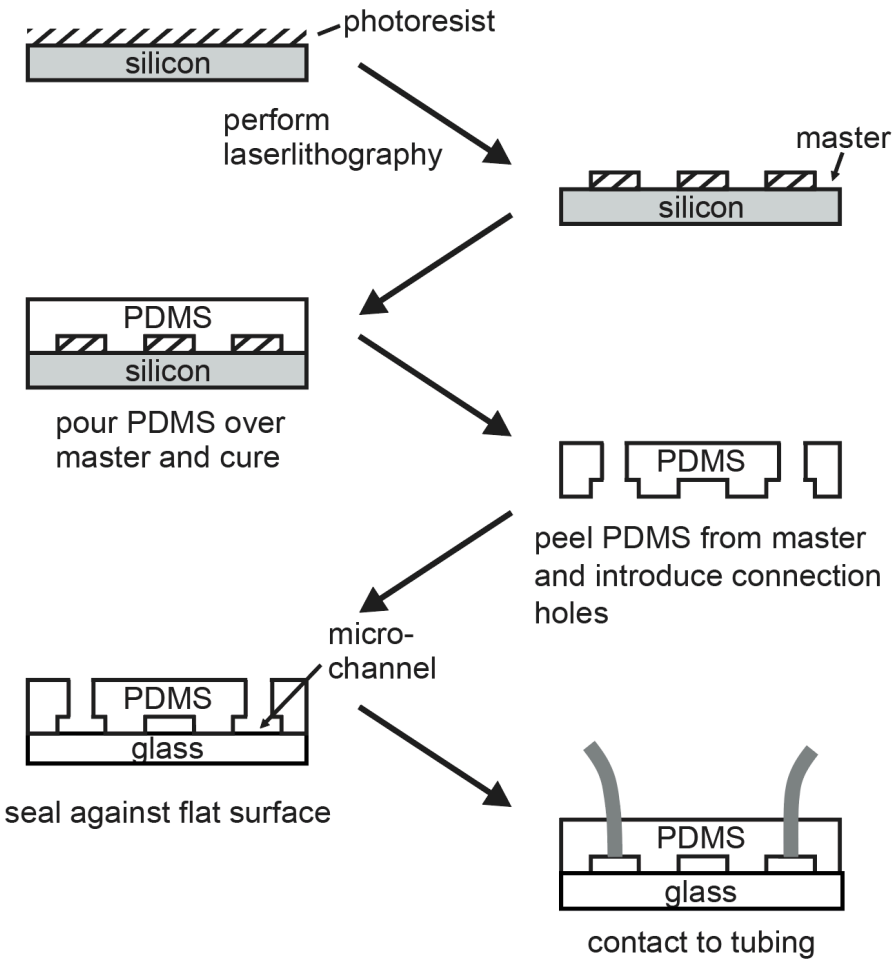

Figure 31 Production process of microfluidic devices.

First, a silicon wafer is spin-coated with the photoresist of choice. The design is lasered into the photoresist, which hardens the structure. The non-exposed regions are removed with a developer and the structure on the silicon wafer becomes visible. PDMS is poured over the structure and cured. Afterwards the connection holes are punched into the peeled PDMS structure and sealed against a glass. Finally, the tubings are attached. Figure adapted from Seemann et al., 2012.[301]

3.1.2 *Droplet production devices*

In order to produce water-in-oil droplets, various device geometries can be implemented. Here, a general overview of the used devices is given.

3.1.2.1 *Single inlet production device*

In order to establish simple water-in-oil droplets, it is necessary to use a production device with a flow-focusing junction (Figure 32). The used oil phase is coming from two sides of the junction, cutting off the protein mixture stream at the flow focusing junction (Figure 32, red square). The tubing with the oil phase is connected to the device over the oil inlet (Figure 32A), while the aqueous phase is connected to the inner inlet (Figure 32B). The produced droplets are collected over the outlet into an Eppendorf tube (Figure 32C). In order to establish 30 – 40 µm droplets in diameter, the flow rates are set to 600 µl/h for the oil phase and 300 µl/h for the aqueous phase.

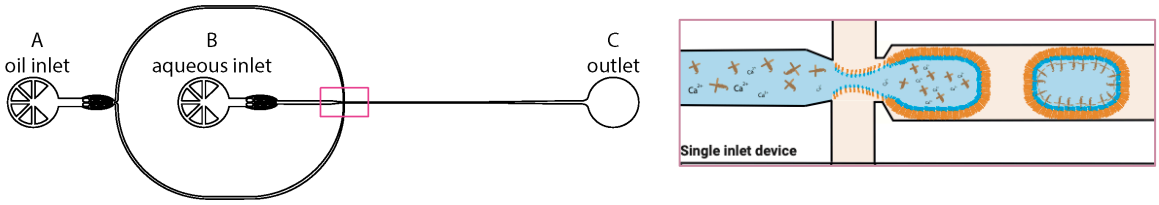

Figure 32 Schematic drawing of a single inlet droplet production device.
The aqueous inner phase is encapsulated by the outer oil stream due to a flow focusing device geometry. The oil phase (A) is redirected into two channels coming from the sides to cut off the aqueous stream (B). Homogenous droplets in size are produced and collected over the outlet (C).

3.1.2.2 *Double inlet production device*

To encapsulate single cells in water-in-oil droplets a double inlet production device is needed. Here, the oil phase is introduced to the system over inlet A, while two different aqueous phases are connected over inlets B and C (Figure 33). The produced droplets are collected over the outlet (D) (Figure 33). The concentration

for the oil phase is the same as for the single production device. Here, it is important to point out that the aqueous phases are diluted by half inside the droplet based on two parallel laminar flows. Hence, the protein concentrations and ionic conditions have to adjusted. The flow rates are also adjusted to the following parameters, 800µl/h for the oil and 200µl/h for each aqueous phase.

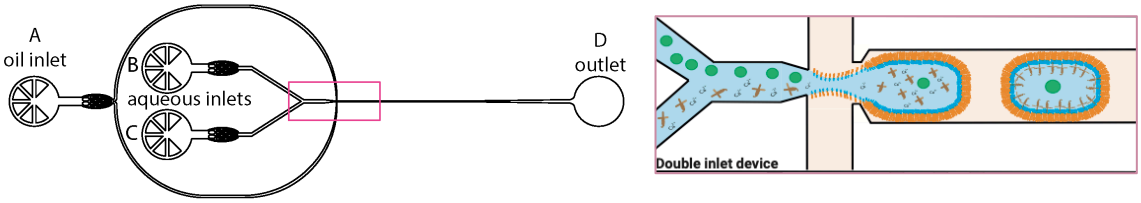

Figure 33 Schematic drawing of a double inlet production devices with an enlarged flow-focusing droplet production area (right).
The oil phase (A) is redirected into two channels coming from the sides to cut off the two aqueous streams in the middle (B and C). Homogenous droplets in size are produced and collected over the outlet (D). Square: Representative encapsulation of cells and proteins in parallel.

3.1.2.3 Aqueous two-phase system

In order to establish PEGDA crescent microparticles a different microfluidic double inlet device is designed (Figure 34). The difference to the previously described double inlet production device is that two flow-focusing junctions are aligned behind each other. First, the aqueous phases B and C are creating a parallel flow (Figure 34, pink square) until they reach the oil junction. At this point, droplets are established by the oil which is cutting off this stream of the two phase-separated aqueous phases. Further a mixing area is needed to fully separate the phases in the droplet. Finally, the droplets are collected over the outlet (Figure 34D). Note, the channel geometry was altered for this particular device. The channel sizes are 60 µm in width and 80 µm in height. In order to achieve a 80 µm height of the photoresist SU-8 3050, the chemical is spin coated at 1700 rpm for 30 s and soft baked at 65 °C for 1 minute first and followed by 30 min at 95 °C. The micropattern Generator µPG 101 is used to mask the design into the photoresist by using 50 mW output power and 30 % pixel pulse duration.

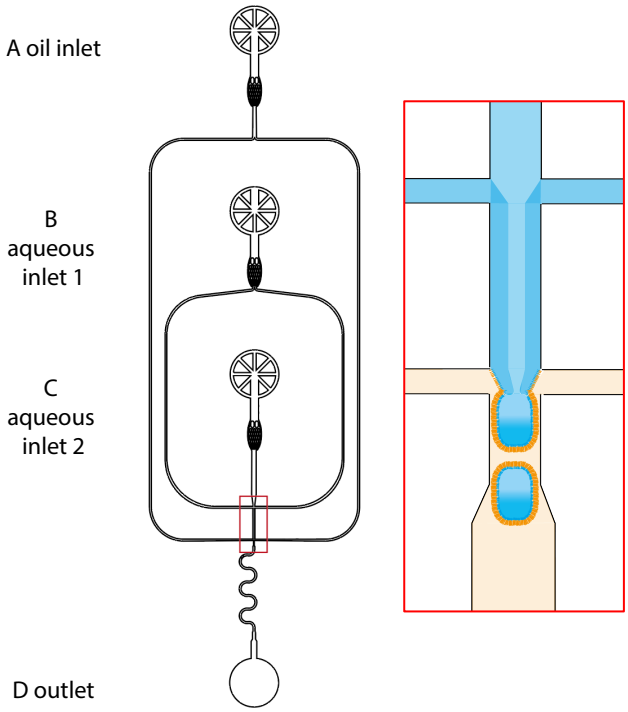

Figure 34 Aqueous two-phase system.
Two aqueous inlets (B and C) are designed behind each other in order to create an aqueous parallel flow (red square) which is cut by the oil coming from the top inlet (A). The droplets are mixed on chip first before they are collected over the outlet (D).

3.1.3 *Pico-injection device*

The biggest advantage of the pico-injection technology is that it is possible to inject any wanted content, for example a fluorescent dye, ions, enzymes, proteins or even living cells into previously established droplets.[276] In order to do so, a special design is needed. Figure 35 shows the general set up for a pico-injection device, where the oil phase is introduced to the system over inlet A, the aqueous phase over inlet B and the injection nozzle is attached over a channel to inlet C. Figure 35, red square shows the enlarged injection area with the injection nozzle and droplets passing by and being injected with single cells. In order to be able to apply an electric field, electrodes are attached to the devices through four prepared inlets (Figure 35D). To insert the electrodes, the device is put on a hot plate and heated up to 100 °C to melt a low melting-point alloy (51IN-32.5BI-16.5SN, Indium Corporation of America,

USA) inside the electrode microchannels.[302] Electric wires (Farnell, 1219343,Draht, Massivdraht, Schaltdraht, PVC, 23 AWG, 0.28 mm²) are inserted into the melted solder carefully. After quickly testing the resistance to check for functionality of the electrodes, the wires are stabilized with a UV-hardening glue (Loctite 352, Henkel, Germany). Before using the device, Sigmacote® is applied to the microchannels and flushed with HFE-7500 after 5 min at 65 °C.

The pico-injection procedure *per se* works with an electrical field generated in the injection area. Two electrodes, a shielding and an active electrode are connected to a function generator. For the injection of cells, I generate an electric field of 900 Hz and 900 V. The field, together with the geometry of the device, allows the droplet wall to stretch and destabilize shortly. As soon as the droplet is passing by the injection nozzle, the inner droplet aqueous phase is connecting with the aqueous phase of the injection channel and with pressure on the injection channel the content of choice can be injected. Immediately after the droplet passes the injection nozzle it stabilizes again and the injected substance stays encapsulated. The droplets are produced on chip by using syringe pumps to introduce the various phases. The flow rate of the (1) oil phase is set to 800 µl/h, (2) encapsulated aqueous phase is 300 µl/h and (3) injected aqueous phase is at 100 µl/h.

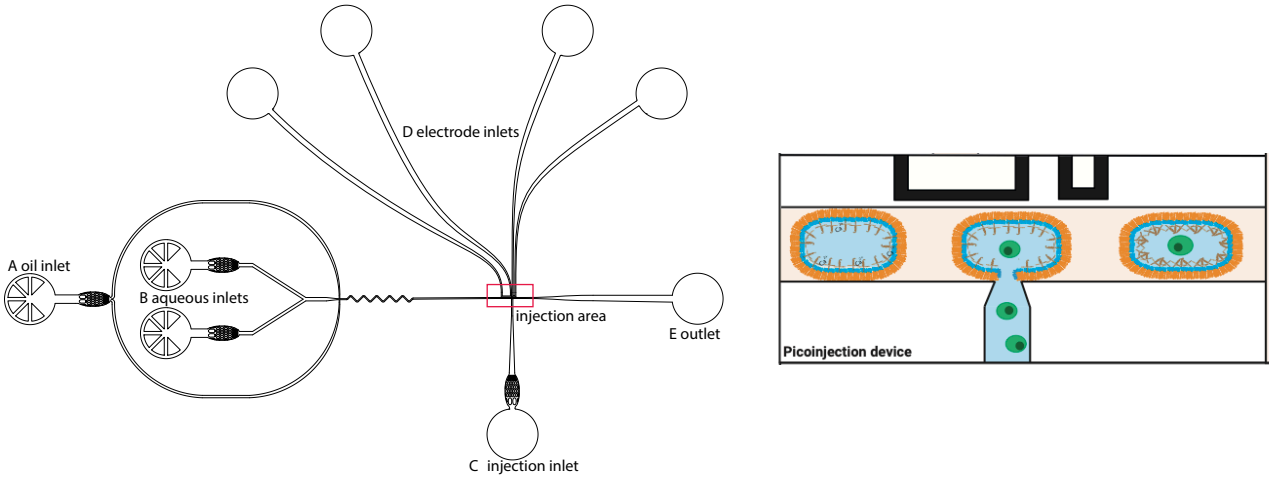

Figure 35 Pico-injection device with build-in double droplet production.
Injection of any wanted content into produced droplets on the same microfluidic design. A) Inlet for oil phase. B) Aqueous inlets. C) Injection inlet. D) electrodes. E) outlet. Square: Enlarged injection area. Laminin-111 containing droplets coming from the production area and getting injected with single cells at the injection nozzle.

3.1.4 Release devices

In order to remove the stabilizing oil shell around the droplets, two different microfluidic release devices are designed and implemented. One works based on the mechanism of a parallel aqueous flow and the destabilization of the droplet by electric fields, while the other is basically a bulk release method on chip, where the destabilization of the droplet wall is ensured by excessive contact between the droplets and a destabilizing agent before an interaction with the release media is facilitated.

3.1.4.1 Parallel microfluidic release device

To release the content of water-in-oil droplets carefully and individually a parallel microfluidic release device is used. The working mechanism is based on the application of an electric field, which destabilizes the outer oil shell. A parallel aqueous flow is introduced in which the released content of the destabilized water-in-oil droplets is collected. Inlet A introduces the previously made droplets to the

system, inlet B consists of pure HFE-7500 oil, which is needed to separate the droplets (Figure 36A, B). By introducing a destabilizing agent in the separation channel, it is possible to support the electric release process. Electrodes are attached as described previously (Chapter 3.1.3 Pico-injection device). The aqueous release media is introduced to the device via inlet C (Figure 36C). For this design two outlets are needed, outlet E collects the released content from the droplets, while outlet F is collecting the oil waste. The microfluidic release area is enlarged, showing the release process (Figure 36). First, the droplet is squeezed inside the channel, which is destabilizing the droplet wall to an extent already. Further, a contact between the droplet and the aqueous flow is established and the electric field initiates the complete destruction of the oil shell, leading to the release of the content of the droplet. In my case, cell-laden or empty protein microcapsules are collected over the collection outlet, while the oil waste is collected separately. The results are depicted in Chapter 4.4.4 Release of ProCaps via a microfluidic release device.

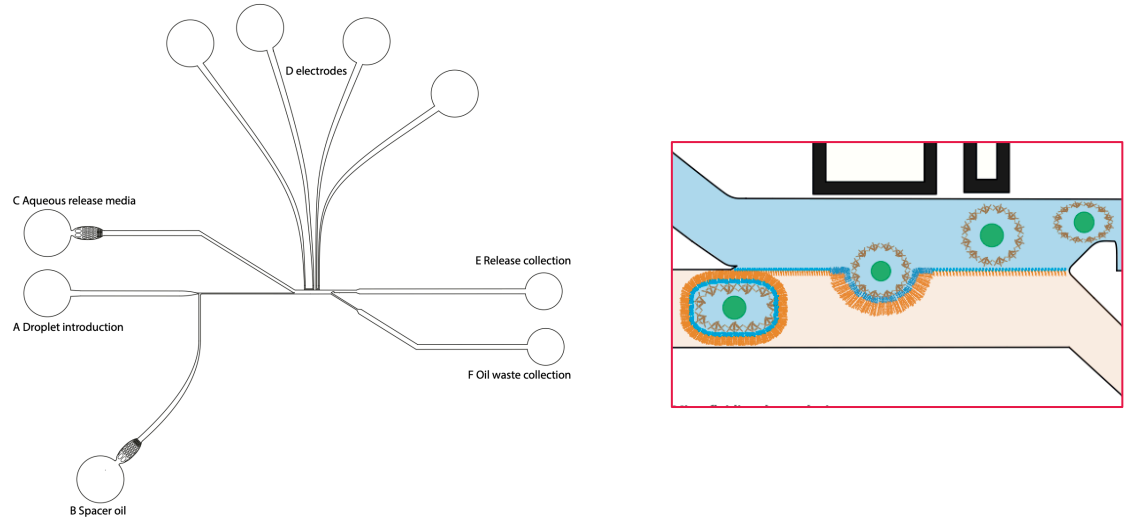

Figure 36 Schematic overview of the microfluidic release device.
The inset shows the first contact of a cell-laden water-in oil droplets with the aqueous phase. Next, the oil phase is removed and the content is released.

3.1.4.2 Circular microfluidic release device

In addition to the parallel release microfluidic device, I designed another channel geometry to accelerate the process and increase the yield of especially smaller protein microcapsules (Figure 37). Briefly, the idea is to destabilize the wall of the

droplets by interspersing them with a destabilizing agent (1H,1H,2H,2H-Perfluoro-1-octanol, PFO). The droplets are loaded with a syringe into one inlet channel and interspersed in the circle with the destabilizing agent coming from the second inlet channel. To maximize the time of contact, a circle structure is implemented (Figure 37a). The flow rates are set to 100 µl/h for the droplets and 150 µl/h for the destabilizing surfactant phase. An aqueous flow is generated with 1x PBS loaded in a syringe introduced to the system with 180 µl/h crossing the mixed droplet/destabilizing surfactant phase (Figure 37b). Further downstream, electrodes are installed to help the fusion of the destabilized droplets with the PBS inside the channels (Figure 37c). The electric field is set to 900 V and 900 Hz. The capsules are collected together with the oil waste over one outlet but because of phase separation properties of the oil and the water phase, the generated capsules remain in the aqueous phase and are easily collected.

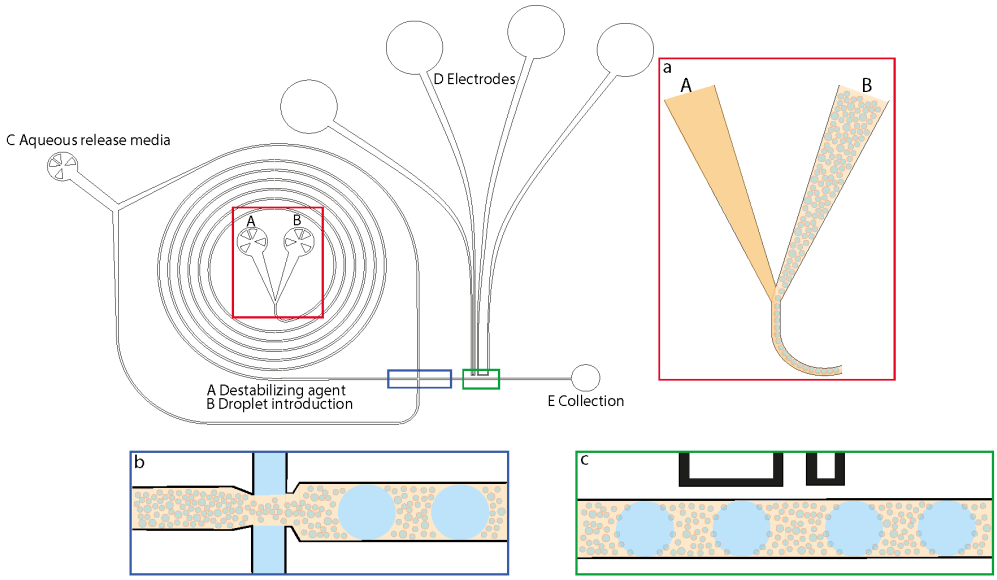

Figure 37 Schematic drawing of circular release device.
a) Schematic drawing of droplets being introduced to the device over inlet B with a destabilizing agent in parallel added over inlet A. b) The aqueous release media is introduced via inlet C and merges with the droplet-destabilizing surfactant mixture. c) Electrodes are connected over D and support the destabilization of the droplets. Finally, the released content is collected over outlet E.

3.1.5 *Droplet deformation device*

In general, this device is used to analyze the interfacial tension (IFT) of single water-in-oil droplets on a microfluidic chip.[303] However, I make use of this device in order to investigate the broad effects of the encapsulated proteins on the viscoelastic properties of the droplets. Droplets are produced on the chip and are flowing through 100 relaxation chambers before collected over the outlet. The droplets are squeezed in the narrow channels and relax in the chambers. The channel sizes for this particular device geometry is 10 µm for the channels and 30 µm in width and 30 µm in length and height for the chamber. With high speed cameras it is possible to analyze the form of the droplet before it is squeezed again into the next chamber (Figure 38).

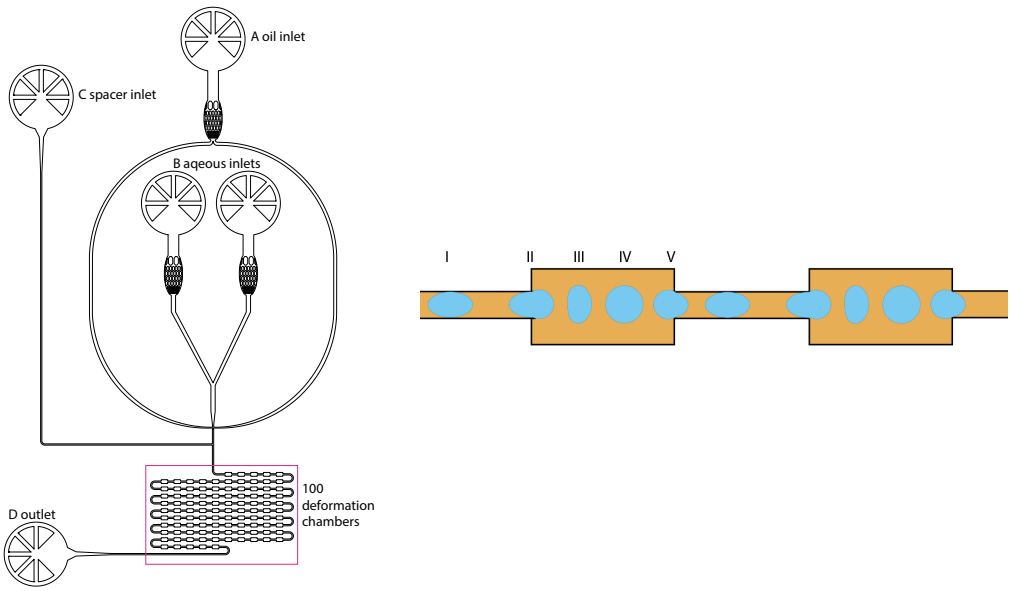

Figure 38 Schematic representation of the deformation chamber and the theoretical behavior of a droplet through a chamber.

Droplets are produced by the surfactant containing oil phase (inlet A) cutting of the aqueous flow (inlet B) and separated by the spacer oil (inlet C). Droplets are going through 100 deformation chambers before they are collected at the outlet (D). Droplets are undergoing theoretically following stages in the deformation chamber: I) Droplet is squeezed inside the channel. II) Droplet entering the chamber. III) Start of relaxation of the droplet. IV) Full reconstitution to its shape. V) Leaving the deformation chamber into the next channel.

3.2 High-speed camera

A high-speed camera is used to obtain images of the production, injection and release of droplets. Two different high-speed cameras are used. A Phantom V2511 is used to observe the injection of contents into droplets and the release of contents from destabilized water-in-oil droplets by the parallel microfluidic device or the circular microfluidic release device. High-speed videos of injection and release are obtained at a resolution of 500x280. A Photron FASTCam Mini UX100 is used to image water-in-oil droplet production and PEGDA crescent droplet production. Images for the droplet production and circle release are obtained at a resolution of 1280x1024 and at 4000fps. Videos are saved as TIFFs and analyzed with ImageJ.

3.3 Fluorescent labelling of Laminin-111 and Bovine Plasma Fibronectin

In order to be able to detect the generated microcapsules by confocal laser scanning microscope (CLSM), the proteins of choice are labelled. To do so, first, laminin-111 (Laminin from Engelbreth-Holm-Swarm murine sarcoma basement membrane, 1-2 mg/ml in Tris buffered NaCl, Sigma, L2020) or bovine fibronectin (Gibco™, 1mg/ml) is dialyzed (Slide-A-Lyzer™ MINI Dialysis Device, 3.5K MWCO, 0.5ml, Thermo Scientific) against sterile 1x PBS at 4 °C. Every hour the PBS in the flask is exchanged and as a final step the dialysis is left overnight. The next day, 50 µg NHS-Ester DyLight™ 550 (Thermo Scientific) is diluted with either 500 µl of freshly dialyzed laminin-111 in 1x PBS or 250 µl dialyzed bovine plasma fibronectin. The vials are shaken for 1 hour at 4 °C on a test tube shaker at 600 rpm. Afterwards the solutions are dialyzed against 1xPBS to remove any unbound dyes. The PBS in the tube is exchanged hourly and as a final step it is left to dialyze overnight. The labeled protein solutions are aliquoted and stored at -20 °C until further usage.

3.4 Statistical analysis of protein attraction in dsProCaps

In order to analyze the intensity of the proteins at the periphery of the droplets, approximately 100 droplets are imaged for each condition. The LSM 900 (Zeiss) is set to 5 % laser power and 600 V gain. The mean intensity values are obtained by integrating the intensity values of 20 individual line profiles per condition. The integrated values are normalized to the first time point plotted using Prism9. To analyze the significance between the timepoints a two-way ANOVA was performed. Several ImageJ Macros are listed in Chapter 7.1.12.

3.5 Generation of ECM-based dsProCaps

In this section I am focusing on the detailed production of ECM-based droplet-stabilized protein microcapsules (dsProCaps). Different surfactant types and the tested concentration ranges, together with the varying constellation of the aqueous phase are discussed thoroughly.

3.5.1 Generation of dsProCaps with negatively charged PEG-based fluorosurfactants

For the generation of ECM-based microcapsules, it is needed to establish water-in-oil droplets, with a charged water-oil interphase, serving as a scaffold for the attraction of ECM proteins. By making use of a flow-focusing single inlet droplet production device stable water-in-oil droplets are produced with 5 w% Perfluoro-polyether-poly(ethylene)glycol (PFPE-PEG) block-copolymer fluorosurfactants (008 PEG-based fluorosurfactants from Ran Biotechnologies, Inc., USA) and 8 mM Krytox™ (157FSH, Chemours, 680-272-0) dissolved in HFE-7500 oil (3M, USA) being the stabilizing oil phase. As discussed in the introduction Chapter 1.7.3 Surfactants, the Krytox™ surfactant is known for its negative charge attached to the PEG molecule. From here on, droplets established with Krytox™ are termed negatively charged dsProCaps. The aqueous phase consists of a mixture of the

protein of choice (i.e. laminin-111, Matrigel® or bovine plasma fibronectin) with its individual polymerization cocktail in the aqueous phase. Matrigel® is used because of two reasons. First, it consists of laminin-111 (60 %), collagen type IV (30 %) and entactin (8 %), and several growth factors such as TGF-β, IGF-1 and others. Entactin serves as a bridging molecule between laminin-111 and collagen type IV, and supports the structural organization.[304] Using Matrigel® allows to investigate the establishment of protein capsules made out of a mixture of proteins. Second, Matrigel® is widely used for the growth of spheroids and known for the proper interaction of cells with proteins. In order to attract and polymerize the proteins inside negatively charged droplets, 1.17 µM laminin-111 or 1.4 µM Matrigel® are mixed with 10 mM $CaCl_2$ in PBS. In the case of bovine plasma fibronectin, 25 mU Transglutaminase 2 (T5398, Sigma Aldrich), 250 mM NaCl (3975.1, Roth), 40 mM Tris (AE15.1, Roth), 5 mM CaCl2 (A431982, Merck), 1 mM DTT (646563-10X.5ml, Sigma Aldrich) are added to polymerize 0.5g/L fibronectin (1.14 µM) in PBS. For producing 30-40 µm droplets in diameter, the oil mixture and aqueous phase of choice are loaded into separate syringes (Omnifix®-F, B.Braun, Germany), connected by a cannula (Sterican®, 0.4 x 20 mm, BL/LB, B.Braun, Germany) and PTFE-tubing (0.4 x 0.9 mm, Bola, Germany) and inserted into the prepared connection holes of the PDMS device. The flow rates are set on the syringe pumps (Standard Infuse/Withdraw Pump 11 Elite Programmable Syringe Pump, Harvard Instruments) for the oil phase at 600µl/h and 300µl/h for the aqueous phase. Laminin-111, bovine plasma fibronectin and Matrigel® droplets are collected in a 1.5 ml Eppendorf tube and stored for several hours at 37 °C in order to attract and polymerize the proteins inside the droplets. The exact time points are indicated in the appropriate result sections.

3.5.2 *Generation of dsProCaps with positively charged PEG-based fluorosurfactants*

Another charge-mediated approach to attract proteins to the inner periphery of a droplet's wall, is the use of positively charged surfactants (Figure 39). Martin Schröter (Ph.D. Student, MPImR, Prof. Spatz Department) synthesized a N(Me)3-PEG-PFPE block-co-polymer, which has a positive charge attached to a PEG molecule, leading to the positive charge facing into the aqueous phase. Here, 20 mM of this surfactant is prepared in HFE-7500 and either diluted to 5 mM for simple dsProCaps production or directly used for the encapsulation of cells inside the droplets, to ensure higher droplet stability. In the case of positively charged dsProCaps, 0.8 µM laminin-111 or 1.4 µM Matrigel® with 10 mM $CaCl_2$ are diluted in DMEM cell culture media containing 1 % FBS. This specific condition proved to attract the proteins most efficiently to the inner periphery of positively charged dsProCaps. The flow rates for simple droplet production are 200µl/h and 600µl/h for the aqueous and oil phase, respectively. It is important to mention here, that this special fluorosurfactant interacts highly with the PDMS of the microfluidic chips. In order to generate stable positively charged dsProCaps, the devices are rendered hydrophobic with Ombrello instead of Sigmacote®. Ombrello is a stronger chemical and no incubation time is needed. The solution is introduced to the channels with a syringe and flushed shortly. Afterwards, HFE-7500 is filtered through a PTFE-filter (0.2 µm, Polytetrafluorethylen, ROTILABO®) and used to flush the device to remove the remaining Ombrello particles. Devices can be used immediately after rendering or stored until further usage.

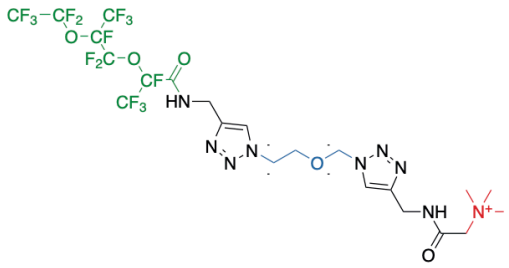

Figure 39 Chemical structure of N(Me)3-PEG-PFPE surfactant.

3.5.3 *Generation of negatively and positively charged small dsProCaps*

The production of small ECM-protein microcapsules is based on the same mechanism as the large microcapsules. The term "small dsProCaps" refers to the smaller droplet diameter. The proteins are attracted to the inner periphery by charges, with the main difference being the shorter adsorption depth, which the proteins have to overcome. Both charge mediated attraction mechanisms are applied to establish small dsProCaps with Krytox™/PEG-PFPE or N(Me)3-PEG-PFPE. The difference to the bigger microcapsules lays on the one hand in the production process *per se* and on the other hand, the concentration of the used proteins. Instead of preparing droplets with a microfluidic chip, I am making use of an emulsifier (T 10 basic ULTRA-TURRAX®, IKA) for the so-called one-pot assembly of small dsProCaps. This machine is producing small heterogenic droplets in the range of 1 to 100 µm in diameter, depending on the settings, by using high shearing and expanding forces.[257] The aqueous phase consists of the protein of choice and the polymerization factors needed for each protein. For laminin-111 droplets, 0.3 µM protein with 10 mM $CaCl_2$ is mixed together, while in the case of Matrigel® droplets 0.2 µM protein and 10 mM $CaCl_2$ is needed to attract the proteins to the periphery. To establish fibronectin droplets 0.3 µM protein is mixed with 25 mU Transglutaminase 2, 250 mM NaCl, 40 mM Tris, 5 mM $CaCl_2$ and 1 mM DTT. In order to generate the droplets, the protein mixture is added on top of the oil phase (Figure 40A), consisting of 8 mM Krytox™/5 w% PEG-PFPE or 5mM N(Me)3-PEG-PFPE both diluted in HFE-7500 as the stabilizing surfactants and dispersed with the rotor-stator machine (Figure 40B). To generate approximately 10 µM droplets in diameter 400 µl of the aqueous phase and 600 µl of the oil phase are mixed at 26,334 rpm (level 5 on the emulsifier) for 35s. The droplets are incubated for several hours at 37 °C.

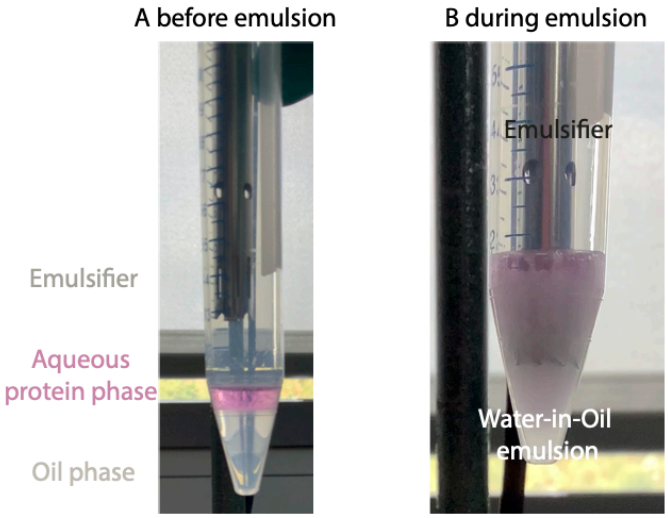

Figure 40 Production of small droplet-stabilized protein capsules (dsProCaps) by using an emulsifier. A) Before starting the emulsification process the aqueous protein mixture is added carefully on top of the oil phase, consisting of Krytox™/PEG-PFPE or N(Me)3-PEG-PFPE. B) The emulsifier head is situated inside the oil phase and the process is started. The two phases are mixed thoroughly through this technique.

3.6 IFT measurements by pendant drop

To understand some physical properties of the newly synthesized surfactant and its interplay with ECM proteins, I conduct pendant drop measurements to shed light on the interfacial tension (IFT) properties in contact with ECM proteins. The basic principle of my experiment lays on the production of an oil drop hanging from a blunt needle into an aqueous phase. Images are captured and analyzed by using the SCA 20 contact angle software and IFT values in mN/m are obtained. The physics behind this analysis is described in detail in Chapter 1.7.4 Physical Properties of droplet stabilization. The used oil conditions in my particular experiment, are 5 mM or 20 mM of the positively charged surfactant diluted in HFE-7500. Two different buffer conditions are tested, 1) PBS only and 2) pure laminin-111 without additional $CaCl_2$. Five values are obtained for each condition and plotted using Prism9. An ordinary one-way ANOVA is used to determine the statistical difference. The results of those experiments are explained in Chapter 4.10.3 Interfacial Tension Measurements of N(Me)3-PEG-PFPE.

3.7 FRAP measurements

FRAP measurements are conducted to understand the polymerization pattern of proteins inside dsProCaps. By encapsulating 2mg/ml 70 kDa FITC-dextran molecules with the labelled proteins I want to analyze protein polymerization at the periphery at different time points. First, droplets containing DyLight555 labelled laminin-111 in PBS with or without 10 mM $CaCl_2$ are produced. The difference of the droplets lays in their oil constellation. Two different concentrations of the positively charged surfactant are used (5 mM and 20 mM), while the third condition consists of 5 w% PEG-PFPE and 8 mM Krytox™ dissolved in HFE-7500. The droplets are imaged directly after production, 2 h and 24 h after incubation at 37 °C. FRAP measurements are conducted using the LSM 980. First, 100 % of laser power at 488 nm was used to bleach different regions. Three droplets are bleached and analyzed, while one droplet served as the non-bleach control and another ROI was set to obtain the background noise. Three images are taken before the regions are bleached for 20 s and recovery is imaged for 100 s. The image resolution is set to 128x128, which reduces the imaging quality, however based on the fast diffusion properties of FITC-dextran molecules in several testing conditions, higher image resolutions could not fully capture the recovery. The values for each time point are subtracted with the background. Next, the mean of five measurements and three droplet values at each measurement are plotted with Prism9. The results of those experiments are explained in Chapter 4.3.1 Measuring protein diffusivity in dsProCaps and Chapter 4.11.1 Analysis of protein diffusion in positively charged dsProCaps.

3.8 Deformation chamber

In order to analyze the deformation of either previously or on-chip produced droplets the liquids are introduced to the system with a microfluidic flow controller (Elveflow OB1 MK3+). Here, the phases are prepared in 1.5 ml Eppendorf tubes and attached to adapters which are connected to the controller over vacuum channels.

The content is introduced into the chip via PTFE-tubing (0.4 x 0.9 mm, Bola, Germany). The system controls the liquid flow over pressures, which are indicated at the results. For the experiments, I produce laminin-111 droplets directly on chip by introducing the production oil via the oil inlet and the laminin-111(1.2 µM)-$CaCl_2$ (10 mM) mixture through one aqueous inlet. The used oil concentration is 1 w% PEG-PFPE and 5 mM Krytox™ diluted in HFE-7500. The spacer oil consists of the same oil as used for the production, in order to not dilute the surfactant molecules. For the second approach, I produced droplets a day before and incubated them over night at 37 °C and introduced them to the system through one aqueous inlet channel, using again the same production oil as the spacer. The used flow rates for each set up are indicated at Chapter 4.3 Analysis of the Mechanical Properties by Rapid Microfluidic-Based Deformation of dsProCaps.

3.9 Cell culture of eukaryotic and prokaryotic cells

All used eukaryotic cells for this study are cultured following the same protocol. HaCat-YFP Keratin (kind gift from Prof. Rudolph Leube, University of Aachen) are seeded in T-125 flasks and cultured in DMEM GlutaMAX®, supplemented with 10 % FBS and 1 % Pen/Strep. To detach the cells Trypsin EDTA 0.25 % is added to the flasks for 8 min and the collected cells are centrifuged at 1200 rpm for 5 min. Cell pellets are resuspended in 1x PBS and diluted to have a cell number of $2x10^6$ cells/100ul for each experiment. 500,000 cells are seeded in T-125 flasks to further keep the culture.

For culturing Jurkat cells (kind gift from Prof. Benjamin Geiger, Weizmann Institute of Science, Israel), RPMI 1640 medium supplemented with 10% FBS is used. $2x10^6$ cells/100 µl are used per experiment. To work with the amount needed, all cells are collected in 15 ml tubes (Falcon) and centrifuged at 300 g for 10 min. Afterwards, the supernatant is aspirated and the pellet is resuspended in the amount needed. In order to differentiate dead cells from healthy cells inside the droplets, a live/dead dye (7-Aminoactinomycin D, 7-AAD, A1310, ThermoFischer

Scientifc, 1.5 µl per 2x10^6 cells/100 µl cell suspension or Propidium iodide P1304MP at 1.5µg/ml) is mixed with the cells.

To prepare *E. coli* for the bacterial experiments a 50 mg/ml Kanamycin (Roth, T832.2 (sulfat)) stock in ddH_2O is prepared. Further, 12.5 g of LB powder (AppliChem A0954, lot# 0954-1/162) are dissolved in 500 ml ddH_2O and autoclaved. To start the culture, kanamycin is mixed at 1:1000 (50 µg/ml) in 500 ml LB medium and 20 ml of the prepared media is transferred in a small-sized glass beaker. *E. coli* are scratched from the frozen surface with a sterile pipette tip and incubated in the glass beaker for 6 - 7 hours at 37 °C at 250 rpm. Afterwards, 15 µl of the expanded culture are transferred in a new glass beaker and incubated overnight at the same incubation conditions. The next day, the bacteria culture is collected and centrifuged to remove the supernatant. To induce the GFP of the used *E. coli*, 20 µl of IGPF (Isopropyl-β-D-thiogalactopyranosid, VWR, CAS-NR.367-93-1) is added to a high density of bacteria and let shake overnight again.

3.10 Analysis of the pH inside dsProCaps

For encapsulating cells inside droplets, it was important to analyze and understand the pH values in this confined environment. In order to do so, first a calibration curve with water-in-oil droplets is established. PBS samples are prepared with a pH meter (Mettler Toledo) with different pH values ranging from pH 3 to 9 in 0.5 steps. The calibration curve is prepared by producing water-in-oil droplets with an oil phase consisting of 1.4 w% PEG-PFPE in HFE-7500 and an aqueous phase with the different PBS buffers containing pH values mixed with 100 µM pyranine (L11252, Alfa Aesar). 50 droplets per condition are imaged by using the LSM 900 (ZEISS), with 5 % laser power and 600 V gain. The intensity of each droplet is measured and analyzed using ImageJ. The mean grey values of 50 droplets are plotted with Prism9. Statistical differences are obtained by using an ordinary one-way ANOVA. The experimental conditions are prepared with the oil concentration and aqueous phases indicated at the results in chapter 4.9 Analysis of pH inside dsProCaps and

4.10.2 Analysis of pH inside positively charged dsProCaps and the analysis of the experiments is performed the same way as for the calibration curve.

3.11 Bulk polymerization of laminin-111 in different pH values

To understand the polymerization behavior of laminin-111 in different physiological conditions and investigate the pH dependency, a bulk experiment is performed. Hereto, I seeded 100,000 HaCaT Keratin-YFP cells together with 1.2 µM of laminin-111 and 10 % DyLight555-labelled laminin-111 in 10 wells of a 96-well plate in buffers with pH values ranging from 3 to 9 and in cell culture media. The cells and labelled proteins are imaged directly after seeding, 4 h and 24 h after incubation at 37 °C and 5 % CO_2. CLSM images are obtained with the Zeiss LSM980 (5 % laser settings, 600 V). The results of this experiment are explained in Chapter 4.9 Analysis of the pH inside dsProCaps.

3.12 Release of microcapsules into physiologically relevant media

In order to remove the outer oil shell of dsProCaps, several different release approaches can be conducted. Here, I am presenting the bulk release approach, which is the most used in my thesis. The other methods, are performed in order to validate the possible ProCaps generation in a broader spectrum.

3.12.1 Bulk release

To investigate the interaction of the encapsulated organisms with the ECM-protein of choice the microcapsules needed to be released out of the surfactant-stabilized shell. This is performed by using a previously described bulk-release method.[253] Briefly, 20µl 1x PBS is added to the Eppendorf tube in which the droplets are collected and polymerized at 37 °C (Figure 41A). Afterwards 20µl PFO

(destabilizing surfactant) (Sigma, 370533-25G) are added dropwise from the top (Figure 41B). By tilting and rotating the tube slowly the microcapsules are released into PBS (Figure 41C). In order to image the resulting ProCaps, they are collected on a glass cover slide, and observed with an LSM 900 (5 % laser power, 600 V gain) and analyzed with ImageJ.

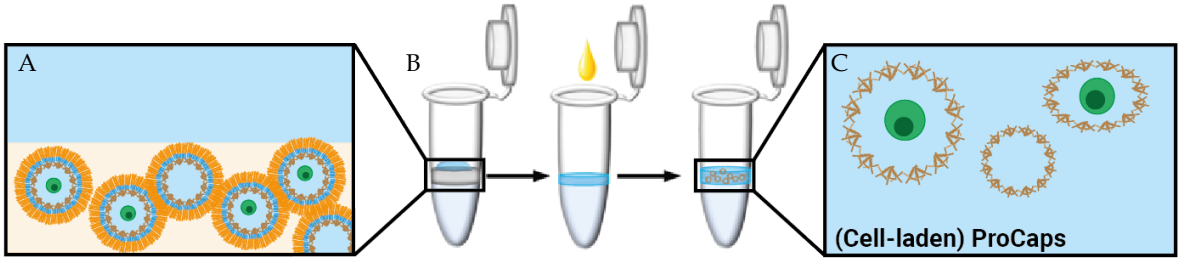

Figure 41 Bulk release approach in three simple steps.
A) Droplets are collected in 1.5 ml Eppendorf tubes and covered with 1x PBS. Droplets start accumulating at the water-oil interface. B) Destabilizing surfactant (yellow droplet) is added to the PBS-droplet mix. C) Over time microcapsules are released into the PBS without any remaining surfactants.

3.12.2 *Petri dish release*

To observe the release mechanism, a new release method is invented. First, a special oil phase consisting of 30 % destabilizing surfactant (370533-25G, Sigma) diluted in HFE-7500 is prepared in a petri dish. 1x PBS covered the oil phase, establishing two separate layers. Previously prepared laminin-111 droplets in 5 w% PEG-PFPE with 8 mM Krytox™ are loaded in the oil phase of the petri dish. The release of the capsules is observed in a time lapse by an upright, water-immersion confocal microscope (Leica SP5). Capsules are imaged with 40 % laser power, and 100 % smart gain. The results of those experiments are explained in Chapter 4.4.3 Observing the release mechanism of ProCaps.

3.12.3 *Microfluidic release*

This method falls into the broad category of droplet-based microfluidic tools. Here, an oil stream and an aqueous stream are generated in order to release any contents

from the droplets into the parallel release media. Hereby, I introduced previously established droplets, the aqueous release phase and a spacer stream for the droplets with a microfluidic pressure device (Fluigent) (Chapter 3.1.4.1 Parallel microfluidic release device). The used pressure values are 100 mbar, for the droplets, 150 mbar for the spacer and 300 mbar for the aqueous phase. Finally, to allow the full destabilization of the droplets and hence the release of the content, an electric field is implemented. Here, a field of 900 V and 900 Hz are generated with a function generator (Rohde & Schwarz HM8150) and a High Voltage Power Amplifier (TREK Model 623B). The released ProCaps are collected over a separate outlet and are observed by a LSM900 (5 % laser settings, 600 V gain) (Zeiss). The results of this experiment are explained in Chapter 4.4.4 Release of ProCaps via a microfluidic release device.

3.13 Characterization of ECM-based protein capsules

3.13.1 Immunofluorescence staining of ProCaps

Since only 10% labeled protein is used for establishing the microcapsules, it is needed to stain the capsules with various antibodies to visualize the protein organization after the release of the capsules. The staining process is the same for the different protein capsules, simply the primary antibody is changed. In general, the released capsules are loaded on glass cover slides and marked carefully with circles. 4% Paraformaldehyde (PFA) is added to the 20 µl drop of released capsules and incubated for 30 min at room temperature (RT). Afterwards the slides are washed gently three times for 5 min each with 1x PBS. The marked areas are covered with 1 % BSA (approximately 50 µl) and incubated for another 30 min at RT. The used primary antibodies are rabbit polyclonal anti-laminin (abcam ab11575 LOT:GR262966-1) and rabbit polyclonal anti-collagen IV (abcam, ab6586). All are diluted 1:100 in 1% BSA and 100 µl antibody solution is transferred to each marked circle and incubated overnight at 4°C. The next day, the slides are washed gently 3x for 5 min each with 1x PBS. The secondary antibody (chicken anti-rabbit 488,

Invitrogen, A21441 lot: 1697089) is diluted 1:500 in PBS and used for all capsules. 100 µl of the antibody solution is added to the circled spots and left for 1h at RT to incubate. Finally, the slides are washed for a last time, 3x for 5min each with 1x PBS and then mounted in Fluoromount-G® 0100-01 and gently covered with another glass cover slide. The results of those experiments are explained in Chapter 4.4.5.1 Immunological staining of ProCaps.

3.13.2 FITC-dextran release studies

For studying the mesh size of our protein capsules, 2 mg/ml of either 4 kDa or 70 kDa FITC-dextran are mixed together with the protein of choice and its specific polymerization factors. dsProCaps containing laminin-111, Matrigel® or fibronectin are produced as stated before (Chapter 3.5 Generation of ECM-based dsProCaps**)** and polymerized for approximately 24 h at 37 °C. Droplets are observed with the LSM 900 (Zeiss, 5 % laser power Ex/Em: 488nm/512nm, 800 V gain) directly after production and 24 h later. The mean intensity values are obtained with the ImageJ software and plotted using Prism9. With a two-way ANOVA the differences in intensity are evaluated. By implementing the bulk release approach, the microcapsules are released and imaged for remaining FITC-dextran signals (5 % laser power Ex/Em: 488nm/512nm, 600 V gain). A line intensity profile depicts representative intensity plots for the labelled protein and the different FITC signals. The results of those experiments are explained in Chapter 4.4.5.2 ProCaps porosity investigation with FITC-dextran.

3.14 Adhesion experiments of cells to negatively and positively charged ProCaps

Since the production of ProCaps involves many chemicals and can be harsh to natural proteins, the question arose, if the proteins denature during this process. In order to contradict this hypothesis and confirm protein functionality, the simplest experiment is to understand the attachment of cells to ProCaps from the outside.

Hence, dsProCaps containing 0.8 µM laminin-111, 10 % labelled proteins and 10 mM $CaCl_2$ and stabilized by either 5 mM N(Me)3-PEG-PFPE or 5 w% PEG-PFPE/8 mM Krytox™ are produced. Further positively and negatively charged ProCaps are released using the bulk release approach. The capsules are loaded into a glass bottom 6-well dish and 200,000 HaCaT YFP cells are seeded simultaneously. Images are obtained directly 24 h, 48 h and 72 h after culturing at 37 °C and 5 % CO_2 with a LSM980 (5 % laser settings, 600 V gain). The results of those experiments are explained in Chapter 4.9 Analysis of pH inside ds ProCaps and Chapter 4.9 Analysis of pH inside dsProCaps and 4.12 Generation of ProCaps by implementing the bulk release approach.

3.15 ECM deposition analysis of HaCaT cells

Based on the generally known fact that adhesion cells deposit their own ECM proteins after complete adhesion to surfaces, I set out to investigate potential release of ECM proteins by the cells prior to their full attachment and spreading. 30,000 HaCaT cells are seeded in either media or PBS in two 24 glass bottom well-plates. Table 1 shows the set up for two 24-well plates.

Table 1 Experimental set up for the analysis of ECM deposition over time.
Three different protein types are analyzed, LN, laminin-111; FN, fibronectin; colIV, collagen type IV. Deposition of each protein is observed at 30min (0.5h), 1h, 2h, 3h, 4h, 24h, 48h, and 72h in cell culturing media or PBS.

0.5h LN Media	0.5h LN PBS	0.5h FN Media	0.5h FN PBS	0.5h colIV Media	0.5h colIV PBS
1h LN Media	1h LN PBS	1h FN Media	1h FN PBS	1h colIV Media	1h colIV PBS
2h LN Media	2h LN PBS	2h FN Media	2h FN PBS	2h colIV Media	2h colIV PBS
3h LN Media	3h LN PBS	3h FN Media	3h FN PBS	3h colIV Media	3h colIV PBS
4h LN Media	4h LN PBS	4h FN Media	4h FN PBS	4h colIV Media	4h colIV PBS
24h LN Media	24h LN PBS	24h FN Media	24h FN PBS	24h colIV Media	24h colIV PBS
48h LN Media	48h LN PBS	48h FN Media	48h FN PBS	48h colIV Media	48h colIV PBS
72h LN Media	72h LN PBS	72h FN Media	72h FN PBS	72h colIV Media	72h colIV PBS

The cells are fixed at the indicated time points with 4 % PFA for 10 min at 37 °C without disturbing the other conditions. PFA is washed 3 times from the according timepoint with PBS and remained untouched until all cells from each 24-well plate are fixed. Afterwards, the cells are blocked with 1 % BSA and incubated for 30 min at RT. Three different antibody mixtures are prepared. Rabbit polyclonal anti-laminin-111 (abcam, ab11575), rabbit polyclonal anti-collagen IV (abcam, ab6586) and rabbit polyclonal anti-fibronectin (abcam, ab2413) are diluted 1:100 in three separate falcon tubes. Primary antibody staining is performed overnight at 4 °C and after three washing steps, the cells are incubated with the secondary antibody (chicken anti-rabbit 488, Invitrogen, A21441, dilution factor 1:500). After three washing steps with PBS, five images are taken with the LSM 980 (laser power 5 %, 600 V gain). Analysis is performed by measuring the mean intensity of each image with ImageJ and plotting the mean of each using Prism9.

3.16 Pico-injection of eukaryotic and prokaryotic cells into surfactant-stabilized droplets

For the encapsulation of various organisms, a specially designed production and pico-injection microfluidic design is used (Figure 35). dsProCaps are produced with a flow-focusing junction on the same device. The flowrates for the oil phase are set to 600 µl/h and the aqueous-protein phase to 200µl/h. An electric field (900V and 900 Hz) is generated using a function generator (Rohde & Schwarz HM8150) and a High Voltage Power Amplifier (TREK Model 623B) to destabilize the polymer membrane of the droplets directly at the injection nozzle and inject the fluid containing the organisms of choice. The organisms are injected with 50 µl/h using a third syringe pump. To observe the production and injection process a high-speed camera (Phantom v2512) attached to an Olympus IX7 microscope is used. Movies are analyzed using ImageJ. The injected droplets are collected and incubated for several hours at 37 °C with 5 % CO_2. Bacteria images are obtained with a confocal laser scanning microscope (Leica, SP5) and cell-laden dsProCaps images are taken with the LSM 900 (Zeiss).

3.17 Trajectory analysis of bacteria inside laminin-111 ProCaps

In order to analyze the movement of single bacteria inside laminin-111 ProCaps a Plugin on Fiji is utilized. TrackMatev6.0.1 is an open platform for the tracking of single-particles published by Tinevez *et al.*[305] The plugin is a very handy tool, since it is guiding through the analysis step by step. For my analysis is used the Laplacian of Gaussian (LoG) detector, which applies a filter to the image and allows for calculation made in the Fourier space. The maxima in the images are used to track movement and further maxima too close to each other are suppressed, allowing for single particle tracking. The pixel width and height are set to 0.691 µm each and the voxel depth to 1 µm. The estimated blob diameter is set to 5 µm with a threshold at 10. This tool allows even for sub-pixel localization by fitting a quadratic scheme onto the image. After choosing this detector, it is necessary to adjust the diameter and the threshold, which is different from image to image. The best settings are determined with the preview tool. After running the analysis, the HyperStack Displayer is chosen which overlays the spots and tracks. Next, the simple Linear Assignment Problem (LAP) tracker is used to link the detected spots over the frames and build a track segment. In a second step the spots are investigated in order to search for missing detection and if the tracking of any spots is lost over the frames, the script closes the gaps. This tracker is suitable for Brownian motion, based on the ability of gap-closing. By displaying the spots and the tracks individually it is possible to adjust the colors.

3.18 Encapsulation of cells into positively charged dsProCaps

In order to encapsulate single cells inside positively charged dsProCaps I re-purposed the aqueous two-phase system microfluidic design (Experimental Section 3.1.2.3. ATPS device, Figure 34). Hereby, I made use of 20 mM N(Me)3-PEG-PFPE dissolved in HFE-7500 as the oil phase, by which the cell-laden droplets are

stabilized. 1.17 µM laminin-111 with 10 % labelled laminin-11 and 10 mM $CaCl_2$ are diluted in PBS and introduced into the first aqueous inlet. $2x10^6$/100 µl HaCaT cells are taken into a syringe and connected to the second aqueous inlet on the microfluidic design (Figure 34). This particular design is used to ensure the encapsulation of cells without diluting the protein phase excessively, as it is the case by implementing a standard double inlet droplet production device. Cell-laden dsProCaps are produced by using 800 µl/h as the oil phase flow rate, 200 µl/h as the cell flow rate and 300 µl/h for laminin-111.

3.19 Production of PEGDA crescent particles

An aqueous two-phase system device is used in order to establish PEGDA/dextran containing droplets (Figure 34, Experimental Section 3.1.2.3. ATPS device). For the formation of PEGDA crescent microparticles droplets are prepared with 40 w% PEGDA (700g/mol) containing 1.5 w% LAP and 40 w% dextran (40,000g/mol). Two syringes are prepared containing either PEGDA-LAP, or dextran. It is very important to protect the PEGDA-LAP mixture from light, otherwise the polymerization occurs in the syringe. The oil phase consists of 0.5 w% PEG-PFPE surfactant dissolved in HFE-7500. In order to produce homogeneous droplets, the syringes are connected to the device in the appropriate connection holes and the flow rates are set to 4 µl/min for the oil phase, 1 µl/min for the PEGDA-LAP phase and 0.25 µl/min for dextran. Shortly before the droplets are collected over the outlet, a focused laser light using a DAPI filter generates a UV beam which is polymerizing the droplets on chip. After the successful polymerization the PEGDA phase is solid, and the non-polymerized dextran phase is easily removed by several washing steps. The release process involves the removal of the excessive oil layer underneath the droplet-stabilized particles. Next, 30 % PFO is added to destabilize and remove the oil layer around the droplets. After a short centrifugation, the particles are further washed with 70 % EtOH for several times. Afterwards several washing steps are conducted in sterile PBS in order to ensure sterility for the cell experiments.

3.19.1 Production of laminin-111 coated PEGDA crescent microparticles

For producing crescent particles with a laminin-111 layer only in the cavity, the protein is mixed in the dextran phase and encapsulated directly. In order to have high concentrations of RGD for the cells to anchor, I prepared 1.17 µM laminin-111 with 10 % of DyLight550-labelled laminin-111 and 1 mM additional RGD (A8052, Sigma Aldrich). By incorporating the protein, it is needed to lower the dextran percentages. The protein-RGD solution is used to dissolve 30 w% dextran directly and left overnight on a shaker at 4 °C at 700 rpm to dissolve the dextran homogenously with the protein. Since the protein increases the viscosity, the flow rates for the production of droplet-stabilized particles were adjusted. Here, I used 5 µl/min for the oil phase, 1 µl/min for the PEGDA-LAP phase and 0.3 µl/min for laminin-111/dextran. The PEGDA/LAP concentration stayed the same as used previously. The droplets are polymerized on chip with the DAPI filter and the dextran phase is removed as previously stated. Note, that by introducing laminin-111 to the dextran phase, the removal of the dextran was only conducted by several washing steps using first 30 % PFO and PBS. No additional use of 70 % EtOH is needed. In order to coat the entire particles with laminin-111, previously produced crescent microparticles are incubated with 1.17 µM unlabeled laminin-111 over night at 37 °C at 700 rpm. The results of these experiments are explained in Chapter 4.15.1 Generation of ECM coated PEGDA crescent microparticles.

3.19.2 Immunostaining of laminin-111 on coated PEGDA crescent microparticles

In order to visualize the protein coating around the coated particles, an antibody staining is performed. The particles are centrifuged and the supernatant is discarded. The pellet is resuspended in 4 % PFA to fix the proteins to the particles. PFA fixation is carried out for 30 min at RT at 400 rpm. Afterwards the particles are centrifuged shortly to remove the PFA solution and wash the particles with PBS for

three times, always for 5 min at 400 rpm. Then the particles are incubated with 1 % BSA for 30 min at RT at 400 rpm and the three washing steps with PBS for 5 min each, are repeated. The primary antibody (rabbit polyclonal anti-LN, abcam, ab11575) is prepared (1:100) in 1 % BSA and left on the shaker at 4 °C at 400 rpm overnight. After removing the supernatant, three washing steps at 400 rpm for 5 min are performed to remove unbound primary antibody. The secondary antibody (chicken anti-rabbit 488, Invitrogen, A21441) is diluted 1:500 in PBS and added to the particles. Incubation took 1 h at RT at 400 rpm. The secondary antibody is also washed away for three times at 400 rpm for 5 min each. Images are obtained with the LSM 900 (5 % laser power, 600 V gain). The results of this experiment are explained in Chapter 4.15.1 Generation of ECM coated PEGDA crescent microparticles.

Results and Discussion

4 Results and Discussion

After explaining the materials and methods used in my thesis, I will concentrate on the results which are obtained within the framework of my doctoral thesis. In the context of generating ECM-based containers for single cell observations, two different approaches are established. Hence, I structured the results and discussion section in two main parts.

In the first part, I elaborate on the generation of droplet-stabilized ECM-based protein microcapsules (dsProCaps) by the means of droplet-based microfluidics as an important tool to mimic ECM-based microenvironments. The core section of the first part is about the sequential release of protein microcapsules (ProCaps), into a physiological environment, based on the removal of the outer oil phase. The generation of microcapsules consisting entirely of ECM proteins has never been shown before, thus it withholds major advantages and a broad application range, which are highlighted in more detail throughout the description of my results. Finally, I will present the obstacles in the context of developing cell-laden dsProCaps and describe possible solutions in order to encapsulate healthy cells for investigating the mechanism of interaction of single cells and ECM proteins.

The second part of my thesis evolves around the development of crescent PEGDA microparticles as a versatile tool to allow investigating the behavior of single cells in curved 3D environments. In here, I explain the general assembly methods to incorporate an ECM layer in the cavity of those polymer particles and finally, shed light on the culturing of cells inside such cavities. The combination of ECM proteins with curved surfaces for the culture of single cells has never been shown before and opens up several possibilities for investigating cellular behavior within a confined 3D curved microenvironment.

Part I

4.1 Microfluidic approaches for the generation of ECM-based droplet-stabilized protein microcapsules (dsProCaps)

In the following sections, I describe the results pertaining to the formation and comprehensive characterization of cell-laden protein microcapsules that I accomplish in the context of this thesis. Figure 42 represents a general overview of the modular approach that enables the establishment of cell-laden ECM-protein-based microcapsules. I design and implement a modular droplet-based microfluidic platform that produces a technology to encapsulate, manipulate, and monitor proteins and cells within water-in-oil polymer-stabilized droplets. Finally, I release these protein-based capsules into physiological conditions and characterize their biophysical properties marking the completion of the development of this approach. Future uses and applications of this new biomedical tool-set is discussed in Chapter 6 Outlook.

To form the simplest version of the droplet templates that this new technology is based on, I use a single inlet droplet production microfluidics device whereby proteins and ions are premixed in the aqueous phase for encapsulation while the oil phase comprises different mixtures of neutral and charged fluorosurfactants dissolved in fluorinated oil. Different types of ECM proteins are attracted to the inner droplet periphery by charge mediated interactions which yield so-called **d**roplet-**s**tabilized **pro**tein micro**cap**sules (dsProCaps). I implement two different device architectures to produce cell-laden dsProCaps. Incorporation a cell encapsulation module requires a slightly more sophisticated device as premixing of ECM proteins and cells cause excessive interaction of proteins and proteins, leading to a lower concentration of free protein to assemble dsProCaps. Taking advantage of the laminar flows in the microfluidic channels[237], a double aqueous inlet device is therefore designed and implemented to minimize the exposure of proteins and cells prior to their co-encapsulation. As an alternative approach a pico-injection microfluidic unit may also be used to inject cells into the preformed dsProCaps. Following the successful formation of cell-laden or empty dsProCaps, protein

microcapsules (ProCaps) are released from the stabilizing surfactant layer into physiological conditions. This is achieved by either using a microfluidic release device, where capsules are released separately or in a bulk release approach which happens off-chip.

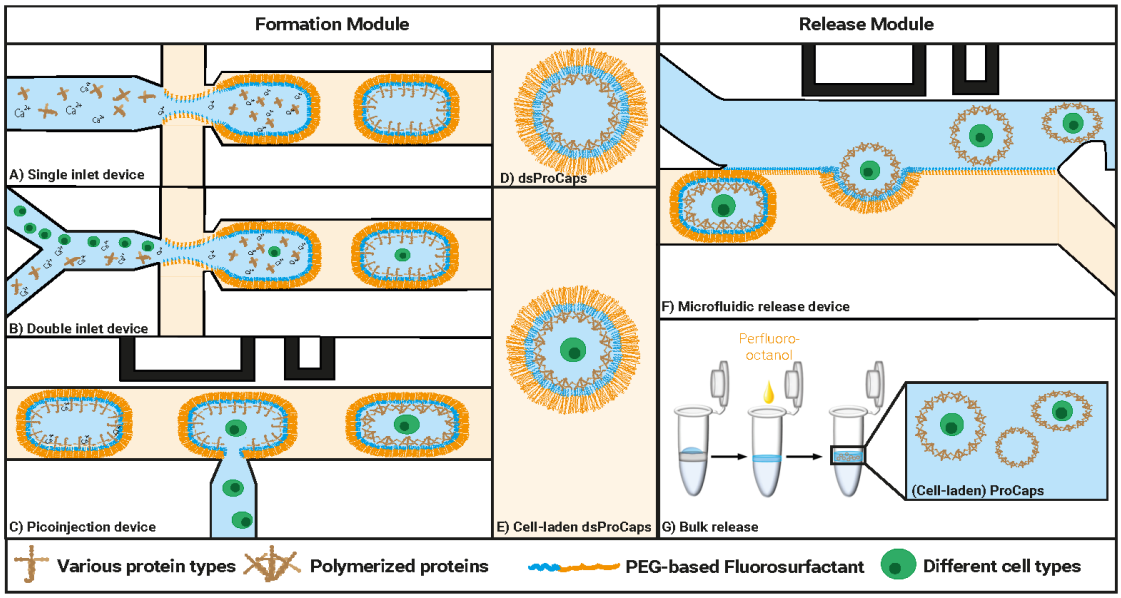

Figure 42 Schematic representation of modular droplet-based microfluidic technology for the charge-mediated assembly of empty or cell-laden protein capsules.
Formation Module. A) Formation of droplet-stabilized protein microcapsules (dsProCaps) can be performed by using single inlet devices. Proteins and divalent ions are diluted in the same aqueous phase and encapsulated in water-in-oil droplets stabilized by charged fluorosurfactants dissolved in fluorinated oil. D) The proteins are attracted to the periphery by charge-mediated interactions and crosslinked by calcium ions. B) Cell-laden dsProCaps can be produced by two different approaches. In a parallel flow, cells and proteins/ions are introduced in a double inlet device consisting of two aqueous inlet channels and being encapsulated. C) The second approach is to produce first the dsProCaps and pico-inject cells and ions into the preformed dsProCaps. Following the injection of cells and ions the proteins undergo polymerization on the inner droplet interface (E; cell-laden dsProCaps). Release Module. Upon the polymerization of the proteins two different methods can be applied to release the protein microcapsules (ProCaps) from the oil phase into an aqueous environment. F) By using a microfluidic release device, droplets can be released individually into a parallel aqueous phase under the influence of an electric field. G) In a bulk release approach many ProCaps are released simultaneously in a one pot procedure. This is achieved by chemical destabilization of the fluorosurfactant layer at the droplet interface with perfluoro-octanol.

4.2 Generation of ECM-based droplet-stabilized protein microcapsules (dsProCaps)

The very first step in assembling ECM-based microcapsules is producing a supporting scaffold out of fluorosurfactants facing into the inner surface of the droplets such that ECM-proteins may ionically interact and form a nucleation point that then lays the foundation for the protein capsule. The different device geometries to achieve such a scaffold are described in section 3.1.1 Microfluidic device fabrication. To now describe the chemistry more specifically, the oil phase consists of Poly(ethylene)glycol-Perfluoropolyether (PEG-PFPE) and Krytox™ dissolved in Hydrofluorether (HFE)-7500. Native tissues in the body are composed of varying degrees of a variety of proteins.[3,306] Therefore, I narrow down the design of my studies around the most commonly used ECM proteins for *in vitro* cell cultures, that being laminin-111, fibronectin and the well-known ECM substitute, Matrigel®. Matrigel® is composed mostly of laminin-111 and collagen type IV.[304] The selection of these ECM proteins is important for the two following reasons. First, the assembly of microcapsules consisting solely of ECM proteins has not been shown in literature so far, making the proteins relevant and interesting building blocks. Second, ECM molecules provide strong interactions with cells and trigger various intracellular activation pathways upon cell-ECM contact.[33,92] By establishing a 2.5D environment out of ECM molecules, I will gain an understanding for the behavior of cells upon interaction with ECM components from multiple sides.

The water phase of the droplets varies depending on the protein of choice and an associated polymerization factor (Figure 43A). In the case of laminin-111 and the laminin-111/collagen IV mixture (Matrigel®), $CaCl_2$ is needed for the polymerization[307] while fibronectin is polymerized in a transglutaminase 2 and dithiothreitol (DTT) solution, mixed with NaCl and $CaCl_2$.[57] The formation of protein capsules, rather than gel-like solid structures, necessitates additional charge-mediated interactions between the proteins and the inner droplet periphery. Towards this end, Krytox™ surfactant molecules orient at the water-oil droplet

interface based on hydrophobicity and importantly create a negatively-charged droplet periphery (Figure 43A1). This net-negative charge on the inner droplet periphery attracts first positively charged Ca^{2+} ions (Figure 43A2) and subsequently negatively charged ECM proteins. Over time and under physiological conditions (37 °C, 5% CO_2), the proteins align at the inner periphery of the droplet (Figure 43A3) where polymerization occurs (Figure 43A4). The modularity of the devices and droplet-based emulsion chemistries developed in this thesis require thorough characterization to obtain a mechanistic and well characterized understanding of the formation of protein capsules. As the formation of the surfactant layer supplies the charge-mediated formation of the protein capsules and lays the foundation for the protein scaffold itself, I investigate different Krytox™ and PEG-PFPE surfactant ratios (Supplementary Figure 1) to optimize this important first step.

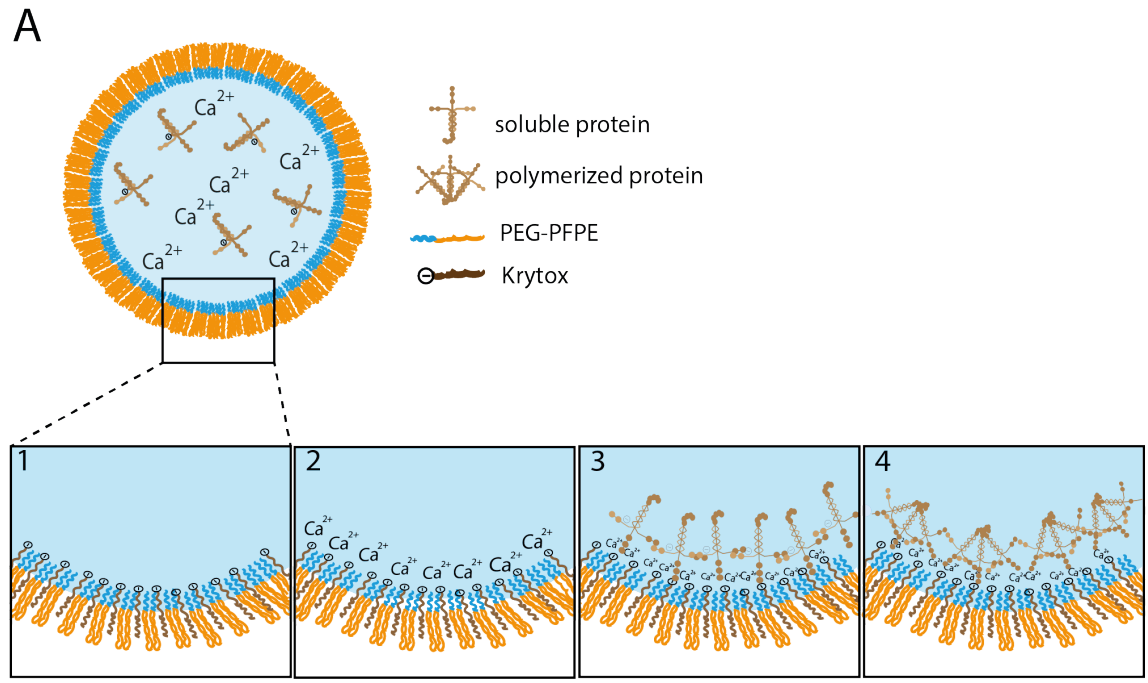

Figure 43 Charge-mediated attraction of protein molecules to the inner droplet periphery.
A) All components for a successful attraction of the protein to the periphery are encapsulated within water-in-oil droplets. 1) The oil phase consists of PEG-PFPE and Krytox™ fluorosurfactants contributing to the stability of the droplet and introducing a negative charge to the water-oil-interface. 2) A positively charged Ca^{2+} ions layer is created by the attraction of those ions to the negatively charged periphery. 3) Negatively charged laminin is attracted to the positively charged Ca^{2+} layer. 4) The Ca^{2+} ions are also required for polymerization of laminin at the periphery.

In Figure 44Ai-Ci, the representative confocal fluorescence microscopy images of dsProCaps consisting of either laminin-111 (A), fibronectin (B) or Matrigel® (C) are presented. The images are taken directly after production of the droplets, indicating fast charge-mediated attraction of proteins to the periphery, proven by the insets which represent the fluorescence intensity distribution profiles of the accumulated protein. The peaks represent the successful attraction of the protein to the periphery with very low amount of protein remaining in the center of the droplet. Incubating the droplets for 24 h and repeated intensity profiles measurements allowed for the same observation (Figure 44Aii-Cii). The graph in Figure 44D depicts the general attraction intensity of the proteins to the inner periphery over time. Laminin-111 attraction is increased over time, while fibronectin and Matrigel® are attracted immediately and do not allow for further protein accumulations. Interestingly, laminin-111 and Matrigel proteins have a higher attraction to the inner droplet periphery compared to fibronectin because the mean grey values of fibronectin are lower when compared to the other two proteins. I postulate that this difference is caused by the variation in protein conformations between laminin, collagen and fibronectin.

To demonstrate that the attraction of the protein to the periphery is not an artifact of surface tension or non-specific interactions, I encapsulate Matrigel® with their polymerization factors inside water-in-oil droplets stabilized with PEG-PFPE but lacking Krytox™. By confocal fluorescence microscopy I could observe an aggregation of protein-$CaCl_2$ molecules in the water compartment (Supplementary Figure 2).

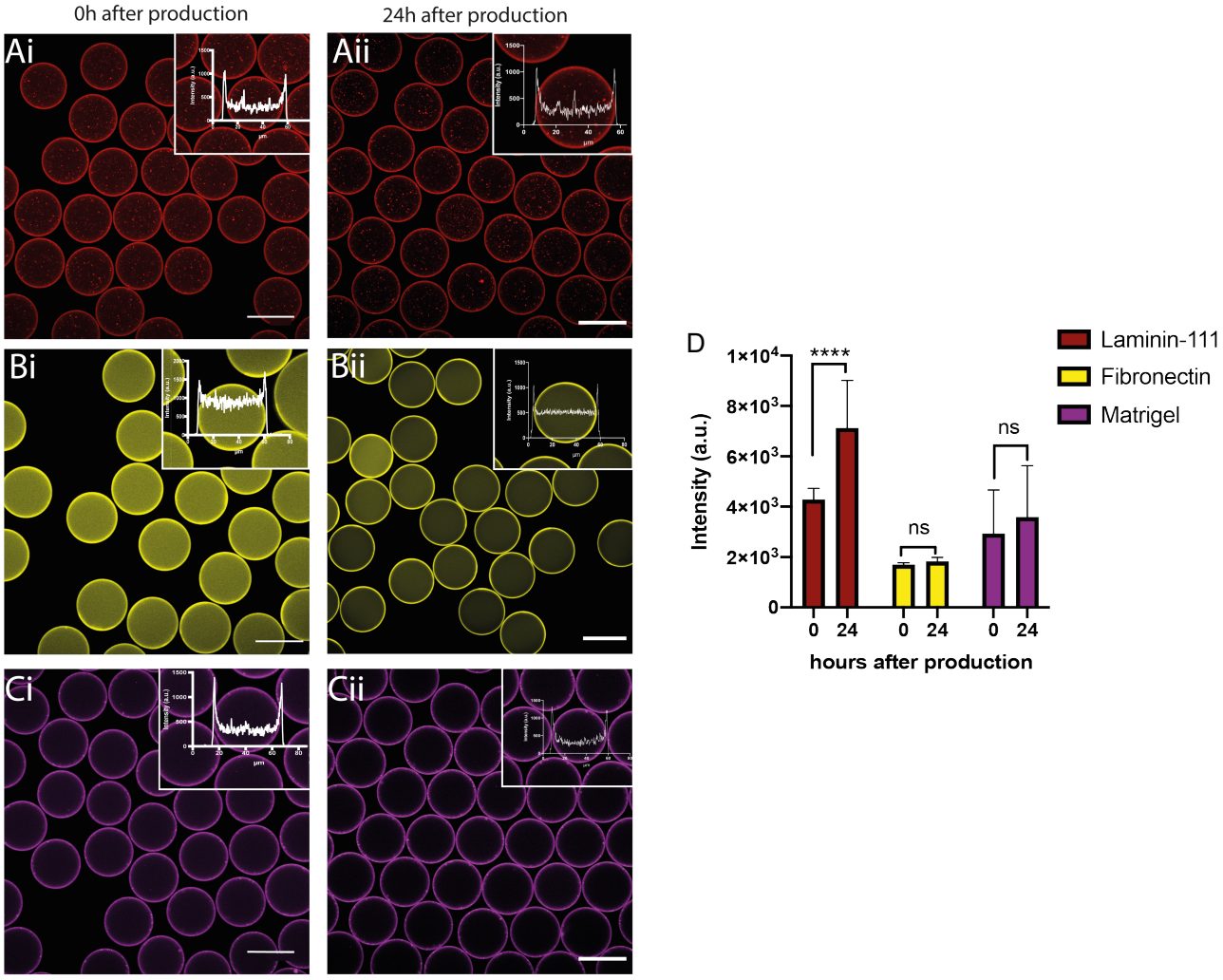

Figure 44 Krytox™/PEG-PFPE surfactant stabilized dsProCaps.
ECM-protein coated droplets establish a homogenous distribution of laminin-111 (Ai), fibronectin (Bi) or Matrigel®(Ci) after production or after 24 h (Aii, Bii, Cii) on the inner periphery of the droplet. Scale bar, 50 µm. D) Analytical comparisons are provided for each protein at both timepoints (0 h and 24 h) after production. Error bars are representing standard deviation. Two-way ANOVA, LN: p<0.0001, FN: 0.9958, MG: 0.7327.

4.2.1 *Production of small dsProCaps by emulsification*

After the successful attraction of proteins to the inner periphery, the next investigation is to test various droplet sizes, which enables a deeper understanding for the kinetics and functionality of the system. Further, smaller protein capsules could be used for various biomedical applications, such as the delivery of drug molecules. Using an emulsifier instead of a microfluidic droplet generation device, high shear forces are introduced to the protein-oil mixture in bulk, which allows for

a fine dispersion of protein-containing droplets in oil[257] (Experimental Section 3.5.3 Generation of negatively and positively charged small dsProCaps). The driving mechanism of generating small ECM-based droplets is based on the same charge-mediated mechanism as for the larger dsProCaps. Figure 45 shows confocal fluorescence microscopy images and depicts the successful attraction of laminin-111 (Ai), fibronectin (Bi) and Matrigel®(Ci) after production to the inner periphery of droplets with 5 – 20 µm in diameter, highlighted by the intensity profile insets. Low intensity values in the center for laminin-111 (A) and Matrigel® (C) droplets are visible, an in parallel the protein is strongly attracted to the inner periphery proven by the height of the spatially encoded intensity peaks. In the case of fibronectin (Figure 45B inset) the intensity values do not drastically decline between the intensity peaks, indicating remaining protein in the center of the droplet. This observation is also underlined by the low attraction intensity values to the periphery of the droplet (Figure 45D). Interestingly, observing the droplets after 24 h again, the intensity of Matrigel® declines, while laminin-111 and fibronectin are attracted immediately and do not change over time. The reason for this observation is not known currently.

It is important to mention here, that the concentration of the proteins was scaled to account for the reduced droplet sizes, but despite the lowered protein concentrations, the overall intensities of e.g. laminin-111 dsProCaps are higher (intensity value $2x10^6$) than in 30 µm sized droplets (intensity value $6x10^3$). The increased intensities correlate with the smaller droplet size, leading to the assumption that the attraction mechanism is enhanced by shorter adsorption depths, which the proteins need to overcome in order to align at the periphery. Another hypothesis is that the charge-mediated attraction is enhanced, with the charges of the proteins and the periphery being closer to each other. Both hypotheses taken together might account for the elevated protein attraction in smaller dsProCaps.

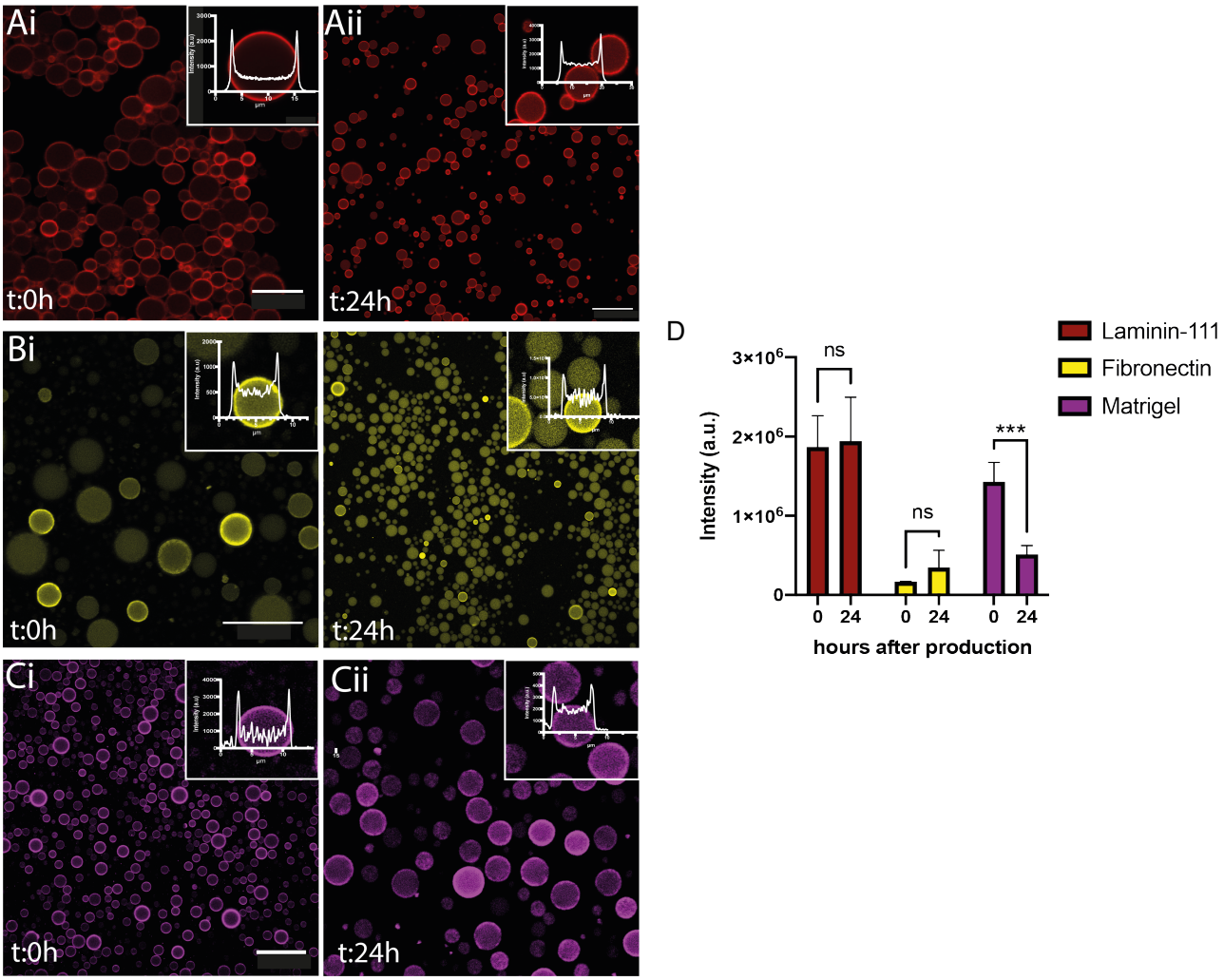

Figure 45 Small ECM-protein based water-in-oil droplets.

Three different types of proteins are attracted to the periphery of surfactant-stabilized water-in-oil droplets (A, laminin-111; B, fibronectin; C, Matrigel®) and imaged after 24h again. The insets of each class of protein depict the intensity values of proteins attracted to the periphery. Scale bar, 30 µm. D) Intensity comparison between differently sized dsProCaps. Mean gray values are plotted against the incubation time of dsProCaps made out of laminin-111, fibronectin or Matrigel®. Error bars are representing standard deviation. LN: p>0.999, FN: p> 0.999, MG: p> 0.0003. n = 3 independent experiments, 50 droplets analyzed for each protein and time point.

4.3 Analysis of the Mechanical Properties by Rapid Microfluidic-Based Deformation of dsProCaps

A microfluidic deformation chamber device is a fast method to analyze the dynamic interfacial properties of droplets under flow conditions. Therefore, to understand the effect that proteins might have on the surface properties of the droplets two different experimental settings are designed and implemented. Laminin-111 is encapsulated into droplets with 1 w% PEG-PFPE and 5 mM Krytox™ in HFE-7500 and polymerized overnight prior to introduction into the droplet-deformation chamber device. Three different flow rate conditions are applied; 1) 1000 mbar droplets, 1050 mbar spacer oil, 2) 1000 mbar droplets, 1150 mbar spacer oil, 3) 2150 mbar droplets, 2000 mbar spacer. Figure 46A-C shows the representative brightfield time lapse images of laminin-111 dsProCaps deformation under the different flow rates. The deformation of all droplets is immense, with the third parameter settings being the harshest, nearly rupturing the droplets. The deformation of the droplets is transient over several chambers until they permanently rupture. Because of the unusual deformation morphologies observed, quantitative analysis is not feasible due to a lack of fit with deformation profiles that normally enable measurement of interfacial tension changes. Figure 46D shows the control experiment with a standard water-in-oil droplet and the related deformation morphologies that are suitable for the computational analysis. Observing the immense deformation of dsProCaps produced 24 h prior to the deformational experiments, I set out to investigate the effects of soluble proteins inside water-in-oil droplets before the potential interactions with the periphery affect the deformability of the inner aqueous phase of the droplet. Therefore, the deformation chamber is used to produce the droplets on-chip and test the deformation before polymerization of the proteins occur. However, for the questionable droplets depicted in Figure 46E the results are difficult to be confident in. The polymerization of the protein helped with the shape of the droplet, while the soluble and unpolymerized proteins turned the construct into rods rather than droplets. Interestingly, the rod structures stayed in those shapes and are pushed

from one chamber into another. This leads to the assumption that the deformational forces from the microfluidic device affect the protein polymerization inside the droplets, potentially creating a viscous gel. In order to understand the interplay between the proteins and the surfactants in more details, I conducted FRAP measurements.

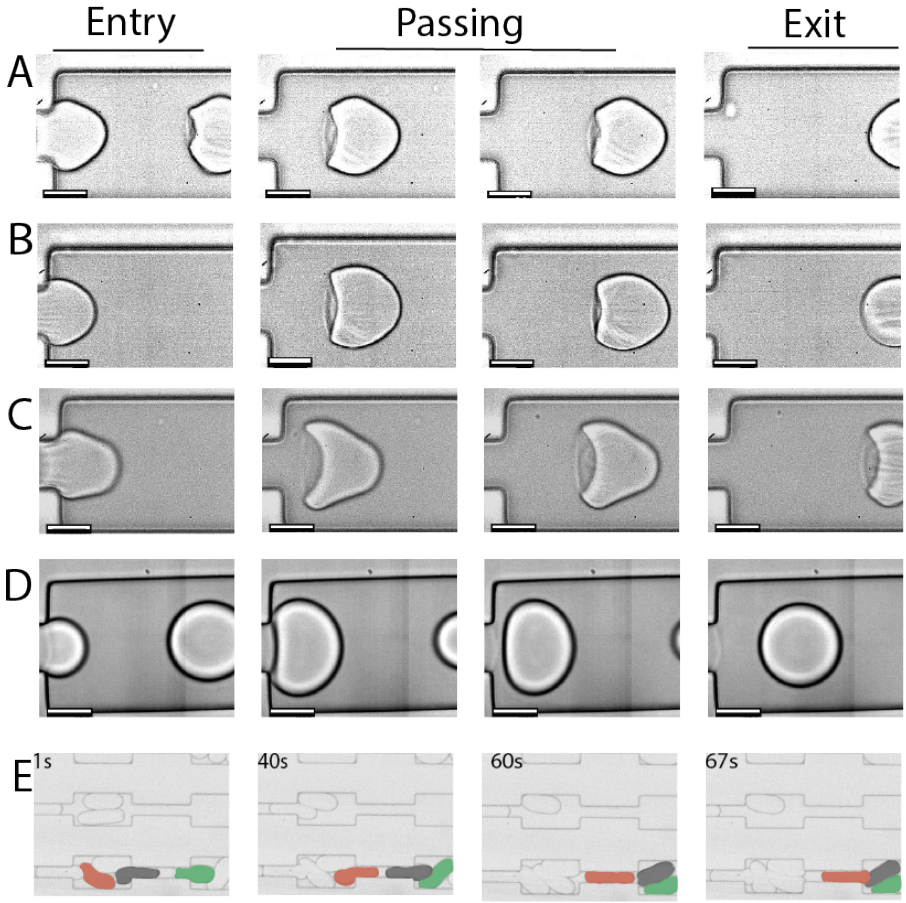

Figure 46 Deformation experiment of dsProCaps with a microfluidic deformation device. Laminin-111 droplets are produced the day before and introduced to the system with the following flowrates A) 1000 mbar droplets, 1050 mbar spacer oil, B) 1000 mbar droplets, 1150 mbar spacer oil, C) 2150 mbar droplets, 2000 mbar spacer oil. D) Simple water-in-oil droplets as control for the deformation introduced with 1000 mbar and separated with 1050 mbar. Scale bar, 10 µm. E) Laminin-111 droplets are produced on the deformation chamber device. Rod-shaped structures are pushed through the channels (green, red, black colored brightfield image).

4.3.1 Measuring protein diffusivity in dsProCaps by FRAP

The surprising results obtained from the previously described deformation experiments, lead me to the investigation of protein diffusivity at the periphery of the established dsProCaps. In order to investigate the movements of proteins I conducted FRAP measurements. I set out various conditions to analyze the behavior of the proteins 1) directly after production, 2) after several hours of incubation at 37 °C and 3) under the effect of the polymerization factors. First, I generate dsProCaps as previously stated, containing laminin-111 and 10 mM $CaCl_2$ in PBS as the appropriate polymerization buffer (Experimental Section 3.7 FRAP measurements). However, the first attempt showed no recovery of fluorescent laminin-111 (Supplementary Figure 3). This phenomenon is explained by the immediate attraction and interaction of the protein to the negatively charged periphery of water-in-oil droplets as already seen in Figure 44. Further the attracted proteins might interact strongly with the Krytox™ molecules, hindering free proteins to be exchanged at the periphery. Based on this fundamental observation, a different question is raised. Can the immediate accumulation of the protein at the periphery be set in relation to the polymerization of the protein? In order to answer this question, I encapsulate 70 kDa FITC-dextran molecules together with the labelled proteins to understand the diffusivity of such small molecules through polymerized protein meshes. If no polymerization is present, I expect a detectable recovery of the FITC-dextran molecules. First, FITC-containing laminin-111 dsProCaps with $CaCl_2$ are measured directly after production, 2 h and 24 h after incubation at 37 °C. Not surprisingly, no recovery of the FITC-dextran molecules is detected, meaning that the proteins are fully polymerized (Figure 47). The protein meshes are hindering the molecules to diffuse freely throughout the droplets. To control the polymerization behavior, FRAP measurements are conducted on droplets containing FITC-dextran and labelled laminin-111, but lacking the polymerization factor $CaCl_2$. Surprisingly, also no recovery could be observed under this particular condition and the potential reason will be explained in Chapter 4.9 Analysis of pH in dsProCaps. Another interesting occurrence is the decrease of intensity over time. Having a closer look at the graph in Figure 47 shows

that the FITC intensity is lowered in droplets containing $CaCl_2$ at all time points and droplets missing $CaCl_2$ are also lower in intensity after 24 h. The potential reason for the loss in intensity is discussed in Chapter 4.9 Analysis of pH in dsProCaps.

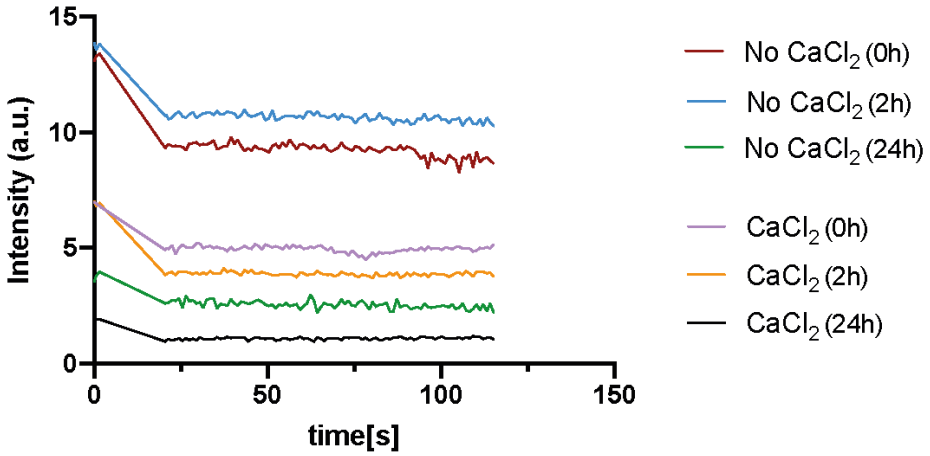

Figure 47 FRAP measurements inside dsProCaps.
Diffusivity of 70 kDa FITC-dextran molecules in laminin-111 containing dsProCaps stabilized with Krytox™/PEG-PFPE. No recovery of the bleached regions can be observed at any time point (0h, 2h, 24h) or polymerization condition (with or without $CaCl_2$). n = 5 measurements per each condition.

4.4 Generation of ECM protein-based microcapsules (ProCaps)

As the final intention for the protein capsules is to serve as a platform for the investigation of biophysical and biochemical properties of cell-ECM interactions, it is important that the ProCaps are situated in physiological conditions. Therefore, the assembled dsProCaps are released from the stabilizing oil-surfactant layer to an aqueous condition, which will enable nutrient and waste transport and facilitate a biocompatible environment for cells within the capsules. Towards this end, I design and implement several release approaches to determine the most efficient method for the formation of ProCaps.

4.4.1 Releasing ECM ProCaps with the bulk release approach

After polymerization of the proteins inside the droplet scaffold, I release the protein capsules into physiological media. The bulk release method allows for a fast and efficient release of capsules made entirely out of laminin-111 (A), fibronectin (B) or Matrigel®(C) (Figure 48). To optimize the release approach, laminin-111, fibronectin and Matrigel® dsProCaps are produced at stated before (Experimental Section 3.5 Generation of ECM-based dsProCaps) and released at several time points to finally release stable ECM-protein based microcapsules (Supplementary Figure 4). The most efficient time point to release stable laminin-111 ProCaps, is determined to be directly after production and after incubating the droplets for 2 h at 37 °C. This observation is in line with the conducted FRAP measurements for laminin-111. Protein polymerization occurs instantly and is sufficient for the release of ProCaps without incubation at 37 °C. The reason behind this observation is stated at Chapter 4.9 Analysis of the pH inside dsProCaps. Interestingly, fibronectin and Matrigel® ProCaps are established after 4 h of incubation. Moreover, ProCaps cannot be released after the mentioned time points. The reason for this specific phenotype is highlighted in Chapter 4.4.3 Observing the release of ProCaps. For all three types of protein microcapsules, characteristic filamentous polymerization patterns are visible. Brighter and more dense areas of protein accumulation are visible in all three cases, which leads to the assumption of the formation of a porous capsule structure. Because of the lack of additional polymeric support, the purely protein-based capsules keep a rounded shape, however, collapsing of the capsules upon release and contact with the glass observation slide.

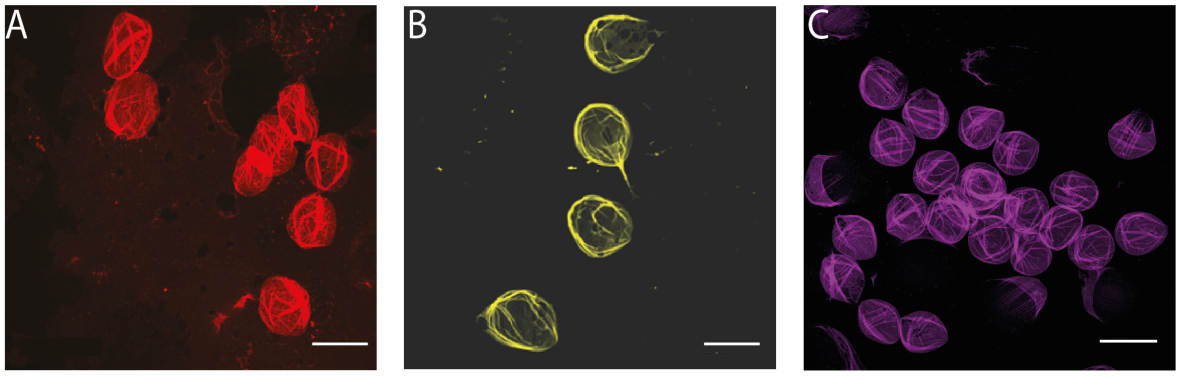

Figure 48 ECM-protein based microcapsules (ProCaps).
Laminin-111 (A), fibronectin (B) and Matrigel® (C) microcapsules are released out of oil phase and the surfactant stabilizing layer. The observed fibrillar structures indicate the effective polymerization of the proteins, which helps maintaining the round shape of the capsules. Scale bar, 30 µm.

4.4.2 *Release of small dsProCaps by using different release approaches*

After the establishment of small dsProCaps by means of an emulsifier, I set out to produce small ProCaps using two different release approaches, the bulk release approach and a circular release device (Chapter 3.1.4.2 Circular microfluidic release). Figure 49A-C depicts the successful release of small capsules based on laminin-111, fibronectin and Matrigel® respectively. In the case of laminin-111 and fibronectin, the small capsules are connected to each other via protein nets. Those nets are consisting of polymerized proteins, which did not assemble at the inner periphery of droplets to establish ProCaps. The emulsification process produces droplets in a heterogeneous size range (Figure 45) and because the encapsulated protein concentration is decreased, to establish protein microcapsules with approximately 10 µm in diameter, likely not enough protein is available to be attracted to the inner periphery of droplets with larger diameters. This leads to the consecutive polymerization of the proteins based on $CaCl_2$ and temperature in the water compartment of the droplets, however, the amount of protein is not sufficient to be attracted to the periphery and generate stable ProCaps. This leads to the release of protein nets around successfully established small ProCaps. In the

confocal fluorescence micrographs in Figure 49A-C, white arrow heads are indicating small capsules for all three protein types.

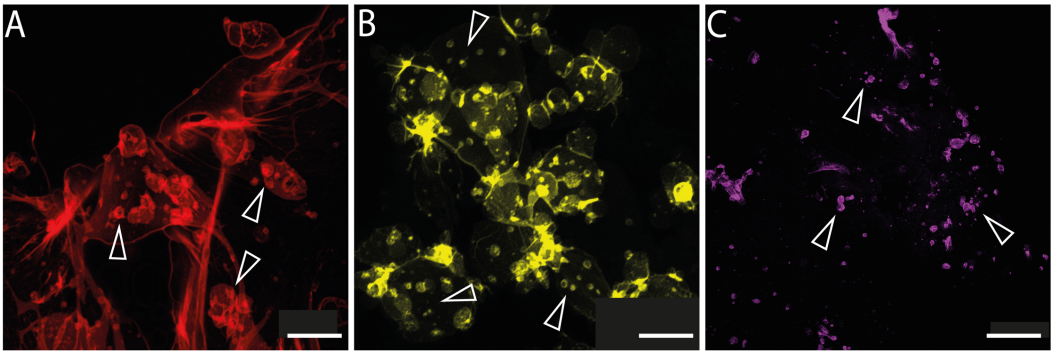

Figure 49 Small ECM-protein based microcapsules (ProCaps).
Laminin-111 (A), fibronectin (B) and Matrigel® (C) small ProCaps are indicated by white arrow heads. Protein networks are connecting the small individual capsules with each other. Scale bar, 20 µm.

Since the emulsification method allows for the generation of a high number of dsProCaps in a relatively short amount of time (Figure 40), the newly designed release device is implemented (Chapter 3.1.4.2 Circular release) to accelerate the release process. The design is a combined version of the bulk release approach on a microfluidic chip. Hereby, the release of ProCaps is facilitated in a fast manner. I introduce the droplets and the destabilizing agent (PFO) through the inner inlets and establish the release media flow from the outer side. By this technique, I increase the droplet contact and duration with PFO, which destabilizes the outer oil-shell layer (Supplementary Figure 5A). Upon interaction with the release media, the destabilized droplets fuse and release their content into the release media, which flows in the same outlet channel as release media droplets (Supplementary Figure 5B). Additionally, an electric field is introduced to support the fusion to the release medium (Supplementary Figure 5C). The collection outlet is the same for the protein capsules and the remaining surfactant molecules and both phases are collected together. However, collecting the ProCaps becomes feasible by the phase separation of the oil and the aqueous phase inside the collection tube. Supplementary Figure 6 depicts small laminin-111 and Matrigel® protein microcapsules, proving for the successful implementation of the release device. Comparing these resulted capsules to ProCaps established with the bulk release

method, no difference in quality of the capsules can be determined. The major advantage of this method over the conventional bulk release approach is reflected in the high number of protein capsules released in a much shorter time.

4.4.3 Observing the release mechanism of ProCaps

The implementation of a different release approach inspired the direct observation of the particular process. To observe the release of capsules, a cell culture dish is filled with the destabilizing agent (Perfluoro-octanol, PFO) and covered with a release media of interest. Previously produced droplets as stated in Chapter 3.5 Generation of ECM-based dsProCaps, are loaded at the bottom of the well and because of their density, the water-in-oil droplets float to the interface between water and oil in the dish. With a water-immersion objective the release process of laminin-111 capsules is observed (Figure 50A). Since the release process is rapid, the focus of the objective is placed at the water phase (Figure 50BI). After 40s (Figure 50BII) the droplets become unstable and the protein capsules are released. The process ends after roughly 300s, as soon as the characteristic capsule structures are visible (Figure 50BIV). However, with this release process it is not possible to transfer the established capsules from the water phase to a glass cover slide without damaging the capsules. The interactions between the capsules and the oil phase are too strong for a safe removal. This release process shows that all capsules are released out of their stabilizing oil shells, but due to the strong Krytox™-protein interactions, the majority of the capsules stay at the interface and hence, are lost. This is the main reason why the time point of release is of utmost importance, to yield the highest number of successfully released droplets. Longer incubation times strengthen the Krytox™-Protein interactions and hindering a successful release (Supplementary Figure 4).

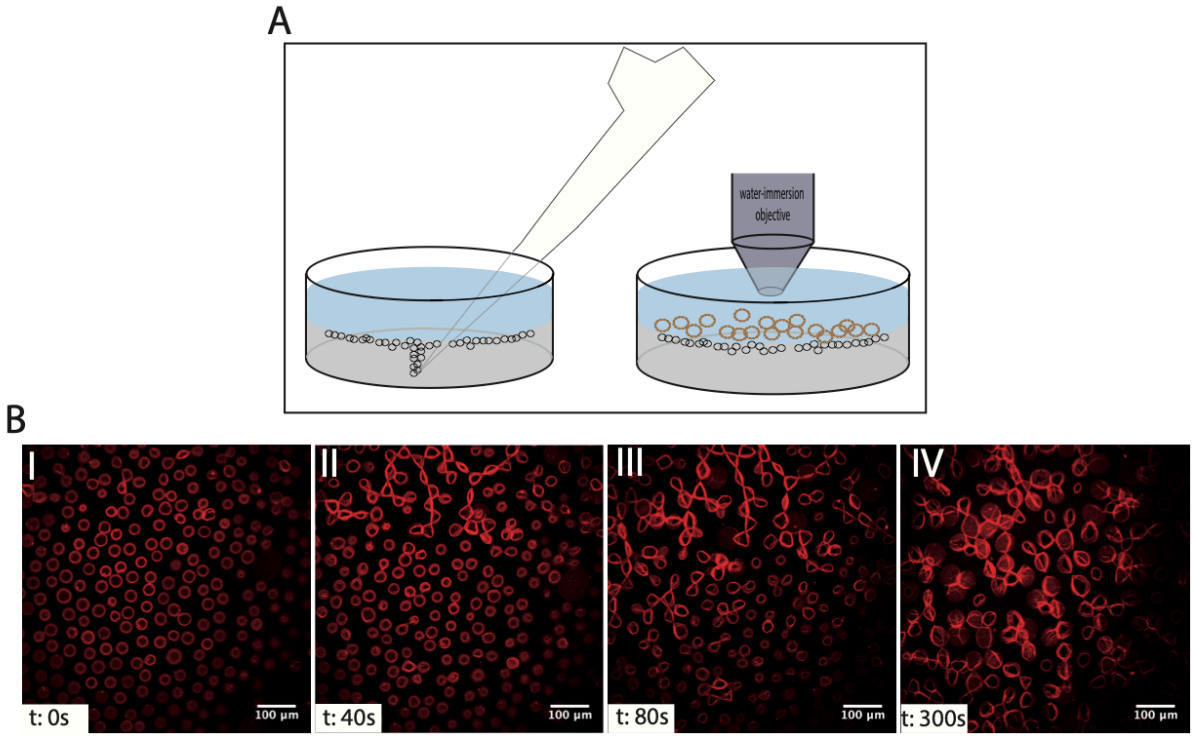

Figure 50 Observation of the release of protein-based microcapsules.
A) Experimental set up for the observation of the ProCaps release. Droplets are loaded into an oil phase, consisting of destabilizing surfactant diluted in HFE-7500 and covered with PBS. The release process is observed live with an upright water-immersion objective. BI) Droplets are visible in the oil phase. BII) After approximately 40s the microcapsules are released. BIII) During the release process, the proteins connect to the neighboring capsules, which are also released. BIV) The release process is completed after 300s.

4.4.4 *Release of ProCaps via a microfluidic parallel release device*

Another promising release approach is the use of microfluidic release devices (Experimental Section 3.12.3 Microfluidic release). Using a flow controller, the preformed dsProCaps are loaded into the microfluidic device and destabilized by an electric field, supported by a destabilizing agent in the droplet-separating channel. Due to destabilization of the surfactant layer the dsProCaps are fused with the parallel aqueous flow and release the polymerized ProCaps into an aqueous phase. The droplet is introduced to the system via the droplet insertion channel (Supplementary Figure 7-1), then the first contact between the droplet and parallel aqueous flow is generated (Supplementary Figure 7-2). Based on the electric field

and the destabilizing surfactant the droplet is ruptured and the content is released (Supplementary Figure 7-3). The oil waste and the released aqueous phase are collected separately (Supplementary Figure 7-4). In comparison to the bulk release approach, the microfluidic technique allows for the spatially separated release of capsules, however, it is more time consuming and complicated in the set up. The established capsules do not differ in appearance when released by the bulk release approach or the microfluidic device (Supplementary Figure 8).

4.4.5 Characterization of ECM ProCaps

Following the formation of ProCaps I set out to establish several methods for their biochemical, structural and mechanical characterization. Two different experiments are conducted in order to visualize the general structure. In the first experiment I stain the ProCaps with appropriate antibodies. The other characterization method focuses on the pore size of the capsules by encapsulating FITC-dextran of different molecular weights and observe I aim to understand the mesh size of the capsules, by the retention or release of the FITC-dextran molecules.

4.4.5.1 Immunofluorescence staining for complete ProCaps visualization

The ECM microcapsules are produced with 10% labelled protein and a porous shape is apparent upon release (Figure 48). However, to discover the actual structure of the capsules, I develop an antibody staining protocol to obtain a clearer representation of the total proteinaceous structure. The detailed staining protocol is described in the section 3.13.1 Immunofluorescence staining of ProCaps. Briefly, in the case of laminin-111 microcapsules, the protein is stained with an anti-laminin antibody (Figure 51A) and detected with an AlexaFluor 488-secondary antibody (Figure 51Ai). It is clear, that the capsules are not completely represented by the initial 10% label. The overlay of the initial microcapsule and the antibody-stained image (Figure 51Aii) demonstrate a significant discrepancy in the amount of space contained by the protein. Although, some pores do remain between the densely

polymerized structures, leaving space for molecules and nutrients to pass through the protein membrane. Matrigel® capsules (Figure 51B) are stained with collagen IV antibodies (Figure 51Bi) since it mostly consists of collagen type IV and laminin-111. Here, I observed a similar structural assembly. Collagen IV molecules are not only detectable inside the polymerized areas (Figure 51Bii) but also fill most of the holes, which are normally observed, making the capsules less porous than assumed.

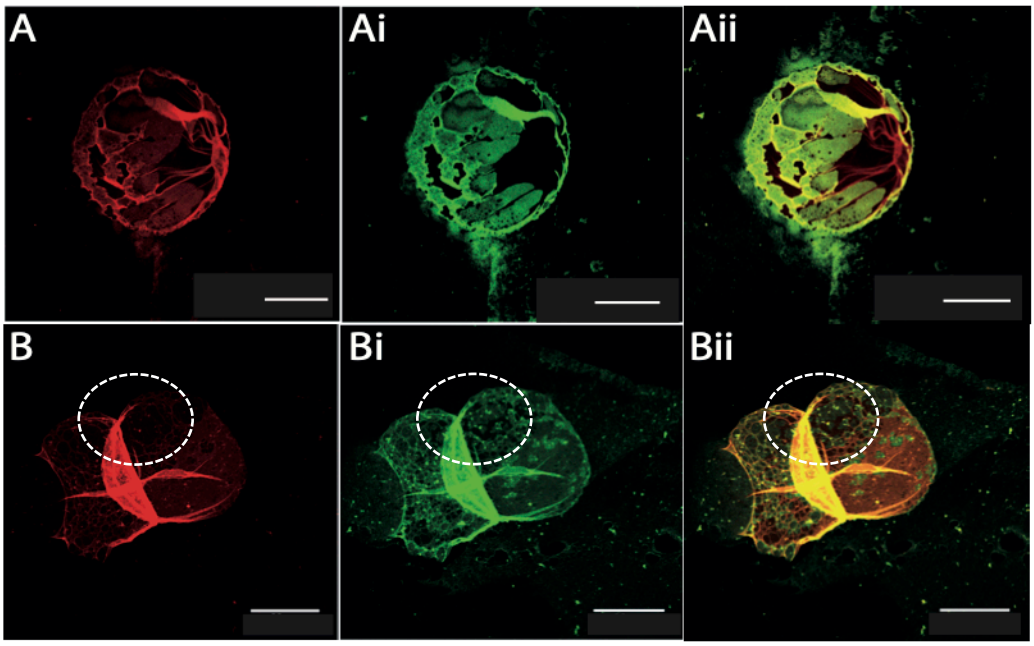

Figure 51 Antibody staining of ProCaps.
A) Laminin-111 capsules produced with 10 % labelled laminin (red). Ai) Laminin-111 capsules stained with an α-LN antibody. Aii) The overlay image highlights the porosity of the capsule, since the complete capsule is not stained. B) Matrigel capsules produced with 10 % labelled laminin (red). Bi) Matrigel capsules stained with an α-colIV antibody. Bii) The overlay image reveals that collagen type IV is intertwined deeply in the capsule wall (dotted circle). Scale bar, 30 µm.

4.4.5.2 ProCaps porosity investigation with FITC-dextran

After revealing the porosity of the capsules by an immunofluorescent staining, I design an investigation towards the actual mesh size of the ProCaps using FITC-dextran of various molecular weights. First, 4k FITC-dextran or 70k FITC dextran are encapsulated together with the proteins in the water phase and droplets are produced as previously described (Experimental Section 3.13.2 FITC-dextran release studies). The droplets are imaged by CLSM directly after production and

the mean intensity values of 4 kDa FITC and laminin-111(A), fibronectin(B), and Matrigel®(C) (Figure 52, t: 0 h) or 70 kDa FITC (Figure 53, t: 0 h) are measured using Fiji software. After 24 h of incubation at 37 °C the proteins are still assembled evenly at the droplet periphery and importantly FITC-dextran is still homogenously distributed inside the droplet. This observation shows that these molecules do not interfere with the dsProCaps generation and are not binding to the protein, which would falsify the results. The 4 kDA FITC fluorescence intensity decreased slightly in case of Matrigel® overnight, however no diffusion to the oil phase is detected. Surprisingly the 70 kDa FITC-dextran fluorescence intensity values inside fibronectin dsProCaps decreased while it did not change in laminin-111 and Matrigel® dsProCaps. A potential reason for this phenomenon might be the pH reactivity of FITC.

Following the assembly of FITC-dextran-loaded dsProCaps, I release the protein capsules and capture an overlay confocal fluorescence micrograph of the proteins and the FITC-dextran. The observation reveals no retention of 4 kDa FITC-dextran in the ProCaps made of laminin-111, fibronectin and Matrigel® (Figure 54A, B and C). It is clearly visible that 4 kDa FITC-dextran is released out of the capsules and not aggregated within the droplet wall, since negligible fluorescence intensity, or values equal to background signal, is detected in the intensity graphs. However, the intensity values of 70 kDa FITC dextran are higher than the 4 kDa condition (Figure 54Ai, Bi, Ci). The peaks in the graphs showing protein aggregation of the capsule are also increased in the FITC plot, suggesting that higher amounts of the 70 kDa FITC dextran are retained inside the established ProCaps. This observation leads to the conclusion that the pore sizes of the established ProCaps are still bigger than the radius of gyration of 70 kDa FITC-Dextran molecules (7 nm), since only small amount of the molecule could be retained inside the capsules. To analyze the maximum size of the pores a further test is required, for instance using larger sized beads with known diameters on the micro-scale level. Important to the aim of this thesis, is that the pore-sizes of the capsules are such that encapsulated cells retain viability within the capsules, implying mass transport phenomena that supports nutrient supply and waste removal (see the following sections).

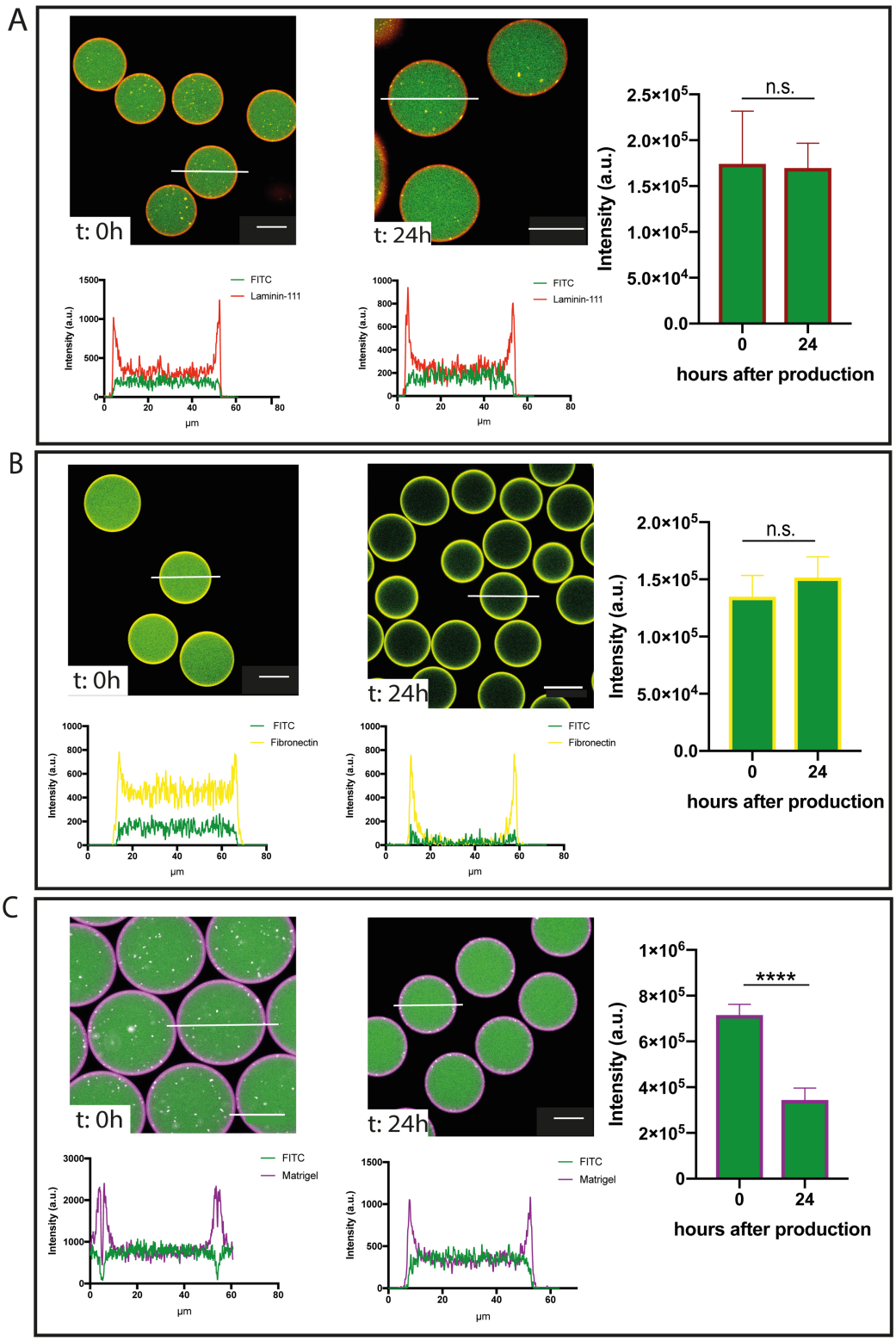

Figure 52 Encapsulation of 4 kDa dextran-FITC into protein droplets.
Laminin-111 (A), fibronectin (B) and Matrigel® (C) droplets directly after production and after 24h polymerization. Intensity graphs underneath the images show the grey values of the proteins and FITC-dextran for both time points. The graphs next to the images indicate the intensity of FITC-dextran over time. LN: $p = 0.9604$, FN: $p < 0.0827$, MG: $p < 0.0001$. Error bars are representing standard deviation. Scale bar, 30 µm.

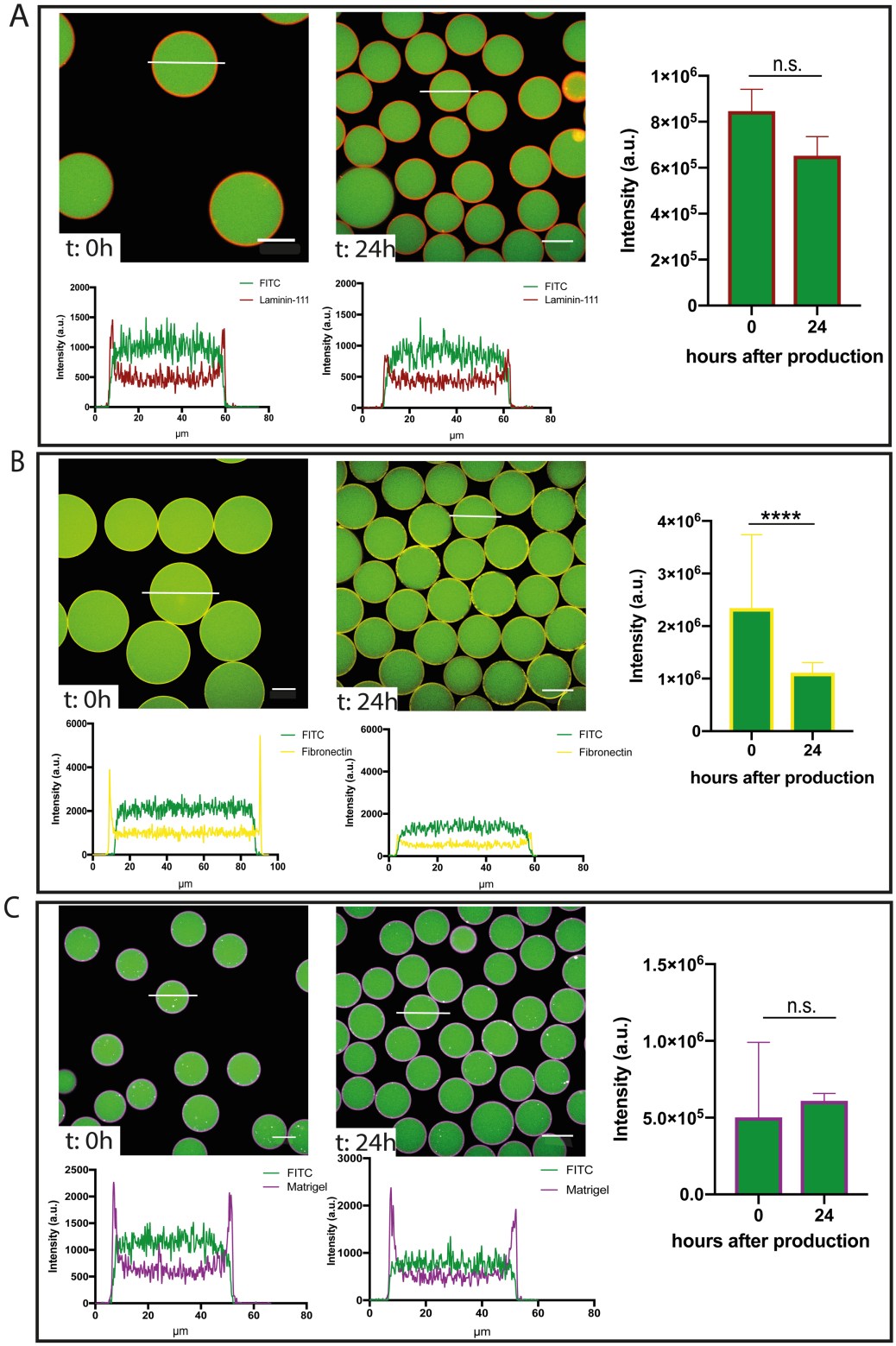

Figure 53 Encapsulation of 70 kDa dextran-FITC into protein droplets.

Laminin-111 (A), fibronectin (B) and Matrigel® (C) droplets directly after production and after 24h polymerization. Intensity graphs underneath the images show the grey values of the proteins and FITC-dextran for both time points. The graphs next to the images indicate the intensity of FITC-dextran over time. LN: $p = 0.1962$, FN: $p < 0.0001$, MG: $p = 0.6207$. FITC-dextran values are significantly decreased only when encapsulated with fibronectin. Error bars are representing standard deviation. Scale bar, 30 µm.

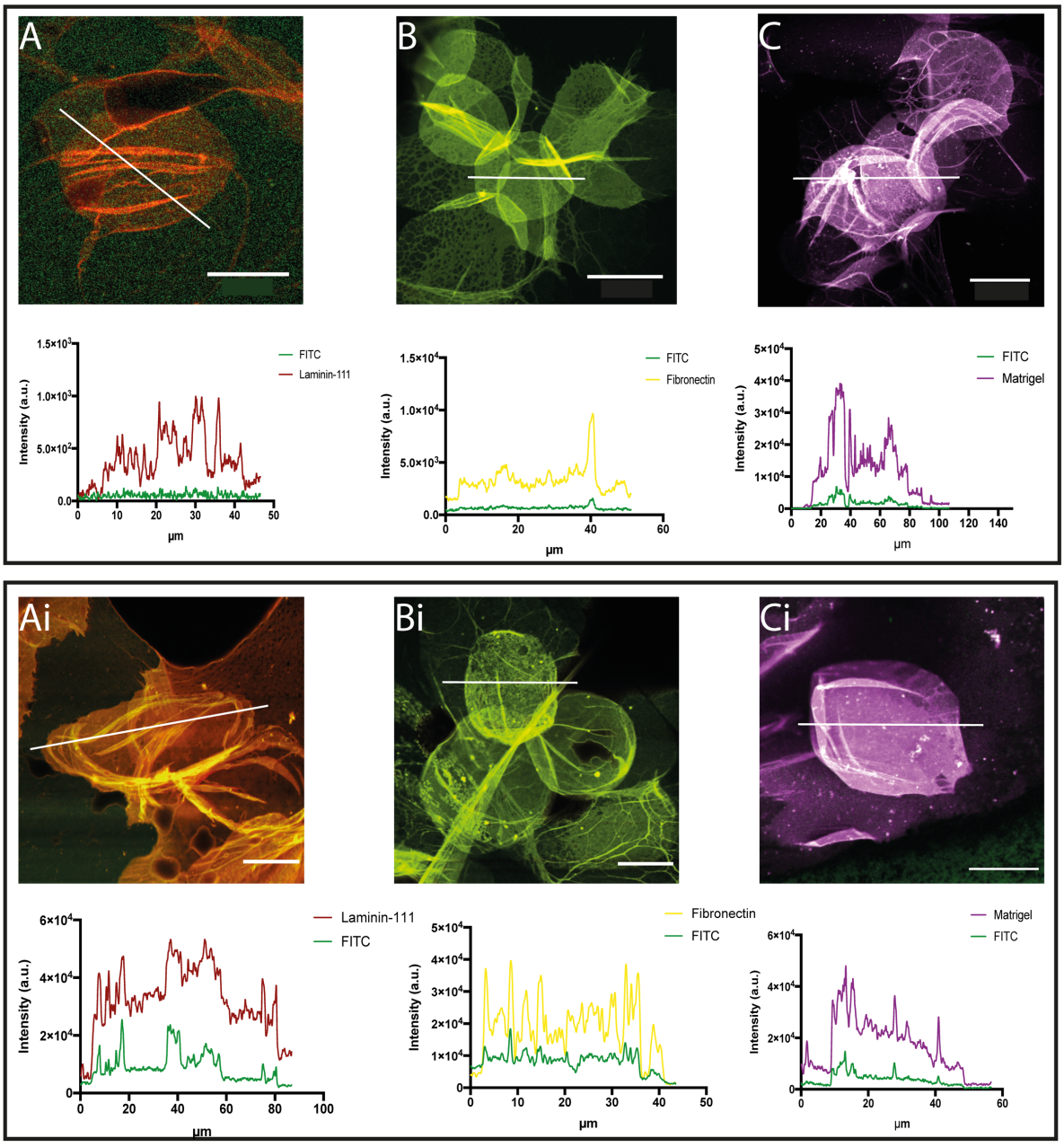

Figure 54 FITC-dextran loaded protein capsules with the according intensity graphs. Laminin-111 (A), Fibronectin (B) and Matrigel (C) ProCaps containing 4 kDa dextran FITC with the according intensity graphs. Laminin-111 (Ai), Fibronectin (Bi) or Matrigel (Ci) ProCaps containing 70 kDa dextran FITC with the according intensity graphs. Scale bars, 20 µm.

4.5 Encapsulation of various organisms inside ProCaps

To demonstrate the versatility of cargo-laden ProCaps, I start with incorporating two different organisms, namely *Escherichia coli* (E. coli) bacteria and Malaria Ookinetes, inside dsProCaps. Thereby, I investigate the interactions of different organisms with the proteins assembling the capsule's wall.

4.5.1 Pico-injection of Escherichia coli into dsProCaps and the sequential release of bacteria-laden ProCaps

By encapsulating *E. coli* cells, I evaluate the retention of a model bacteria strain within capsules. I consider two major aspects that will affect the successful formation of cell-laden ProCaps. First, due to potential affinity between bacteria and proteins, it could be necessary to minimize the exposure between bacteria and proteins prior to dsProCaps formation. Second, since the microcapsules are extremely robust after polymerization of the proteins, it is not possible to introduce any micro-scale organisms to the capsule without breaking its structure. Therefore, I implement a microfluidic pico-injection technology for the sequential delivery of bacteria into pre-polymerized dsProCaps (Experimental Section 3.16 Pico-injection of eukaryotic and prokaryotic cells into surfactant-stabilized droplets). This method enables the generation of water-in-oil droplets and facilitates injection of proteins, dyes or even living organisms in any aqueous solution on the same device (Figure 35). The working principle is based on an electric field, combined with narrow microchannels to stretch the droplet, specifically the water-oil interface. By this means, the wall is loosened and the inner aqueous phase fuses with the aqueous phase from the injection nozzle. The content is introduced into the droplet and the cell-laden droplet is collected. The major advantage of this device is that the proteins are attracted to the inner droplet periphery and are still soluble because the process is performed in the millisecond timescale. Supplementary Figure 9 shows the injection of a single droplet with *E. coli*. Supplementary Figure 9I shows the first contact between the droplet and the bacteria arriving from the injection channel. In

Supplementary Figure 9II, electric field-mediated fusion of the droplet aqueous phase with the aqueous phase from the injecting channel is shown. The pressure in the injection nozzle is adjusted so that a precise amount of aqueous phase is injected. Due to the relatively small size of bacteria in comparison to the device channel dimensions, it is difficult to observe the bacteria in the injection nozzle. For better observation, it would be possible to use a fluorescence microscope to observe the injection process, since the *E. coli* are fluorescently labelled. In Figure 55, I demonstrate several examples of the successful pico-injection of bacteria in dsProCaps. Figure 55 is depicting E. coli-containing droplets with three different types of ECM-proteins, laminin-111 (A), fibronectin (C) or Matrigel® (E). The overlay confocal fluorescence microscopy images illustrate the captured bacteria inside dsProCaps. These results reveal that encapsulated *E. coli* are not interfering with the charge-mediated mechanism of capsule formation, showing that proteins are attracted to the periphery regardless of cargo classification. This mechanism becomes more evident with the successful release of the microcapsules from the oil phase into physiologically relevant media. Figure 55 B, D and F are depicting E. coli-laden ProCaps, made out of laminin-111, fibronectin, and Matrigel®, respectively. To follow the movements of the bacteria on the inside of laminin-111 ProCaps, their trajectories are tracked using ImageJ analysis (Experimental Section 3.17 Trajectory Analysis of bacteria inside laminin-111 ProCaps). *E. coli* are captured inside capsules over several hours and trajectory tracking (of the first 10 min) shows that occasionally bacterial motility is hindered when in contact with the protein (Figure 56). Several bacteria demonstrate movement until becoming attached to the protein layer of the capsule shell. These exemplary bacteria are then not able to detach from the laminin-111 capsules anymore. These results indicate that laminin-111 capsules might be used as coatings on different materials to capture bacteria and hinder motility. Finally, these observations hint at a potential application in implantation medicine as a coating material.

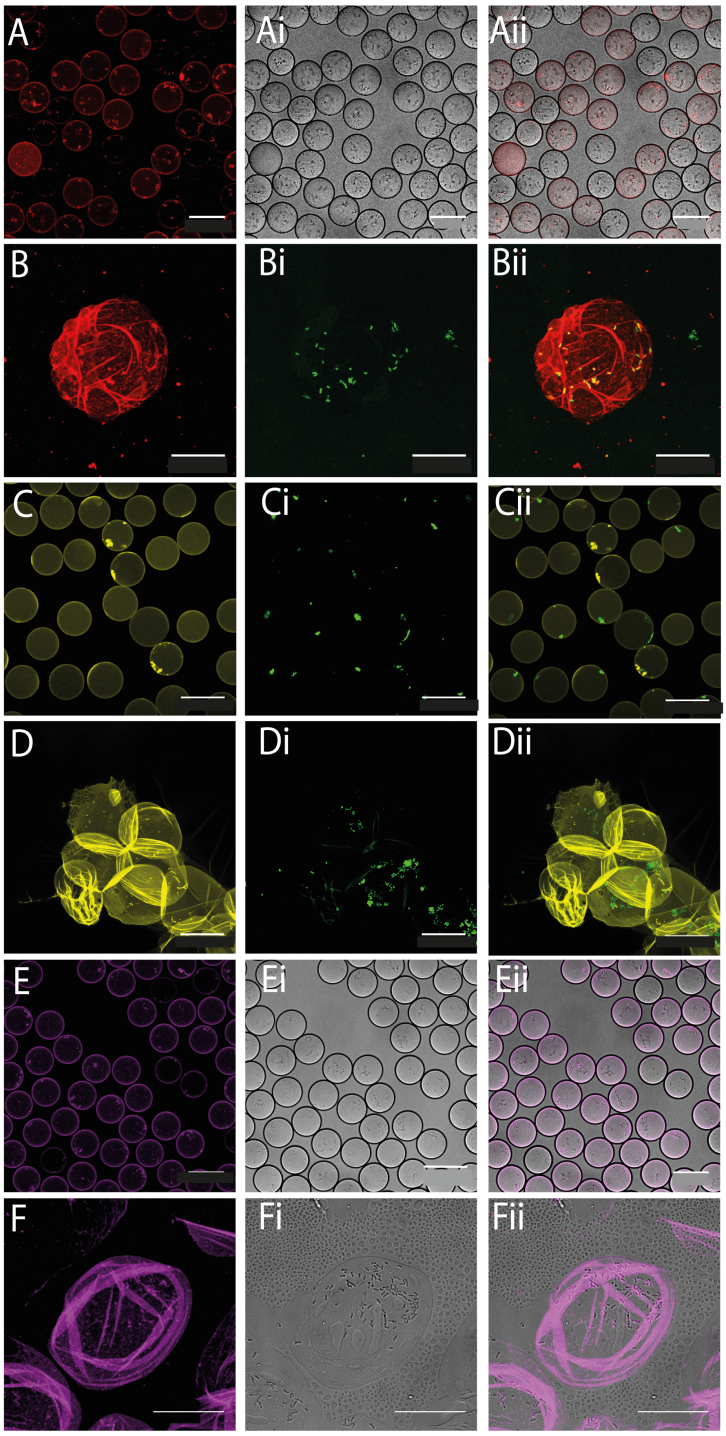

Figure 55 E. coli-loaded dsProCaps and ProCaps.
Laminin-111 (A), fibronectin (C) and Matrigel® (E) droplets loaded with E. coli by pico injection. CLSM images show the protein attraction to the periphery (A, C, E), with the brightfield image highlighting the E. coli (Ai, Ci, Ei). Aii, Cii, Eii) dsProCaps and E. coli overlay images depict the successful retention of E. coli (Aii, Cii, Eii). Scale bar, 50 µm. Laminin-111 (B), fibronectin (D) and Matrigel® (F) ProCaps. Bi, Di, Fi) Only GFP-E. coli. Bii, Dii, Fii). ProCaps and E. coli overlay images depict the successful encapsulation of E. coli. Scale bar, 30 µm.

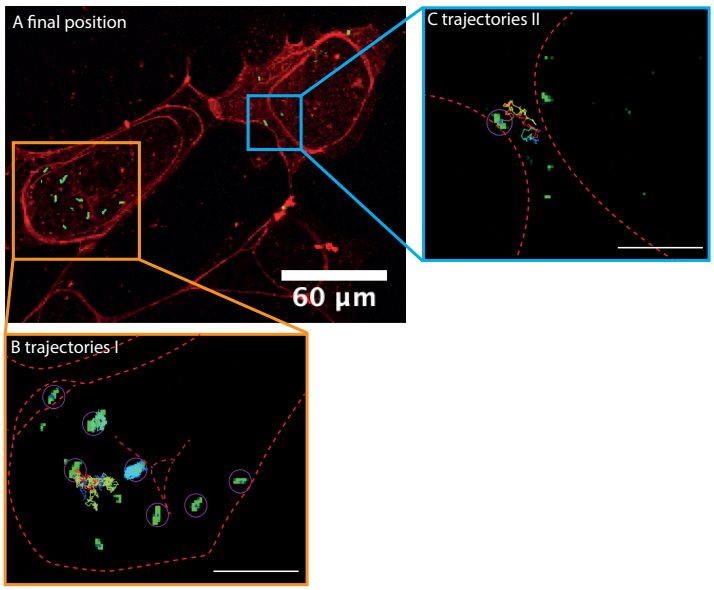

Figure 56 E. coli are observed over time in protein microcapsules after encapsulation and release. A) Image depicts the last time point of a 600s timelapse. B) Trajectories of eight different bacteria show that bacteria in contact with protein fibers are trapped and do not move, while other single bacteria can move in the cavity of the capsule freely. C) Trajectories of two other bacteria are shown, where a clear pattern is visible. One bacterium is moving until it interacts with the protein wall. Then its movement is inhibited, while the other bacterium is trapped from the beginning, hence no trajectory is recorded. Scale bar, 20 µm.

4.5.2 *Encapsulation of Ookinetes into laminin dsProCaps and the subsequent release of ProCaps*

In the life cycle of Malaria parasites, ookinetes play a crucial role. Ookinetes migrate through the midgut of the host mosquito where they produce an oocyst.[308] This oocyst comprises laminin proteins and serves as a protective capsule for ookinetes to grow and mature.[309] Once ookinetes mature into sporozoites, the oocyst bursts and the cells migrate to the salivary gland of the mosquito.[310] Then upon a mosquito bite, the mosquito transfers sporozoites to the human where they are transported through fluids to the liver, produce merozoites and further infect red blood cells. While it is widely known that the oocyst is mostly made out of laminin, little is known about the outbreak reaction of sporozoites.[311] In this section, I investigate the use of laminin ProCaps for the encapsulation of ookinetes to build a platform that will shed light on the outbreak mechanism. By establishing a synthetic oocyst, it will become possible to observe the formation and further outbreak of sporozoites

and investigate this mechanism closely. Here, I use a simple single inlet droplet production device to encapsulate ookinetes together with proteins in dsProCaps. Droplets are produced as previously stated (Experimental section 3.6 Generation of ECM-based dsProCaps). Laminin-111 and the ookinetes are mixed in PBS containing 10mM $CaCl_2$. As the main aim here is to establish the encapsulation technique, ookinetes are fixed prior to encapsulation and only end point experiments are discussed. It is also important to mention here, that the stabilizing oil phase consists of a positively charged surfactant instead of using the negatively charged Krytox™ molecules. The motivation behind the change of the oil phase is discussed thoroughly in Chapter 4.9 Analysis of pH inside dsProCaps. Upon encapsulation of proteins and ookinetes, proteins are evenly attracted to the inner periphery of the dsProCaps (Figure 57A) without proteins aggregating around ookinetes (Figure 57C). Further, by implementing the already discussed bulk release approach, I release laminin-111 ProCaps containing single ookinetes (Figure 57D). The orthogonal view depicts the protein surrounding single ookinetes (Figure 57E). By evaluating fixed ookinetes, I prove the successful production of synthetic oocysts and demonstrate the retention of the cells within the capsules. The next steps involve encapsulation of living ookinetes and time-dependent studies of the behavior inside laminin-111 ProCaps.

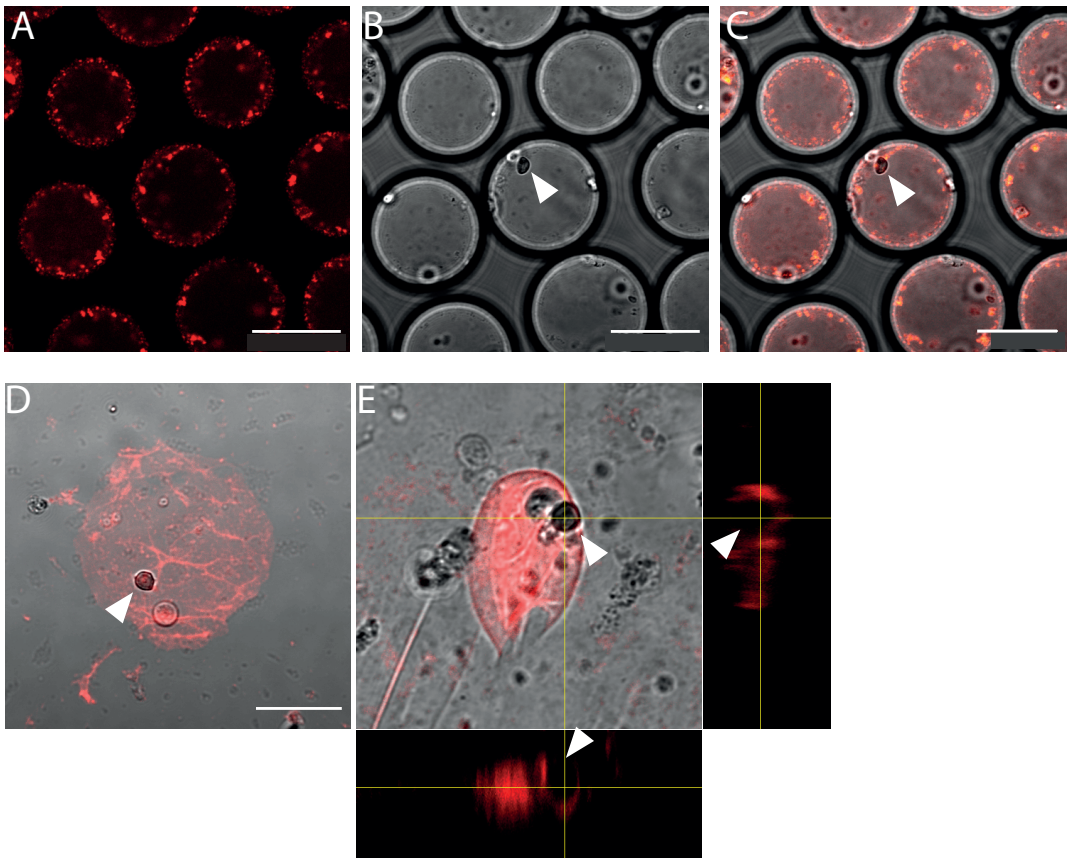

Figure 57 Single Ookinete encapsulation.
Laminin-111 dsProCaps (red signal, A) containing single Ookinetes (brightfield, B). C) Overlay of a single ookinete encapsulated in a laminin-111 dsProCaps. Scale bar, 50 µm. D) Single ookinete encapsulated in a laminin-111 ProCaps. E) Orthogonal view of a single ookinete encapsulated in a ProCaps. Side views show the encapsulated cell inside laminin-111. White arrows show single Ookinetes. Scale bar, 20 µm.

4.6 Encapsulation of keratinocytes in dsProCaps and the subsequent release of cell-laden ProCaps

After the establishment of microcapsules comprising ECM-proteins and the successful encapsulation and retention of small *E. coli* and larger ookinetes, the next step was to encapsulate eukaryotic cells. Keratinocytes (HaCaT) are used because of their excessive contact to ECM *in vivo*.[135] Cell-laden dsProCaps are produced using a pico-injection device with a single inlet droplet production channel incorporated (Figure 35). Laminin-111, fibronectin, or Matrigel® are mixed in the aqueous phase and the resulting droplets are stabilized with Krytox™/PEG-PFPE

to incorporate a negative charge on the inner periphery (Experimental Section 3.16 Pico-injection of eukaryotic and prokaryotic cells into surfactant stabilized droplets). After the establishment of the protein droplets, cells are injected sequentially over the injection nozzle of the device. Supplementary Figure 10 shows the stepwise injection of a single cell into a droplet. First, a contact between the droplet and the injection nozzle is facilitated by an electric field, which destabilizes the wall of the droplets. Next, based on the flow rate set on the syringe pump since cells are injected and as soon as the droplet leaves the injection are, the wall is stabilized again and the content stays encapsulated. Figure 58 show HaCaT cells encapsulated after pico-injection into laminin-111 (A), fibronectin (B), and Matrigel®(C) dsProCaps. Interestingly, the labelled proteins are not only going to the periphery of the droplets but are also coating the cells, which gives the impression of fluorescently labelled cells upon observation by CLSM (Figure 58). The potential reason for the attraction of the protein to the cells might be the high affinity of the protein to the cells rather than the inner periphery of the droplets. The accumulation of protein on the cells lead to the concern that the stability of the resulting ProCaps is affected because of a lower protein concentration getting attracted to the inner periphery of droplets. However, despite aggregation of proteins around the cells, enough additional protein is left to align at the inner periphery and polymerize to form stable capsules after the release. The success of the release is demonstrated by CLSM and qualitative observation of the structure of ProCaps containing the cells (Figure 58Ai, Bi, Ci). The tilted tent-like shapes of the cell-laden ProCaps highlight the successful polymerization of the proteins.

By using a cell viability detection molecule, propidium iodide (PI), it is observed that despite the successful encapsulation, cells did not survive the ProCaps formation process. The experiments are initially conducted in PBS, a solution that is osmotically stable but lacking essential nutrients for cell viability and therefore optimization of culture conditions is required. The following chapters focus on optimizing the technique to prevent cell death inside the protein capsules.

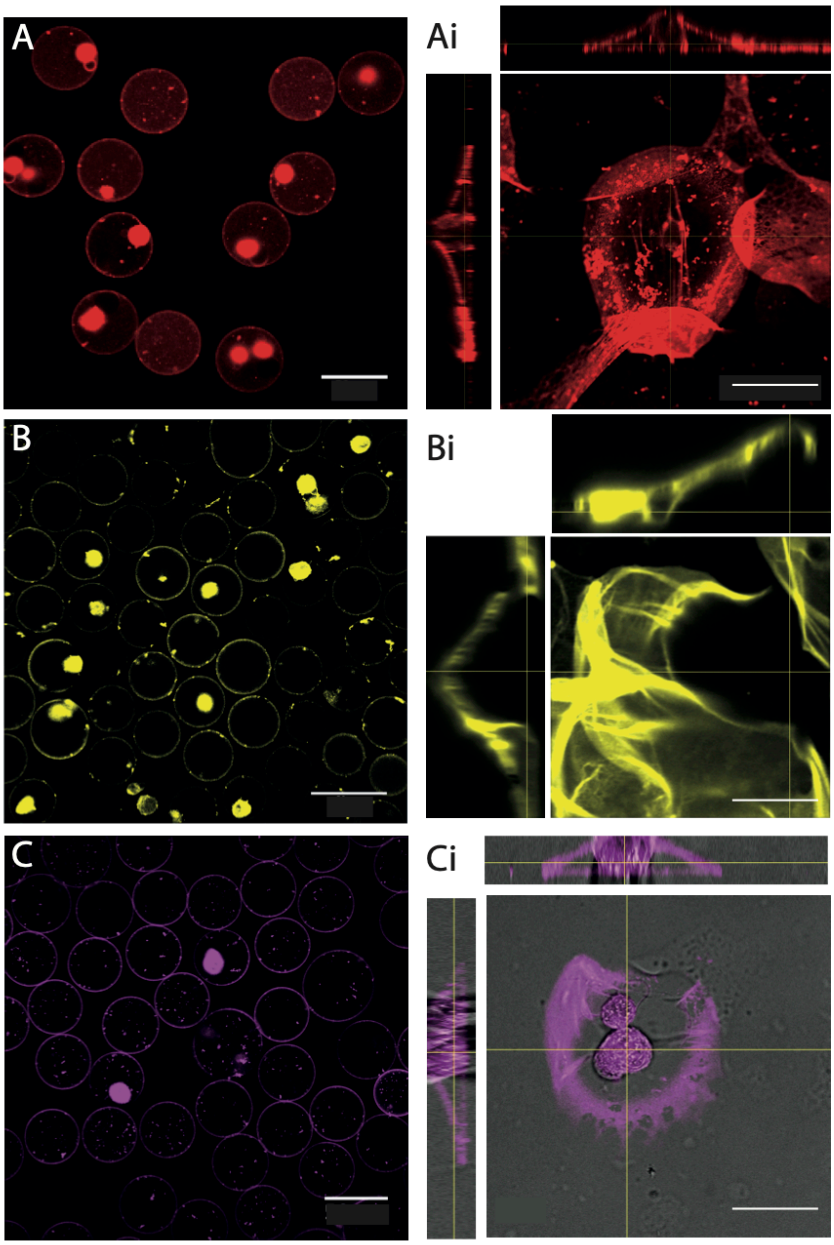

Figure 58 Laminin-111 (A), fibronectin (B) and Matrigel®(C) dsProCaps containing HaCaT cells. The bright color around the cells are simply soluble protein molecules coating the cells. Scale bar, 50 µm. After release, ProCaps made out of laminin-111 (Ai), fibronectin (Bi) or Matrigel®(Ci) containing single cells are generated. The stability of the protein is visible by the tent like structure around the cells. Scale bar, 30 µm.

4.7 Production of dsProCaps with cell culture media

To test the hypothesis that the aqueous phase lacking nutrients resulted in cell death, dsProCaps are produced in cell culture media instead of PBS. The generation of dsProCaps remains the same as described in Chapter 3.5 Generation of ECM-based dsProCaps. However, the proteins and the polymerization factors are diluted in cell culture media containing 1 % FBS instead of PBS. Because the ionic conditions are different in this aqueous phase, I establish simple dsProCaps to ensure the successful charge-mediated attraction of the proteins to the inner periphery before incorporating cells. Figure 59A-C shows the attraction of laminin-111, fibronectin, and Matrigel® to the periphery of the droplets, respectively. Even though the protein is distributed at the periphery, the impression of holes in the protein layer arises. This phenomenon is explained by the addition of unlabeled 1 % FBS to cell culture medium, which is also attracted to the periphery of the droplet based on its slightly negative charges (pKa value = 5.7).[312] To prove that FBS is not interfering with the formation of microcapsules, release into physiologically relevant media is conducted and ProCaps are established as seen in the insets of Figure 59A-C.

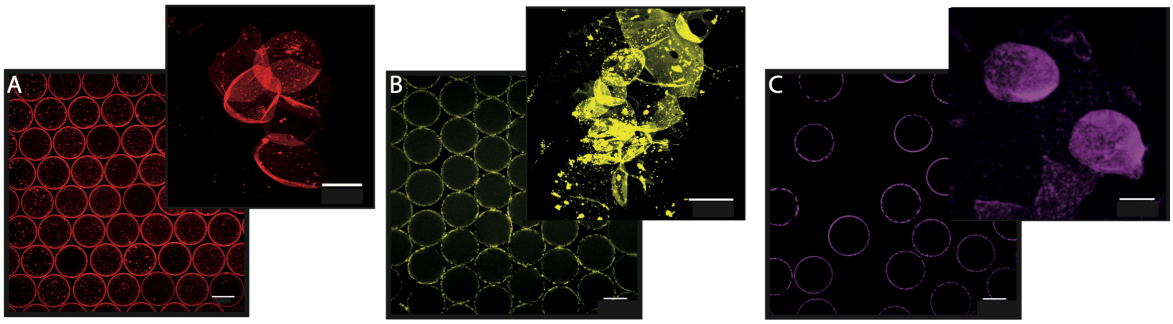

Figure 59 dsProCaps established with cell culture media and the subsequent release of polymerized ProCaps. Laminin-111 (A), fibronectin (B) and Matrigel® (C) proteins are attracted to the periphery of the droplets. The successfully released microcapsules are depicted on the upper right corner. Scale bar 50 µm dsProCaps, 30 µm ProCaps.

4.8 Encapsulation of Jurkat cells inside dsProCaps and the subsequent release of cell-laden protein microcapsules

Previously, the death of adhesion cells inside dsProCaps and ProCaps was observed and discussed. The question arose if the absence of adhesion points for adhesive cells lead to apoptosis. To test whereas suspension cells will better tolerate the ProCaps formation processes I encapsulate Jurkat cells in RPMI-1640 media supplemented with 1%FBS by pico-injection into dsProCaps (Experimental Section 3.16 Pico-injection of eukaryotic and prokaryotic cells into surfactant stabilized droplets). Figure 60 shows single Jurkat cells inside laminin-111 (A), fibronectin® (B), or Matrigel® (C) consisting dsProCaps. Similarly, to the HaCaT cell encapsulation (Figure 58), the proteins accumulate around the cells. The previous hypothesis was that the proteins have a higher affinity towards the adhesion cells rather than the negatively charged inner periphery. However, seeing the laminin-111 accumulation around suspension cells leads to the assumption of a different hypothesis which is going to be explained in more detail in Chapter 4.9 Analysis of the pH inside dsProCaps. By encapsulating a 7-AAD, a live/dead stain which is taken up only by apoptotic cells, the death of encapsulated cells inside laminin-111 and Matrigel® dsProCaps is detected (Figure 60A and C). Interestingly, the cells inside fibronectin dsProCaps do not reveal the uptake of the apoptosis marker. Suggesting the viability of the cells inside fibronectin dsProCaps. Nevertheless, I release all types the cell-laden dsProCaps and observe protein capsules bearing cells on their inside, albeit dead cells. The famous tent-like release shape is proven by CLSM imaging, which is covering the cells with green staining of cells inside fibronectin ProCaps (Figure 60Bi), while the cells in the other two ProCaps express the 7-AAD dye very poorly, suggesting cell death in each condition (Figure 60Ai and Ci). This result shows that encapsulating suspension cells inside dsProCaps with the preferred media conditions is not mitigating cell death. Even though the results do not lead to the preferred outcome, valuable information towards future experimental design is obtained. Neither using cell culture media as the inner aqueous media nor the use of suspension cells could save the cells from apoptosis.

Taken together, this leads to testing the pH values inside Krytox™/PEG-PFPE stabilized droplets to determine the reason behind cell death.

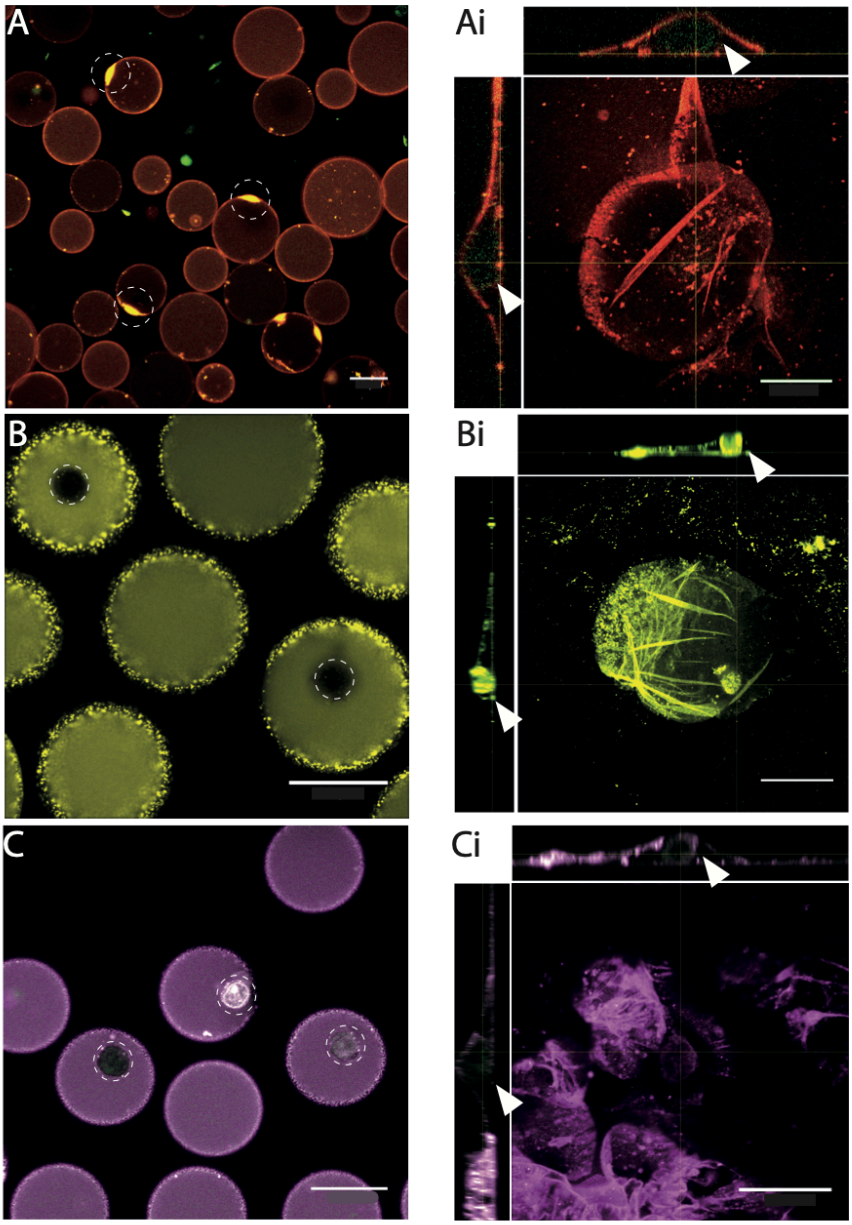

Figure 60 Encapsulation of Jurkat cells in negatively charged dsProCaps.
Jurkat cells inside Krytox™ stabilized dsProCaps made out of A) laminin-111, B) fibronectin or C) Matrigel®. Scale bar, 50 µm. Ai) Laminin-111, Bi) fibronectin or Ci) Matrigel® ProCaps with single cells encapsulated (white arrow heads). 7 – AAD (green) signals of the cells label apoptotic cells inside dsProCaps and ProCaps. Scale bar, 30 µm.

4.9 Analysis of the pH inside dsProCaps

In the previously described chapters I observe the death of HaCaT cells inside Krytox™/PEG-PFPE stabilized protein droplets. Based on the negative charges present on the Krytox™ molecules, I hypothesize that the environmental conditions inside dsProCaps are in an acidic pH range. The ionic conditions needed to attract and polymerize the ECM proteins might further enhance the acidic pH conditions.[243] Therefore, pyranine is added to the dsProCaps system to measure the internal pH parameter. Figure 61 depicts the calibration curve which is generated in different pH values in PBS inside simple PEG-PFPE droplets. It is used to understand the pH values of the dsProCaps (Experimental Section 3.10 Analysis of the pH inside dsProCaps).

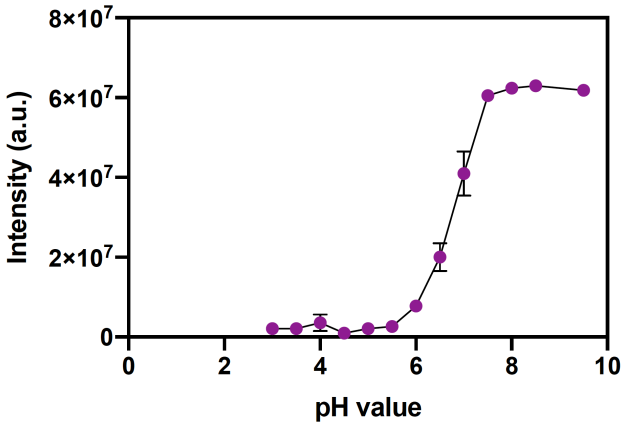

Figure 61 pH Calibration curve with 100 µM pyranine measured at Ex:488 nm/Em:512nm. pH values from 3 to 9.5 are measured inside PBS-in-oil droplets stabilized with 1.4 w% PEG-PFPE and their intensity values are plotted using Prism9.

By applying the same CLSM acquisition conditions for the calibration curve and the experiments, I obtain the corresponding pH values for different conditions inside dsProCaps. The final environment for cells inside dsProCaps comprises laminin-111, the Live/Dead dye 7-AAD, 10 mM $CaCl_2$ diluted in HEPES, and the surrounding stabilizing Krytox™/PEG-PFPE oil phase (Experimental Section 3.5 Generation of ECM-based dsProCaps). The effects of every component on the pH are tested individually (Supplementary Figure 11). Independently from the tested contents, the pH values inside droplets stabilized with Krytox™/PEG-PFPE are relatively low. Pyranine intensities obtained from droplets containing all the

necessary components for the generation of dsProCaps are around $1.6x10^6$ (Figure 62), which represent a pH value around 5. In contrast, droplets stabilized by PEG-PFPE surfactants only, showed intensity values of around $7x10^6$ that correspond to the physiological pH value 6 (Figure 62). Interestingly, the pH decreases in the fully equipped dsProCaps conditions, while the lack of $CaCl_2$ molecules, increases the pyranine intensities (Supplementary Figure 12). Comparing the pH values between Krytox™ and only PEG-PFPE stabilized droplets, shows that the decrease in pH is clearly caused by Krytox™ molecules acting as proton donors at the water-oil interface. The carboxylic group (COOH) on the Krytox molecules dissociates, releasing H^+ ions to the aqueous phase, which leaves behind the COO^- group on the periphery of the droplet. This leads to the attraction of counter ions such as Ca^{2+} to the interface to ensure electroneutrality of the COO^- group on the Krytox™ surfactant.[243] The free H^+ ions causing a drop in pH in the inner aqueous droplet phase. Without the presence of charges provided by Krytox™, cell viability is restored, proven by the lack of uptake of a live/dead dye (Supplementary Figure 13). Additionally, the cells are not attracting the surrounding protein as it was shown before (Figure 58). However, no charges are present for the calcium molecules to interact with, which results in the loss of protein attraction to the inner droplet periphery.

Based to the newly detected low pH values inside dsProCaps, the effect on the charges of the protein needs to be considered. The overall charge of the proteins is negative at pH values around 7.4 of laminin-111 (UniProt: LAMA1_MOUSE (pI: 6.28), LAMB1_MOUSE (pI: 4.82), LAMC1_MOUSE (pI: 5.08)) and bovine serum fibronectin (UniProt: FINC_BOVIN (pI: 5.32)). The pI values are determined by the ExPASY server with the "Compute pI/MW" tool.[313] Following these values, the overall charge of the proteins is slightly positive at a pH of 5, which is the condition inside dsProCaps. Based on this observation, the charge-mediated attraction of the proteins to the periphery is facilitated by the Ca^{2+} ions together with the positive charge of the protein *per se*. This explains the immediate attraction of the protein to the inner periphery of dsProCaps (Figure 44).

The low pH inside the droplets is detrimental to cell viability, however when it comes to the proteins, studies have shown that an acidic pH neither denatures nor affects the functionality of proteins.[59] The self-assembly and polymerization of laminin[314] and the conformational changes needed for fibronectin to undergo fibrillogenesis are promoted at acidic pH, and further still allow for the adhesion and migration of cells.[59] Based on these literature findings, I conduct two bulk experiments to investigate the polymerization and functionality of ECM proteins exposed to acidic pH conditions inside dsProCaps. Hereby, I investigate the polymerization of laminin-111 at different pH values over certain time points (Supplementary Figure 14) and further analyzed the adhesion pattern of HaCaT cells to previously established and released laminin-111 ProCaps (Supplementary Figure 15). The first bulk polymerization experiment revealed the elevated polymerization pattern of laminin-111 at pH values 5 and 6 after 4 h in culture. However, no increased protein-cell interactions are observed. After another 24 h complete polymerization of laminin-111 is observed in all conditions lower than pH6. Laminin-111 in pH 7 and higher revealed the lack of a prominent polymerization pattern (Supplementary Figure 14). After proving enhanced polymerization at lower pH values, I proceed to test the functionality of the ProCaps. HaCaT cells are seeded on top of ProCaps and imaged by CLSM after 24 h, 48 h and 72 h. A confluent cell layer grows over the capsules, proving the remaining functionality of the proteins and the adhesion ability of cells to the capsules.

The detection of such low pH values is also explaining the results of the previously described FRAP measurements (Chapter 4.3.1 Measuring protein diffusion in dsProCaps by FRAP). The potential reason for the missing recovery of proteins inside dsProCaps lacking $CaCl_2$ molecules at any time point, is the acidic pH environment. Based on literature and the bulk polymerization experiment (Supplementary Figure 14) conducted, the polymerization of laminin-111 is facilitated at pH 5, independent of the presence $CaCl_2$ molecules. Hence, the FITC-dextran molecules used in the FRAP experiments are trapped inside a polymerized protein net from an early time point on. Additionally, the pH sensitivity of FITC further explains the decrease in intensity of the FRAP measurement curves over

time and in $CaCl_2$ containing droplets and in the porosity experiment (Chapter 4.4.5.2 ProCaps porosity investigation with FITC-dextran).

Taken together I can conclude that the acidic pH conditions inside dsProCaps are not affecting the functionality of the proteins, on the contrary, those conditions are favorable for protein polymerization as proven by a polymerization experiment and FRAP measurements. However, cell viability cannot be ensured in the acidic pH environment and still remains an issue to be solved. Therefore, instead of Krytox™, positively charged surfactants (see next Section) are implemented to maintain the charge-mediated attraction mechanism.

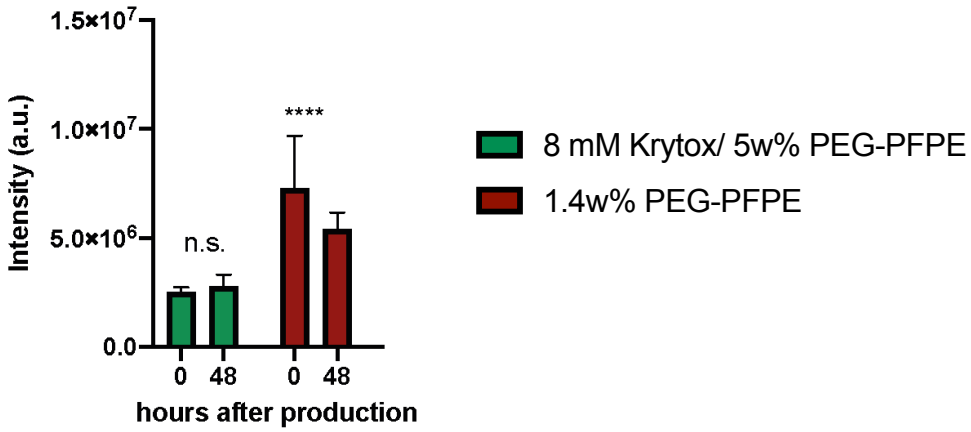

Figure 62 pH analysis in laminin-111 dsProCaps.
Measured pyranine intensities in laminin-111 droplets stabilized with and without Krytox™ are depicted over time. Low intensities reflect low pH values. Intensities for Krytox™/PEG-PFPE stabilized droplets are significantly lower than in droplets stabilized by the neutral fluorosurfactant PEG-PFPE only. Krytox: $p = 0.6085$, PEG-PFPE: $p < 0.0001$. Error bars are representing standard deviation.

4.10 Implementation of a newly synthesized positively charged surfactant

By using a positively charged surfactant I hypothesize to ensure the charge-mediated production of dsProCaps and simultaneously promote cell viability by mitigating the low pH inside the droplets otherwise caused by Krytox™. In the next chapters I discuss the droplet-stabilizing abilities of the positively charged

surfactant and some fundamental characterization properties, important for the final ProCaps generation.

4.10.1 Mechanism of positively charged surfactant-mediated dsProCaps formation

After detecting that the Krytox™ molecules are the source of the acidic pH environment inside the dsProCaps and hence leading to cell death, I sought out to find a new solution to generate cell-laden ProCaps and ensure biocompatibility. To attract the proteins to the inner periphery a positively charged surfactant is generated and kindly provided to me by my colleague Martin Schröter (Ph.D. Student, MPImR, Prof. Spatz Department) who synthesized them for the first time. This surfactant has a positively charged methylgroup (N(Me)3) attached to PEG, which is further attached to a PFPE hydrophobic domain (Experimental Section 3.5.2 Generation of dsProCaps with positively charged PEG-based fluorosurfactants). This positively charged mechanism negates the use of Krytox™ as a driving force to attract proteins to the inner periphery. Further, the negative charges no longer face into the aqueous phase leading to acidification of droplets. Figure 63 depicts a schematic representation of the charge-mediated attraction mechanism for the formation of dsProCaps using the positively charged surfactant. The droplet wall consists only of positively charged molecules (Figure 63A1) and the negatively charged protein molecules are attracted directly to the periphery (Figure 63A2). The proteins, in turn, are attracting Ca^{2+} ions (Figure 63A3) which are important for the polymerization of laminin-111 (Figure 63A4). Whenever this surfactant is used, I call the resulting droplets positively charged dsProCaps with their corresponding positively charged ProCaps.

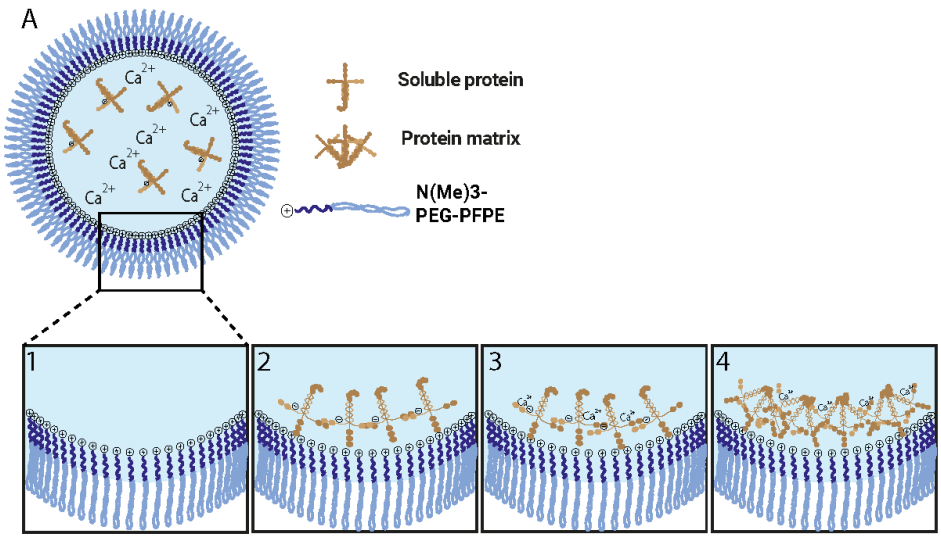

Figure 63 Attraction of proteins to the periphery of droplets established with positively charged surfactant, shown at the example of laminin-111.

A) Water-in-oil droplets stabilized with N(Me)3-PEG-PFPE containing $CaCl_2$ and soluble laminin-111 to establish positively charged dsProCaps. 1) The hydrophilic side of the surfactant molecule PEG-N(Me)3 faces towards the inside and presents the positive charge to the aqueous phase. 2) Negatively charged laminin-111 is attracted to the periphery and aligns at the wall. 3) $CaCl_2$ molecules are attracted to the proteins. 4) $CaCl_2$ is necessary to polymerize the proteins which accumulated at the periphery of the droplet.

4.10.2 *Analysis of pH inside positively charged dsProCaps*

Before encapsulating cells inside droplets stabilized with the positively charged surfactant, it is necessary to determine the effects of this surfactant on the pH inside dsProCaps. The analysis is performed exactly as in the conditions for negatively charged droplets and are explained in detail in the experimental section 3.10 Analysis of the pH inside dsProCaps. The dsProCaps are stabilized with 5mM positively charged surfactant dissolved in HFE-7500 and contain 0.8 µM laminin-111 with 10 mM $CaCl_2$ in PBS. Labelled laminin was left out in order to not interfere with the pyranine signal. Comparing the intensity values of the experiment with the previously established calibration curve, I could determine that the pH of this particular aqueous phase is at approximately 7 (Figure 64, Supplementary Table 1) This value is at the physiological range for cell survival, and more promising than the values obtained inside droplets stabilized with Krytox™. Similar to droplets established with PEG-PFPE only, $CaCl_2$ decreases the pyranine intensities in the

droplets stabilized with the positively charged surfactant (Supplementary Figure 16). The hypothesis is that upon interaction of the Ca^{2+} ions with laminin-111, H^+ ions are released, which leads to a decrease in pH inside the droplet.[65,307,314] Not surprisingly, the pH values are significantly higher with $CaCl_2$ dissolved in 1M HEPES than with 10mM HEPES because 1M HEPES stabilizes the pH better than lower values (Supplementary Figure 16).

For a better comparison, the pH values of droplets stabilized with Krytox™ and only PEG-PFPE are depicted next to dsProCaps stabilized with N(Me)3-PEG-PFPE again (Figure 64). The pH in the positively charged surfactant is significantly higher ($p < 0.0001$) than in droplets produced with PEG-PFPE fluorosurfactant only, suggesting that the positively charged surfactant in combination with $CaCl_2$ is not affecting the pH drastically and still harbors a hospitable environment for cells (Figure 64). After 48 h of incubation the pH decreases in both conditions significantly, which might be due to the increase of higher numbers of H^+ ions over time. However, cell-laden droplets are not incubated in such a long period of time. The reason for the lower pH of PEG-PFPE surfactant stabilized droplets might lay in the synthesis process of this surfactant. During the synthesis and purification, some Krytox™ residues might remain in the surfactant and hence lower the pH. The low amount of Krytox™ molecules most probably affects the pH but is not charging the periphery sufficiently enough in order to attract proteins to the inner periphery (Supplementary Figure 2).

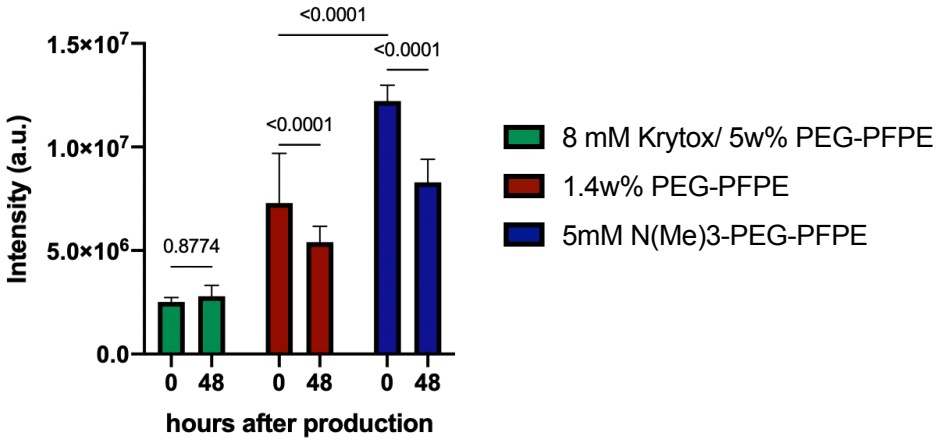

Figure 64 Comparison of pH values between various oil phases.
Intensity values between different oil conditions after production (t0h) and 48h later. Error bars are representing standard deviation. n = 50 droplets per condition of two independent experiments. Pyranine intensities are measured at Ex:488 nm/Em:521 nm.

4.10.3 Interfacial Tension Measurements of N(Me)3-PEG-PFPE surfactants

To further characterize this newly synthesized surfactant and investigate its interactions with proteins, pendant drop measurements are performed to understand the surface tension of water-in-oil droplets stabilized with different surfactant concentrations. In this regard, I measure two different surfactant concentrations against PBS and pure protein (Figure 65) (Experimental Section 3.6 IFT measurements). An accountable difference between the IFT of 5 mM (22 mN/m) and 20 mM (19.4 mN/m) N(Me)3-PEG-PFPE measured against water can be determined. With the higher surfactant concentration, the IFT decreases, which is caused by an increase in interfacial coverage by the surfactant (Chapter 1.7.4 Physical properties of droplet stabilization). The higher the number of surfactants aligning at the oil-water interphase, the more those molecules are preventing the coalescence of water-in-oil droplet by stabilizing the periphery. The higher the number of surfactants at an interphase, the lower the IFT values become. Measuring the IFT against pure protein leads to a significant decrease in both surfactant conditions. The IFT at 5 mM of the surfactant is measured at around

15 mN/m, while the value is reduced by half with 20 mM of the surfactant measured against laminin-111 (7.5 mN/m) (Figure 65). The low IFT values can be further explained, based on the negative charges of the proteins. The charge-mediated interaction of the positively charged surfactant and the proteins is facilitated. This attraction leads to a high surface coverage of the protein to the oil phase, causing the IFT to decrease. With the much lower values at 20 mM of the positively charged surfactant, I assume a higher attraction of the protein to the droplet, leading to a less dense packing of the surfactant molecules caused by the steric hindrance. The proteins might interact with the surfactants at the interface, hindering the exchange of molecules and hence lowering its surface tension.

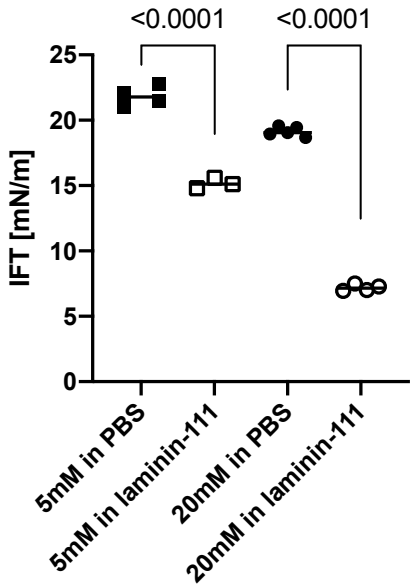

Figure 65 Interfacial tension (IFT) measurements of N(Me)3-PEG-PFPE.
Two different concentrations (5 mM and 20 mM) are measured against PBS or 1.17 µM laminin-111.

4.11 Production and characterization of positively charged dsProCaps

After manifesting that the pH values inside positively charged dsProCaps are in a physiological range and that by means of pendant drop an attraction of proteins to the surfactant-water interphase is achievable, I commenced with the generation of dsProCaps. This step is important to understand if the generation of ProCaps using

a positively charged approach is possible. The production of positively charged ECM-based dsProCaps is dependent on the establishment of water-in-oil droplets to function as scaffolds first. In order to find the right oil-surfactant concentration to successfully attract proteins to the inner periphery, I tested various concentrations to understand the optimal conditions for the attraction of proteins to the inner periphery (Supplementary Figure 17). For this experiment Matrigel® is used as a model system. It can be clearly seen, that droplets stabilized with pure positively charged surfactant are able to attract the protein to the periphery. Interestingly, 5 mM and 20 mM of the surfactant are attracting the proteins to the periphery, while in the droplet population stabilized with 10 mM of the surfactant the establishment of dsProCaps is not facilitated. However, the images are taken 2 h after production. This time window might be too short to attract proteins to the inner periphery. After discovering the right concentrations for the successful attraction of proteins, different proteinaceous aqueous phases are introduced to a single inlet droplet production device with an oil phase, consisting of either 5 mM or 20 mM positively charged surfactant diluted in HFE-7500. Fibronectin or Matrigel® are mixed at the same concentrations used for the establishment of negatively charged dsProCaps, with the appropriate polymerization factors, while laminin-111 is slightly adjusted. The detailed production steps are described in the Experimental Section 3.5.2 Generation of dsProCaps with a positively charged surfactant. The oil phase is used to cut off the protein stream and produce evenly sized water-in-oil droplets. The attraction of laminin-111 and Matrigel® is feasible and allows for the generation of dsProCaps over time. Laminin-111 is attracted initially to the inner periphery and increases over time (Figure 66, intensity insets). Matrigel® dsProCaps have a very interesting morphology. The proteins are homogenously distributed directly after production in some droplets (Figure 66Bi), while in others, the protein is attracted immediately to the inner periphery. The intensity profiles demonstrate homogenous protein distribution inside the droplets. After 2 h, the protein is attracted to the periphery of all droplets (Figure 66Bii, intensity inset). Interestingly, with this newly synthesized surfactant it is not possible to attract fibronectin molecules to the inner periphery of the droplets (Figure 66Ci and Cii).

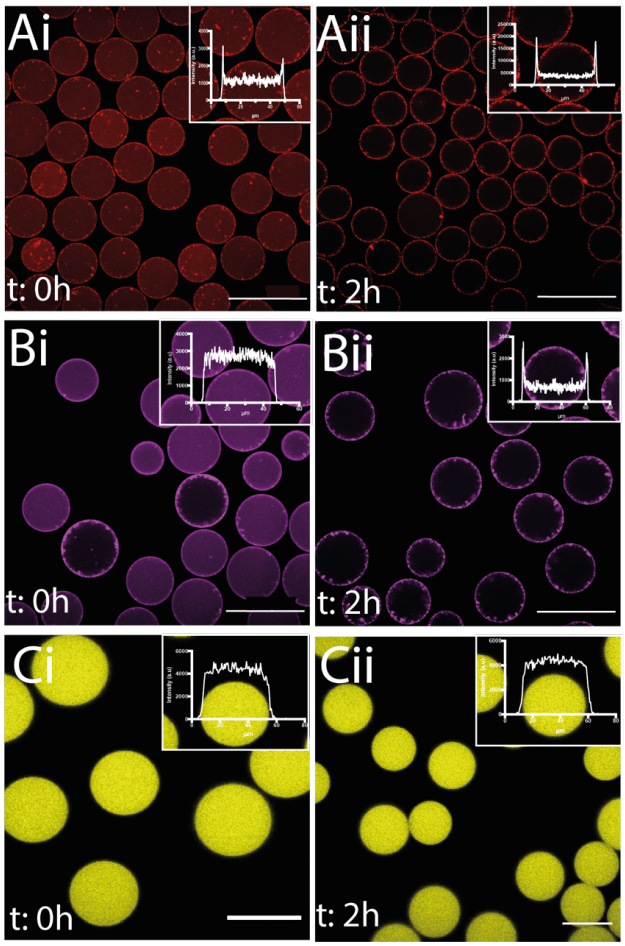

Figure 66 positively charged dsProCaps over time.
ECM-coated water-in-oil droplet stabilized by positively charged surfactants. Laminin-111 (Ai) droplets after production. Intensity inset depicts the slight attraction of protein to the inner periphery. Bi) Intensity inset depicts the homogenous distribution of Matrigel® inside the droplets. Laminin-111 (Aii) and Matrigel® (Bii) show an increase of protein attraction after 2 hours of. Intensity insets are proving the successful attraction of the protein at the periphery. Ci,Cii) Fibronectin is neither attracted to the periphery after production nor after 2 h. Scale bar, 50 µm.

The attraction of laminin-111, Matrigel® and fibronectin to the periphery is measured every two hours over a time course of eight hours and a raising trend is observable for laminin-111 and Matrigel®, while fibronectin is not attracted to the periphery at any time point given (Figure 67). Those intensity values are also in line with the images taken for each time point (Supplementary Figure 18). The reason for this might lay in two varying protein conformations in which fibronectin exists. Prior to activation, fibronectin occurs in a coiled conformation. After interaction with sulfonic acid groups it unravels into longer fibronectin chains which can

undergo fibrillogenesis.[315] Studies have shown that by coating fibronectin on negatively charged surfaces, the interaction with sulfonic acid groups can be mimicked and trigger conformational change.[59] I hypothesize that by encapsulating fibronectin inside Krytox™/PEG-PFPE droplets, negative charges are interacting with the coiled fibronectin structures and lead to unwrapping and fibrillogenesis of the protein. When using the positively charged surfactant, no negative charges are present, and hence fibronectin stays in the round conformation and cannot assemble at the inner droplet periphery.

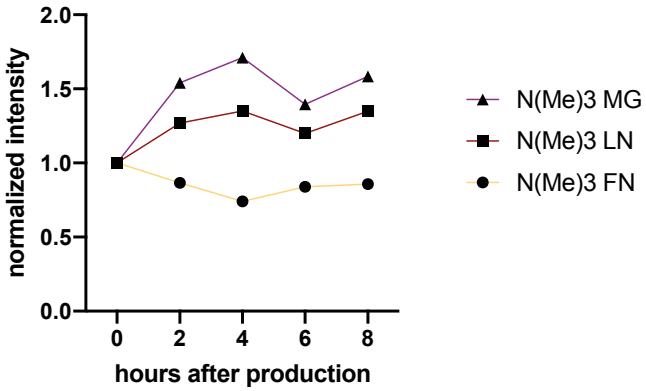

Figure 67 Time observation of the attraction of proteins to the inner periphery of positively charged dsProCaps. Normalized mean intensity grey values are plotted for Matrigel®(MG), laminin-111 (LN) and fibronectin (FN) in droplets stabilized with N(Me)-PEG-PFPE surfactants.

A difference in continuity of the protein layer at the positively charged periphery can be detected (Figure 66) in comparison to negatively charged dsProCaps (Figure 44). In positively charged dsProCaps protein-Ca^{2+} complexes assemble on the inside of dsProCaps and are further attracted to the inner periphery. This phenotype is caused by the delay of protein attraction (Figure 66), which supports the assumption that divalent ions are not the driving force as it is the case in Krytox™ mediated protein attraction. The overall charge of the proteins is negative at pH values around 7.4 of laminin-111 (UniProt: LAMA1_MOUSE (pI: 6.28), LAMB1_MOUSE (pI: 4.82), LAMC1_MOUSE (pI: 5.08)) and bovine serum fibronectin (UniProt: FINC_BOVIN (pI: 5.32)). The proteins keep their overall negative charges, since the pH inside positively charged dsProCaps is higher than their isoelectric point. This explains, that in the case of the positively charged

surfactants, proteins are attracted directly to the positively charged inner periphery without the help of small ions.

To further test this hypothesis, I produce droplets stabilized with either 5 mM or 20 mM of the positively charged surfactant, without the addition of $CaCl_2$ molecules (Supplementary Figure 19). Directly after production, no attraction of the protein to the periphery is observed. After the incubation of the droplets for 2 h at 37 °C the proteins started getting attracted towards the inner periphery of the droplets. This observation is more evident in droplets stabilized with 20 mM N(Me)3-PEG-PFPE. The next day, the proteins are nicely attracted to the periphery in both concentration conditions, proving the hypothesized working mechanism in Figure 63. This mechanism gives the proteins and $CaCl_2$ molecules time to aggregate. This observation is in line with droplets containing $CaCl_2$ (Figure 66). The continuous protein layer inside $CaCl_2$-missing droplets proves the assembly of protein-Ca^{2+} complexes in droplets established with $CaCl_2$.

To investigate if the adsorption kinetics can be improved and protein aggregation prevented, I produce small dsProCaps stabilized with N(Me)3-PEG-PFPE by emulsification (see Chapter 3.5.3 Generation of small dsProCaps stabilized with negatively and positively charged PEG fluorosurfactants for more details). The idea is to decrease the adsorption depth of the proteins to the inner periphery, leading to a faster attraction of the protein without the risk of generating protein-Ca^{2+} complexes. The instantaneous attraction of laminin-111 and Matrigel® is detected, without the generation of protein aggregations prior to the attraction to the inner periphery (Figure 68). This result supports the hypothesis that reducing the distance to the periphery allows for a faster attraction of the proteins to the inner periphery. The reason for this might be the interplay between the decreased adsorption depth, which supports the faster adsorption of the proteins to the periphery, and the closer proximity between the opposite charges on the proteins and the droplet interface. This reduces the interaction time of the calcium molecules and proteins, preventing the generation of protein-Ca^{2+} complexes. However, in these conditions, fibronectin could still not be attracted to the inner periphery (Figure 68), possibly explained by a lack of negative charges inside droplets stabilized with N(Me)3-PEG-PFPE surfactants. Further, as a proof-of-concept

experiment the dsProCaps are released. Not surprisingly, fibronectin ProCaps could not be established, while laminin-111 and Matrigel® ProCaps assembled as expected (Supplementary Figure 20).

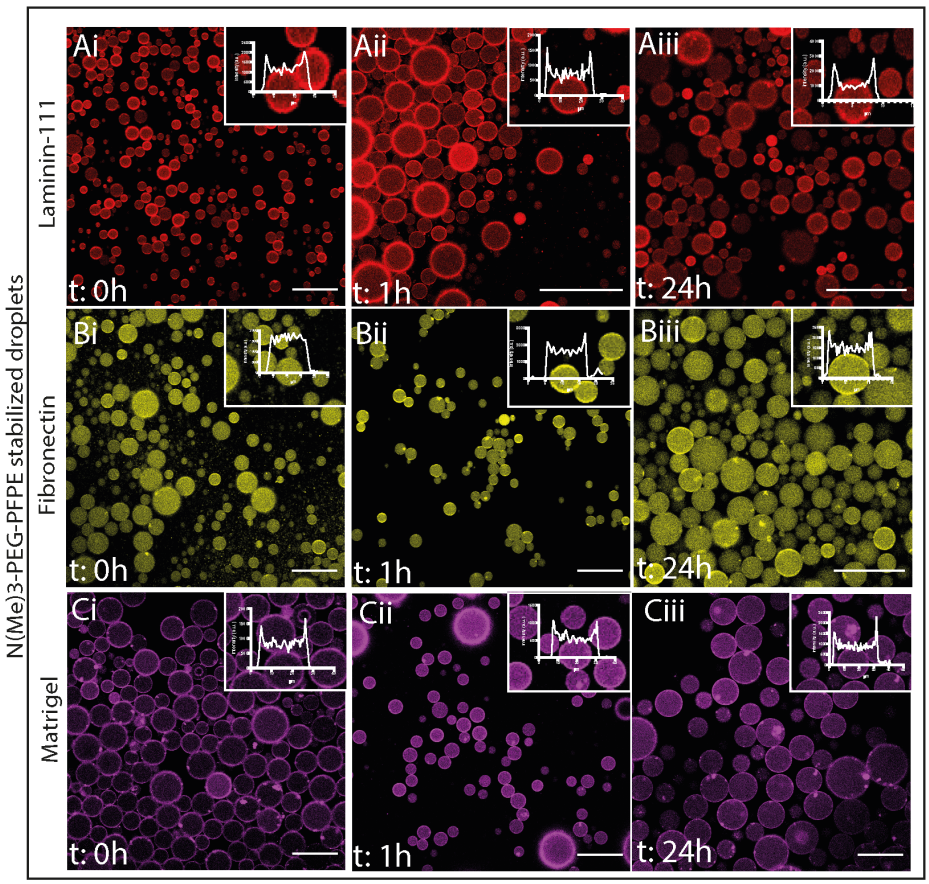

Figure 68 Small dsProCaps stabilized with 5 mM positively charged surfactant.
Laminin-111(Ai), fibronectin (Bi) and Matrigel® (Ci) droplets are established by using an emulsifier to generate droplets approximately 5 - 20 µm in diameter and observed immediately. Laminin-111 (A) and Matrigel®(B) proteins stay attracted to the periphery over time. High intensity peaks in the insets can be observed at each timepoint for both protein types (0h: Ai, Bi; 1h: Aii, Bii; 24h: Aiii,Biii). Ci, Cii, Ciii) Fibronectin could not be attracted at any time point tested. Scale bar, 20 µm.

4.11.1 Analysis of protein diffusion at the interphase of positively charged dsProCaps

Another important aspect on understanding the protein dynamics inside positively charged dsProCaps is the diffusivity of the protein at the periphery. In order to investigate the general movement pattern of the proteins, FRAP measurements are conducted. Interestingly, no recovery of the fluorescently labelled protein could be detected at any time point (Supplementary Figure 21). This observation is in line with the FRAP measurements conducted for negatively charged dsProCaps (Chapter 4.3.1 Measuring protein diffusion in dsProCaps by FRAP). The result indicates the same as previously stated. The lack of diffusion of the protein, which can be explained by the interaction between the soluble proteins and the charged periphery is occurring at an earlier time point than initially assumed. However, those results indicate the assembly of the protein at the periphery, but no information are gained on the polymerization pattern of the proteins. To investigate the polymerization in more detail, FRAP measurements are conducted on FITC-dextran molecules encapsulated with laminin-111 proteins (Experimental Section 3.7 FRAP measurements). The basic idea is to understand the diffusion of those small molecules inside polymerized protein meshes. Laminin-111 is encapsulated with 70 kDa FITC-dextran with and without the polymerization factor $CaCl_2$ in two different surfactant concentrations to understand the impact on protein polymerization. Figure 69A shows the recovery of FITC-dextran molecules inside 5 mM dsProCaps with and without $CaCl_2$ molecules, measured at 0 h, 2 h and 24 h after production. A pronounced recovery behavior of the FITC-dextran molecules is established at any time point when no $CaCl_2$ molecules are present. This observation underlines the lack of polymerization of the protein, without $CaCl_2$ ions. While having a closer look at the recovery pattern inside droplets containing the polymerization factors, no recovery can be observed at any timepoint. This result indicates the polymerization of proteins at the periphery of the droplets happening at a very early stage, leading to the trapping of the small FITC-dextran molecules inside the protein nets. The FRAP results obtained within droplets

stabilized by 20 mM positively charged surfactants are mostly in line with the previously described droplets, except the loss in recovery of FITC-dextran molecules in droplets without $CaCl_2$ incubated for 24 h. The reason for this might lay in the polymerization ability of laminin-111 inside lower pH values. As it was shown earlier in this thesis, the pH decreases inside the dsProCaps over time, which might lead to the polymerization of the protein without the presence of $CaCl_2$ (Chapter 4.9 Analysis of the pH inside dsProCaps and Chapter 4.10.2 Analysis of pH inside positively charged dsProCaps).

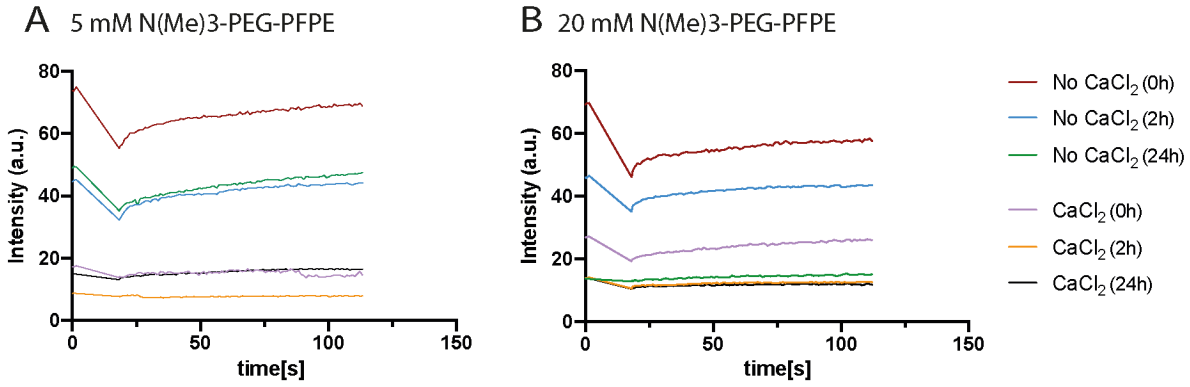

Figure 69 FRAP measurements inside positively charged dsProCaps.
Diffusivity of 70 kDa FITC-dextran molecules in laminin-111 dsProCaps stabilized with A) 5mM or B) 20mM N(Me)3-PEG-PFPE concentrations. Fluorescent recovery of the bleached regions can be observed at any time point (0h, 2h, 24h) without $CaCl_2$. The introduction of the polymerization factors hinders the diffusion. n = 5 measurements per each condition.

4.12 Generation of ProCaps by implementing the bulk release approach

By proving the protein polymerization abilities inside positively charged dsProCaps by conducting FRAP measurements, I set out to release ProCaps. By implementing the bulk release approach polymerized laminin-111 and Matrigel® capsules are released after 2 h (Figure 70A, B). Despite the generation of protein-Ca^{2+} complexes and their subsequent attraction (Figure 66), nicely shaped ProCaps could be released. This experiment ultimately proves the successful accumulation and polymerization of proteins inside dsProCaps. The morphology of the capsules

differs from negatively charged capsules (Figure 48), based on the protein aggregations which are assembled inside the droplets prior to the alignment at the inner periphery. Further, a time release study is conducted to observe the release efficiency of the ProCaps over a time course of 8 h. A heat map depicts the strict polymerization time point of fully released ProCaps (green, 1) and partially released ProCaps (orange, 0.5) or not released (red, 0) (Figure 70C). It becomes clear that in the case of laminin-111 ProCaps, after 4 h no protein microcapsules are released anymore, most likely caused by highly polymerized proteins and intense interactions with the stabilizing outer oil shell. For Matrigel® based ProCaps, fully generated capsules can be released only after 2 h of incubation, limiting the time window of a successful release. The proteins might interact with the charged surfactants on the inner periphery of the droplets creating covalent bonds, preventing the release of protein microcapsules. This hypothesis is supported by previous experiments explained in Chapter 4.4.3 Observing the release mechanism of ProCaps. There it can be seen that the polymerized proteins are interacting with the oil surface, hindering the capsules to be removed from this surface. However, this particular experiment is performed with Krytox™ droplets and needs to be validated for positively charged dsProCaps.

To investigate the remaining adhesive properties of the ProCaps a bulk adhesion experiment is performed as previously completed for negatively charged ProCaps (Chapter 4.9 Analysis of the pH inside dsProCaps and Experimental Section 3.14 Adhesion experiments of cells to negatively and positively charged ProCaps). HaCaT cells are seeded on ProCaps and imaged by CLSM after 24 h, 48 h and 72 h. A confluent cell layer grew over the capsules, proving the functionality of the proteins (Supplementary Figure 22).

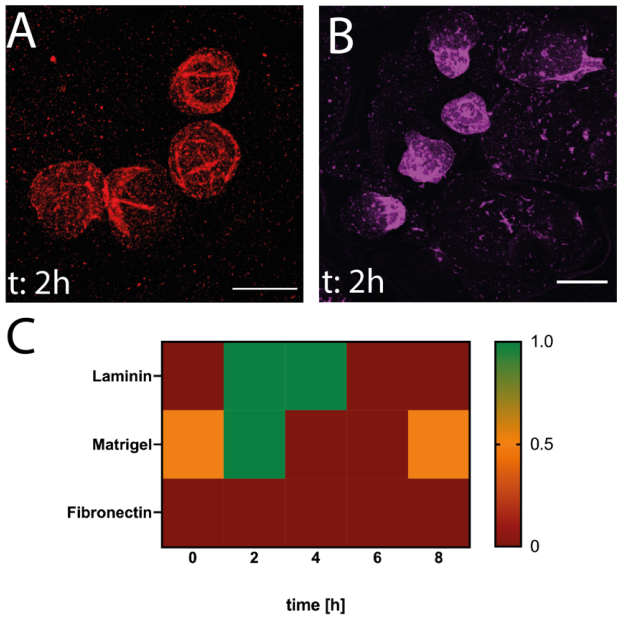

Figure 70 Positively charged ProCaps generation.
Laminin-111 (A) and Matrigel®(B) capsules are released by the bulk release approach after 2 h incubating at 37 °C. Scale bar, 30µm. C) Heat map for the visualization of the relevant timepoints to release laminin-111 or Matrigel® ProCaps. Fibronectin ProCaps are not established at any time point. Fully released ProCaps (green, 1), partially released ProCaps (yellow, 0.5) or not released (red, 0).

4.13 Production and analysis of cell-laden dsProCaps

The final goal of this thesis is the generation of cell-laden ECM ProCaps to serve as a new technology for further investigations such as cell-ECM interactions from various sides of the cell. For such observations, cells have to be healthy and not impaired in their natural behavior. Following the successful implementation of the positively charged surfactants for the formation of dsProCaps with pH levels in a physiological range, I set out to establish cell-laden dsProCaps. I chose HaCaT and Jurkat cells again. HaCaT cells, which are keratinocytes, are known for their extensive interactions with ECM proteins *in vivo* and make the perfect cell model to study behavioral changes of cells inside dense ECM capsules.[135] Jurkat cells are immortalized human T lymphocytes, and interact with ECM molecules after trans endothelial migration during migration to inflammation sites.[316] To overcome the limitations related to pico-injection technology, such as low injection efficiency and complexity I decide to implement a double aqueous inlet device. HaCaT cells expressing keratin-YFP or Jurkat cells are encapsulated simultaneously in a parallel

flow with either laminin-111 or Matrigel®. HaCaT cells and Jurkat cells are individually encapsulated in laminin-111 (Figure 71A, C) or Matrigel® (Figure 71B, D) consisting dsProCaps (Experimental Section 3.18 Encapsulation of cells in positively charged dsProCaps).

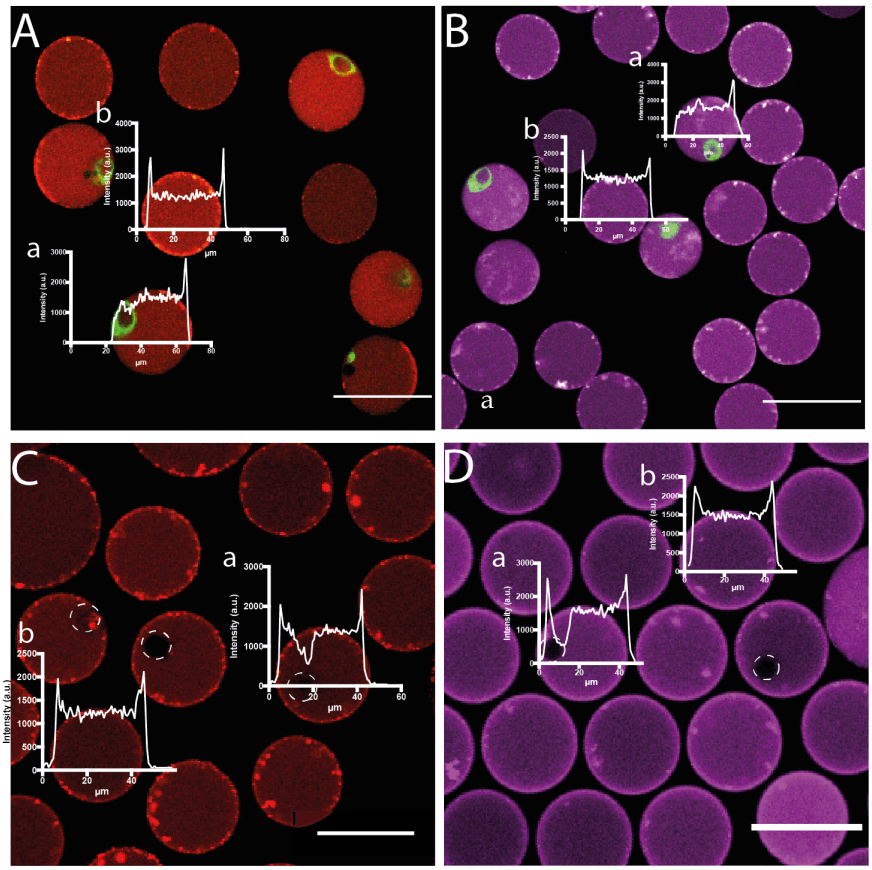

Figure 71 Encapsulation of two different cell types inside dsProCaps stabilized with N(Me)3-PEG-PFPE surfactants.

HaCaT Keratin-YFP (green) cells encapsulated in laminin-111(A) or Matrigel®(B) dsProCaps. Insets show the intensity profiles of cell-laden (a) or empty (b) dsProCaps. Jurkat cells encapsulated in laminin-111 (C) or Matrigel®(D) dsProCaps. Insets show the intensity profiles of cell-laden (a) or empty (b) dsProCaps. Dotted circles point out the unlabeled Jurkats. Scale bar, 50 µm.

Further, cell viability is investigated by encapsulating propidium iodide together with the cells and the proteins. As expected by the determination of a physiological pH environment (Figure 64), no uptake of the red dye is observed by CLSM, confirming the viability of cells. Interestingly, in every HaCaT containing droplet, the fluorescently labelled protein, which represents only 10 % of the containing protein, is attracted mostly on the opposing side of HaCaT cells, as shown by the

intensity profiles insets in the image. A clear two-peak profile is visible for empty dsProCaps while the protein attraction in cell-laden dsProCaps is clearly higher on one side of the droplet (Figure 71A, B). The theory behind this observation is that HaCaT cells produce and secrete their own ECM proteins, leading to the repulsion of the labelled protein. A first hint in the direction of this particular hypothesis, can be seen when comparing the encapsulated HaCaT cells to the Jurkat cells. In both of the two ECM conditions (laminin-111 and Matrigel®), the proteins to not accumulate on the opposite side of the Jurkat cells, as it is highlighted by the insets in Figure 71C, D. It is generally known, that suspension cells do not produce and deposit their own ECM proteins, which is underlying the phenomenon occurring in dsProCaps containing adherent HaCaT cells. Unfortunately, no literature is currently available to prove or deny this hypothesis. Most of the ECM deposition studies investigate the release of ECM proteins in a time span starting at 24 h and beyond after cell adhesion occurs.[317] In the dsProCaps, cells are observed over 2 hours only and in non-spreading conformations, revealing this repulsion phenomenon already. In order to evaluate the ECM deposition of cells over shorter time spans, I conducted a bulk ECM deposition experiment of HaCaT cells. The exact experimental conditions are explained in 3.15 ECM deposition analysis of HaCaT cells. Briefly, I seed HaCaT cells in either normal cell culture media or PBS (pH 7.4), to account for normal behavior of cells in nutritious environments and to mimic the conditions inside water-in-oil droplets, respectively. The cells are fixed 30 min, 1 h, 2 h, 3 h, 4 h, 24 h, 48 h and 72 h after seeding and stained with either anti-laminin-111, anti-fibronectin or anti-collagen type IV antibodies. Figure 72A shows the intensities of each stained protein in either media or PBS compared in one graph. Interestingly, the cells deposit the same amount of each protein in both culturing conditions after 30 min of culturing. In cell culture media after 1 h, collagen type IV is deposited first and then decreases again to allow for the deposition of laminin after another two hours in culture. Finally, fibronectin is deposited after 48 h in culture (Figure 72B). Since, the encapsulation of cells in dsProCaps occurs in PBS, the results of the deposition in PBS are more relevant to the hypothesis and highlighted separately (Figure 72C). The proteins are deposited at the same levels after 30 min of culture but also decrease together after another

30 min in culture. Interestingly, in comparison to the media conditions, fibronectin is deposited first after 2 h in culture. This result fits perfectly to the observations made in the positively charged dsProCaps. A time study shows the attraction of the labelled protein to one side of the droplet over the time course of 90 min. Intensity profiles are depicted for empty (1) and cell-laden (2) laminin-111 dsProCaps (Supplementary Figure 23). The overall intensity increases in empty droplets, while the protein accumulates on the opposite side of the cells, which is pointed out by the intensity graphs of the cells and the proteins of cell-laden droplets.

After 4 h in culture collagen type IV and fibronectin increase in intensity, while laminin-111 stays at low levels. Although interesting, this time point is not relevant for the repulsion effect in cell-laden ProCaps, since ProCaps are released after 2 h. Further, the cells did not survive in only PBS for such long time periods, which was observed by the lack of adhesion of the cells, compared to the media conditions. Nevertheless, the increase in deposition of fibronectin and collagen type IV is of particular interest, because it occurs after cell death. If there is a correlation between cell death and the excessive deposition of ECM proteins after apoptosis, it still needs to be determined.

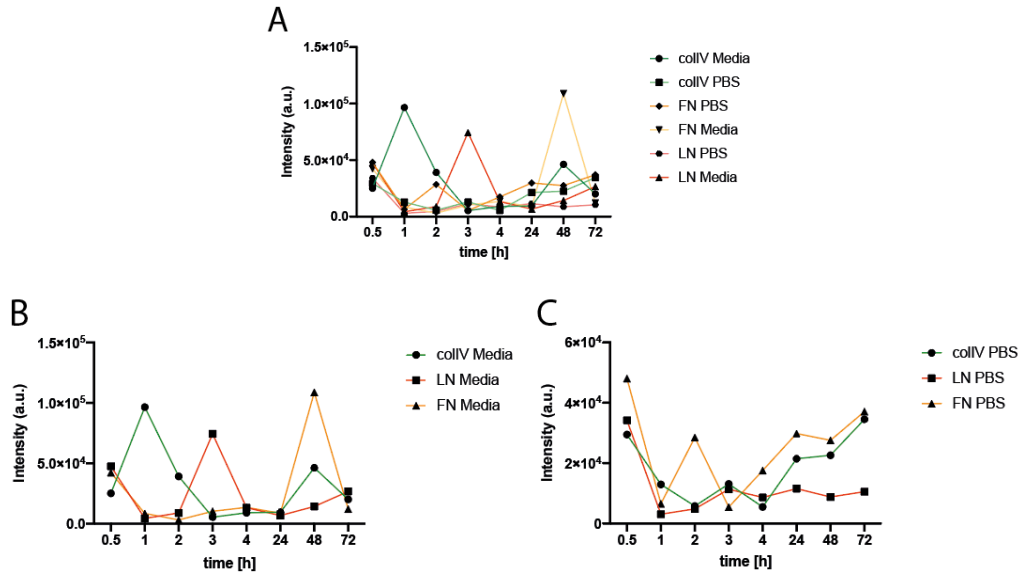

Figure 72 ECM deposition of HaCaT cells over short time periods. A) laminin, fibronectin and collagen type IV deposition inside cell culture media or PBS. B) ECM deposition of cells cultured in media. C) ECM deposition of cells cultured in PBS. Graphs are shown separately again to point out the increased deposition in PBS.

In contrast to cells encapsulated inside Krytox™/PEG-PFPE stabilized droplets (Figure 58), neither HaCaTs nor Jurkat cells are covered by the ECM proteins (Figure 71). The initial hypothesis was that the proteins are accumulating around the cells because of the higher affinity of the protein towards the cells than the charged droplet's inner periphery. This statement however is not validated after observing the missing attraction of the protein to the encapsulated cells inside dsProCaps stabilized by the positively charged surfactant. There are two possible explanations for the previous observation of proteins coating cells in negatively charged dsProCaps. First, the previously described ECM deposition experiment in PBS shows an increase in ECM deposition after the probable cell death. Further, the cells inside Krytox™ stabilized droplets are also undergoing apoptosis in the acidic pH conditions, as shown previously (Chapter 4.6 Encapsulation of keratinocytes in dsProCaps and chapter 4.9 Analysis of pH inside dsProCaps). Taken together, apoptotic cells might consequently deposit ECM proteins, which might further attract the surrounding proteins, leading to the coverage of cells by the proteins. The second hypothesis is split in two equally important aspects, which are both partly supported by literature findings. First, it was shown by Freire et al.[314] that laminin-111 polymerizes more efficiently under acidic pH conditions. I repeated this experiment in bulk and could confirm these findings (Supplementary Figure 14). Laminin-111 polymerizes most efficiently at pH 5 after 4 h at 37 C, establishing prominent polymerization patterns. This pH value is also representative of the conditions inside Krytox™/PEG-PFPE stabilized droplets as discovered and discussed earlier in this thesis (Chapter 4.9 Analysis of pH inside dsProCaps). Therefore, the proteins are already in their preferred polymerization environment, leading to an increased polymerization behavior. Secondly, another study by Paradise *et al.*[318] showed an increase in integrin activation at the lower end of the physiological pH range of cells. The authors show the opening of the headpiece of integrin $\alpha_v\beta_3$ at the pH of 6.[318] Taken together, the elevated ECM deposition of dying cells, the enhanced laminin polymerization at pH 5 and the increased activation of the laminin-specific integrin $\alpha_v\beta_3$ at pH 6 are possible explanations for the accumulation of proteins around cells inside negatively charged dsProCaps.

4.14 Creation of cell-laden ProCaps in physiological media

The successful attraction of the proteins to the inner periphery of positively charged dsProCaps and the encapsulation of living cells led to the final step of my PhD thesis. I implement the bulk release approach to release laminin-111 (Figure 73A, C) or Matrigel® (Figure 73B, D) ProCaps containing HaCaT (Figure 73A, B) or Jurkat cells (Figure 73C, D). Comparing to the previously established cell-laden ProCaps, also here the tent-like structure around the cells is visible. The proteins still undergo strong interactions with the underlying glass and force the capsules to flatten out, however, the tilted structures highlight the successful polymerization of the proteins. A future experiment to prevent those glass-ProCaps interactions could be the seeding of such capsules on passivated glass surfaces. This approach focuses on the interaction of cells with the surrounding capsule and might further reveal cell growth in ECM ProCaps only.

The success of this experiment is not only given by the perfectly assembled polymerized structures around the encapsulated cells, but more importantly, the viability of the cells is in the focus of this particular experimental result. The missing propidium iodide staining, reveals the well-being of the cells inside the ProCaps after release. By CLSM, I observe the cells inside ProCaps, showing a high interaction between cells and the proteins and the underlying glass substrate. The HaCaT cells start adhering and further proving their viability. Comparing this phenomenon to the same cell line encapsulated in negatively charged capsules (Figure 58), highlights the viability even more so. Cells inside negatively charged ProCaps keep their round morphology and do not establish any interactions with the proteins, likely exposing the cell death. Those interactions are not present in Jurkat-containing ProCaps, but based on their nature, those cells do not adhere and stretch in order to migrate. The lack of the uptake of propidium iodide ensures the cell viability of Jurkat cells inside laminin-111 and Matrigel® ProCaps. To further ensure cell viability a live dead assay was conducted. Laminin-111 ProCaps containing HaCaT cells are released into standard cell culture media and stained

directly after seeding. Thereby, no cell death was observed, supporting the viability of the cells during the production of ProCaps (Supplementary Figure 24).

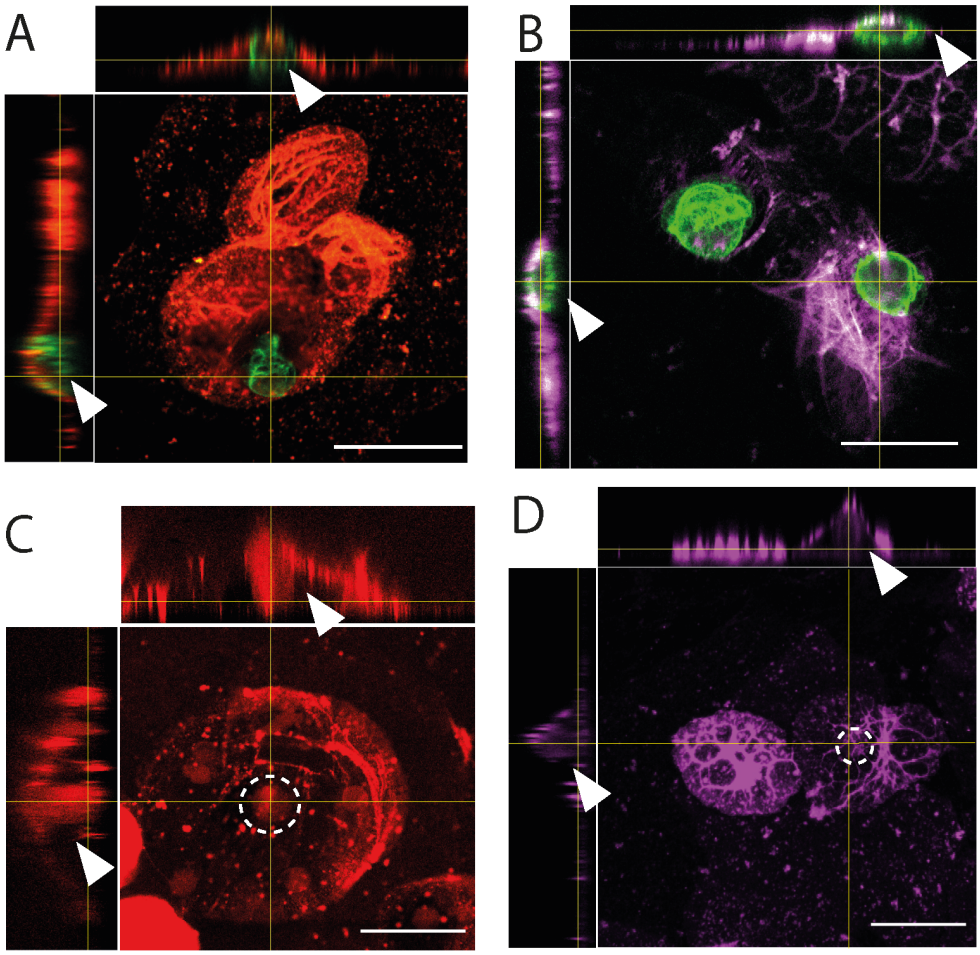

Figure 73 Generation of cell-laden ProCaps containing two different cell types.
HaCaT (green) cells encapsulated in laminin-111(A) or Matrigel®(B) ProCaps. The tent-like structure around the cells proves the successful polymerization of the proteins and the containment of HACATs (white arrow heads). Jurkat cells encapsulated in laminin-111 (C) or Matrigel®(D) ProCaps. Dotted circles point out the unlabeled Jurkats. The tent-like structure around the cells proves the successful polymerization of laminin-111 or Matrigel® and the containment of Jurkats (white arrow heads). Scale bars, 50 µm.

After the production of protein microcapsules containing living cells, the follow up study is to observe the cells over longer time periods. Here, only the observation of HaCaT cells inside laminin-111 protein capsules is chosen to investigate the effect of protein capsules on the cell. HaCaT cells are known to interact highly with laminin proteins.[135] Following the assembly of cell-laden ProCaps, a time-lapse

observation of HACAT cells inside laminin-111 protein capsules is performed. Despite the fact that the HaCaT cells are alive inside the ProCaps (REF), no cellular motility has been observed within 20 h of observation. Because the live/dead staining did not reveal cell death, the reason for this phenomenon has yet to be discovered. One potential hypothesis is that based on the stiffness values obtained by AFM indentation measurements (Chapter 7.2 Preliminary stiffness measurements of ProCaps by AFM), the capsules appear to be very soft (Supplementary Figure 27). The lack of stiff ECM proteins might hinder the movement of the cells. It is known that cells need anchoring points and stiff substrates in order to initiate actin cytoskeleton rearrangement to pull the cell towards specific directions.[81,85] In this case, the capsules provide anchoring points, since RGD is present in the proteins. However, based on the soft material and the lack of a stiff capsule wall, the cells might be just trapped in compliant ECM without the possibility of anchorage and further migration.[15] Further experiments are needed in order to investigate this hypothesis in more details and moreover generate stiffer ProCaps.

Part I: Summary

In the first part of my thesis, I was able to generate the very first microcapsules consisting solely of ECM-proteins. By the means of droplet-based microfluidics, a modular approach for the charge-mediated attraction of proteins to the periphery is established. I was able to implement two different charges at the periphery of the droplets, allowing the generation of positively or negatively charged dsProCaps. Upon release into physiologically relevant aqueous conditions single ProCaps are finally established. Further, I could show the incorporation of single cells inside dsProCaps and the subsequent release of cell-laden ProCaps. To sum up, by implementing droplet-based microfluidics the generation of ECM-based ProCaps is feasible and is a useful addition to the field of single cell-ECM investigations.

Part II

4.15 Implementation of crescent microparticles for biomedical applications

In the previous chapters, I established a platform technology – based on the development of ECM-based protein microcapsules consisting out of full-length laminin-111, Matrigel® or fibronectin – to investigate the mechanism of interaction between single cells and components of the ECM in 2.5D. Even though these ECM-based protein microcapsules allow to investigate the interaction of single cells with ECM proteins, which play a pivotal role in influencing cell adhesion[319], differentiation[320], migration[83] and phenotype stability, another important aspect in tissue organization and cell behavior is the anisotropic distribution of cellular constituents.[12] For example, specific tissue architectures rely on the coordination of cell forces, cell polarities (e.g., shape anisotropy) and cell-ECM protein interactions.[321,322] Therefore, within the context of mimicking the 3D organization of the ECM, it is important to recapitulate (1) the wide variety of topological features, which are often smooth and curved, that single cells are experiencing, and (2) the close contact of cells with ECM-based proteins. To this extent, it was shown already that curved surfaces impact the migratory behavior of T cells[323], that mesenchymal stem cells are heavily impacted by concave or convex structures in terms of their differentiation and migration behavior[324], and that the directionality of migration can be reorganized by curved surfaces.[325] However, our fundamental understanding on the impact of curvature on the behavior of cells with ECM proteins remains elusive and the underlying mechanisms continues to be unclear.

4.15.1 Generation of ECM-coated PEGDA crescent microparticles

The advantage of PEGDA crescent microparticles is the possibility of studying the attachment, spreading or migration of single cells in three-dimensional curved containers. The benefit of this particle shape is that the open bucket allows nutrients to be exchanged at all times while simultaneously providing a niche for single cell

analysis. I aimed to develop a tunable hydrogel-based system with minimal anisotropy and low roughness to highlight the interactions of single cells with laminin-111 functionalized curved surfaces. To this extent, I prepared crescent microparticles using a combination of droplet-based microfluidics, an aqueous two-phase system (ATPS) and PEG polymer chemistry (of which the mechanical properties can be tuned depending on the molecular weight and relative concentration) to obtain precise control over the size and internal structure of these gel microparticles. I use photo-polymerizable poly-(ethylene glycol) diacrylate (PEGDA) and non-polymerizable dextran (See Experimental Section 3.19 Production of PEGDA crescent particles.)

PEGDA-LAP and dextran, with or without laminin- 111 are introduced to an ATPS microfluidic device (Figure 74A) to establish a phase-separated laminar flow of these two phases. Droplets containing both phases are produced by an oil flow consisting of 0.5 w% PEG-PFPE surfactant dissolved in HFE-7500. Hereafter, a meandering channel (with a constant width of 40 μm) ensures the homogenization of the ATPS mixture after which complete phase separation occurs (Figure 74B). The perfectly phase separated droplets (Figure 74C) are selectively polymerized using high intensity UV light with a DAPI filter. After crosslinking the droplets are collected at the outlet of the microfluidic device.

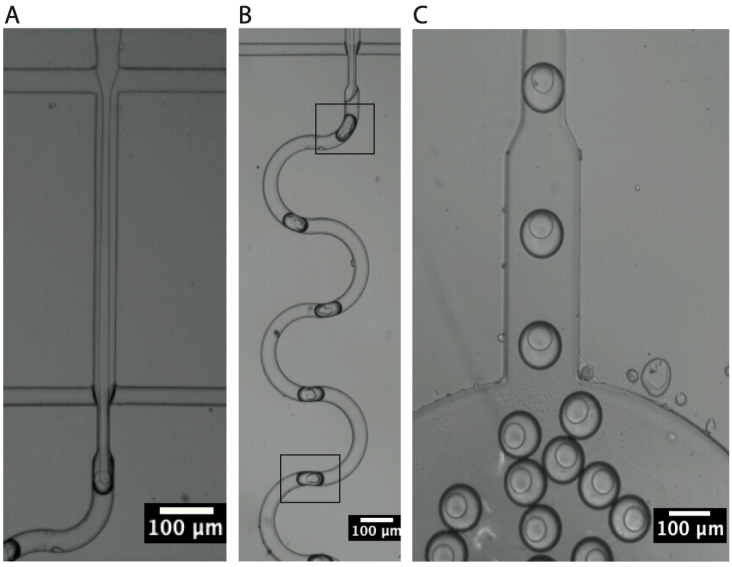

Figure 74 On chip production of PEGDA crescent microparticles.
A) Two aqueous phases consisting of PEGDA-LAP and dextran, with or without laminin-111, are establishing a parallel flow after the first flow-focusing junction of the device. With oil introducing to the system, the aqueous stream is cut and droplets can be produced at the second flow-focusing junction. B) The droplets are mixed before polymerization to ensure a phase separation inside the droplet. C) The nicely phase separated droplets with a clear dextran phase and the PEGDA bucket are polymerized on chip directly before collection.

In general, I observed that the production of phase-separated ATPS droplets, which results in crescent microparticles upon polymerization and subsequent removal of the dextran phase, follows several rules: (1) At very low concentrations of PEGDA and dextran, phase separation does not take place and results in normal spherical particles. (2) Increasing the polymer concentration leads to an enlargement of the relative opening diameter of the inner bucket. (3) The relative size of the particle cavity can be adjusted by tuning the concentration ratio of the dextran phase and the PEGDA phase. (4) Increasing the volume fraction of the dextran phase towards the PEGDA phase, results in two aqueous phases that do not completely phase separate in the microfluidic channel. (5) Finding the right UV-light intensity is crucial for the efficient and fast photo-polymerization of the PEGDA component to prevent non-uniformity of the particles. Taken together, the successful production of crescent microparticles depends on the interplay of the molecular weight of the ATPS components, the concentration of the ATPS components, the used flow rates, the concentration of the photo-initiator and the intensity of the UV light.

As mentioned before, the curved cavity of crescent microparticles are perfect containers for the investigation of single cell-ECM interactions. Therefore, I aimed to functionalize the cavity of the crescent microparticles with laminin-111 in a simple coating process. To this extent, I prepare unmodified crescent microparticles and mix them with a solution of pure laminin-111 after polymerization and the removal of dextran (detailed protocol in Experimental section 3.19 Production of PEGDA crescent microparticles). Figure 75A depicts the complete coating of the particles with a homogeneous layer of laminin-111 (antibody staining, green). This indirectly indicates the preference of laminin-111 to accumulate at a solid-liquid interface. The orthogonal view of a z-stack from CLSM shows the complete coverage of the particle with protein, present also in the cavity (figure 75B). The generation method used to prepare crescent microparticles at first and followed by the incubation with a sterile laminin-111 solution, I call the "two-step methodology". Here, the thickness of the protein layer covering the crescent microparticles is very consistent and reproducible. In general, this two-step methodology allows to investigate the mechanism of interactions of single cells with components of the ECM in 3D curved environments in more detail. These fully coated particles could be used for the investigation of cells with convex curved surfaces from the outside of the particle, while the cavity mimics concave shapes. By altering the molecular weight of PEGDA, it also becomes feasible to tailor the stiffness of the particles and investigate the changes in single cell behavior on differently stiff substrates.

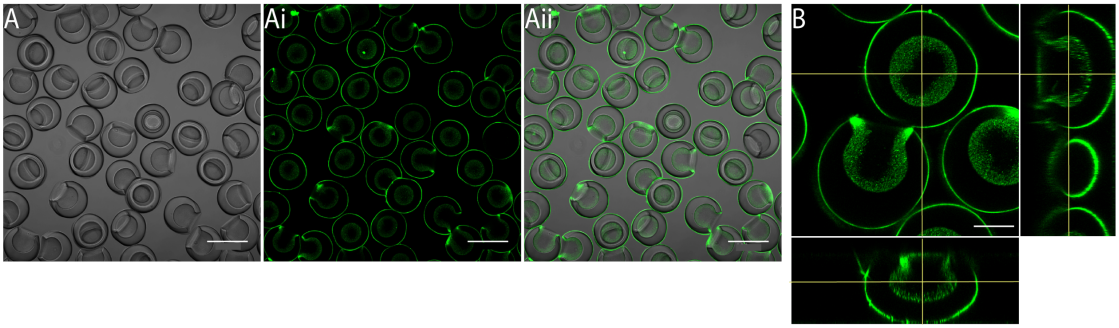

Figure 75 Coating of previously produced crescent particles with laminin-111.
A) Particles are coated in protein and stained with an anti-LN antibody (green). Scale bar, 100 µm.
B) Orthogonal view of a z-stack of protein coated particles. Continuous protein coating can be detected around the entire particle and the bucket. Scale bar, 50 µm.

After confirming the successful assembly of Laminin-111 onto crescent microparticles from multiple sides following a two-step process, I aim to restrict the protein functionalization of the cavity to a single step. Laminin-111 and 10 % fluorescently-labeled laminin-111 is added to the dextran phase, and ATPS droplets are formed at the volume rates of dextran to PEGDA at 1:5 (See Experimental section 3.19 Production of PEGDA crescent microparticles). Before using an UV light to polymerize the PEGDA particles, most of the protein accumulates at the PEGDA-Dextran interface (Figure 76A), with some residues in the cavity. The difference between polymerized and non-polymerized droplets becomes clear with Figure 76B. Here, the droplet shape is transformed due to the contraction of the crosslinked PEGDA phase. The droplet formation is changed and a bucket structure is already clearly visible. The protein strongly accumulates at the interface between PEGDA and dextran, coating the bucket of the crescent PEGDA microparticles. It is important to mention here that even though I use an UV photo-polymerization reaction for the polymerization of PEGDA microparticles, laminin-111 is only exposed shortly to the high intensity. In addition, several studies have shown the crosslinking of hydrogels and laminin-111 isoforms and demonstrated the functionality of laminin after short exposure times.[326] After several washing steps, the non-polymerized dextran phase is removed and the final product is visible. Two crescent particles are depicted, one from the top, were the round shape is clearly visible, with a red laminin- 111 ring on the inside. The second particle is shown from

the side, with a separated laminin-111 layer clearly only in the inside of the bucket (Figure 76C). This is also a clear indication for the successful removal of dextran, since no protein molecules remained in the middle of the bucket. After release of the fully polymerized crescent particles, before the removal of the dextran phase, laminin-111 residues are visible in the cavity (Supplementary Figure 25).

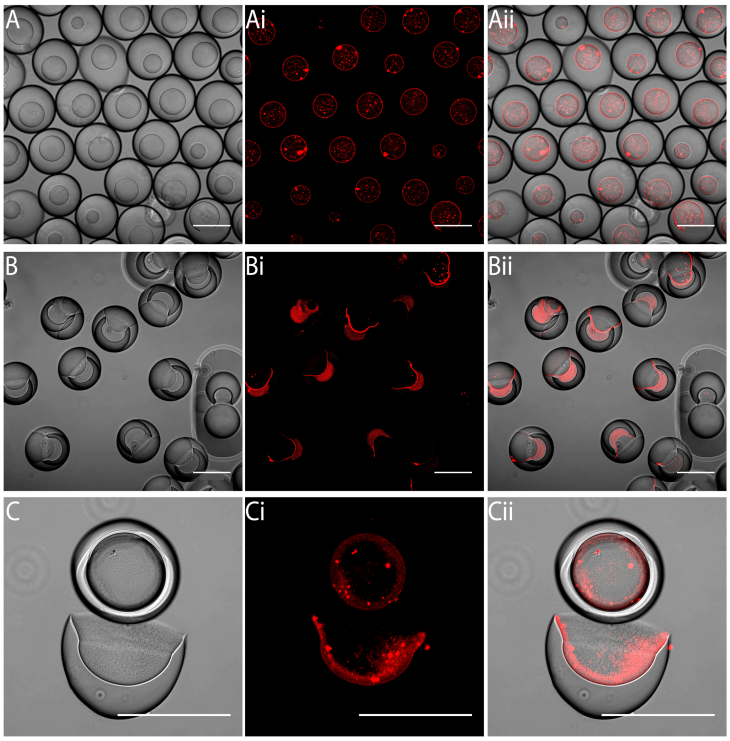

Figure 76 Production of laminin-111 coated crescent microparticles.
A) Brightfield image PEGDA-Dextran+Laminin-111 droplets produced on chip and collected without polymerization of the PEGDA phase. Ai) Laminin-111 (red) distribution inside the dextran phase. Aii) Overlay of brightfield with laminin-111 depicts the restriction of the protein to the inner dextran phase. B) Brightfield image PEGDA-Dextran+Laminin-111 droplets polymerized on chip. Bi) Laminin-111 (red) attraction towards PEGDA phase after polymerization of the droplets. Bii) Overlay of brightfield with laminin-111 depicts the accumulation of the towards PEGDA. C) Brightfield image of released PEGDA crescent particles. Ci) Lamininn-111 distribution on the bucket periphery. Cii) Overlay of PEGDA microparticle with an inner cavity coating of laminin-111. Scale bar, 100 µm.

4.15.2 Single cell analysis in PEGDA crescent particles

Until now, I have shown that crescent microparticles can be prepared using an ATPS system and droplet-based microfluidics. Moreover, I could show that the cavity of my crescent microparticles can be selectively functionalized by adding Laminin-111 to the dextran phase. After polymerization of the crescent microparticles by focused UV light, the dextran phase can be easily removed after several washing steps in PBS, leaving behind cavities of which the surface is functionalized with laminin-111 given its preferred partition towards the PEGDA phase. These crescent microparticles remain stable for several weeks in aqueous solutions (PBS, cell culture media, etc.).

I optimized the fabrication parameters in such a way that single cells can be seeded onto the crescent microparticles. In order to seed cells onto the crescent microparticles, a confluent monolayer of crescent microparticles is pipetted onto the bottom of a well plate. Given the unique morphology of the microparticles, they spontaneously rotate to settle with their cavities facing upwards as a consequence of gravitational forces. Exploiting this feature, cells can be easily seeded over the particles and allowed to settle and attach as a consequence of the presence of laminin-111. Here, HaCaT-Keratin YFP cells are used to follow the shape changes of the cells over time, without the need of an additional staining. Figure 77 depicts a single crescent bucket with a laminin-111 coating loaded with two single HaCaT cells. After observing that the labelled laminin-111 signal is reducing over time, I assumed that the encapsulated cells take up the laminin-111 by endocytosis (Supplementary Figure 26). This leads to the loss of ECM-cell contacts inside the buckets and further results in cell death. The subsequent addition of pure RGD molecules rescued the cells and allowed the attachment to the curved cavity. This implies that the crescent microparticles, functionalized with ECM protein allow the investigation of the initial contacts of cells with ECM proteins and the fundamental mechanism of action. I use an orthogonal view tool in ImageJ to show the enclosing of the cells inside the buckets. Seeding the cells inside the bucket is a bulk approach, which leads to additional cells seeded around the particles (Figure 77). In the future,

it might be interesting to investigate whether the size and opening diameter of the crescent microparticles needs to be enlarged in order to allow a more efficient cell loading capacity. However, based on the interactions between the cells and the buckets, it is feasible to transfer the cell-laden crescent microparticles to a new observation plate, to remove the additional cells in the surrounding. However, here I keep the cells surrounding the particles as an internal control for cell survival.

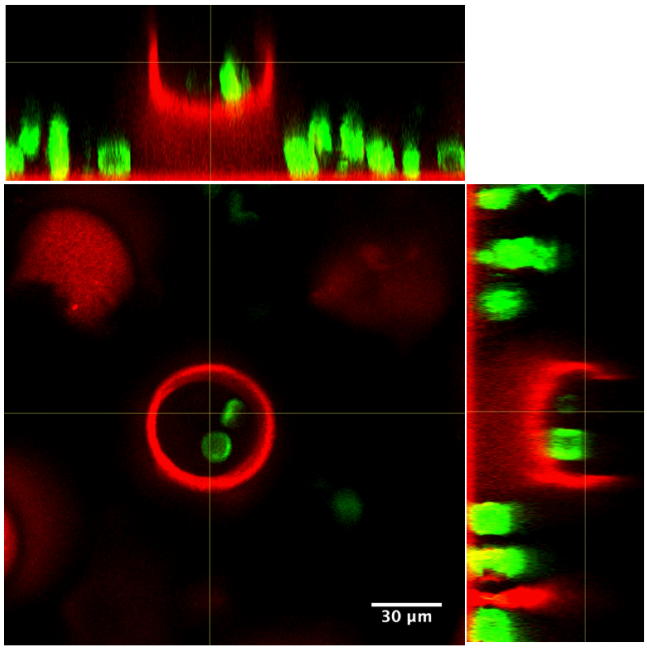

Figure 77 HaCaT cells loaded into laminin111-coated crescent particles.
Orthogonal view of a crescent particle with laminin-111 (red) coating and two HaCaT cells (green) inside the particles. Image was taken directly after cell seeding, many cells are seeded around the bucket on the bottom of well plate.

Subsequently, I imaged the cell-laden crescent microparticle for 11 hours and could observe the successful division of cells inside the ECM coated cavity (Figure 78). After 260 min of culture, the cell starts dividing and two daughter cells are detected after 560 min. Moreover, the third cell inside the bucket starts spreading slightly and adhering to the bucket after 600 min. This stunning occurrence strengthens the hypothesis that the cells are in tight interaction with their underlying ECM inside the bucket, further supported by studies that show cells need anchoring points to divide.[25,88,327] In the future, I am planning to execute several immunostaining in order to further understand the interactions of single cells with ECM proteins. The

observation of cell division suggests the ability to mimic environments that support cell division and other cellular functions in a 3D environment but without the need of complete cellular adhesion and elongation. This observation shows that laminin-functionalized crescent microparticles are a useful tool to study single cell biology in curved 3D environments in more detail.

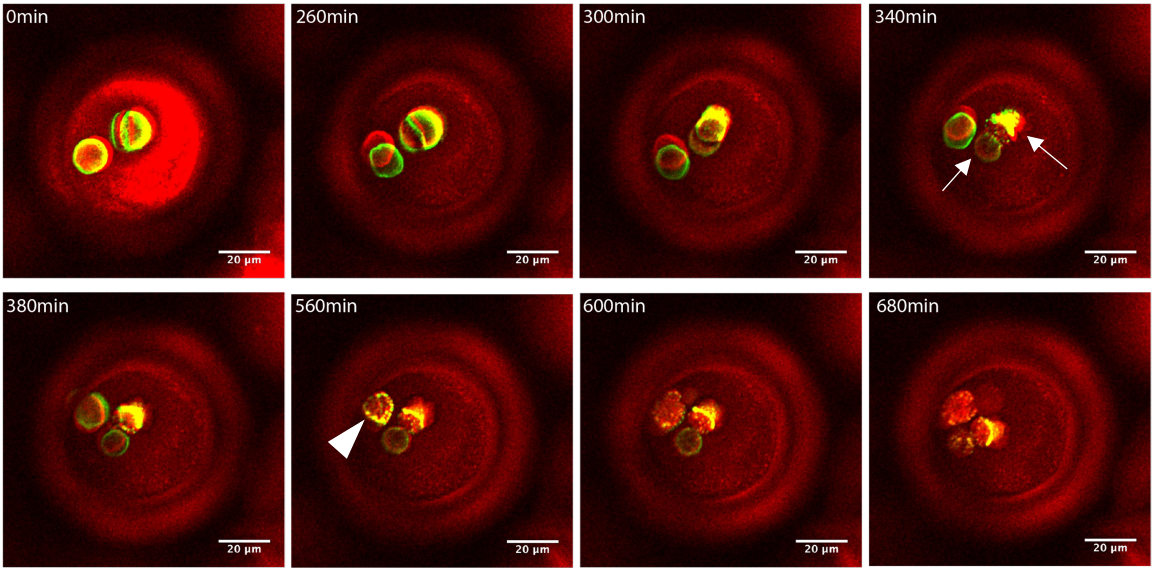

Figure 78 Cell division of a single HaCaT cell inside a laminin-coated crescent particle.
Time observation of a single cell dividing in a laminin coated crescent bucket. White arrows show the dividing cell and the daughter cell after 340 min. White arrow head shows the third cell attaching to the particle after 560 min.

Part II: Summary

In the second part of my thesis I established the successful functionalization of crescent microparticles with laminin-111. To this extent, I developed a broadly applicable one-step process to coat the cavity of crescent PEGDA microparticles taking advantage of the phase separation of the components of the ATPS system and the preferred accumulation of protein at the solid-liquid interface. In addition, I demonstrated the successful loading and adherence of (single) cells within the curved and ECM-coated surfaces of the crescent microparticles. The successful interaction and division of a single cell inside these ECM-coated curved cavities supports the potential use of crescent microparticles to investigate single cell behavior in 3D microenvironments.

Summary and Outlook

5 Summary

Many cellular functions are known to depend both on the mechanical properties of their environment and on the distribution of available biochemical ligands.[68,145] In the current state of the art systems, ECM-cell interactions are mainly analyzed on either protein-coated 2D planar surfaces[328] or in 3D constructs made out of protein-containing hydrogels.[329] The drawbacks of the 2D approaches are the lack of the interaction with ECM-proteins from the basal and apical sides. In the case of 3D hydrogel-based systems the independent control over the mechanical properties that are mainly dictated by the cross-linked polymers and the biochemical triggers affected by the proteins is the significant limitation.[124] Hence, to study cell-ECM interactions the aim of my PhD thesis was to implement modular droplet-based microfluidic technology in order to design and develop cell-laden microcapsules consisting entirely of extracellular matrix proteins. Particularly, I focused on the generation of two new systems: 1) ECM-protein based microcapsules and; 2) ECM-protein coated PEGDA crescent microparticles.

Currently, there is a wide range of capsule sizes, production techniques and components available. At the first glance the broad variety of capsules might be overwhelming. By tuning the search parameters in a literature research to capsules in the micrometer range rather than nanocapsules, the number of existing capsules is attenuated. Most of the capsules are made out of polymers such as PSS[208], PNIMPAM[197] or PLL[209], which are shown to be biocompatible and stable. However, these capsules made of synthetic polymers cannot be designed for cell-ECM interactions studies, but rather are implemented for drug delivery applications. Adding the term "protein-based" in front of "microcapsules", shortens the literature list even further. Currently, protein-based microcapsules are mainly consisting of human serum albumin (HSA) [185,187,188], which does not have a very important role in the activation of important cellular functions. However, it is an abundant protein and allows for the fast and stable polymerization around templates. Finally, tailoring the literature search to "ECM protein-based microcapsules" does not yield any results

currently. This makes it even more interesting to establish such protein-based microcapsules, not only for the detailed investigations of cell-ECM interactions from their basal and apical side, but also to fill the general gap in the spectrum of currently existing microcapsules.

In my PhD thesis I discuss two novel methods for the cell-laden dense ECM compartments. One method allows for the encapsulation of cells in microcapsules consisting entirely of ECM proteins, while in the other approach cells are interacting with ECM proteins coating the inner surface of curved PEGDA microparticles. Both strategies have the potential to highlight unknown characteristics of cell behavior upon ECM contact on differently shaped surfaces.

In order to generate protein-based microcapsules, I implemented the modular droplet-based microfluidic technology and used water-in-oil droplets as basic scaffolds for the generation of protein microcapsules. Various production and characterization steps were needed in order to establish such unique ProCaps. In **Chapter 4.2** I focused entirely on the basic principles of dsProCaps assembly processes. By stabilizing water-in-oil droplets with a combination of neutral and negatively charged PEG-based fluorosurfactants, it became possible to apply charge-mediated attraction between different kinds of ECM proteins and ions to the charged interface. This charge-mediated interaction is the key to the successful generation of protein-based microcapsules. Here, I used positively charged ions as mediators for the attraction between the negatively charged proteins and the charged water-in-oil droplets surfaces in order to establish droplet-stabilized protein microcapsules (dsProCaps). Many characterization experiments were performed for a better understanding of the basic mechanics behind the attraction, assembly and polymerization of the proteins (**Chapter 4.3**). I showed the assembly of dsProCaps in a size range of 5 – 100 µm in diameter, showing the wide range of potential applications. Following the successful assembly of dsProCaps I set out to analyze their physicochemical and biological properties. For the very first characterization experiment I use a microfluidic deformation chamber device, by which it was possible to analyze the dynamic interfacial properties of single water-in-oil droplets. Those results revealed the complex dynamics of such dsProCaps. Those first impressions of

the polymerization pattern lead to the investigation of the diffusivity of proteins at the interface of water-in-oil droplets by FRAP (**Chapter 4.3.1**). In **Chapter 4.4** I proceed to the release of ProCaps out of the stabilizing oil shell. Attracting the proteins to the inner periphery of droplets and hence establishing dsProCaps achieves the first step of establishing ECM protein-based microcapsules (ProCaps). By implementing a bulk release approach, the outer oil shell layer of the droplets is removed and allows for the successful release of such ProCaps. For the first time in the history of microcapsules it is possible to generate microcapsules, consisting entirely of ECM proteins.

Two major characterization experiments are performed to understand the morphology of the capsules in more details. First, an immunostaining was conducted in order to visualize the complete structure of the ProCaps (**Chapter 4.4.5.1**). In a second experiment I encapsulated FITC-dextran molecules of different molecular weights to investigate the diffusivity through the porous capsule wall (**Chapter 4.4.5.2**). Thereby, I detected that the capsules are less porous than previously assumed.

After the successful assembly of ECM-based protein capsules and the range of characterization experiments, I started to incorporate various eukaryotic and prokaryotic cells. First, I focused on prokaryotic cells in order to observe the retainment of organisms in the ProCaps (**Chapter 4.5**). Those experiments showed the successful assembly of ProCaps containing bacteria and allowed for the first impression of the capsule shape containing bigger organism such as ookinetes.

To finalize my PhD thesis, I encapsulate single eukaryotic cells inside dsProCaps (**Chapter 4.6**). With the so-called pico-injection technique, I inject different cell types after the charge-mediated assembly of a protein layer at the interphase of water-in-oil droplets. However, the cell viability in negatively charged ProCaps was immensely impaired and led to cell death. Further studies revealed that the well-being of the cell was reduced by the acidic pH environment generated by the negatively charged surfactant molecules. Based on this observation, cell-laden ProCaps were further only produced by using a positively charged surfactant, where I measured a physiological pH environment (**Chapter 4.10.2**). Cell survival was ensured and I could release cell-laden ProCaps and observe cell viability (**Chapter 4.14**). Studying the cells inside the ProCaps reveals their elongation and attachment to the protein surface, which leads to

the conclusion of healthy and interactive cells. The establishment of ECM ProCaps allows, on the one hand for the investigations of various kinds of healthy and diseased cell types with their surrounding ECM, and on the other hand for mimicking 3D tissues *in vitro* when using such capsules as building blocks for 3D bioprinting. Additionally, to the broad application aspect of the ProCaps, the capsules *per se* count as a novel technology. Within the scope of my thesis, I add a new production process for the establishment of microcapsules to the list of existing capsule-generation technologies. Further, those microcapsules consist of a new and versatile material, which are not yet used in literature. Using a charge-mediated approach for the attraction of various kinds of proteins and molecules allows for the generation of a range of general protein-based microcapsules. Any wanted content can be introduced to the droplets prior to polymerization of the capsule wall.

In the second part of my thesis, I produce ECM-coated PEGDA crescent microparticles (**Chapter 4.15**). The technology of crescent microparticles is already well known and established. I advanced this technology by coating the inner cavity with a layer of laminin-111. The coated cavity enables the attachment of cells on curved substrates. The main advantage of this system is the possible investigations of cells with their underlying ECM substrate on a curved shape. Further, by the open structure of the microparticle, constant supply of nutrients is ensured. Those advantages were proven by the successful cell division of a single cell in contact with the laminin-111 layer inside the bucket. In this thesis, the attachment properties of cells inside these crescent microparticles are investigated and suggest the great potential of PEGDA microparticles for cell microencapsulation. The importance of different cellular behaviors such as curvotaxis, proliferation and migration in rounded environments can be studied using this newly created ECM container. Further, it becomes feasible to mimic various tissue types by tailoring the stiffness of the PEGDA containers. This possibility opens up various stiffness studies, combined with ECM interactions. Furthermore, showing the successful coating of the inner bucket shape paves the way for the coating with various molecules and investigations of different types of cell contacts, ranging from cell-cell or various cell-pathogen interactions.

6 Outlook

In the first part of my thesis, I concentrate on the generation of microcapsules consisting entirely of ECM proteins. I further show the successful encapsulation of single cells. The second part of my thesis focuses on the addition of an ECM layer in the cavity of crescent PEGDA hydrogel-microparticles. Both achievements open up investigations of various cell-ECM interactions and the consequent changes on cell behavior.

6.1.1 Proposed applications for cell-ECM studies inside ProCaps

Establishment of ProCaps allows for the exploration of cell behavior within ECM-based compartments. Particularly, it will be exciting to analyze cell motility and adhesion processes in 3D confined spaces with systematic modulation of the mechanical and biochemical capsule properties. As I already demonstrated in Chapter 4.2**,** the properties of the capsules can be adjusted to mimic the best tissue conditions for a given cell type. Additionally, this system will enable investigations on the outbreak of cancer cells from compact ECM, which can be modulated and studied intensively on a single-cell level. Further, these capsules could be designed to induce stresses on cells which, in turn, would have an effect on the intracellular arrangement of the cytoskeleton and impacts the tensegrity of the cell. Tensegrity *per se*, is a subfield of mechanobiology. It focuses on the effects mechanical stress has on the internal cytoskeleton of the cells, rather than inducing motility of the cells. Continuous tension inside the cell is working against the forces influencing the cell from the outside, leading to changes of the actomyosin cytoskeleton. By encapsulating cells inside dense ECM capsules the effects of mechanical stress on the internal arrangement of the cells can be studied.

6.1.1.1 *Cancer cell behavior in confined ECM capsules*

The effects of mechanical stress on tumor progression were shown previously.[89,113,330,331] Cancer cells were driven towards invasive and aggressive phenotypes when under constant mechanical stress.[332,333] Currently, various stress levels are exerted on cancer cell monolayers or tumor spheroids by co-culturing cells with microbeads in differently stiff agarose gels.[334] An application possibility for my newly generated ProCaps is to investigate if mechanical stress can drive normal cells towards cancerous lineages. Hereto, natural cells can be trapped in stiff ECM confinements, such as the ProCaps are offering, and observed for a potential change in the phenotype towards cancer cells (Figure 79). Rho-dependent cytoskeletal arrangements were shown to be activated under constant stress.[331] Based on the upregulation of Rho, focal adhesion generation is induced, which further activates the actin cytoskeleton and induces cell migration, which in the case of cancer cells leads to metastasis and invasion. The question arises, if the same pathways can be induced by the encapsulation of healthy cells inside ECM capsules, or ultimately new connections between mechanotransduction and cancerous pathways can be established. The impact on cancer cell generation can be analyzed by this novel technology and further genetic information can be gathered by simply collecting and sequencing the trapped cells.

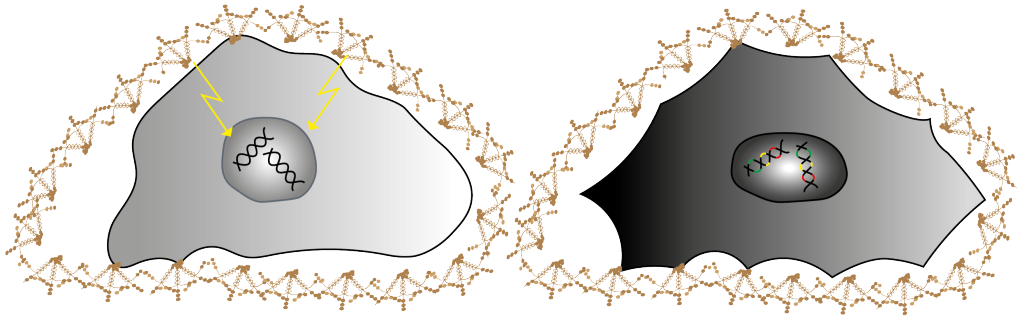

Figure 79 Mechanically induced cancer cell formation.
By the encapsulation of healthy cells and the constant force, is it possible to trigger cancer cell phenotypes?

6.1.1.2 *Cell migration through dense ECM capsule walls*

Another study enabled by the development of my capsule technology is the observation of cancer cells escaping out of tight ECM-protein microcapsules. It is well known, that the ECM of the tumor-microenvironment is stiff and consists mostly out of laminin-111 and fibronectin.[108,118,335,336] Therefore, it is possible to adjust the mechanical properties of capsules and to encapsulate aggressive cancer cells into such microcapsules and observe their outbreak over time. By imitating tight confinements, it becomes possible to trigger tissue-specific MMP release and observe the degradation of the ECM capsules and the subsequent controlled migration of cells out of ProCaps (Figure 80). These specific conditions would couple actin cytoskeleton rearrangement and lamellipodia assembly on single cells as they crawl out of 3D confinements. Further, close observations of integrin rearrangement can be performed to understand the interactions of cancer cell outbreaks with more complexity. Next to the mechanical changes inside the cells which are taking place during outbreak, the release of additional enzymes and molecules is also of interest for understanding the survival of cancer cells in stiff confinements. After analyzing and understanding the interaction between physical and biochemical mechanisms behind cancer cell outbreak, the emergent pathways could be directly targeted in tumor therapy.

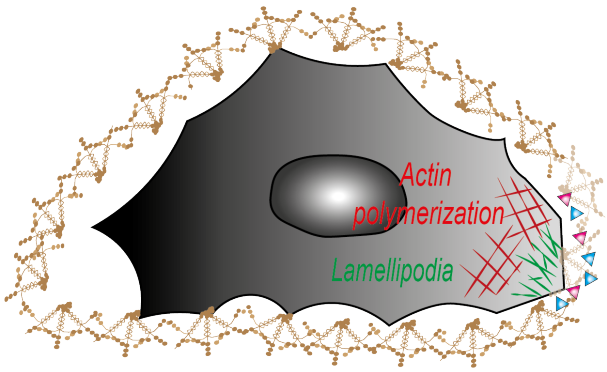

Figure 80 Can we trigger MMP-based ECM degradation, migration of cancer cells out of the capsule and further observe and the effects on the actin cytoskeleton?

6.1.1.3 *Immunological studies within ECM-based ProCaps*

As demonstrated in Chapter 4.14 it is possible to encapsulate a variety of different cells inside ProCaps consisting of various proteins. Thereby a broad study approach focusing on cytokine release of immune cells out of a confined ECM environment becomes feasible.[337] As it is known, effector T cells are attracted to inflamed tissues by the incorporation of various chemoattractants inside the ECM.[338] The encapsulation of immune cells in ProCaps would allow for the detailed analysis of the effect of ECM on the cytokine release profile and the subsequent attraction of other cell types (Figure 81).[323] Towards this end, co-encapsulation of specially designed beads for cytokine sensing together with cytotoxic cells would lead to the immediate analysis of the immunological mechanisms within different tissues.[23] Ultimately, the interaction between immune cells and cancer cells through a shielding ECM barrier can be investigated by encapsulating cancer cells and allowing the attraction of immune cells from the surrounding environment. This experimental setup can highlight the close enzymatic and cytokine-based interaction between immunological and diseased cells. With the approach of confining cells inside dense ECM, the goal is to simulate ECM niches *in vitro* and further observe cell-cell communication of various cell types and to the surrounding condition.

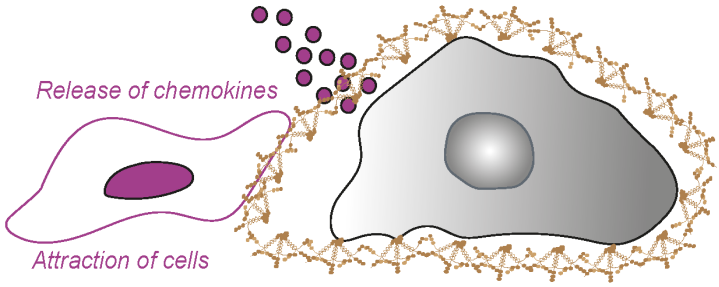

Figure 81 Immune cell attraction.
Encapsulated cells will most likely release various kinds of chemokines, which in turn can attract surrounding cells. This mechanism allows for the investigation of different cell interactions through the ECM microcapsule wall.

6.1.1.4 *3D bioprinting of cell-laden protein microcapsules*

Another very interesting implementation of the ProCaps technology is the usage for 3D bioprinting applications. Much effort has been invested in the printing of tissues *in vitro* by using cell sheets surrounded by polymers or proteins embedded in hydrogels.[339-341] Here, the idea is to use protein capsules as three-dimensional building blocks, with single cells enclosed by their own extracellular matrix (Figure 82). Tissue construction would benefit from the suggested approach based on the porosity of the capsules, which allows for constant nutrient transport. The 3D generated construct would mimic the *in vivo* situation with higher fidelity to natural environments than artificially constructed cell stacks, given the use of native proteins in the generation of ProCaps. Further, ECM degradation and deposition by the incorporated cells would be induced at an earlier timepoint than using polymer-based constructs.[125,341-343]

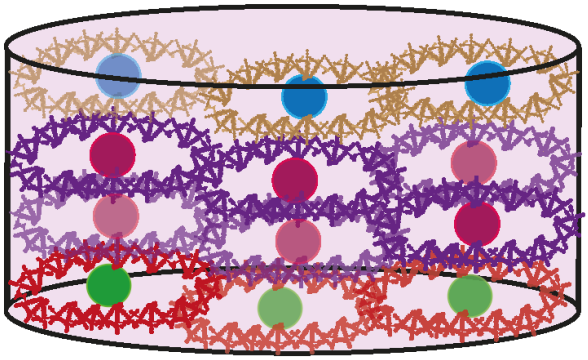

Figure 82 3D bioprinting with cell-laden ECM microcapsules.
The established cell-laden microcapsules can be used as building blocks for the arrangement of various tissue types in vitro. Here, different cell types can be encapsulated in any ECM-protein of choice and used to build any tissue-like structure of choice by mix & match.

6.1.1.5 *Investigations of SynCell-ECM interactions*

The field of bottom up synthetic biology has emerged in the recent years and basically combines an engineering mindset with biology.[344] Synthetic biological projects range from the simple generation of biological shapes by osmotic pressures[345] over recombinant DNA technology[346] to the synthesis of microbial genomes[347] and the generation of protocells.[348] In the scope of my thesis, I am interested more in the generation of simplified artificial cells and ECMs.[349,350] Synthetic cells and synthetic ECMs have been discretely built, and the effects of synthetic ECMs on natural cells is observed.[351,352] However the combination of synthetic cells in contact with natural ECM has not yet been investigated. Encapsulating synthetic cells inside ProCaps consisting of different ECM proteins would enable the analysis of simple adhesion patterns with protein-specific or unspecific integrins incorporated into the synthetic cell membrane (Figure 83). This type of approach removes uncontrollable variables from the experimental design and once the fundamental role of a protein like integrin is understood, can incorporate more complexity. For example, by encapsulating MMPs and a built-in release process which is triggered upon deformation of the SynCell through specific integrin binding, ECM degradation can be mimicked. The release itself would be accomplished by incorporating shorter tailed lipid molecules inside the SynCells to provide a breaking point upon deformation.

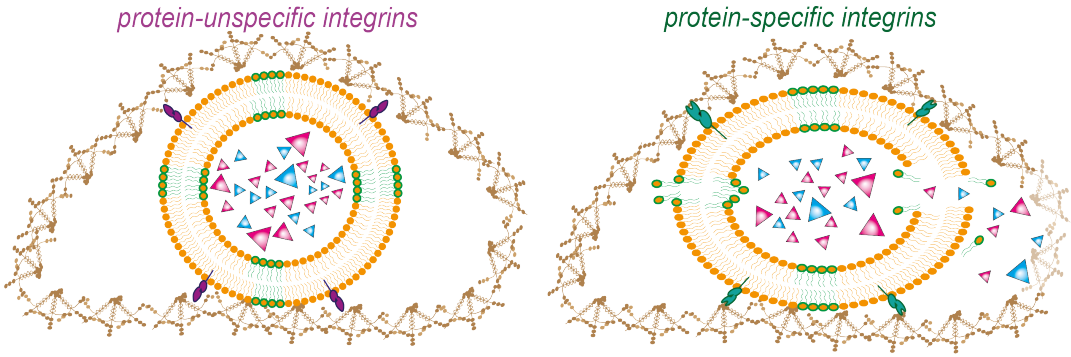

Figure 83 SynCell-ECM interaction inside ECM-based microcapsules.
Can we trigger the release of MMPs out of SynCells upon the binding of specific integrins?

6.1.2 General application possibilities for crescent microparticles

The generation of crescent-shaped PEGDA hydrogels and their use in biomedicine is a relatively new field which holds many promising application possibilities by altering the cavity of such particles.[219,221] Many researchers are loading differently coated crescent particles with cells and observe general interactions such as the spreading of cells on gelatin coated cavities[222] or the simple loading, transport and release of cells on RGD containing cavities.[221]

6.1.2.1 Single cell studies inside PEGDA crescent microparticles

One major application of the crescent PEGDA microparticles is to investigate the complete spreading of cells on various ECM proteins used to coat the inner bucket of the cavities and evaluate the movements of single cells on curved surfaces (Figure 84A). It was shown that curvotaxis influences collective cell migration on curved landscapes and that these movements are directed by an interplay of the nucleus and cytoskeleton.[353] However, those studies are conducted on concave structures with only 10 µm in diameter, allowing the cells to migrate over hill-like structures. In contrast, encapsulating cells in our crescent microparticles with bucket sizes around 40 - 60 µm in diameter will allow for the complete spreading and potential generation of FAKs at the cell surface. Another investigation follows the results achieved by Dobre *et al.*, where they generate hydrogels containing various laminin isoforms and tissue specific growth factors, showing stem cell differentiation towards osteogenic lineages.[326] Here, the idea is to coat the inner bucket with various laminin isoforms and selectively bind growth factors to allow cell adhesion and differentiation towards specific lineages.[326] It is widely known that the abundance of different laminin isoforms are tissue dependent and have higher affinities to tissue specific growth factors and hence trigger cell differentiation towards osteogenic or neuronal tissues.[354] By coating the bucket of the crescent microparticles with tissue specific proteins and the corresponding growth factors, it becomes possible to trigger stem cell differentiation and proliferation towards a specific lineage (Figure 84B).

The beauty of the crescent technology is that coating the cavity is not limited to laminin proteins exclusively. Another biomedical application of the crescent particles is to trigger antibody release upon B cell encapsulation. B cells are important immunological players, which secrete specific antibodies upon contact with antigens. By loading B cells inside the crescent microparticles it becomes possible to establish a close contact to specific antigens used to coat the cavity. Hereby, it is possible to select and produce hyper-secreting B cell populations for the generation of highly monoclonal antibodies (Figure 84C).

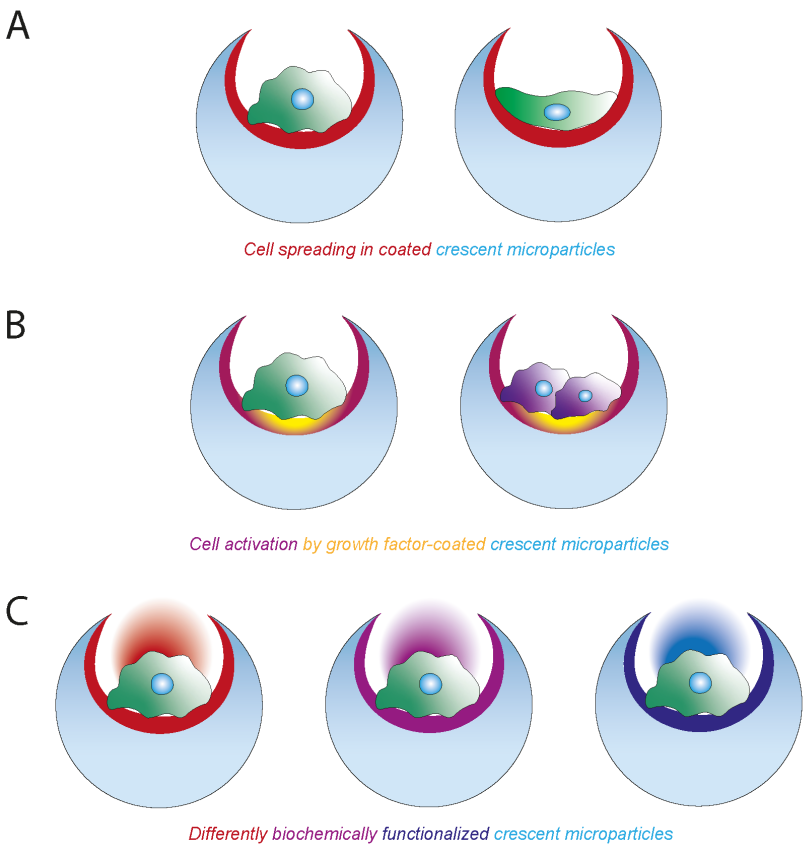

Figure 84 Application possibilities for coated PEGDA hydrogel crescent microparticles.
A) Cell spreading in adhesion coated crescent particle cavities. B) Stem cell differentiation and proliferation on cytokine coated particles. C) Implementation of various antigens and observation of antibody release from B cell populations.

6.1.2.2 *Crescent microparticles as containers for controlled spheroid cultures*

The previously mentioned applications of single-cell based crescent microparticles, shows the great potential for evaluating the impact of curved substrates for biomedical applications. Importantly, the applications are not limited to single cell studies only. By adjusting the cavity diameter of the microparticles it is feasible to collect several cells (Figure 85A) and serve as incubation containers for cell growth that eventually leads to spheroid formation (Figure 85B). By providing cells with a curved ECM layer on the basal side, cells have a mechanical support to initialize proliferation that will lead to deposition of native ECM proteins and formation of spheroids. (Figure 85C). The major advantage of those particles is the that the spheroids will be the same size and together with the open cavity of the particles a constant nutrient supply is ensured. Changing the functionalization depending on the cell type of interest, various spheroid types can be generated. Finally, by changing the molecular weight and relative concentration of PEGDA the stiffness of the particles can be tuned to closely investigate spheroid formation on differently rigid substrates.

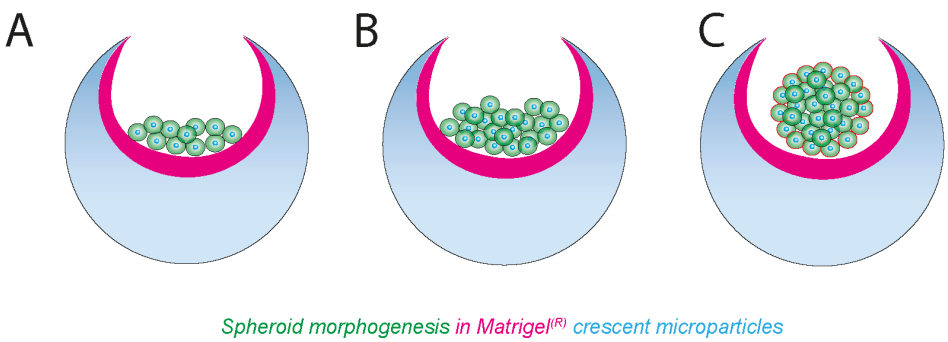

Figure 85 Step-wise spheroid formation inside crescent microparticles.

7 Appendix

7.1 Supplementary Figures and Tables

7.1.1 Characterizing dsProCaps established with Krytox™/PEG-PFPE

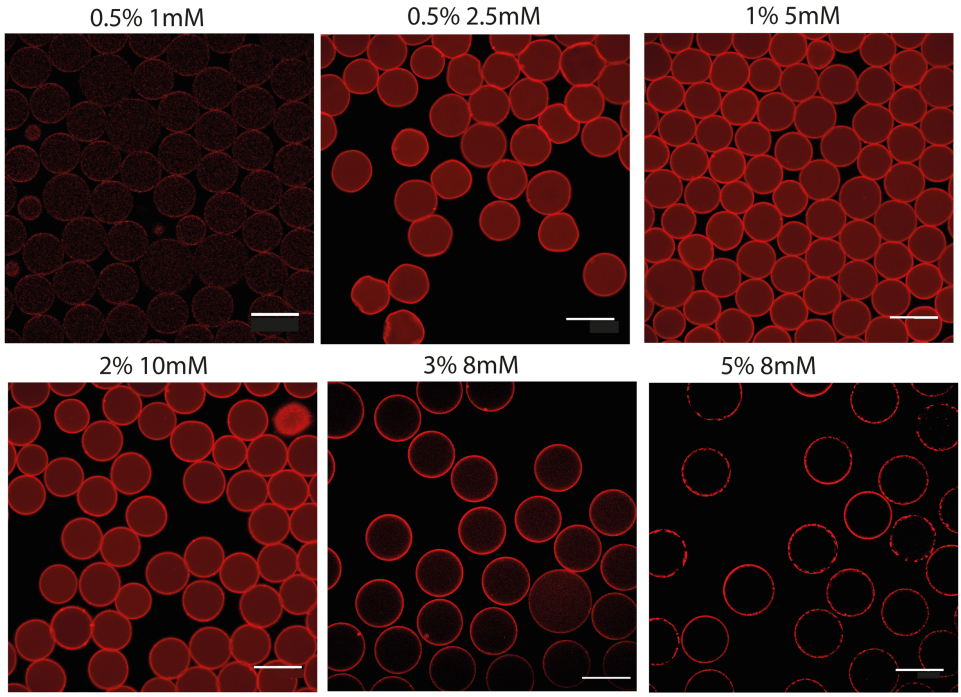

Figure SI 1 Concentration study for an efficient protein attraction.
Different Krytox™-to-PEG-PFPE conditions tested to determine droplet stability and protein attraction to the inner droplet periphery. Higher Krytox™ (mM) and PEG-PFPE surfactant (w%) concentrations stabilize the droplets better and allow for a clean attraction of laminin-111 to the inner periphery. Scale bar, 50 µm.

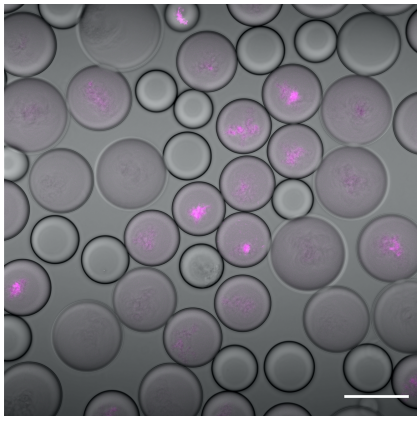

Figure SI 2 Matrigel® encapsulation in 1.4 w% PEG-PFPE stabilized droplets without Krytox™.
Scale bar, 50 µm.

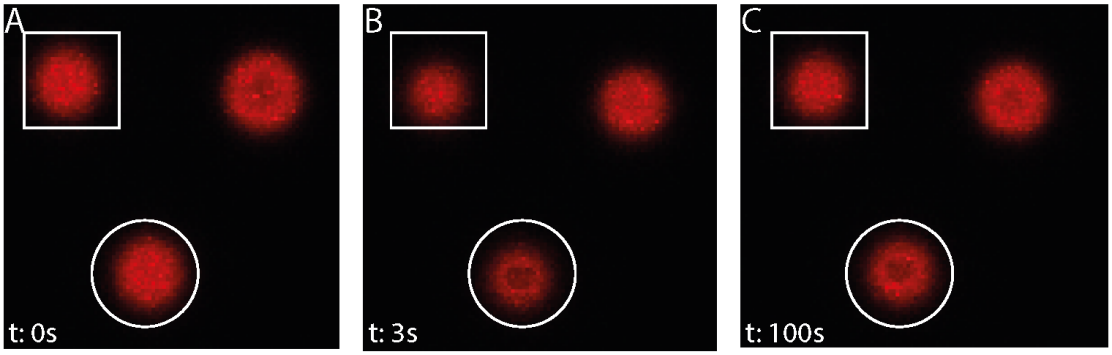

Figure SI 3 FRAP measurements on Krytox™/PEG-PFPE stabilized laminin-111 dsProCaps. One droplet serves a non-bleach control (Square). B) Bleaching occurs after 3s. C) No fluorescence laminin-111 recovery is detected over 100s (Circle).

7.1.2 Estimation of the right time point for ProCaps generation

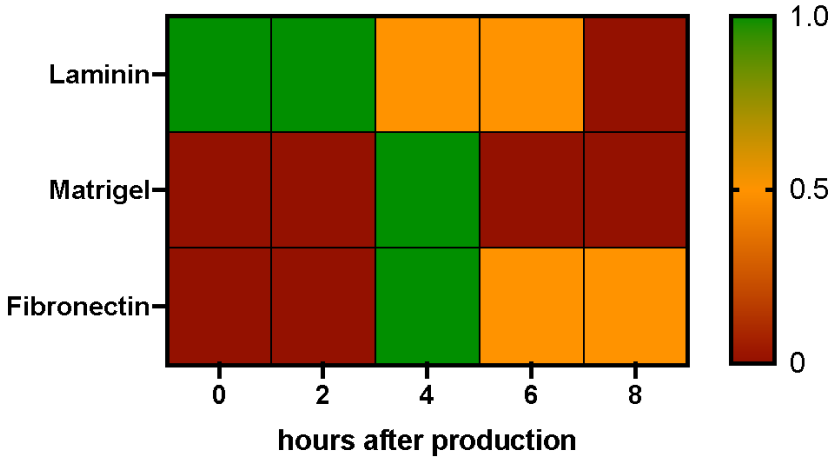

Figure SI 4 Release efficiency of ProCaps generated out of Krytox™/PEG-PFPE stabilized dsProCaps over time. Three different ProCaps types are released every 2h after incubation at 37 °C. 1; fully released capsules, 0.5; half-released protein capsules, 0; no capsules formed.

7.1.3 *Release of differently sized ProCaps with various microfluidic release devices*

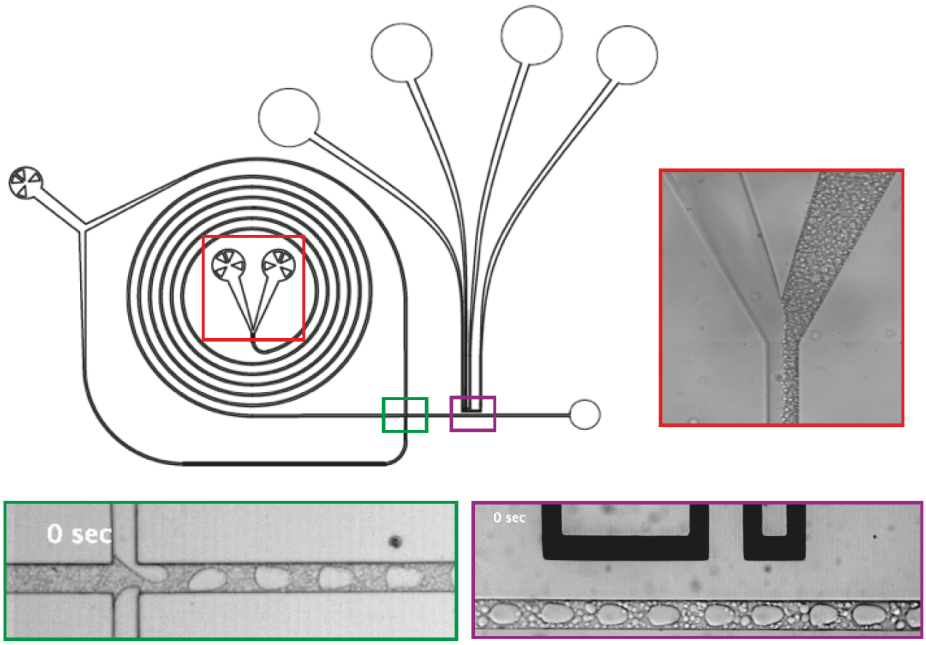

Figure SI 5 Release process with circular microfluidic release device.
Small dsProCaps and a destabilizing agent are introduced in parallel to the circular release device (red square). The release media is introduced from the outer inlet channel and mixed with the droplet/PFO mixture at the flow focusing junction (green square). Before the released capsules are collected through the outlet channel, an electric field supports the destabilization of the droplets (purple square).

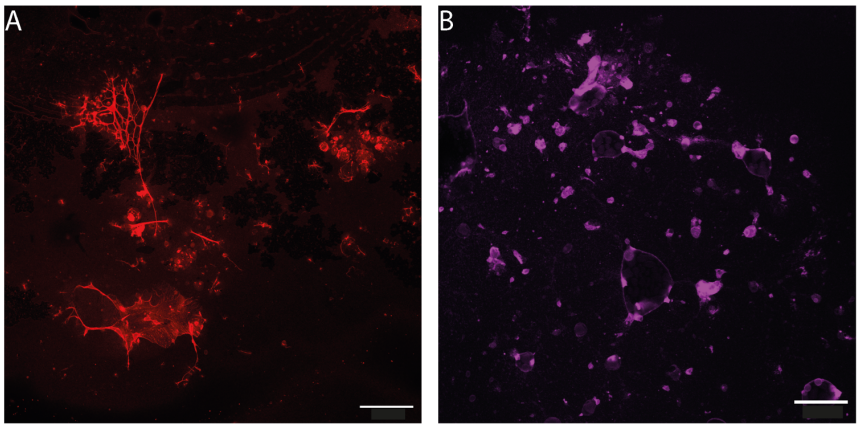

Figure SI 6 Small ProCaps established with the circular microfluidic release device.
Laminin-111 (A) and Matrigel (B) protein microcapsules can be detected in high numbers. Scale bar, 20µm.

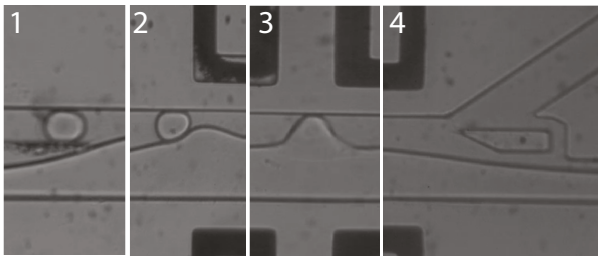

Figure SI 7 Workflow of ProCaps being released by an electric field implemented on a parallel flow release device.

1) A single droplet is introduced to the release area. 2) The first contact to the parallel aqueous phase is established. 3) The electric field impacts the droplet stability and allows for the coalescence of the droplet with the aqueous stream. Hereby, the content is released. 4) Two separate streams are collected. The upper stream collects the remaining oil waste and the lower aqueous phase contains the released microcapsules.

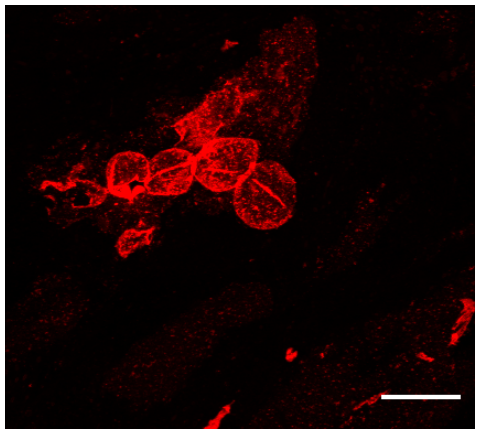

Figure SI 8 Laminin-111 ProCaps generated with the microfluidic parallel release device. Scale bar, 30 µm.

7.1.4 Pico-injection of different contents into preformed dsProCaps

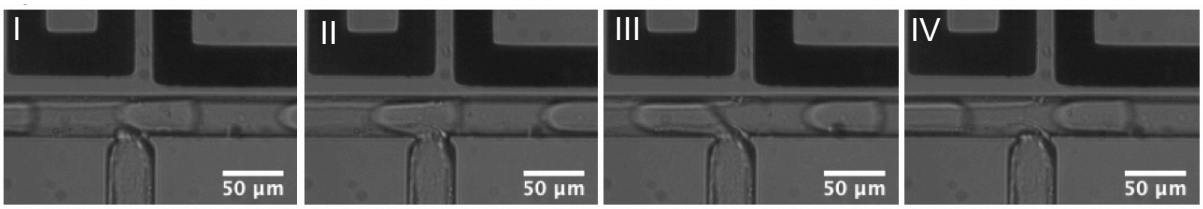

Figure SI 9 Injection of E. coli into protein-coated droplets in a pico-injection device.

I) The first contact between the droplet and the aqueous phase containing the bacteria, coming from the injection nozzle is established. II) The two aqueous phases fuse under the effect of the electric field. With the pressure on the injection nozzle the organisms are injected. III) The droplet stays in contact with the injection nozzle until it passes by completely. IV) After the droplet passed on it stabilizes again and the injection nozzle is sealed by the constant oil flow.

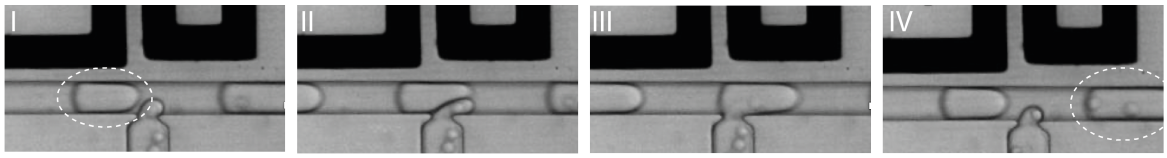

Figure SI 10 Injection of cells inside dsProCaps.
I) The first contact between the droplet and the aqueous phase containing the cells, coming from the injection nozzle is established. II) The two aqueous phases fuse under the effect of the electric field. With the pressure on the injection nozzle the organisms are injected. III) The droplet stays in contact with the injection nozzle until it passes by completely. IV) After the droplet passed on it stabilizes again and the injection nozzle is sealed by the constant oil flow and the cells stay encapsulated.

7.1.5 Analysis of the pH inside negatively charged dsProCaps

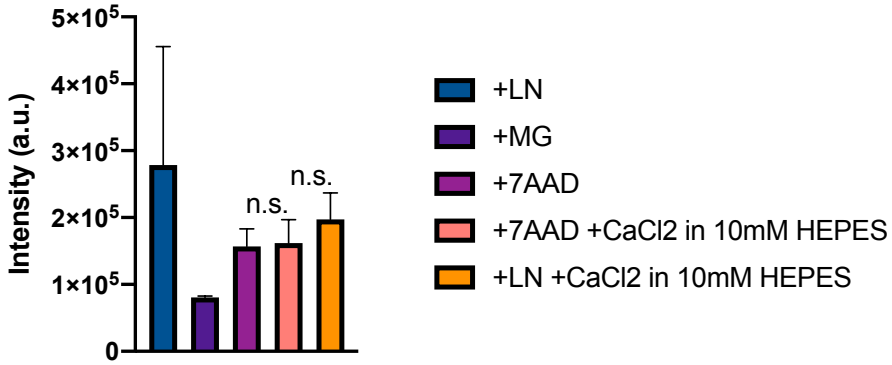

Figure SI 11 pH analysis inside water-in-oil droplets established with Krytox™.
Krytox™ molecules decrease the intensity values immensely inside droplets with various contents. No differences can be spotted at such low intensity values.

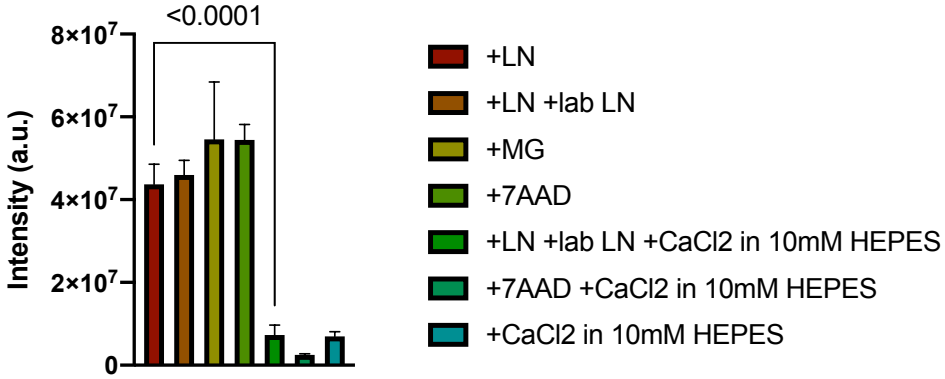

Figure SI 12 pH analysis inside water-in-oil droplets stabilized only with PEG-PFPE fluorosurfactant.
pH values are in normal areas, when no ions are added into the droplets. Upon the encapsulation of $CaCl_2$ ions, the intensity values drop drastically.

7.1.6 *Effects of the pH in negatively charged dsProCaps on proteins and cells*

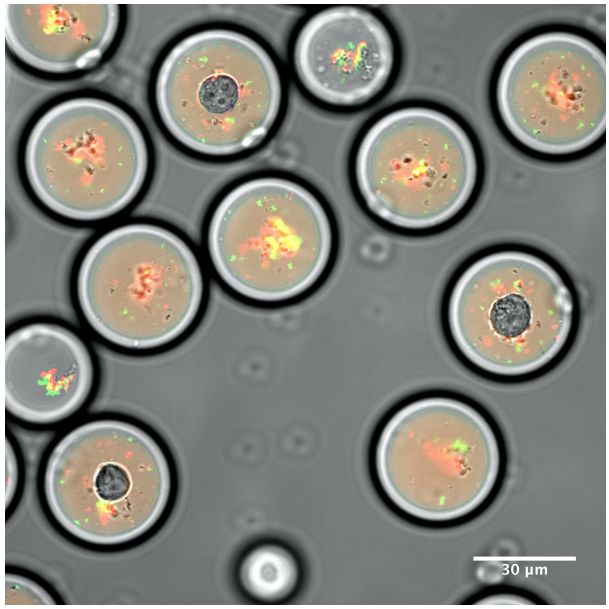

Figure SI 13 Jurkat cells inside laminin-111 dsProCaps stabilized with PEG-PFPE.
The lack of Krytox™ molecules shows no attraction of the protein and further proves cell viability by the lack of 7-AAD uptake by the cells.

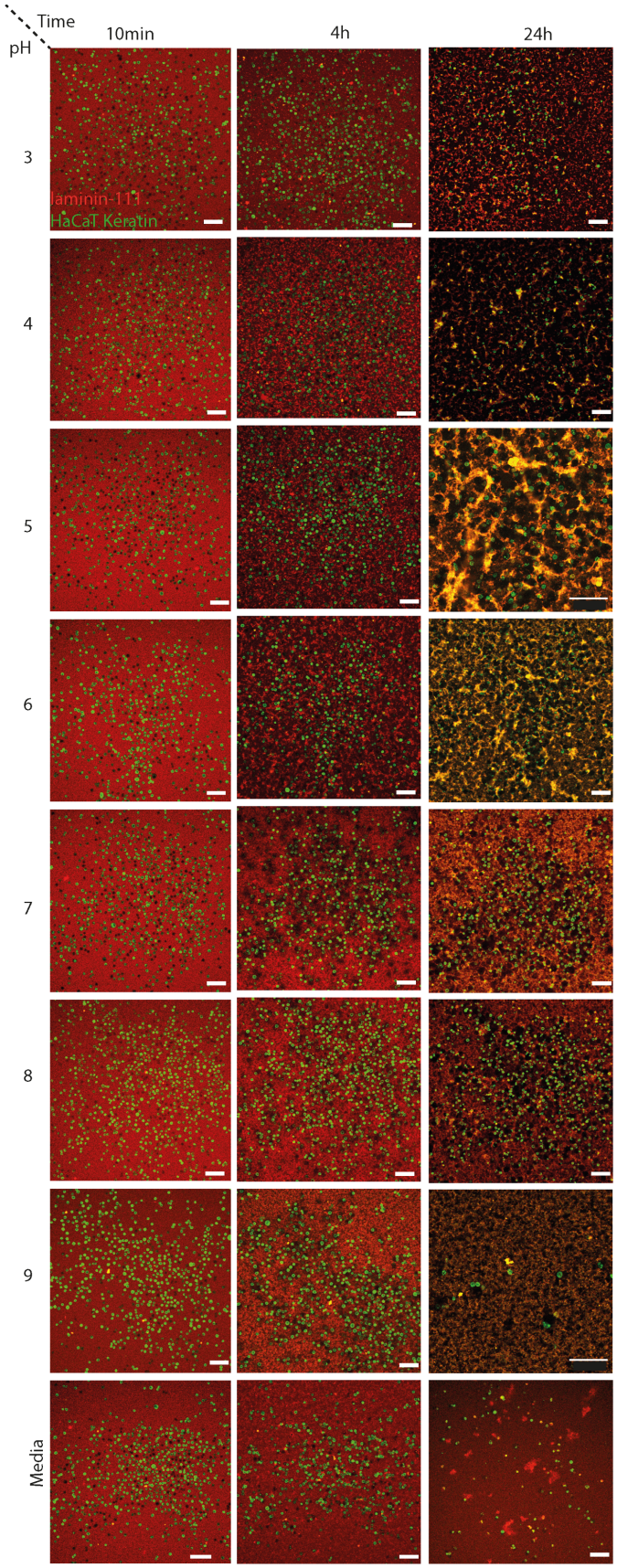

Figure SI 14 Laminin-111 polymerization efficiency under the effect of various pH over time. Scale bar, 100 µm.

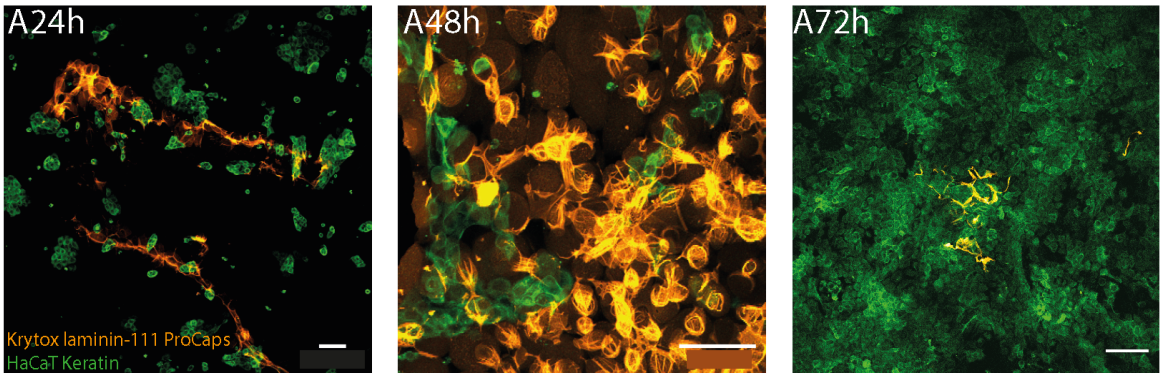

Figure SI 15 HaCaT cell adhesion to ProCaps established with positively charged surfactants. Cell growth was tracked over 24 (A24h), 48 (A48h) and 72 h (A72h). Scale bar, 50 µm.

7.1.7 Analysis of the pH inside positively charged dsProCaps

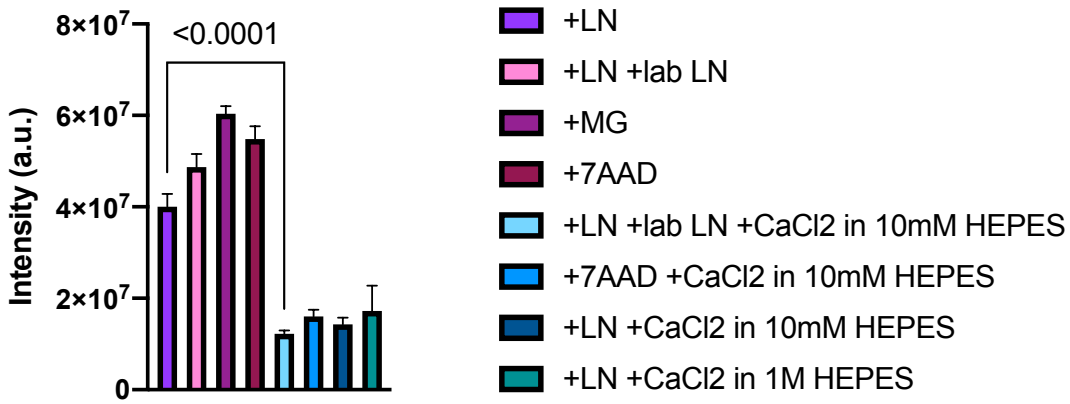

Figure SI 16 pH analysis inside water-in-oil droplets stabilized with N(Me3)-PEG-PFPE fluorosurfactant. pH values are in normal areas, when no ions are added into the droplets. Upon the encapsulation of $CaCl_2$ ions, the intensity values drop.

7.1.8 Characterization of dsProCaps stabilized with positively charged surfactant

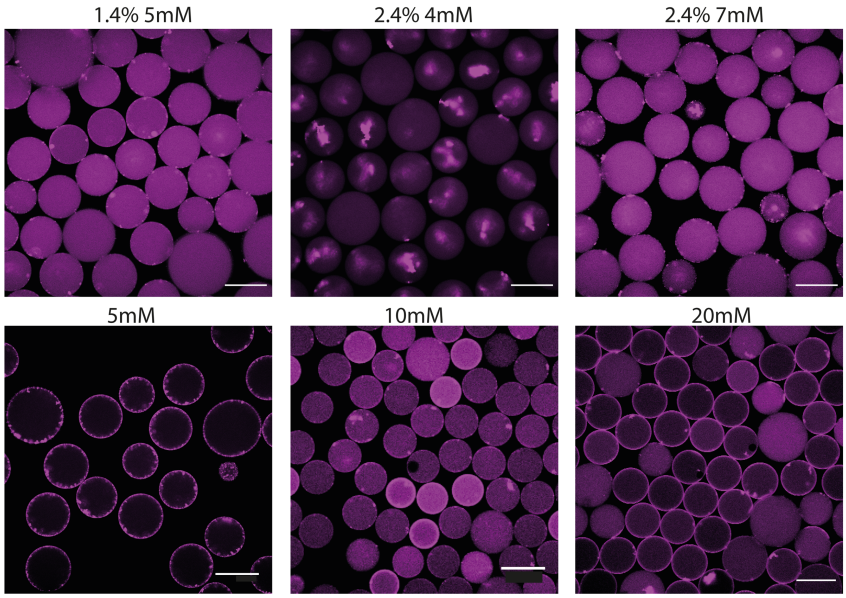

Figure SI 17 Various surfactant concentrations were tested in order to find the suitable balance between protein attraction and oil stability. Three different concentrations of the positively charged surfactant (mM) mixed with various ratios of 008-fluorosurfactant (%). Matrigel® was used as the model protein. Scale bar, 50 µm.

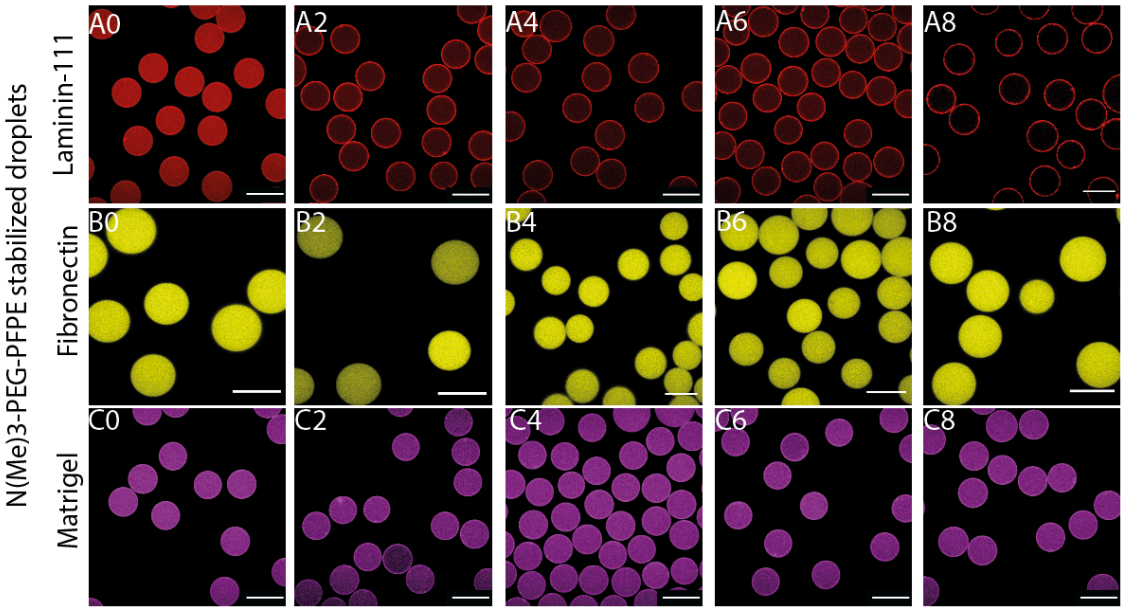

Figure SI 18 Time study for the attraction of laminin-111, fibronectin and Matrigel® to the periphery of N(Me)3-PEG-PFPE stabilized droplets. Scale bar, 50 µm.

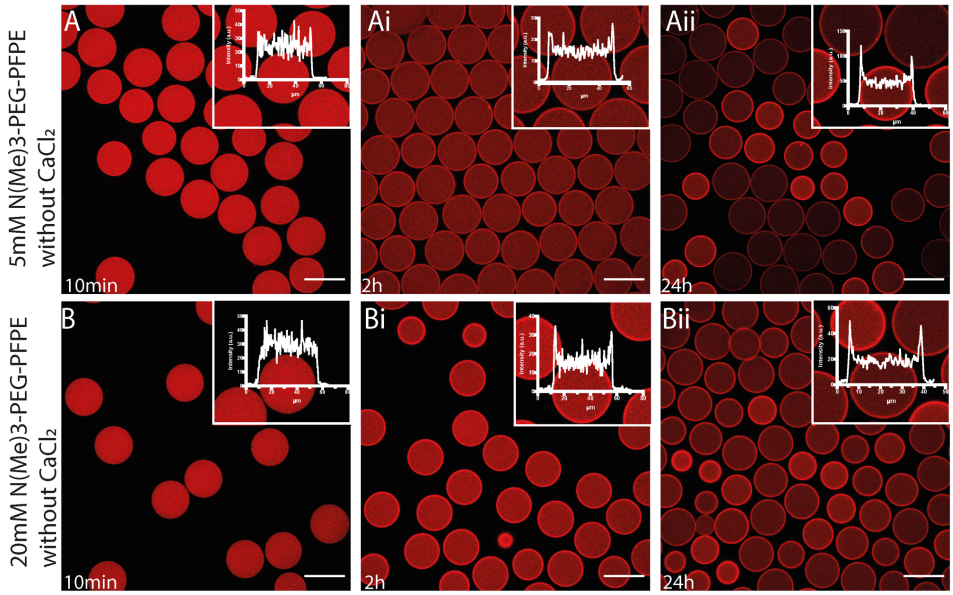

Figure SI 19 Attraction of laminin-111 in N(Me)3-PEG-PFPE droplets without $CaCl_2$. Laminin-111 encapsulated inside water-in-oil droplets stabilized with 5 mM (A) or 20 mM (B) positively charged surfactants, without the addition of $CaCl_2$ molecules. Time observation after 10min (Ai, Bi), 2h (Aii, Bii) and 24h (Aii, Bii) revealed the attraction of the protein to the periphery. Validated by representative intensity plots. Scale bars, 50 µm.

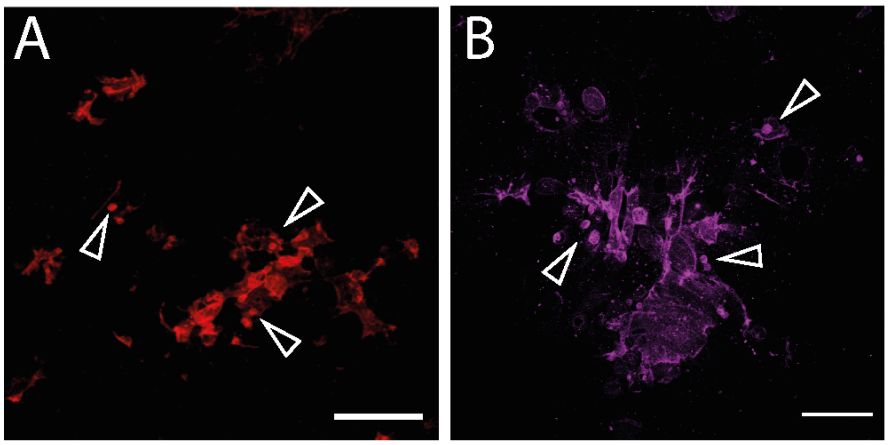

Figure SI 20 Release of small positively charged ProCaps. Laminin-111 (A) and Matrigel® (B) ProCaps generated (white arrow heads). Scale bar, 30µm.

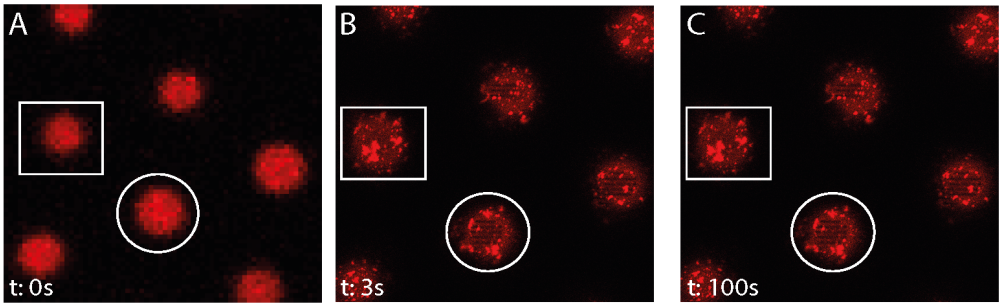

Figure SI 21 FRAP measurements on N(Me)3-PEG-PFPE stabilized laminin-111 dsProCaps. One droplet serves a non-bleach control (Square). Bleaching occurs after 3s and no recovery is detected over 100s (Circle).

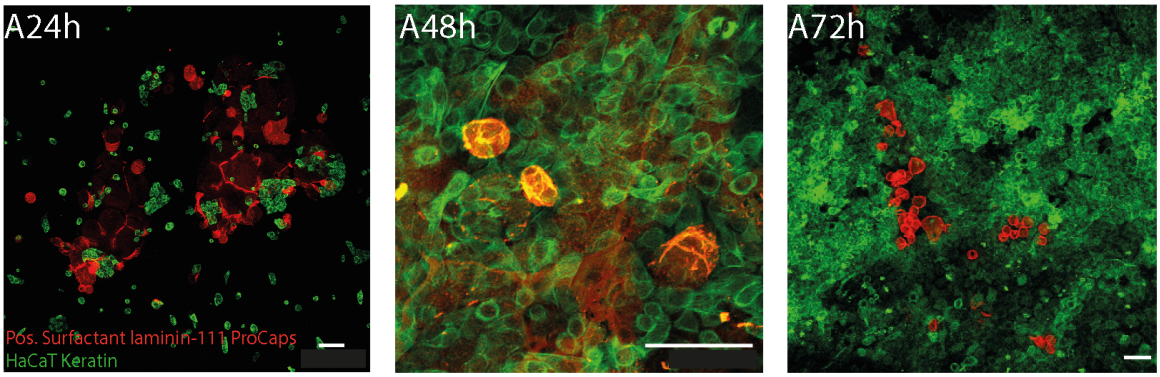

Figure SI 22 HaCaT cell adhesion to ProCaps established with positively charged surfactants. Cell growth was tracked over 24 (A24h), 48 (A48h) and 72 h (A72h). Scale bar, 100µm.

7.1.9 *Protein attraction in cell-laden dsProCaps*

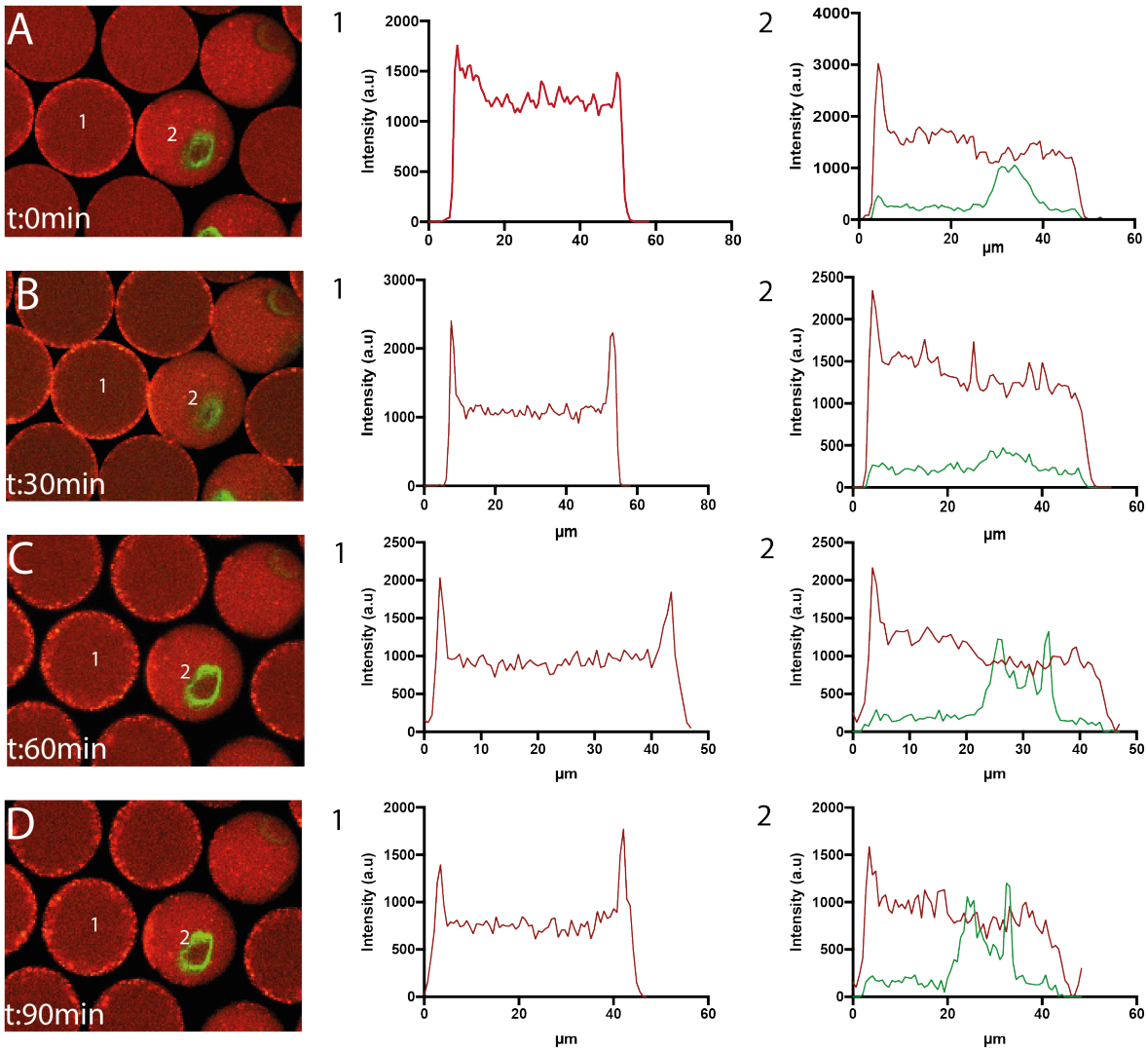

Figure SI 23 Observation of HaCaT-YFP cells in positively charged laminin-111 dsProCaps over 90 min. Intensity plots laminin-111 only (1) or in combination with HaCaT cells (2) of droplets 1 and 2 are depicted next to each time point.

7.1.10 Live/Dead staining of cells released from laminin-111 positively charged ProCaps

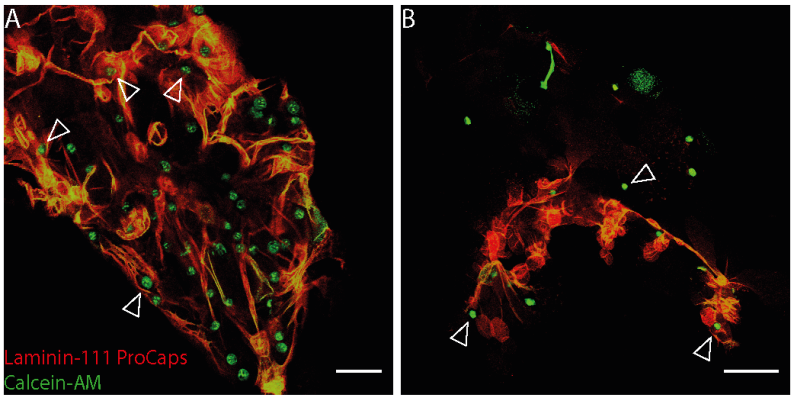

Figure SI 24 Live/Dead imaging of HaCaT cells (white arrow heads) inside laminin-111 ProCaps. A) Viable cells trapped in laminin network upon release of capsules. Scale bar, 50µm. B) Living cells in laminin-111 ProCaps and in the surrounding. Scale bar, 100µm. Calcein-AM signal ex/em 488 nm/515 nm, laminin-111 ProCaps and propidium iodide ex/em 570nm/602 nm.

7.1.11 Laminin-111 consumption by cells over time

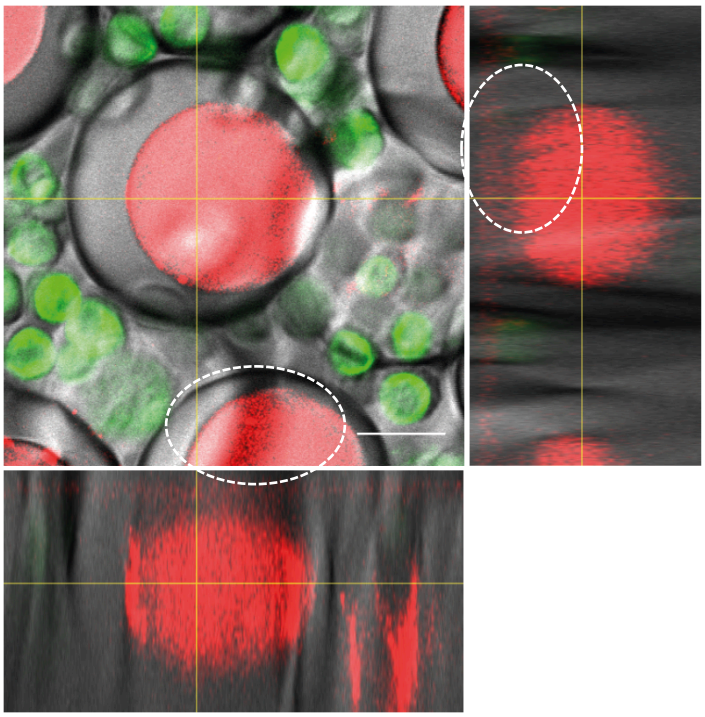

Figure SI 25 Laminin-111/Dextran residues inside the crescent microparticles. HaCaT YFP cells (green) cannot be loaded into the filled cavity.

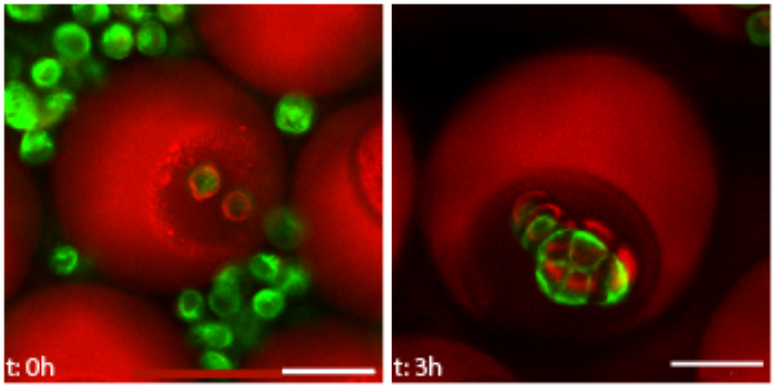

Figure SI 26 Decrease of laminin-111 signal inside buckets of crescent microparticles.
After addition of the cells (t:0h) a strong red signal is visible, which cannot be detected after another 3h in culture. HaCaT-YFP cells seem to consume the laminin-111.

7.1.12 Various Macros for the analysis of fluorescent images

Merging multi-channel images

```
run("Split Channels");
run("Merge Channels...");
run("Enhance Contrast", "saturated=0.35");
waitForUser("adjust brightness/contrast");
run("Scale Bar...", "width=100 height=5 font=20 color=White background=None location=[Lower Right] bold overlay");
saveAs("Tiff");
saveAs("Jpeg");
```

Thresholding

```
run("Set Measurements...", "area mean standard min median limit display redirect=None decimal=3");
run("Smooth");
setAutoThreshold("Otsu dark");
waitForUser("adjust threshold");
run("Analyze Particles...", "size=20-Infinity pixel circularity=0.80-1.00 show=Outlines display exclude include summarize");
close();
saveAs("Results");
```

Assigning LUTs

```
run("Red");
run("Enhance Contrast", "saturated=0.35");
waitForUser("adjust brightness/contrast");
run("Scale Bar...", "width=30 height=5 font=25 color=White background=None location=[Lower Right] bold overlay");
saveAs("tiff");
saveAs("jpeg");
close();

run(„Magenta“);
run("Enhance Contrast", "saturated=0.35");
waitForUser("adjust brightness/contrast");
run("Scale Bar...", "width=30 height=5 font=25 color=White background=None location=[Lower Right] bold overlay");
saveAs("tiff");
saveAs("jpeg");
close();

run(„Yellow);
run("Enhance Contrast", "saturated=0.35");
waitForUser("adjust brightness/contrast");
run("Scale Bar...", "width=30 height=5 font=25 color=White background=None location=[Lower Right] bold overlay");
saveAs("tiff");
saveAs("jpeg");
close();
```

7.2 Preliminary stiffness measurements of ProCaps by AFM

Based on the lack of movement of cells encapsulated inside laminin-111 ProCaps (See Chapter 4.14 Creation of cell-laden ProCaps), I set out to investigate the stiffness of the established protein microcapsules. Positively and negatively charged dsProCaps with laminin-111 and Matrigel® are produced and released after 2 h at 37 °C. The preliminary results are indicating the stiffness range of the positively and negatively charged capsules being between 100 to 600 Pa (Supplementary Figure 27). Interestingly, the stiffness increases significantly ($p = 0.0437$) between laminin capsules generated with the positively (POS LN) or negatively charged (KRY LN) surfactants. The reason for this might lay in the more efficient attraction of proteins to the negatively charged inner droplet periphery rather than the positively charged surfactant (Figure 44 and 66). With more proteins being attracted, stiffer and thicker protein capsules can be established. The lack of difference in stiffness between POS MG and KRY LN and between POS LN and POS MG cannot be fully trusted based on the low number of measured protein capsules. Note, the AFM measurements were conducted only once with a low number of measured capsules. Hence, the experiments have to be repeated. However, the most important outcome of this preliminary experiment is the generally low stiffness values for each of the used conditions.

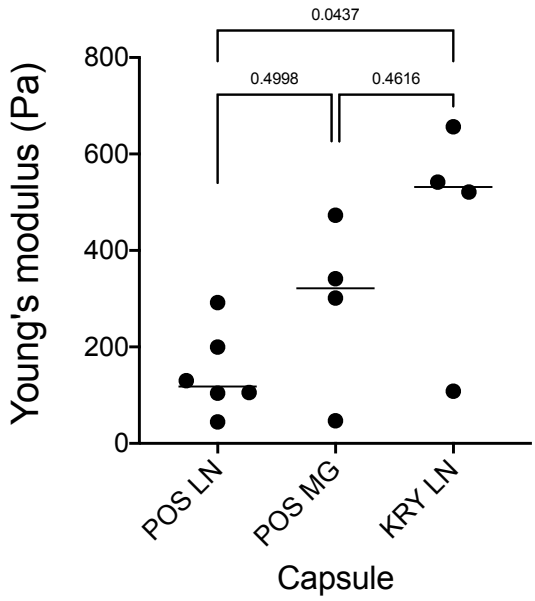

Figure SI 27 AFM indentation measurements of ProCaps to define stiffness values. Positively charged (POS) and negatively charged (KRY) capsules are generated with laminin-111 (LN) or Matrigel®(MG). Ordinary one-way ANOVA was used to generate statistical values.

7.3 List of Publications

Published

R Luo, **S Pashapour**, O Staufer, I Platzman, JP Spatz, Polymer-based Porous Microcapsules as Bacterial Traps, Adv. Functional Materials 30 (17), 1908855, March 2020.

C Frey, K Göpfrich, **S Pashapour**, I Platzman, JP Spatz, Electrocoalescence of Water-in-Oil Droplets with a Continuous Aqueous Phase: Implementation of Controlled Content Release, ACS Omega 5 (13), 7529-7536, March 2020.

In Submission

S Pashapour, M Schröter, C Frey, I Platzman, JS Spatz, Generation of Extracellular Matrix-based Microcapsules for Investigating Single Cells

In Preparation

J De Lora, **S Pashapour**, I Platzman, JS Spatz, Mechanical Manipulation of Cells in vitro by Ferrofluidic Synthetic Cells

7.4 List of Figures

7.5 Bibliography

1. Theocharis AD, Manou D, Karamanos NK. The extracellular matrix as a multitasking player in disease. *FEBS J* 2019;**286**(15):2830-2869.
2. Pickup MW, Mouw JK, Weaver VM. The extracellular matrix modulates the hallmarks of cancer. *EMBO Rep* 2014;**15**(12):1243-53.
3. Frantz C, Stewart KM, Weaver VM. The extracellular matrix at a glance. *J Cell Sci* 2010;**123**(Pt 24):4195-200.
4. McKee TJ, Perlman G, Morris M, Komarova SV. Extracellular matrix composition of connective tissues: a systematic review and meta-analysis. *Sci Rep* 2019;**9**(1):10542.
5. Niessen CM, Leckband D, Yap AS. Tissue organization by cadherin adhesion molecules: dynamic molecular and cellular mechanisms of morphogenetic regulation. *Physiol Rev* 2011;**91**(2):691-731.
6. DeSimone TRDW. The Extracellular Matrix In Development and Morphogenesis: A Dynamic View. *Dev Biol* 2010.
7. C. K. Regulation of embryonic cell adhesion by the cadherin cytoplasmic domain. . *Cell* 1992.
8. JP. T. Epithelial-mesenchymal transitions in tumour progression. *Nat Rev Cancer* 2002;**2**.
9. Townes PL HJ. Directed movements and selective adhesion of embronic amphibian cells. *J Exp Zool* 1955.
10. Nagafuchi A SY, Okazaki K, Yasuda K, Takeichi M. Transformation of cell adhesion properties by exogenously introduced E-cadherin cDNA. *Nature* 1987;**329**.
11. Sun Z, Guo SS, Fassler R. Integrin-mediated mechanotransduction. *J Cell Biol* 2016;**215**(4):445-456.
12. Sara A. Wickström CNN. Cell adhesion and mechanics as drivers of tissue organization and differentiation: local cues for large scale organization. *Curr Opin Cell Biol* 2018.
13. Matvey E. Lukashev ZW. ECM signalling: orchestrating cell behaviour and misbehaviour. *trends in CELL BIOLOGY* 1998;**8**.
14. Lin JH, Chang HY, Kao WL, et al. Effect of surface potential on extracellular matrix protein adsorption. *Langmuir* 2014;**30**(34):10328-35.
15. Humphrey JD, Dufresne ER, Schwartz MA. Mechanotransduction and extracellular matrix homeostasis. *Nat Rev Mol Cell Biol* 2014;**15**(12):802-12.
16. Theocharis AD, Skandalis SS, Gialeli C, Karamanos NK. Extracellular matrix structure. *Adv Drug Deliv Rev* 2016;**97**:4-27.
17. Yue B. Biology of the extracellular matrix: an overview. *J Glaucoma* 2014;**23**(8 Suppl 1):S20-3.
18. Farach-Carson MC, Carson DD. Perlecan--a multifunctional extracellular proteoglycan scaffold. *Glycobiology* 2007;**17**(9):897-905.
19. ARISTIDIS S. CHARONIS ECT, PETER D. YURCHENCO. Binding of Laminin to Type IV Collagen: A Morphological Study. *The Journal of Cell Biology* 1985;**100**:5.
20. Parkin JD, San Antonio JD, Pedchenko V, et al. Mapping structural landmarks, ligand binding sites, and missense mutations to the collagen IV heterotrimers predicts major functional domains, novel interactions, and variation in phenotypes in inherited diseases affecting basement membranes. *Hum Mutat* 2011;**32**(2):127-43.
21. Mak KM, Mei R. Basement Membrane Type IV Collagen and Laminin: An Overview of Their Biology and Value as Fibrosis Biomarkers of Liver Disease. *Anat Rec (Hoboken)* 2017;**300**(8):1371-1390.
22. Hansen NU, Genovese F, Leeming DJ, Karsdal MA. The importance of extracellular matrix for cell function and in vivo likeness. *Exp Mol Pathol* 2015;**98**(2):286-94.
23. Tomlin H, Piccinini AM. A complex interplay between the extracellular matrix and the innate immune response to microbial pathogens. *Immunology* 2018;**155**(2):186-201.
24. Czirok Z, Filla, Little, Rongish. Extracellular matrix macroassembly dynamics in early vertebrate embryos. *Curr Top Dev Biol* 2006.
25. Doyle AD, Petrie RJ, Kutys ML, Yamada KM. Dimensions in cell migration. *Curr Opin Cell Biol* 2013;**25**(5):642-9.
26. Doyle AD WF, Matsumoto K, Yamada KM. . One-dimensional topography underlies threedimensional fibrillar cell migration. *J Cell Biol* 2009.

27. Cukierman E PR, Stevens DR, Yamada KM. Taking cell-matrix adhesions to the third dimension. *Science* 2001.
28. Mao Y SJ. Stimulatory effects of a three-dimensional microenvironment on cell-mediated fibronectin fibrillogenesis. *J Cell Sci* 2005.
29. Davidson LA DB, Keller R, Desimone DW. Live imaging of cell protrusive activity, and extracellular matrix assembly and remodeling during morphogenesis in the frog, Xenopus laevis. *Dev Dyn* 2008.
30. DJ. C. Syndecans: multifunctional cell-surface co-receptors. . *Biochem* 1997.
31. Kupperman E AS, Osborne N, Waldron S, Stainier DY. . A sphingosine-1-phosphate receptor regulates cell migration during vertebrate heart development. *Nature* 2000.
32. Oehrl W PG. Modulation of growth factor action by the extracellular matrix. *Connect Tissue Res* 2008.
33. Beqaj S JS, Mattingly RR, Pan D, Schuger L. . High RhoA activity maintains the undifferentiated mesenchymal cell phenotype, whereas RhoA down-regulation by laminin-2 induces smooth muscle myogenesis. *J Cell Biol* 2002.
34. Guilak F CD, Estes BT, Gimble JM, Liedtke W, Chen CS. . Control of stem cell fate by physical interactions with the extracellular matrix. *Cell Stem Cell* 2009.
35. Alford D BD, Geyp M, Pitha P, Taylor-Papadimitriou J. . Integrin-matrix interactions affect the form of the structures developing from human mammary epithelial cells in collagen or fibrin gels. *J Cell Sci* 1998.
36. Dzamba BB, MA.; DeSimone, DW. . The integrin family of cell adhesion molecules. *Cell Adhesion* 2001.
37. Flanagan LA RL, Derzic S, Schwartz PH, Monuki ES. . Regulation of human neural precursor cells by laminin and integrins. *J Neurosci Res* 2006.
38. Palecek SP LJ, Ginsberg MH, Lauffenburger DA, Horwitz AF. Integrin-ligand binding properties govern cell migration speed through cellsubstratum adhesiveness. *Nature* 1997.
39. Pankov R, Yamada KM. Fibronectin at a glance. *J Cell Sci* 2002;**115**(Pt 20):3861-3.
40. Chiquet-Ehrismann R, Tucker RP. Tenascins and the importance of adhesion modulation. *Cold Spring Harb Perspect Biol* 2011;**3**(5).
41. Midwood KS, Chiquet M, Tucker RP, Orend G. Tenascin-C at a glance. *J Cell Sci* 2016;**129**(23):4321-4327.
42. Khoshnoodi J, Pedchenko V, Hudson BG. Mammalian collagen IV. *Microsc Res Tech* 2008;**71**(5):357-70.
43. Grover CN, Gwynne JH, Pugh N, et al. Crosslinking and composition influence the surface properties, mechanical stiffness and cell reactivity of collagen-based films. *Acta Biomater* 2012;**8**(8):3080-90.
44. Ricard-Blum S. The collagen family. *Cold Spring Harb Perspect Biol* 2011;**3**(1):a004978.
45. Kadler KE, Baldock C, Bella J, Boot-Handford RP. Collagens at a glance. *J Cell Sci* 2007;**120**(Pt 12):1955-8.
46. Makareeva E LS. Procollagen triple helix assembly: An unconventional chaperone-assisted folding paradigm. *PloS One* 2007.
47. Sauk JJ NN, Siavash H. . Hsp47 a novel collagen binding serpin chaperone, autoantigen and therapeutic target. *Front Biosci* 2005.
48. JM. M. Lysyl oxidases in mammalian development and certain pathological conditions. *Histol Histopathol* 2009.
49. Anazco C, Lopez-Jimenez AJ, Rafi M, et al. Lysyl Oxidase-like-2 Cross-links Collagen IV of Glomerular Basement Membrane. *J Biol Chem* 2016;**291**(50):25999-26012.
50. Pischon N. Bedeutung der extrazellulären Kollagenmodifikationen für die Osteoblastendifferenzierung und Entstehung von Knochengewebe. *Habilitationsschrift* 2012.
51. Herchenhan A, Uhlenbrock F, Eliasson P, et al. Lysyl Oxidase Activity Is Required for Ordered Collagen Fibrillogenesis by Tendon Cells. *J Biol Chem* 2015;**290**(26):16440-50.
52. Romberger DJ. Fibronectin. *Int J Biochem Cell Biol* 1997;**29**.
53. Magnus K. Magnusson DFM. Fibronectin Structure, Assembly, and Cardiovascular Implications. *Arterioscler Thromb Vasc Biology* 1998.
54. Schwarzbauer JE, DeSimone DW. Fibronectins, their fibrillogenesis, and in vivo functions. *Cold Spring Harb Perspect Biol* 2011;**3**(7).

55. Benjamin Geiger AB, Roumen Pankov and Kenneth M. Yamada. TRANSMEMBRANE EXTRACELLULAR MATRIX–CYTOSKELETON CROSSTALK. *Nature Reviews* 2001;**2**.
56. Hynes R. MOLECULAR BIOLOGY OF FIBRONECTIN
. *Ann Rev Cell Biol* 1985;**1**.
57. Nelea V, Nakano Y, Kaartinen MT. Size distribution and molecular associations of plasma fibronectin and fibronectin crosslinked by transglutaminase 2. *Protein J* 2008;**27**(4):223-33.
58. Deravi LF ST, Paten JA, Ruberti JW, Bertoldi K, Parker KK. Differential Contributions of Conformation Extension and Domain Unfolding to Properties of Fibronectin Nanotextiles. *Nano Lett* 2012.
59. Ahn S, Deravi LF, Park SJ, et al. Self-organizing large-scale extracellular-matrix protein networks. *Adv Mater* 2015;**27**(18):2838-45.
60. Jens Ulmer BGaJPS. Force-induced fibronectin fibrillogenesis in vitro. *Soft Matter* 2008.
61. Miller CG, Budoff G, Prenner JL, Schwarzbauer JE. Minireview: Fibronectin in retinal disease. *Exp Biol Med (Maywood)* 2017;**242**(1):1-7.
62. Durbeej M. Laminins. *Cell Tissue Res* 2010;**339**(1):259-68.
63. Hamill KJ, Kligys K, Hopkinson SB, Jones JC. Laminin deposition in the extracellular matrix: a complex picture emerges. *J Cell Sci* 2009;**122**(Pt 24):4409-17.
64. McKee KK, Aleksandrova M, Yurchenco PD. Chimeric protein identification of dystrophic, Pierson and other laminin polymerization residues. *Matrix Biol* 2018;**67**:32-46.
65. Armony G, Jacob E, Moran T, et al. Cross-linking reveals laminin coiled-coil architecture. *Proc Natl Acad Sci U S A* 2016;**113**(47):13384-13389.
66. Di Russo J, Luik AL, Yousif L, et al. Endothelial basement membrane laminin 511 is essential for shear stress response. *EMBO J* 2017;**36**(2):183-201.
67. Marcel BRUCH RLaJE. Dissection of laminin by cathepsin G into its long-arm and short-arm structures
and localization of regions involved in calcium dependent stabilization
and self-association. *Biochemistry* 1989;**185**.
68. Chiquet M, Gelman L, Lutz R, Maier S. From mechanotransduction to extracellular matrix gene expression in fibroblasts. *Biochim Biophys Acta* 2009;**1793**(5):911-20.
69. W Z. ECM and Cell Surface Proteolysis:
Regulating Cellular Ecology. *cell* 1997;**91**.
70. Rohani MG, Parks WC. Matrix remodeling by MMPs during wound repair. *Matrix Biol* 2015;**44-46**:113-21.
71. Cox TR, Erler JT. Remodeling and homeostasis of the extracellular matrix: implications for fibrotic diseases and cancer. *Dis Model Mech* 2011;**4**(2):165-78.
72. Keller KE, Aga M, Bradley JM, Kelley MJ, Acott TS. Extracellular matrix turnover and outflow resistance. *Exp Eye Res* 2009;**88**(4):676-82.
73. Engler AJ, Sen S, Sweeney HL, Discher DE. Matrix elasticity directs stem cell lineage specification. *Cell* 2006;**126**(4):677-89.
74. Franck Verrecchia AM. Transforming growth factor-β and fibrosis. *World J Gastroenterol* 2007.
75. Hinz B. The extracellular matrix and transforming growth factor-beta1: Tale of a strained relationship. *Matrix Biol* 2015;**47**:54-65.
76. Larsen M, Artym VV, Green JA, Yamada KM. The matrix reorganized: extracellular matrix remodeling and integrin signaling. *Curr Opin Cell Biol* 2006;**18**(5):463-71.
77. Zeinab Jahed HS, Mehrdad Mehrbod, Mohammed R.K. Mofrad. Linking the Extracellular Matrix to the Nucleus. *International review of cell and molecular biology* 2014;**310**.
78. Campbell ID, Humphries MJ. Integrin structure, activation, and interactions. *Cold Spring Harb Perspect Biol* 2011;**3**(3).
79. Srichai MB, Zent R. Integrin Structure and Function. *Cell-Extracellular Matrix Interactions in Cancer*, 2010;19-41.
80. Humphries MJ, McEwan PA, Barton SJ, et al. Integrin structure: heady advances in ligand binding, but activation still makes the knees wobble. *Trends in Biochemical Sciences* 2003;**28**(6):313-320.
81. Shellard A, Mayor R. Durotaxis: The Hard Path from In Vitro to In Vivo. *Dev Cell* 2021;**56**(2):227-239.

82. Zheng Y, Nan H, Liu Y, et al. Modeling cell migration regulated by cell extracellular-matrix micromechanical coupling. *Phys Rev E* 2019;**100**(4-1):043303.
83. Friedl P, Brocker EB, Zanker KS. Integrins, cell matrix interactions and cell migration strategies: fundamental differences in leukocytes and tumor cells. *Cell Adhes Commun* 1998;**6**(2-3):225-36.
84. Yamada KM, Collins JW, Cruz Walma DA, et al. Extracellular matrix dynamics in cell migration, invasion and tissue morphogenesis. *Int J Exp Pathol* 2019;**100**(3):144-152.
85. Lo CM, Wang, H.B., Dembo, M., and Wang, Y.L. Cell movement is guided by the rigidity of the substrate. *Biophys J* 2000.
86. Espina JA, Marchant CL, Barriga EH. Durotaxis: the mechanical control of directed cell migration. *FEBS J* 2021.
87. Li S, Huang NF, Hsu S. Mechanotransduction in endothelial cell migration. *J Cell Biochem* 2005;**96**(6):1110-26.
88. Lock JG, Wehrle-Haller B, Stromblad S. Cell-matrix adhesion complexes: master control machinery of cell migration. *Semin Cancer Biol* 2008;**18**(1):65-76.
89. Romani P, Valcarcel-Jimenez L, Frezza C, Dupont S. Crosstalk between mechanotransduction and metabolism. *Nat Rev Mol Cell Biol* 2021;**22**(1):22-38.
90. Peyton SR, Putnam AJ. Extracellular matrix rigidity governs smooth muscle cell motility in a biphasic fashion. *J Cell Physiol* 2005;**204**(1):198-209.
91. Chun-Min Lo H-BW, Micah Dembo, and Yu-li Wang. Cell Movement Is Guided by the Rigidity of the Substrate. *Biophys J* 2000.
92. Dupont S, Morsut L, Aragona M, et al. Role of YAP/TAZ in mechanotransduction. *Nature* 2011;**474**(7350):179-83.
93. Sirio Dupont LM, Mariaceleste Aragona, Elena Enzo, Stefano Giulitti, Michelangelo Cordenonsi, Francesca Zanconato, Jimmy Le Digabel, Mattia Forcato, Silvio Bicciato, Nicola Elvassore & Stefano Piccolo Role of YAP/TAZ in mechanotransduction. *Nature* 2011.
94. Jeong-Ho Hong ESH, Michael T. McManus, Adam Amsterdam, Yu Tian, Ralitsa Kalmukova, Elisabetta Mueller, Thomas Benjamin, Bruce M. Spiegelman, Phillip A. Sharp, Nancy Hopkins, Michael B. Yaffe. TAZ, a Transcriptional Modulator of Mesenchymal Stem Cell Differentiation. *Science* 2005.
95. Jin Hao YZ, Dian Jing, Yu Li, Juan Li, Zhihe Zhao. Role of Hippo Signaling in Cancer Stem Cells. *J Cell Physiol* 2013.
96. HONG-BEI WANG MD, YU-LI WANG. Substrate flexibility regulates growth and apoptosis of normal but not transformed cells. 2000.
97. Francis SMFaH. Disruption of Epithelial Cell-Matrix Interactions Induces Apoptosis. 1994.
98. Jere E. Meredith J, Babak Fazeli, and Martin A. Schwartz. The Extracellular Matrix as a Cell Survival Factor. *molecular biology of the cell* 1993;**4**.
99. Koninger J, Giese T, di Mola FF, et al. Pancreatic tumor cells influence the composition of the extracellular matrix. *Biochem Biophys Res Commun* 2004;**322**(3):943-9.
100. Rosso F, Giordano A, Barbarisi M, Barbarisi A. From cell-ECM interactions to tissue engineering. *J Cell Physiol* 2004;**199**(2):174-80.
101. Holle AW, Young JL, Spatz JP. In vitro cancer cell-ECM interactions inform in vivo cancer treatment. *Adv Drug Deliv Rev* 2016;**97**:270-9.
102. Wynn TA. Cellular and molecular mechanisms of fibrosis. *J Pathol* 2008;**214**(2):199-210.
103. RODEMANN HPB, ANKE; BURGER, ANKE; GÜVEN, NURI; LÖFFLER, HEIDI; BAMBERG, MICHAEL. The underlying cellular mechanism of fibrosis. *Kidney International supplement* 1996(54).
104. Krenning G, Zeisberg EM, Kalluri R. The origin of fibroblasts and mechanism of cardiac fibrosis. *J Cell Physiol* 2010;**225**(3):631-7.
105. D. Rubel JF, M. Martin, A. Leibnitz, R. Girgert, N. Miosge, B. Eckes, G.A. Muller,, Gross O. Collagen receptors integrin alpha2beta1 and discoidin domain receptor 1 regulate maturation of the glomerular basement membrane and loss of integrin alpha2beta1 delays kidney fibrosis in COL4A3 knockout mice. *Matrix Biol* 2014;**34**.
106. R. Bansal SN, S. Yazdani, J. van Baarlen, A. Venkatesh, A.P. Koh, W.M., Song NG, H. Watanabe, M.B. Beasley, C.A. Powell, G. Storm, N. Kaminski,, H. van Goor SLF, Y. Hoshida, J. Prakash. Integrin alpha 11 in the regulation of the myofibroblast phenotype: implications for fibrotic diseases. *Exp Mol Med* 2017.

107. Schnittert J, Bansal, R., Storm, G. & Prakash, J. . Integrins in wound healing, fibrosis and tumor stroma: high potential targets for therapeutics and drug delivery. *Adv Drug Deliv Rev* 2018.
108. Buchheit CL, Weigel KJ, Schafer ZT. Cancer cell survival during detachment from the ECM: multiple barriers to tumour progression. *Nat Rev Cancer* 2014;**14**(9):632-41.
109. Szot CS, Buchanan CF, Freeman JW, Rylander MN. 3D in vitro bioengineered tumors based on collagen I hydrogels. *Biomaterials* 2011;**32**(31):7905-12.
110. Berens EB, Holy JM, Riegel AT, Wellstein A. A Cancer Cell Spheroid Assay to Assess Invasion in a 3D Setting. *J Vis Exp* 2015(105).
111. Campbell JRPalD. Fibronectin structure and assembly. *Current Biology* 1994.
112. Chellini L, Caprara V, Spadaro F, et al. Regulation of extracellular matrix degradation and metastatic spread by IQGAP1 through endothelin-1 receptor signalling in ovarian cancer. *Matrix Biol* 2019;**81**:17-33.
113. Janiszewska M, Primi MC, Izard T. Cell adhesion in cancer: Beyond the migration of single cells. *J Biol Chem* 2020;**295**(8):2495-2505.
114. Kim W SKY, Soo Kim J, Shin NY, Hanks SK, Song WK The integrin-coupled signaling adaptor p130Cas suppresses Smad3
function in transforming growth factor-beta signaling. *Mol Biol Cell* 2008.
115. Leight JL WM, Chen S, Lynch ML, Chen CS Matrix rigidity regulates a switch between TGF-beta1-induced apoptosis and
epithelial-mesenchymal transition. *Mol Biol Cell* 2012.
116. Liu J AS. Mechanical signals activate vascular endothelial
growth factor receptor-2 to upregulate endothelial cell proliferation
during inflammation. . *J Immunol* 2010.
117. Di Modugno F, Colosi C, Trono P, et al. 3D models in the new era of immune oncology: focus on T cells, CAF and ECM. *J Exp Clin Cancer Res* 2019;**38**(1):117.
118. Najafi M, Farhood B, Mortezaee K. Extracellular matrix (ECM) stiffness and degradation as cancer drivers. *J Cell Biochem* 2019;**120**(3):2782-2790.
119. Huang J, Zhang L, Wan D, et al. Extracellular matrix and its therapeutic potential for cancer treatment. *Signal Transduct Target Ther* 2021;**6**(1):153.
120. Dolor AS, F. C. Jr Digesting a path forward: the utility of collagenase tumor treatment for improved drug delivery. *Mol Pharm* 2018.
121. Liu Jea. TGF-beta blockade improves the distribution and efficacy of therapeutics
in breast carcinoma by normalizing the tumor stroma. *Proc Natl Acad Sci U S A* 2012.
122. Chauhan VPea. Angiotensin inhibition enhances drug delivery and potentiates chemotherapy by decompressing tumour blood vessels. *Nat Commun* 2013.
123. Brun P, Dettin M, Campana LG, et al. Cell-seeded 3D scaffolds as in vitro models for electroporation. *Bioelectrochemistry* 2019;**125**:15-24.
124. Duval K, Grover H, Han LH, et al. Modeling Physiological Events in 2D vs. 3D Cell Culture. *Physiology (Bethesda)* 2017;**32**(4):266-277.
125. Gungor-Ozkerim PS, Inci I, Zhang YS, Khademhosseini A, Dokmeci MR. Bioinks for 3D bioprinting: an overview. *Biomater Sci* 2018;**6**(5):915-946.
126. Kilian YLaKA. Bridging the Gap: From 2D Cell Culture to 3D Microengineered Extracellular Matrices. *Adv Healthc Mater* 2015.
127. Pineda ET NR, Ahsan T. . Differentiation patterns of embryonic stem cells in two- versus three-dimensional culture. *Cells Tissue Organs* 2013;**197**.
128. Menacher A. Traction Force Microscopy. *Friedrich-Alexander Universität Erlangen-Nürnberg* 2012.
129. Smithmyer ME, Cassel SE, Kloxin AM. Bridging 2D and 3D culture: probing impact of extracellular environment on fibroblast activation in layered hydrogels. *AIChE J* 2019;**65**(12).
130. Wan Y, Wang Y, Liu Z, et al. Adhesion and proliferation of OCT-1 osteoblast-like cells on micro- and nano-scale topography structured poly(L-lactide). *Biomaterials* 2005;**26**(21):4453-9.
131. Kleinman HKL-E, L.; Cannon, F.W.; Sephel, G.C. Use of Extracellular Matrix Components for Cell Culture. *Analytical Biochemistry* 1987.
132. Ruoslahti EP, M.D. New perspectives in cell adhesion: RGD and integrins. *Science* 1987.

133. Hauschka SDK, I. R. The influence of collagen on the development of muscle clones. *Proc Natl Acad Sci U S A* 1966.
134. Minor RR, Wootton, J A. M, Prockop, D. J., Patterson, D. F. Genetic diseases of connective tissues in animals. *Curr Prob Dermatol* 1987.
135. Zhang ZG, Bothe I, Hirche F, et al. Interactions of primary fibroblasts and keratinocytes with extracellular matrix proteins: contribution of alpha2beta1 integrin. *J Cell Sci* 2006;**119**(Pt 9):1886-95.
136. Willerth SM, Faxel TE, Gottlieb DI, Sakiyama-Elbert SE. The effects of soluble growth factors on embryonic stem cell differentiation inside of fibrin scaffolds. *Stem Cells* 2007;**25**(9):2235-44.
137. El Bialy I, Jiskoot W, Reza Nejadnik M. Formulation, Delivery and Stability of Bone Morphogenetic Proteins for Effective Bone Regeneration. *Pharm Res* 2017;**34**(6):1152-1170.
138. Arai K, Yoshida T, Okabe M, et al. Fabrication of 3D-culture platform with sandwich architecture for preserving liver-specific functions of hepatocytes using 3D bioprinter. *J Biomed Mater Res A* 2017;**105**(6):1583-1592.
139. Li Y, Kilian KA. Bridging the Gap: From 2D Cell Culture to 3D Microengineered Extracellular Matrices. *Adv Healthc Mater* 2015;**4**(18):2780-96.
140. Beningo KA WY. Double-hydrogel substrate as a model system for three-dimensional cell culture. *Adhes Protein Protoc* 2007.
141. Anna Tourovskaia TB, Bronwyn T. Wickes, Danny Hirdes,, Boris Grin DGC, Kevin E. Healy, and Albert Folch. Micropatterns of Chemisorbed Cell Adhesion-Repellent Films Using Oxygen Plasma Etching and Elastomeric Masks. *Langmuir* 2003.
142. Hadden WJ, Young JL, Holle AW, et al. Stem cell migration and mechanotransduction on linear stiffness gradient hydrogels. *Proc Natl Acad Sci U S A* 2017;**114**(22):5647-5652.
143. Joo S, Yeon Kim J, Lee E, et al. Effects of ECM protein micropatterns on the migration and differentiation of adult neural stem cells. *Sci Rep* 2015;**5**:13043.
144. Falconnet D, Csucs G, Grandin HM, Textor M. Surface engineering approaches to micropattern surfaces for cell-based assays. *Biomaterials* 2006;**27**(16):3044-63.
145. Chaudhuri O, Gu L, Darnell M, et al. Substrate stress relaxation regulates cell spreading. *Nat Commun* 2015;**6**:6364.
146. De Laporte L, Yan AL, Shea LD. Local gene delivery from ECM-coated poly(lactide-co-glycolide) multiple channel bridges after spinal cord injury. *Biomaterials* 2009;**30**(12):2361-8.
147. Chaubey A RK, Leadbetter RM, Burg KJL. Surface patterning: tool to modulate stem cell differentiation in an adipose system. *J Biomed Mater Res B Appl Biomater* 2008;**84**.
148. Foster E, You J, Siltanen C, et al. Heparin hydrogel sandwich cultures of primary hepatocytes. *European Polymer Journal* 2015;**72**:726-735.
149. James C. Y Dunn RGT, and Martin L . Yarmush. Hepatocytes in Collagen Sandwich: Evidence for Transcriptional and Translational Regulation. *The Journal of Cell Biology* 1992;**116**.
150. Pebworth MP, Cismas SA, Asuri P. A novel 2.5D culture platform to investigate the role of stiffness gradients on adhesion-independent cell migration. *PLoS One* 2014;**9**(10):e110453.
151. Robert M. Ezzell MT, Kristin Hendricks, James C.Y. Dunn, Ronald G. Tompkins and Martin L. Yarmush. Effect of Collagen Gel Configuration on the Cytoskeleton in Cultured Rat Hepatocytes. *experimental cell research* 1993.
152. EDWARD L. LECLUYSE KLA, AND JEROME H. HOCHMAN. Formation of extensive canalicular networks by rat hepatocytes cultured in collagen-sandwich configuration. 1994.
153. Beningo KA, Dembo M, Wang YL. Responses of fibroblasts to anchorage of dorsal extracellular matrix receptors. *Proc Natl Acad Sci U S A* 2004;**101**(52):18024-9.
154. Fischer RS, Myers KA, Gardel ML, Waterman CM. Stiffness-controlled three-dimensional extracellular matrices for high-resolution imaging of cell behavior. *Nat Protoc* 2012;**7**(11):2056-66.
155. Chen L, Xiao Z, Meng Y, et al. The enhancement of cancer stem cell properties of MCF-7 cells in 3D collagen scaffolds for modeling of cancer and anti-cancer drugs. *Biomaterials* 2012;**33**(5):1437-44.
156. Wen Z, Liao Q, Hu Y, et al. A spheroid-based 3-D culture model for pancreatic cancer drug testing, using the acid phosphatase assay. *Braz J Med Biol Res* 2013;**46**(7):634-42.

157. Hsiao AY TY-C, Kuo C-H, Mosadegh B, Bedenis R, Pienta KJ, Takayama S. . Micro-ring structures stabilize microdroplets to enable long term spheroid culture in 384 hanging drop array plates. *Biomed Microdevices* 2012;**14**.
158. Torisawa YS TA, Nashimoto Y, Yasukawa T, Shiku H, Matsue T. . A multicellular spheroid array to realize spheroid formation, culture, and viability assay on a chip. *Biomaterials* 2007;**28**.
159. Alessandri K, Feyeux M, Gurchenkov B, et al. A 3D printed microfluidic device for production of functionalized hydrogel microcapsules for culture and differentiation of human Neuronal Stem Cells (hNSC). *Lab Chip* 2016;**16**(9):1593-604.
160. Lv D, Hu Z, Lu L, Lu H, Xu X. Three-dimensional cell culture: A powerful tool in tumor research and drug discovery. *Oncol Lett* 2017;**14**(6):6999-7010.
161. Suri S SC. Cell-laden hydrogel constructs of hyaluronic acid, collagen, and laminin for neural tissue engineering. *Tissue Eng Part A* 2010.
162. Burdick JA CC, Jia X, Randolph MA, Langer R. Controlled degradation and mechanical behavior of photopolymerized hyaluronic acid networks. *Biomacromolecules* 2005.
163. Ji C KA, Dehghani F. . Enhancing cell penetration and proliferation in chitosan hydrogels for tissue engineering applications. *Biomaterials* 2011;**32**.
164. Khalil S SW. Bioprinting endothelial cells with alginate for 3D tissue constructs. *Biomech Eng* 2009;**131**.
165. Han LH LJ, Yu S, Yang F. . Dynamic tissue engineering scaffolds with stimuli-responsive macroporosity formation. *Biomaterials* 2013.
166. Ma NK, Lim JK, Leong MF, et al. Collaboration of 3D context and extracellular matrix in the development of glioma stemness in a 3D model. *Biomaterials* 2016;**78**:62-73.
167. Wolf MT, Dearth CL, Ranallo CA, et al. Macrophage polarization in response to ECM coated polypropylene mesh. *Biomaterials* 2014;**35**(25):6838-49.
168. Faulk DM, Londono R, Wolf MT, et al. ECM hydrogel coating mitigates the chronic inflammatory response to polypropylene mesh. *Biomaterials* 2014;**35**(30):8585-95.
169. Khalili AA, Ahmad MR. A Review of Cell Adhesion Studies for Biomedical and Biological Applications. *Int J Mol Sci* 2015;**16**(8):18149-84.
170. Billiet T, Vandenhaute M, Schelfhout J, Van Vlierberghe S, Dubruel P. A review of trends and limitations in hydrogel-rapid prototyping for tissue engineering. *Biomaterials* 2012;**33**(26):6020-41.
171. Wang RM, Christman KL. Decellularized myocardial matrix hydrogels: In basic research and preclinical studies. *Adv Drug Deliv Rev* 2016;**96**:77-82.
172. Spang MT, Christman KL. Extracellular matrix hydrogel therapies: In vivo applications and development. *Acta Biomater* 2018;**68**:1-14.
173. Rape AD, Zibinsky M, Murthy N, Kumar S. A synthetic hydrogel for the high-throughput study of cell-ECM interactions. *Nat Commun* 2015;**6**:8129.
174. Detsch R, Sarker B, Zehnder T, Frank G, Boccaccini AR. Advanced alginate-based hydrogels. *Materials Today* 2015;**18**(10):590-591.
175. Flores-Torres S, Peza-Chavez O, Kuasne H, et al. Alginate-gelatin-Matrigel hydrogels enable the development and multigenerational passaging of patient-derived 3D bioprinted cancer spheroid models. *Biofabrication* 2021;**13**(2).
176. Hsueh YS, Chen YS, Tai HC, et al. Laminin-Alginate Beads as Preadipocyte Carriers to Enhance Adipogenesis In Vitro and In Vivo. *Tissue Eng Part A* 2017;**23**(5-6):185-194.
177. Lee KY, Mooney DJ. Alginate: properties and biomedical applications. *Prog Polym Sci* 2012;**37**(1):106-126.
178. Karoly Jakab BD, Adrian Neagu, Anatolij Kachurin and Gabor Forgacs. Three-dimensional tissue constructs built by bioprinting. *Biorheology* 2006;**43**.
179. Jakab K, Neagu A, Mironov V, Markwald RR, Forgacs G. Engineering biological structures of prescribed shape using self-assembling multicellular systems. *Proc Natl Acad Sci U S A* 2004;**101**(9):2864-9.
180. Jakab K, Norotte C, Damon B, et al. Tissue engineering by self-assembly of cells printed into topologically defined structures. *Tissue Eng Part A* 2008;**14**(3):413-21.
181. SangJun Moon PD, Syed K. Hasan, M.D.,Young S. Song, Ph.D.,, Feng Xu PD, Hasan Onur Keles, B.Sc., Fahim Manzur, B.Sc., Sohan Mikkilineni,, Jong Wook Hong PD, Jiro Nagatomi, Ph.D., Edward Haeggstrom, Ph.D.,, Ali Khademhosseini PD, and Utkan Demirci, Ph.D.

Layer by Layer Three-Dimensional Tissue Epitaxy by Cell-Laden Hydrogel Droplets. *Tissue Eng Part C* 2010;**16**.
182. Graham AD, Olof SN, Burke MJ, et al. High-Resolution Patterned Cellular Constructs by Droplet-Based 3D Printing. *Sci Rep* 2017;**7**(1):7004.
183. Shimanovich U, Bernardes GJ, Knowles TP, Cavaco-Paulo A. Protein micro- and nano-capsules for biomedical applications. *Chem Soc Rev* 2014;**43**(5):1361-71.
184. Ana Carolina Vale Campos Lisboa MdGdSV, Gisella Grazioli,, Francisco Rolando Valenzuela Díaz MCS. Polymeric Microcapsules Production from Sodium Alginic Acid for Cell Therapy. *Materials Research* 2007;**10**.
185. Lu G, An Z, Li J. Biogenic capsules made of proteins and lipids. *Biochem Biophys Res Commun* 2004;**315**(1):224-7.
186. Tian H, Du J, Wen J, et al. Growth-Factor Nanocapsules That Enable Tunable Controlled Release for Bone Regeneration. *ACS Nano* 2016;**10**(8):7362-9.
187. Zhou J, Hyun DC, Liu H, Wu H, Xia Y. Protein capsules with cross-linked, semipermeable, and enzyme-degradable surface barriers for controlled release. *Macromol Rapid Commun* 2014;**35**(16):1436-42.
188. Li Z, Liu S, Wang S, et al. Synthesis of folic acid functionalized redox-responsive magnetic proteinous microcapsules for targeted drug delivery. *J Colloid Interface Sci* 2015;**450**:325-331.
189. Yuki Itoh MM, Toshiyuki Kida, and Mitsuru Akashi. Enzyme-Responsive Release of Encapsulated Proteins from Biodegradable Hollow Capsules. *Biomacromolecules* 2006.
190. Zhao X, Liu S, Yildirimer L, et al. Injectable Stem Cell-Laden Photocrosslinkable Microspheres Fabricated Using Microfluidics for Rapid Generation of Osteogenic Tissue Constructs. *Advanced Functional Materials* 2016;**26**(17):2809-2819.
191. Campanha-Rodrigues AL, Grazioli G, Oliveira TC, et al. Therapeutic potential of laminin-biodritin microcapsules for type 1 diabetes mellitus. *Cell Transplant* 2015;**24**(2):247-61.
192. Orive G, Hernandez RM, Rodriguez Gascon A, et al. History, challenges and perspectives of cell microencapsulation. *Trends Biotechnol* 2004;**22**(2):87-92.
193. Liu X, Ma PX. Phase separation, pore structure, and properties of nanofibrous gelatin scaffolds. *Biomaterials* 2009;**30**(25):4094-103.
194. Stadler B, Price AD, Chandrawati R, et al. Polymer hydrogel capsules: en route toward synthetic cellular systems. *Nanoscale* 2009;**1**(1):68-73.
195. Zhang X, Xu D, Jin X, et al. Nanocapsules of therapeutic proteins with enhanced stability and long blood circulation for hyperuricemia management. *J Control Release* 2017;**255**:54-61.
196. Damien Mertz JC, Yan Yan, Glyn Devlin, Christophe Chaubaroux, AlexandreDochter, RoxaneAlles, Philippe Lavalle, Jean Claude Voegel, Anton Blencowe, Pascal Auffinger, and Frank Caruso. Protein Capsules Assembled via Isobutyramide Grafts: Sequential Growth, Biofunctionalization, and Cellular Uptake. *American Chemical Society Nano* 2012;**6**(9):10.
197. Huang C-J, Chang F-C. Using Click Chemistry To Fabricate Ultrathin Thermoresponsive Microcapsules through Direct Covalent Layer-by-Layer Assembly. *Macromolecules* 2009;**42**(14):5155-5166.
198. Kim YS, Jeong YI, Jin SG, et al. Release of tissue inhibitor of metalloproteinase-2 from alginate microcapsule encapsulating genetically engineered cells. *Int J Nanomedicine* 2013;**8**:4351-9.
199. Koblinski JE, Wu M, Demeler B, Jacob K, Kleinman HK. Matrix cell adhesion activation by non-adhesion proteins. *J Cell Sci* 2005;**118**(Pt 13):2965-74.
200. Li Z, Yang T, Lin C, et al. Sonochemical Synthesis of Hydrophilic Drug Loaded Multifunctional Bovine Serum Albumin Nanocapsules. *ACS Appl Mater Interfaces* 2015;**7**(34):19390-7.
201. Gang Lu ZA, Cheng Tao, Junbai Li. Microcapsule Assembly of human serum albumin at the liquid/liquid interface by the pendent drop technique. *Langmuir* 2004;**20**.
202. An Z, Lu G, Mohwald H, Li J. Self-assembly of human serum albumin (HSA) and L-alpha-dimyristoylphosphatidic acid (DMPA) microcapsules for controlled drug release. *Chemistry* 2004;**10**(22):5848-52.
203. Campos-Lisboa AC, Mares-Guia TR, Grazioli G, Goldberg AC, Sogayar MC. Biodritin microencapsulated human islets of Langerhans and their potential for type 1 diabetes mellitus therapy. *Transplant Proc* 2008;**40**(2):433-5.

204. Leal-Lopes C, Grazioli G, Mares-Guia TR, Coelho-Sampaio T, Sogayar MC. Polymerized laminin incorporation into alginate-based microcapsules reduces pericapsular overgrowth and inflammation. *J Tissue Eng Regen Med* 2019;**13**(10):1912-1922.
205. Bochenek MA, Veiseh O, Vegas AJ, et al. Alginate encapsulation as long-term immune protection of allogeneic pancreatic islet cells transplanted into the omental bursa of macaques. *Nat Biomed Eng* 2018;**2**(11):810-821.
206. Bidarra SJ, Barrias CC, Granja PL. Injectable alginate hydrogels for cell delivery in tissue engineering. *Acta Biomater* 2014;**10**(4):1646-62.
207. Cui J, van Koeverden MP, Mullner M, Kempe K, Caruso F. Emerging methods for the fabrication of polymer capsules. *Adv Colloid Interface Sci* 2014;**207**:14-31.
208. Edwin Donath GBS, Frank Caruso, Sean A. Davis, and Helmuth Möhwald. Novel Hollow Polymer Shells by Colloid-Templated Assembly of Polyelectrolytes. *Angew Chem Int Ed Engl* 1998;**16**.
209. Hyukjin Lee YJ, and Tae Gwan Park. Shell Cross-Linked Hyaluronic Acid/Polylysine Layer-by-Layer Polyelectrolyte Microcapsules Prepared by Removal of Reducible Hyaluronic Acid Microgel Cores. *Biomacromolecules* 2007.
210. Alexander N. Zelikin QL, and Frank Caruso. Disulfide-Stabilized Poly(methacrylic acid) Capsules: Formation, Cross-Linking, and Degradation Behavior. *chem. mater.* 2008.
211. Chong SF, Chandrawati R, Stadler B, et al. Stabilization of polymer-hydrogel capsules via thiol-disulfide exchange. *Small* 2009;**5**(22):2601-10.
212. Guerzoni LPB, Tsukamoto Y, Gehlen DB, et al. A Layer-by-Layer Single-Cell Coating Technique To Produce Injectable Beating Mini Heart Tissues via Microfluidics. *Biomacromolecules* 2019;**20**(10):3746-3754.
213. Matosevic S, Paegel BM. Layer-by-layer cell membrane assembly. *Nat Chem* 2013;**5**(11):958-63.
214. Esfahani RR, Jun H, Rahmani S, Miller A, Lahann J. Microencapsulation of Live Cells in Synthetic Polymer Capsules. *ACS Omega* 2017;**2**(6):2839-2847.
215. Teramura Y, Kaneda Y, Iwata H. Islet-encapsulation in ultra-thin layer-by-layer membranes of poly(vinyl alcohol) anchored to poly(ethylene glycol)-lipids in the cell membrane. *Biomaterials* 2007;**28**(32):4818-25.
216. Vegas AJ, Veiseh O, Gurtler M, et al. Long-term glycemic control using polymer-encapsulated human stem cell-derived beta cells in immune-competent mice. *Nat Med* 2016;**22**(3):306-11.
217. Kim SH, Abbaspourrad A, Weitz DA. Amphiphilic crescent-moon-shaped microparticles formed by selective adsorption of colloids. *J Am Chem Soc* 2011;**133**(14):5516-24.
218. Ekanem EE, Zhang Z, Vladisavljevic GT. Facile microfluidic production of composite polymer core-shell microcapsules and crescent-shaped microparticles. *J Colloid Interface Sci* 2017;**498**:387-394.
219. de Rutte J, Dimatteo R, van Zee M, Damoiseaux R, Di Carlo D. Massively parallel encapsulation of single cells with structured microparticles and secretion-based flow sorting. *bioRxiv* 2020.
220. Ma S, Thiele J, Liu X, et al. Fabrication of microgel particles with complex shape via selective polymerization of aqueous two-phase systems. *Small* 2012;**8**(15):2356-60.
221. Liu Q, Zhao M, Mytnyk S, et al. Self-Orienting Hydrogel Micro-Buckets as Novel Cell Carriers. *Angew Chem Int Ed Engl* 2019;**58**(2):547-551.
222. Lee S, de Rutte J, Dimatteo R, Koo D, Carl DD. Scalable Fabrication of 3D Structured Microparticles Using Induced Phase Separation. 2021.
223. Shumaker-Parry JS, Rochholz H, Kreiter M. Fabrication of Crescent-Shaped Optical Antennas. *Advanced Materials* 2005;**17**(17):2131-2134.
224. Ralf Seemann MB, Thomas Pfohl, Stephan Herminghaus. Droplet based microfluidics. *IOP Science* 2011;**75**(1).
225. Whitesides GM. The origins and the future of microfluidics. *Nature* 2006;**442**(7101):368-73.
226. Renata F. Gerhardt AJP, Sebastian K. Piendl, and Detlev Belder. Seamless Combination of High-Pressure Chip-HPLC and Droplet Microfluidics on an Integrated Microfluidic Glass Chip. *Anal Chem* 2017.

227. J.Luong RG, M.Hawryluk, R.A.Shellie, H.J.Cortes. Multidimensional gas chromatography using microfluidic switching and low thermal mass gas chromatography for the characterization of targeted volatile organic compounds. *Journal of Chromatography A* 2012.
228. Peter Gravesen JBaOSJ. Microfluidics - a review. *J Micromech Microeng* 1993;**3**.
229. Song H, Chen DL, Ismagilov RF. Reactions in droplets in microfluidic channels. *Angew Chem Int Ed Engl* 2006;**45**(44):7336-56.
230. Mansfield GJaCD. Microfluidic Diagnostics. *Springer Protocols* 2013.
231. Hu YT, Ting Y, Hu JY, Hsieh SC. Techniques and methods to study functional characteristics of emulsion systems. *J Food Drug Anal* 2017;**25**(1):16-26.
232. Li JM. Microfluidics For Single-Cell Analysis. *Springer* 2019.
233. Anwarul Hasan AP, Adnan Memic and Ali Khademhosseini. A multilayered microfluidic blood vessel-like structure. *Biomed Microdevices* 2016.
234. Ingber SNBDE. Microfluidic organs-on-chips. *Nature Biotechnology* 2014.
235. Samantha M. Hattersley JG, and Stephen J. Haswell. The Application of Micro fl uidic Devices for Viral Diagnosis in Developing Countries
. *Gareth Jenkins and Colin D. Mansfi eld (eds.), Microfl uidic Diagnostics: Methods and Protocols, Methods in Molecular Biology,*
vol. 949, DOI 10.1007/978-1-62703-134-9_19, © Springer Science+Business Media, LLC 2013 2013.
236. Sackmann EK, Fulton AL, Beebe DJ. The present and future role of microfluidics in biomedical research. *Nature* 2014;**507**(7491):181-9.
237. Sapienza. Confined Fluid Flow: Microfluidics and Capillarity. 2015.
238. Li JK. Laminar and turbulent flow in the mammalian aorta: Reynolds number. *J Theor Biol* 1988.
239. W J Baars NH, I Marusic Reynolds number trend of hierarchies and scale interactions in turbulent boundary layers. *Philos Trans A Math Phys Eng Sci* 2017.
240. Rojas EC, Staton JA, John VT, Papadopoulos KD. Temperature-induced protein release from water-in-oil-in-water double emulsions. *Langmuir* 2008;**24**(14):7154-60.
241. J Bibette FLCaPP. Emulsions: basic principles. *Rep. Prog. Phys.* 1998.
242. Utada AS. Monodisperse double emulsions generated from a microcapillary device.
. *Science* 2005.
243. Riechers Bea. Surfactant adsorption kinetics in microfluidics. *Proc. Natl. Acad. Sc* 2016.
244. Katepalli H, Bose, A., Hatton, T. A. & Blankschtein, D. . Destabilization of Oil-in-Water Emulsions Stabilized by Non-ionic Surfactants: Effect of Particle Hydrophilicity. *Langmuir* 2016.
245. Adamson AG, A. . Physical Chemistry Of Surfaces. 1997.
246. Taylor P. Ostwald ripening in emulsions: Estimation of solution thermodynamics of the disperse
phase. *Advanced Colloid Interface Science* 2003.
247. Aronson MP. The Role of Free Surfactant in Destabilizing Oil-in-Water Emulsions. *Langmuir* 1989.
248. Nakama Y. Surfactants. *Cosmetic Science and Technology*, 2017;231-244.
249. Guo MT, Rotem, A., Heyman, J. A. & Weitz, D. A. Droplet microfluidics for high-throughput biological assays. *Lab Chip* 2012.
250. Dai BL, L. G. . The mechanism of surfactant effects on drop coalescence. *Phys. Fluids 20* 2008.
251. Ya-Ling Chiu HFC, Kyle K. L. Phua,Ying Zhang,Sissel Juul, Birgitta R. Knudsen,, Yi-Ping Ho aKWL. Synthesis of Fluorosurfactants for Emulsion-Based Biological Applications. *ACS Nano* 2014.
252. DeJournette CJ, Kim J, Medlen H, et al. Creating biocompatible oil-water interfaces without synthesis: direct interactions between primary amines and carboxylated perfluorocarbon surfactants. *Anal Chem* 2013;**85**(21):10556-64.
253. Haller B, Gopfrich K, Schroter M, et al. Charge-controlled microfluidic formation of lipid-based single- and multicompartment systems. *Lab on a Chip* 2018;**18**(17):2665-2674.
254. Baret JC. Surfactants in droplet-based microfluidics. *Lab on a Chip* 2012.
255. Davies JT RE. Interface phenomena. . *NY: Academic Press* 1961.
256. Matsushita Y. Block Copolymers. In: Kobayashi S, Müllen K, eds. *Encyclopedia of Polymeric Nanomaterials*. Berlin, Heidelberg: Springer Berlin Heidelberg, 2015;232-236.
257. Suzuki T. Basics of Emulsification and the Trends in Future. *Oleoscience* 2012.

258. J. Eggers EV. Physics of liquid jets. *Rep Prog Phys* 2008.
259. Holtze Cea. Biocompatible surfactants for water-in-fluorocarbon emulsions. *Lab Chip* 2008.
260. Atkins P. Physical Chemistry. 2006.
261. Gruner P, Riechers B, Chacòn Orellana LA, et al. Stabilisers for water-in-fluorinated-oil dispersions: Key properties for microfluidic applications. *Current Opinion in Colloid & Interface Science* 2015;**20**(3):183-191.
262. Diamant H, Ariel, G. & Andelman, D. . Kinetics of Surfactant Adsorption: The Free Energy *Approach* 2000.
263. A. Bonfillon FS, D. L. . Dynamic Surface Tension of Ionic Surfactant Solutions. *J. Colloid Interface Sciences* 1994.
264. Tadros TF. Applied Surfactants: Principles and Applications. 2006.
265. McDonald. Micelle formation by surfactants. . *Surfactants and interfacial phenomena* 1978;**3**.
266. Nagarajan R, Ruckenstein, E. & Nagarajan, R. . Critical micelle concentration. A transition point for micellar size distribution. *J. Phys. Chem.* 1975.
267. MJ R. Adsorption of surface-active agents at Interfaces. *Surfactants and interfacial phenomena* 1978;**2**.
268. Goddard ED. Surfactants and interfacial phenomena. *Colloids and Surfaces* 1989.
269. Dietzel A. Microsystems for Pharmatechnology: Manipulation of Fluids, Particles, Droplets, and Cells. 2016.
270. Berry JD, Neeson, M. J., Dagastine, R. R., Chan, D. Y. C. & Tabor, R. F. . Measurement of surface and interfacial tension using pendant drop tensiometry. *J. Colloid Interface Sci.* 2015
271. Hansen FKR, G. . Surface Tension by Pendant Drop. *J. Colloid Interface Sci.* 1991.
272. Jin F, Balasubramaniam, R. & Stebe, K. J. . Surfactant adsorption to spherical particles: The intrinsic length scale governing the shift from diffusion to kinetic-controlled mass transfer. *J Adhes.* 2004.
273. Roach LS, Song, H. & Ismagilov, R. F. . Controlling nonspecific protein adsorption in a plugbased microfluidic system by controlling interfacial chemistry using fluorous-phase surfactants. *Anal. Chem.* 2005.
274. Dunstan TSF, P. D. I. . Compartmentalization and separation of aqueous reagents in the water droplets of water-in-oil high internal phase emulsions. *Langmuir* 2011.
275. Damean N, Olguin LF, Hollfelder F, Abell C, Huck WT. Simultaneous measurement of reactions in microdroplets filled by concentration gradients. *Lab Chip* 2009;**9**(12):1707-13.
276. Abate AR, Hung T, Mary P, Agresti JJ, Weitz DA. High-throughput injection with microfluidics using picoinjectors. *Proc Natl Acad Sci U S A* 2010;**107**(45):19163-6.
277. Suea-Ngam A, Howes PD, Srisa-Art M, deMello AJ. Droplet microfluidics: from proof-of-concept to real-world utility? *Chem Commun (Camb)* 2019;**55**(67):9895-9903.
278. Schaerli Y, Hollfelder F. The potential of microfluidic water-in-oil droplets in experimental biology. *Mol Biosyst* 2009;**5**(12):1392-404.
279. Tewhey R, Warner JB, Nakano M, et al. Microdroplet-based PCR enrichment for large-scale targeted sequencing. *Nat Biotechnol* 2009;**27**(11):1025-31.
280. Guo S, Lin WN, Hu Y, et al. Ultrahigh-throughput droplet microfluidic device for single-cell miRNA detection with isothermal amplification. *Lab Chip* 2018;**18**(13):1914-1920.
281. Macosko EZ, Basu A, Satija R, et al. Highly Parallel Genome-wide Expression Profiling of Individual Cells Using Nanoliter Droplets. *Cell* 2015;**161**(5):1202-1214.
282. Jang M, Yang S, Kim P. Microdroplet-based cell culture models and their application. *BioChip Journal* 2016;**10**(4):310-317.
283. Shembekar N, Chaipan C, Utharala R, Merten CA. Droplet-based microfluidics in drug discovery, transcriptomics and high-throughput molecular genetics. *Lab Chip* 2016;**16**(8):1314-31.
284. Klein AM, Mazutis L, Akartuna I, et al. Droplet barcoding for single-cell transcriptomics applied to embryonic stem cells. *Cell* 2015;**161**(5):1187-1201.
285. Monpichar Srisa-Art AJd, and Joshua B. Edel. High-Throughput DNA Droplet Assays Using Picoliter Reactor Volumes. *Analytical Chemistry* 2007.
286. Linas Mazutis AFA, Oliver J. Miller, Jean-Christophe Baret, Lucas Frenz,, Agnes Janoshazi, Valerie Taly, Benjamin J. Miller, J. Brian Hutchison, Darren Link,, Andrew D. Griffiths aMR. Droplet-Based Microfluidic Systems for High-Throughput Single DNA Molecule Isothermal Amplification and Analysis. 2009.

287. Mazutis L, Gilbert J, Ung WL, et al. Single-cell analysis and sorting using droplet-based microfluidics. *Nat Protoc* 2013;**8**(5):870-91.
288. Martino C, deMello AJ. Droplet-based microfluidics for artificial cell generation: a brief review. *Interface Focus* 2016;**6**(4):20160011.
289. Mazutis L, Baret JC, Treacy P, et al. Multi-step microfluidic droplet processing: kinetic analysis of an in vitro translated enzyme. *Lab Chip* 2009;**9**(20):2902-8.
290. Courtois F, Olguin LF, Whyte G, et al. An integrated device for monitoring time-dependent in vitro expression from single genes in picolitre droplets. *Chembiochem* 2008;**9**(3):439-46.
291. Dittrich PS, Jahnz M, Schwille P. A new embedded process for compartmentalized cell-free protein expression and on-line detection in microfluidic devices. *Chembiochem* 2005;**6**(5):811-4.
292. Dressler OJ, Maceiczyk RM, Chang SI, deMello AJ. Droplet-based microfluidics: enabling impact on drug discovery. *J Biomol Screen* 2014;**19**(4):483-96.
293. Ho Cheung Shum J-WK, and David A. Weitz. Microfluidic Fabrication of Monodisperse Biocompatible and Biodegradable Polymersomes with Controlled Permeability. *jacs* 2008.
294. Tumarkin E, Kumacheva E. Microfluidic generation of microgels from synthetic and natural polymers. *Chem Soc Rev* 2009;**38**(8):2161-8.
295. Robert F. Shepherd JCC, Summer K. Rhodes, Darren R. Link,, Manuel Marquez DAW, and Jennifer A. Lewis. Microfluidic Assembly of Homogeneous and Janus Colloid-Filled Hydrogel Granules. *Langmuir* 2006.
296. Casadevall i Solvas X, deMello A. Droplet microfluidics: recent developments and future applications. *Chem Commun (Camb)* 2011;**47**(7):1936-42.
297. Nick J. Carroll SBR, Erin Derbins, Sergio Mendez,, David A. Weitz aDNP. Droplet-Based Microfluidics for Emulsion and Solvent Evaporation

Synthesis of Monodisperse Mesoporous Silica Microspheres. *Langmuir* 2008.

298. Minseok Seo ZN, Shengqing Xu, Michelle Mok, Patrick C. Lewis,, Robert Graham aEK. Continuous Microfluidic Reactors for Polymer Particles. *Langmuir* 2005.
299. Tan WH, Takeuchi S. Monodisperse Alginate Hydrogel Microbeads for Cell Encapsulation. *Advanced Materials* 2007;**19**(18):2696-2701.
300. He Y, Ning T, Xie T, et al. Large-scale production of functional human serum albumin from transgenic rice seeds. *Proc Natl Acad Sci U S A* 2011;**108**(47):19078-83.
301. Seemann R, Brinkmann M, Pfohl T, Herminghaus S. Droplet based microfluidics. *Rep Prog Phys* 2012;**75**(1):016601.
302. Siegel AC, et al. Microsolidics: Fabrication of Three-Dimensional Metallic Microstructures in Poly(dimethyl)siloxane. *Adv Mater* 2007.
303. Brosseau Q, Vrignon J, Baret JC. Microfluidic Dynamic Interfacial Tensiometry (muDIT). *Soft Matter* 2014;**10**(17):3066-76.
304. Corning. Corning® Matrigel® Matrix. *Corning Incorporated* 2012.
305. Tinevez JY PN, Schindelin J, Hoopes GM, Reynolds GD, Laplantine E, Bednarek SY, Shorte SL, Eliceiri KW. . TrackMate: An open and extensible platform for single-particle tracking. . *Methods* 2017.
306. Watt FM, Fujiwara H. Cell-extracellular matrix interactions in normal and diseased skin. *Cold Spring Harb Perspect Biol* 2011;**3**(4).
307. Yi-Shan Cheng M-FC, Robert E. Burgeson, M. Peter Marinkovich,, Yurchenco aPD. Self-assembly of Laminin Isoforms. *Journal of Biological Chemistry* 1997.
308. DSc RSBP, FRS PCCGCMD. THE LIFE-CYCLE OF PRIMATE MALARIA PARASITES. 1982.
309. Karine G. Le Roch YZ, Peter L. Blair, Muni Grainger, J. Kathleen Moch, J. David Haynes, Patricia De la Vega, Anthony A. Holder, Serge Batalov, Daniel J. Carucci, Elizabeth A. Winzeler. Discovery of Gene Function by Expression Profiling of the Malaria Parasite Life Cycle. *Science* 2003.
310. Phillips RS. Current status of malaria and potential for control. *Clin Microbiol Rev* 2001;**14**(1):208-26.
311. Romanico B. G. Arrighi GL, Vassiliki Mahairaki, Inga Siden-Kiamos, Christos Louis. Laminin and the malaria parasite's journey through the mosquito midgut *Journal of Experimental Biology* 2005.
312. TUCKER PJSaA. pH-induced structural transitions of bovine serum albumin

Histidine pK, values and unfolding of the N-terminus during the N to F transition. *Eur J Biochem* 1993.
313. Gasteiger E HC, Gattiker A, Duvaud S, Wilkins MR, et al.. . Protein identification and analysis tools on the ExPASy server. *The proteomics protocols handbook Humana Press* 2005.
314. T FEC-S. Self-assembly of Laminin Induced by Acidic pH. *Journal of Biological Chemistry* 2000.
315. N. Pernodet MR, J. Sokolov , D. Xu , N. Yang , K. McLeod ,. Fibronectin fibrillogenesis on sulfonated polystyrene surfaces. *J Biomed Mater Res A* 2003.
316. M Weismann AHG, L Sorokin, B Bröker, M Frieser, R Hallmann and G W Mayr. Integrin-mediated intracellular Ca2+ signaling in Jurkat T lymphocytes. *J Immunol* 1997.
317. Benny P, Badowski, C., Lane, E.B., Raghunath, M. . Improving 2D and 3D Skin In Vitro Models Using Macromolecular Crowding. . *J Vis Exp* 2016.
318. Ranjani K. Paradise DAL, Krystyn J. Van Vliet. Acidic Extracellular pH Promottes Activation of Integrin avb3. *PLoS One* 2011.
319. Kuschel C, Steuer, H., Maurer, A. N., Kanzok, B., Stoop, R. and Angres, B. . Cell adhesion profiling using extracellular matrix protein microarrays. *Biotechniques* 2006.
320. Campbell A, Wicha MS, Long M. Extracellular matrix promotes the growth and differentiation of murine hematopoietic cells in vitro. *J Clin Invest* 1985;**75**(6):2085-90.
321. Nicolas J, Magli S, Rabbachin L, et al. 3D Extracellular Matrix Mimics: Fundamental Concepts and Role of Materials Chemistry to Influence Stem Cell Fate. *Biomacromolecules* 2020;**21**(6):1968-1994.
322. Padhi A, Nain AS. ECM in Differentiation: A Review of Matrix Structure, Composition and Mechanical Properties. *Ann Biomed Eng* 2020;**48**(3):1071-1089.
323. Michael L Dustin ARdF. Reprograming T cells: the role of extracellular matrix in coordination of T cell activation and migration
. *Curr Opin Immunol* 2001.
324. Smith LR, Cho S, Discher DE. Stem Cell Differentiation is Regulated by Extracellular Matrix Mechanics. *Physiology (Bethesda)* 2018;**33**(1):16-25.
325. Di Meglio I, Trushko A, Guillamat P, Blanch-Mercader C, Roux A. Pressure and curvature control of contact inhibition in epithelia
growing under spherical confinement. *bioRxiv* 2021.
326. Dobre O, Oliva MAG, Ciccone G, et al. A Hydrogel Platform that Incorporates Laminin Isoforms for Efficient Presentation of Growth Factors – Neural Growth and Osteogenesis. *Advanced Functional Materials* 2021;**31**(21).
327. Doyle AD, Yamada KM. Mechanosensing via cell-matrix adhesions in 3D microenvironments. *Exp Cell Res* 2016;**343**(1):60-66.
328. Decaris ML, Binder BY, Soicher MA, Bhat A, Leach JK. Cell-derived matrix coatings for polymeric scaffolds. *Tissue Eng Part A* 2012;**18**(19-20):2148-57.
329. Blanco-Fernandez B, Gaspar VM, Engel E, Mano JF. Proteinaceous Hydrogels for Bioengineering Advanced 3D Tumor Models. *Advanced Science* 2021.
330. Butcher DT, Alliston T, Weaver VM. A tense situation: forcing tumour progression. *Nat Rev Cancer* 2009;**9**(2):108-22.
331. Paszek MJ, Zahir N, Johnson KR, et al. Tensional homeostasis and the malignant phenotype. *Cancer Cell* 2005;**8**(3):241-54.
332. Janet M. Tse GC, James A. Tyrrell, Sarah A. Wilcox-Adelman, Yves Boucher, Rakesh K. Jain, and Lance L. Munn. Mechanical compression drives cancer cells toward invasive phenotype. *Proc Natl Acad Sci U S A* 2012.
333. Josette M. Northcott ISD, Janna K. Mouw, and Valerie M. Weaver. Feeling Stress: The Mechanics of Cancer Progression and Aggression. *Front Cell Dev Biol* 2018.
334. Cheng G, Tse J, Jain RK, Munn LL. Micro-environmental mechanical stress controls tumor spheroid size and morphology by suppressing proliferation and inducing apoptosis in cancer cells. *PLoS One* 2009;**4**(2):e4632.
335. Kai F, Drain AP, Weaver VM. The Extracellular Matrix Modulates the Metastatic Journey. *Dev Cell* 2019;**49**(3):332-346.
336. Lu P, Takai K, Weaver VM, Werb Z. Extracellular matrix degradation and remodeling in development and disease. *Cold Spring Harb Perspect Biol* 2011;**3**(12).
337. Lokmic Z, Lammermann T, Sixt M, et al. The extracellular matrix of the spleen as a potential organizer of immune cell compartments. *Semin Immunol* 2008;**20**(1):4-13.

338. Kim CH. Crawling of effector T cells on extracellular matrix: role of integrins in interstitial migration in inflamed tissues. *Cell Mol Immunol* 2014;**11**(1):1-4.
339. Yamaguchi S, Ueno A, Akiyama Y, Morishima K. Cell patterning through inkjet printing of one cell per droplet. *Biofabrication* 2012;**4**(4):045005.
340. Rutz AL, Hyland KE, Jakus AE, Burghardt WR, Shah RN. A multimaterial bioink method for 3D printing tunable, cell-compatible hydrogels. *Adv Mater* 2015;**27**(9):1607-14.
341. Zhu W, Ma X, Gou M, et al. 3D printing of functional biomaterials for tissue engineering. *Curr Opin Biotechnol* 2016;**40**:103-112.
342. Mandrycky C, Wang Z, Kim K, Kim DH. 3D bioprinting for engineering complex tissues. *Biotechnol Adv* 2016;**34**(4):422-434.
343. Singh D, Singh D, Han SS. 3D Printing of Scaffold for Cells Delivery: Advances in Skin Tissue Engineering. *Polymers (Basel)* 2016;**8**(1).
344. Agapakis CM. Designing synthetic biology. *ACS Synth Biol* 2014;**3**(3):121-8.
345. Leduc S. La biologie synthétique. *Paris: A. Poinat* 1912.
346. Szybalski W, and Skalka, A. Nobel prizes and restriction enzymes. *Gene* 1978.
347. Gibson DG, Glass, J. I., Lartigue, C., Noskov, V. N., Chuang, R.-, Y. A, M. A., Benders, G. A., Montague, M. G., Ma, L., Moodie, M., M. ea. Creation of a bacterial cell controlled by a chemically synthesized genome. *Science* 2010.
348. Mansy S, and Szostak, J. . Reconstructing the emergence of cellular life through the synthesis of model protocells. *Cold Spring Harb Symp Quant Biol* 2009.
349. Fanalista F, Birnie A, Maan R, et al. Shape and Size Control of Artificial Cells for Bottom-Up Biology. *ACS Nano* 2019;**13**(5):5439-5450.
350. Kyburz KA, Anseth KS. Synthetic mimics of the extracellular matrix: how simple is complex enough? *Ann Biomed Eng* 2015;**43**(3):489-500.
351. Haque MA, Nagaoka M, Hexig B, Akaike T. Artificial extracellular matrix for embryonic stem cell cultures: a new frontier of nanobiomaterials. *Sci Technol Adv Mater* 2010;**11**(1):014106.
352. Kim B-S, Park I-K, Hoshiba T, et al. Design of artificial extracellular matrices for tissue engineering. *Progress in Polymer Science* 2011;**36**(2):238-268.
353. Pieuchot L, Marteau J, Guignandon A, et al. Curvotaxis directs cell migration through cell-scale curvature landscapes. *Nat Commun* 2018;**9**(1):3995.
354. Mikaël M Martino 1 PSB, Adrian Ranga, Matthias P Lutolf, Jeffrey A Hubbell. Heparin-binding domain of fibrin(ogen) binds growth factors and promotes tissue repair when incorporated within a synthetic matrix. *Proc Natl Acad Sci U S A* 2013.

8 Acknowledgements

Obtaining my PhD degree at the Heidelberg University and within the Max Planck Institute for Medical Research is a great honor for me. Surrounded by great minds and wandering through the prestigious halls of the MPI motivated and strengthen me every day. The combination of ambitious people, the access to sophisticated instruments and the freedom to perform science helped me to grow and become a better and independent version of myself. Especially at the department for Cellular Biophysics I felt supported by the great working atmosphere and people from all around the world. I am very proud of being part of this sophisticated environment.

First, and most importantly, I want to thank Prof. Dr. Joachim Spatz for offering me a position in his department and giving me the opportunity to conduct research in a great environment. I am very thankful for all the scientific conversations and his support throughout my PhD journey, being it just corrections for poster presentations or even paving the way for new and exciting collaborations. He is an amazing scientist and mentor and was awarded many awards, such as the Leibnitz Preis, and started new institutes and the Max-Planck School in his young life already and still stayed humble and down-to-earth. Joachim Spatz is a role model in every life aspect and I can call myself lucky to have gotten to know him and work with such an incredible person.

I also want to thank Prof. Dr. Reiner Dahint for accepting to review my PhD thesis.

Besides Joachim Spatz, there is one person without whom I would not have achieved what I achieved in the past years. Dr. Ilia Platzman, group leader of the microfluidic subgroup and my close supervisor, supported me since day 1, when I became a "Mikrofluidiker". He introduced me to the world of droplet-based microfluidics and had a lot of patience with me and my 'basic' questions. I am grateful for all his help and scientific advices, and happy that the human/friendship aspect was also present. I could always talk to him about personal situations and joke with him about our Iran-Israel connection. Together with Dr. Rongcong Luo

and other lab members, we had quite some fun evenings at Iranian, Georgian, Chinese, Argentinian and many more dinners. Besides being a great supervisor, he is also a very good friend and important person who shaped me during my PhD time.

This leads me to my present and past colleagues. I am very happy I could meet and share some overlapping fun years together in the lab and more importantly outside the lab with all of you. First, I cannot thank Dr. Barbara Haller, Dr. Christoph Frey and Dr. Kerstin Göpfrich enough for explaining me the basics of droplet-based microfluidics and showing me everything from scratch. Besides technical input they were always open for scientific discussions. Further, I am very happy that Dr. Jacqueline De Lora joined our lab and infected me with her enthusiasm about science. She helped me with various experimental set ups and further introduced me to the world of acoustics and magnetism. Besides, a great co-worker, she became a very good friend and the best office mate. Another very enthusiastic, creative and smart person, who joined our lab recently is Senne Seneca. With his outstanding ideas and motivation for science he ignited my spark for various topics and broaden my horizon. I am especially thankful to Kerstin, Jacqueline and Senne who took their time and corrected parts of my thesis.

Jennifer Diemer was the first person I connected with in the lab and helped me where ever and whenever she could. She and her amazing Mum, Sabine Diemer, basically adopted me and helped me moving (twice) or invited me to family birthday dinners or took me with them to Europapark and Tripsdrill. She turned out to be the best friend I could have ever asked for.

Besides all the scientific greatness those people provide, they are even more amazing and fun people to be around with. With Senne, Jacqueline, Jenny, Jenn, Andrew, Christoph, Babs, Kerstin, Jacopo and Melisa and Franzi we could always go for a beer (or two), watch the super bowl in a cinema, go to the Gay Delight at the Wasen, or have just many, many fun dinner nights. I will never forget the time we all had together and I am very grateful for meeting you.

Besides the whole PhD journey and scientific knowledge, I got to meet Senne at the MPI, with whom I connected on a deeper level. I am very thankful for his support in the final months of writing and conducting experiments in parallel and being by my side through the last year of my PhD. I am looking forward to our next steps in future.

Last, but not least, I want to thank my great family. Without their endless support I could have never taken on the PhD journey in a different country. My parents, Esmail and Parvin Pashapour, are my biggest role models and showed me that with love and affection you can achieve everything you aim for. Most importantly, my sister and best friend Roxana, showed me the importance of a balanced life and supports me no matter what. Without their help I would not have make it to where I am and would not be the person I am today. I am very lucky to have you in my life.

Parts of the research are funded by the Sonderforschungsbereich 1129 (SFB1129) funded by the Deutsche Forschungsgesellschaft (DFG). In the scope of this collaboration I want to thank Prof. Dr. Frischknecht for being a very inspiring collaborator and a great person to work with. His motivation and interest are always very refreshing and lead to fruitful discussions.

NATURWISSENSCHAFTLICH-MATHEMATISCHE GESAMTFAKULTÄT

COMBINED FACULTY OF NATURAL SCIENCES AND MATHEMATICS

RUPRECHT-KARLS-
UNIVERSITÄT
HEIDELBERG

Eidesstattliche Versicherung gemäß § 8 der Promotionsordnung für die Naturwissenschaftlich-Mathematische Gesamtfakultät der Universität Heidelberg / Sworn Affidavit according to § 8 of the doctoral degree regulations of the Combined Faculty of Natural Sciences and Mathematics

1. Bei der eingereichten Dissertation zu dem Thema / The thesis I have submitted entitled

   Generation of Extracellular Matrix Protein-based Microcapsules for Investigating Single Cells

   handelt es sich um meine eigenständig erbrachte Leistung / is my own work.

2. Ich habe nur die angegebenen Quellen und Hilfsmittel benutzt und mich keiner unzulässigen Hilfe Dritter bedient. Insbesondere habe ich wörtlich oder sinngemäß aus anderen Werken übernommene Inhalte als solche kenntlich gemacht. / I have only used the sources indicated and have not made unauthorised use of services of a third party. Where the work of others has been quoted or reproduced, the source is always given.

3. Die Arbeit oder Teile davon habe ich ~~wie folg~~t/bislang nicht[1)] an einer Hochschule des In- oder Auslands als Bestandteil einer Prüfungs- oder Qualifikationsleistung vorgelegt. / I have not yet/have already[1)] presented this thesis or parts thereof to a university as part of an examination or degree.

   Titel der Arbeit / Title of the thesis: ……

   Hochschule und Jahr / University and year: ……

   Art der Prüfungs- oder Qualifikationsleistung / Type of examination or degree: ……

4. Die Richtigkeit der vorstehenden Erklärungen bestätige ich. / I confirm that the declarations made above are correct.

5. Die Bedeutung der eidesstattlichen Versicherung und die strafrechtlichen Folgen einer unrichtigen oder unvollständigen eidesstattlichen Versicherung sind mir bekannt. / I am aware of the importance of a sworn affidavit and the criminal prosecution in case of a false or incomplete affidavit.

Ich versichere an Eides statt, dass ich nach bestem Wissen die reine Wahrheit erklärt und nichts verschwiegen habe. / I affirm that the above is the absolute truth to the best of my knowledge and that I have not concealed anything.

Heidelberg, 30.7.21 ……
Ort und Datum / Place and date

S.Pashapour ……
Unterschrift / Signature

[1)] Nicht Zutreffendes streichen. Bei Bejahung sind anzugeben: der Titel der andernorts vorgelegten Arbeit, die Hochschule, das Jahr der Vorlage und die Art der Prüfungs- oder Qualifikationsleistung. / Please cross out what is not applicable. If applicable, please provide: the title of the thesis that was presented elsewhere, the name of the university, the year of presentation and the type of examination or degree.

The German text is legally binding.